

## A - OPERATION AND ECONOMICS IN TRANSPORT

---

- ASSESSING THE IMPACT OF THREE-WHEELERS ON TRAFFIC FLOW IN INDIA:  
A CASE STUDY USING ANN** **A50**  
M. Mohanty, M. L. Pattanaik, S. R. Samal, Shivam

## B - MECHANICAL ENGINEERING

---

- THE TE33A SERIES DIESEL LOCOMOTIVE BRAKE EQUIPMENT TESTS** **B142**  
S. Abdullayev
- ASSESSMENT OF THE QUALITY INDICATORS OF THE CARRIAGE MOVEMENT  
BY DIRECTLY MEASURING THE FORCES OF INTERACTION BETWEEN  
THE WHEELS AND RAILS** **B155**  
O. Fomin, P. Prokopenko
- INCREASING THE TRAFFIC SAFETY LEVEL OF ROLLING STOCK BY WHEEL  
CONDITION MONITORING USING AN AUTOMATED MEASURING COMPLEX** **B167**  
S. Kliuiev, S. Semenov, E. Mikhailov, J. Dižo, M. Blatnický, V. Ishchuk
- EXEMPLARY DETERMINATION OF THE ADHESION ELLIPSES BASED  
ON SIMULATION OF AN ACCELERATING MOTOR VEHICLE** **B175**  
J. Zalewski
- TRANSPORT EFFICIENCY STRATEGIES IN ASSEMBLY WORKPLACE: A CASE STUDY** **B187**  
D. Plinta, L. Dulina, B. Furmannová, J. Zuzik
- STRUCTURAL ANALYSIS OF DESIGNED TUBES UNDER AXIAL COMPRESSION:  
VARIATIONS OF APPLIED TEMPERATURE, MATERIAL TYPE,  
AND GEOMETRY DESIGN** **B199**  
H. A. Al Kautsar, A. A. Pratama, S. Suryanto, A. R. Prabowo, R. Adiputra, H. Sukanto,  
B. Kusharjanta, H. Carvalho
- STUDY OF THE STRENGTH OF THE OPEN WAGON HATCH DOOR WITH  
RECTANGULAR CORRUGATIONS UNDER STATIC LOADS** **B216**  
J. Gerlici, A. Lovska

## C - ELECTRICAL ENGINEERING IN TRANSPORT

---

- A PARTICLE SWARM OPTIMIZATION BASED FUZZY FLCPI-PSO CONTROLLER  
FOR QUADCOPTER SYSTEM** **C9**  
M. Baba, F. Bounaama, S. Bennaceur, A. Benhammou, M. A. Soumeur
- THE POWER ANALYSIS OF SEMICONDUCTOR DEVICES IN MULTI-PHASE TRACTION  
INVERTER TOPOLOGIES APPLICABLE IN THE AUTOMOTIVE INDUSTRY** **C21**  
J. Simčák, M. Frivaldský, P. Resutík

---

## **D - CIVIL ENGINEERING IN TRANSPORT**

---

### **GENERALIZED ORDERED LOGIT MODEL WITH TESTING ASSUMPTIONS: A CASE STUDY OF USING URBAN LIGHT RAIL IN BURSA**

**D38**

N. Akgun, T. Campisi, M. T. Sunar

### **EXAMINING THE EFFECT OF GEOMETRIC DESIGN FEATURES ON THE SPEED IN HORIZONTAL CURVE ON MOUNTAIN ROAD**

**D52**

E. Ramezani-Khansari, F. M. Nejad, S. Moogehi

---

## **E - MANAGEMENT SCIENCE AND INFORMATICS IN TRANSPORT**

---

### **IMPACT OF AI TECHNOLOGIES ON OPERATIONS OF SMALL AND MEDIUM TRANSPORT BUSINESSES**

**E12**

V. Nićin, S. Nićin, M. Mirkov



Dear colleague,

We would like to send you a copy of the journal Communications - Scientific Letters of the University of Zilina.

Journal Communications - Scientific Letters of the University of Zilina are a well-established open-access scientific journal aimed primarily at the topics connected with the field of transport. The main transport-related areas covered include Civil engineering, Electrical engineering, Management and informatics, Mechanical engineering, Operation and economics, Safety and security, Travel and tourism studies. Research in the field of education also falls under these categories. The full list of main topics and subtopics is available at: [https://komunikacie.uniza.sk/artkey/inf-990000-0500\\_Topical-areas.php](https://komunikacie.uniza.sk/artkey/inf-990000-0500_Topical-areas.php)

Journal Communications - Scientific Letters of the University of Zilina is currently indexed and accepted by CEEOL, Crossref (DOI), DOAJ, EBSCO Host, Electronic Journals Library (EZB), ERIH Plus, Google Scholar, Index Copernicus International Journals Master list, iThenticate, JournalGuide, Jouroscope, Norwegian Register for Scientific Journals Series and Publishers, ROAD, ScienceGate, SCImago Journal & Country Rank, SciRev, SCOPUS, WorldCat (OCLC).

Journal Communications - Scientific Letters of the University of Zilina is preserved in CLOCKSS and Portico to guarantee long-term digital preservation and is archived in the national deposit digitalne pramene.

Authors can share their experiences with publishing in our journal on SciRev.

**Communications was submitted to Web of Science in December 2022. In May 2024 Communications has passed the Web of Science Editorial Triage step evaluation and now is the subject to the editorial evaluation (quality) step.**

I would like to invite authors to submit their papers for consideration. We have an open-access policy and there are **no publication, processing or other fees** charged for published papers. Our journal operates a standard single-anonymised review procedure, the successful completion of which is a prerequisite for paper publication.

The journal is issued four times a year (in January, in April, in July and in October).

I would also like to offer you the opportunity of using already published articles from past issues as source of information for your research and publication activities. All papers are available at our webpage: <http://komunikacie.uniza.sk>, where you can browse through the individual volumes. Our journal offers access to its contents in the open access system on the principles of the license **Creative Commons (CC BY 4.0)**.

For any questions regarding the journal Communications - Scientific Letters of the University of Zilina please contact us at: [komunikacie@uniza.sk](mailto:komunikacie@uniza.sk)

We look forward to future cooperation.

Sincerely

Branislav Hadzima  
editor-in-chief





This is an open access article distributed under the terms of the Creative Commons Attribution 4.0 International License (CC BY 4.0), which permits use, distribution, and reproduction in any medium, provided the original publication is properly cited. No use, distribution or reproduction is permitted which does not comply with these terms.

# ASSESSING THE IMPACT OF THREE-WHEELERS ON TRAFFIC FLOW IN INDIA: A CASE STUDY USING ANN

Malaya Mohanty\*, Madhu Lisha Pattanaik, Satya Ranjan Samal, Shivam

School of Civil Engineering, KIIT Deemed to be University, Bhubaneswar, India

\*E-mail of corresponding author: malaya.mohantyfce@kiit.ac.in

Malaya Mohanty 0000-0002-6116-782X,  
Satya Ranjan Samal 0000-0001-8675-453X

Madhu Lisha Pattanaik 0000-0003-0835-9694,

## Resume

This study explores the significant role of three-wheelers (3W) on urban road traffic, focusing on the reduction in average vehicle speeds and its consequential impact on the Level of Service (LOS) of the road. Data collected from various traffic volumes reveal significant speed reductions ranging from 4% to 35% due to the movement of 3Ws on the road. To model this phenomenon, Artificial Neural Network (ANN) is employed. The resulting reductions in speed, induced by the 3W, trigger LOS degradation, leading to congestion and delays. A noteworthy finding is that the traffic flow naturally gravitates towards the LOS C, underscoring the substantial role played by the 3W in diminishing the overall LOS of the road. This research offers critical insights into the dynamics of urban traffic influenced by the 3W, providing a valuable foundation for traffic management and urban planning efforts.

## Article info

Received 27 February 2024

Accepted 23 May 2024

Online 31 May 2024

## Keywords:

three-wheelers (3W)  
traffic flow  
average speed reduction  
congestion  
level of service (LOS)  
artificial neural network (ANN)  
speed modelling

Available online: <https://doi.org/10.26552/com.C.2024.033>

ISSN 1335-4205 (print version)  
ISSN 2585-7878 (online version)

## 1 Introduction

The world's urban landscapes are constantly evolving, with transportation playing a pivotal role in shaping the dynamics of cities and the flow of traffic [1]. Among the diverse array of vehicles that traverse the streets of bustling metropolises and tranquil towns, the three-wheelers hold a unique position. These small vehicles with three wheels are commonly found in parts of the world with a unique impact on traffic flow. Understanding how three-wheelers affect the traffic is essential for city planners, policymakers, and commuters alike.

Urban transportation systems are continuously evolving, and one essential aspect of this transformation is the role of three-wheelers (3W) in influencing the traffic dynamics [2]. This study sets the stage for a comprehensive exploration of how the 3W impacts urban road traffic. The study delves into the reduction in average vehicle speeds caused by 3W and its subsequent repercussions on the Level of Service (LOS) of roads.

Increase in buildings over the years have increased pressure on the existing infrastructure leading to the building of new roads, flyovers, and expressways [3-8].

India, being a developing country has seen a wave of rapid growth in the road infrastructure over the last few years [9-10]. The major objective of constructing new and wider roads is usually to reduce the time of journey between any two locations, while also keeping in view the safety of the road users. However, in developing countries like India, the problem of heterogeneity or mixed traffic acts as an obstruction in achieving these objectives completely [11]. On the roads of developing countries, various categories of vehicles like two-wheelers, cars, and heavy vehicles are observed. One such category, which is predominately observed as public transport in developing countries are the auto-rickshaws or three-wheelers (3W). While these vehicles offer advantages such as affordability, maneuverability, and accessibility, they also raise concerns regarding their impact on traffic flow. The 3Ws have several advantages as they can easily change lanes [12], are much more affordable, and can provide door-to-door service, which is not possible for other public transportation systems. However, their frequent stop-and-go feature, along with less operating speed as compared to the traffic stream, along with an appreciable composition in traffic flow, makes it a potential cause for reducing the overall quality of

service on roads, thereby increasing the probability of congestion and delays to road users [5, 13-16].

Therefore, in the present study, the effect of the 3Ws as slow-moving vehicles (SMVs) has been assessed utilizing artificial neural network (ANN). Data is collected across various traffic volumes and proportions of vehicles influenced by 3W unveil a significant slowing of traffic, with cars and two-wheelers experiencing the most substantial speed reductions. The modelling of this phenomenon is facilitated by Artificial Neural Networks (ANN). Further, the consequences of these speed reductions reflect through congestion and delays, altering the LOS of roads. The present study leads to a deeper understanding of the role of three-wheelers in the broader traffic ecosystem, which is essential for crafting effective urban transportation policies and planning for a more sustainable and efficient future of mobility.

## 2 Literature review

Not many studies have been found to address the effect of 3W as slow-moving vehicles on the traffic stream in developing countries. However, there are some studies [11, 17-18], which have studied the traffic congestion in developing countries and have indirectly considered the effect of slow-moving vehicles (SMVs) like 3W, and heavy vehicles (HVs) while analyzing the congestion or calculating heterogeneity index. Pinzke and Lundqvist (2004) [14] conducted a comprehensive study on accidents involving slow-moving vehicles on Swedish roads. Another research studied the patterns of elephant racing at moving bottlenecks and explained the non-linear features of complex interactions among vehicles. However, the authors did not specify any single category of vehicle [19]. Slow-moving vehicles are defined as vehicles, which move at speeds between 10-40 km/h [20]. The authors developed a macroscopic model to assess the effect of slow-moving vehicles on traffic congestion where the input parameters consisted of the flows in both directions, the percentage of trucks, the speed and journey length of the slow-moving vehicle; and the outputs provided by the model are number of overtakes; size and duration of disturbance; number of affected vehicles and their delay, etc. Although the speed is a better parameter to judge slow-moving vehicles, developing one model might not apply to different categories of vehicles. Wickes and Nelson (2000) [21] had described the complete physics behind the slow-moving vehicles, their requirement, the necessary emblems to be put on them to prevent hazards and their speed limits. However, since the study was conducted 23-25 years ago, it considered only farm vehicles as slow-moving vehicles. Recently, Del Serrone et al. (2023) [22] assessed the effectiveness of providing climbing lanes to slow-moving vehicles while climbing hills using VISSIM. Although the results exhibited by the authors

are positive, however, unlike the study, in developing countries heavy vehicles are not the only slow-moving vehicles. Further, their study was limited to hilly terrain only. A similar study suggested providing passing bays every 2-4km for slow-moving agricultural vehicles on 2-lane rural roads [23]. Garvey (2003) [24] addressed the shortcomings of the SMV emblem that was used as a safety feature for more than 40 years in the US. He interviewed over 100 male and female drivers on the identification of the SMV emblem, which surprisingly showed that although older drivers understood the meaning of the safety emblem, the understandability of younger counterparts was under 30%. The study was meant for developed countries and talked about poor driver education. Its utilization in developing countries seems to be sparse. Sylla (2021) [25] proposed a model to understand the effect of SMVs on traffic. However, the model although accurate was hugely dependent on the downstream traffic density. Further, the SMVs were defined as vehicles moving in bottlenecks only. Gaur and Sachdeva (2022) [26] opined that SMVs reduce the capacity of the road. The study reported that an increase in HVs from 5 to 15% on the road reduces the capacity of the road by 20%. Another literature [27] studied the effect of SMVs on young drivers at night in Malaysia. All the literature seems to address only HVs or agricultural vehicles as SMVs, whereas, in developing countries like India, selective 3Ws are also SMVs as their average speeds are usually less than 40 km/h. Similarly, machine learning (ML) and deep learning methods have not been used much to study the aspect of SMVs.

A study at a small roundabout in Hlohovec, Slovakia [28], reflected that changing the traffic organization would result in shorter travel times, better traffic flow permeability, and fewer collision points. The study also highlighted the impact of the proposed changes on traffic characteristics, such as stop times, speed, and travel times. Lizbetin and Stopka (2016) [29] proposed a solution for a specific traffic operation in the city of Pilsen. They focused on analyzing traffic survey results in the field. The goal of their study was to increase traffic fluency, safety, and environmental protection in urban areas. Neural networks has also been used in a study to forecast the number of road accidents and the authors opined that neural networks are an effective tool to study traffic scenarios [30]. In a dated study [31], the authors reviewed and suggested various traffic scenarios/contexts, which should be studied in detail; and one of them was to address the travel time by various categories of vehicles. Another research studied the two types of behaviours exhibited by drivers: one being aggressive and another being cooperative. While aggressive behaviours might lead to crashes, excessive cooperative behaviours can lead to long queues and congestion [32]. These drivers need to be studied as they always slow down the traffic stream. Although the study by Metelski (2018) [33], examined various traffic events on the road, the researcher has opined that it



**Figure 1** Snapshot from one of the sites illustrating the temporary road markings

does not delve into all the types of traffic problems related to various categories of vehicles. Authors of [34] presented that cars emit maximum Carbon Di-Oxide to the environment. They also found that standing vehicles and at speeds below 15<sup>th</sup> percentile speeds produce much higher CO<sub>2</sub> to the environment and the reason is attributed to intersections and SMVs. An increase in EVs and autonomous vehicles can decrease the proportions of SMVs like 3-wheelers, which impact the traffic flow, [35]. Therefore, it can be said that many researchers have directly or indirectly addressed the problems faced by SMVs on the road, but have not much assessed it as their objectives were different. Further, with advancements in active learning (AL) and machine learning, the studies need to apply them to make evaluation easier on roads. Therefore, the present study attempts to evaluate the effect of 3Ws in Indian conditions on urban road traffic scenarios utilizing ANN.

### 3 Site selection, data collection and methodology

Data from various mid-block sections on 6-lane divided urban roads within the city of Bhubaneswar, India, were gathered via video recording technique. Bhubaneswar, classified as a tier-II smart city, boasts a population of approximately 1.5 million residents. The selection of this city for our study is based on its representation of a typical tier-II city in India, sharing similar demographic characteristics with many other cities in this category. The test sections were specifically chosen to ensure that the traffic flow at these locations remains unaffected by factors such as horizontal curvature, the presence of intersections downstream or upstream, bus stops, parked vehicles, pedestrian activity, or any form of side friction. Data was collected from various locations at mid-block sections within the urban area, and these collections were carried out at

different time intervals for a comprehensive analysis. Temporary road markings were applied to the road section, as depicted in Figure 1. For the study, data were acquired through video recording techniques, and subsequently retrieved with the aid of Kinovea software, ensuring accuracy and efficiency in the extraction process. The recorded videos were played back on a monitor using Kinovea video editing software, and the following parameters were extracted.

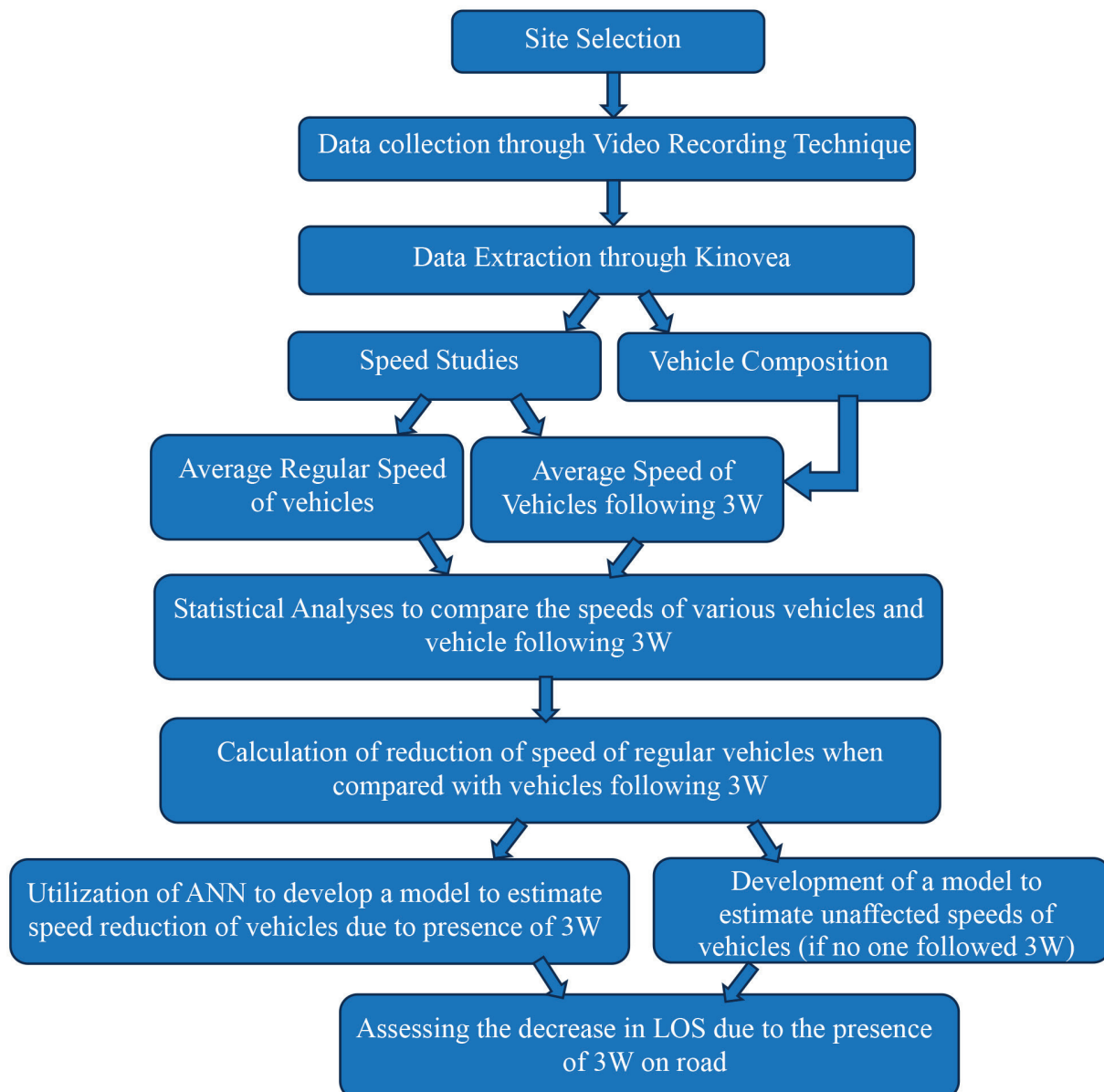
- Traffic Volume.
- Operating speeds of vehicles
- Composition of vehicles.

The extracted data were subjected to various statistical analyses to study the effect of 3W on other categories. The detailed methodology of the study is presented in the form of a flow chart in Figure 2. To identify vehicles following the 3-wheelers (3Ws) for the study, certain criteria were established. This included identifying vehicles that consistently followed 3Ws without the availability of space for overtaking them and exhibited a regular pattern of brake light usage, observed through the tail lamp lights. Additionally, in instances where a queue is formed, vehicles within the queue were considered only if the leading vehicle was a 3W. Analyzing the speeds of both regular vehicles and those following 3Ws offered valuable insights into the impact of 3Ws on the traffic flow, presenting an intriguing avenue for research.

#### 3.1 Artificial neural network

Artificial neural networks (ANN), recognized as one of the foremost data mining techniques for addressing intricate challenges across diverse fields such as fluid mechanics, signal processing, transportation studies, nanotechnology, and atomic physics [36], serve as prevalent nonlinear estimation models [37]. The ANN methodology involves data processing through





**Figure 2** Flowchart for methodology

interactions among virtual neurons, arranged in a layered structure with numerous interconnections [38]. Each neuron's output in each layer serves as input to multiple neurons in the subsequent layer, thus establishing the transfer functions applied to each neuron's input signal.

Numerous studies attest to the ANN's adeptness in accurately predicting various traffic incidents, establishing its reliability [39]. Typically, the ANN configurations with two hidden layers are widely employed in transportation engineering problem-solving. However, inappropriate neuron counts in hidden layers may result in over-fitting or under-fitting, compromising the network's performance and accuracy. Shallow networks with one or two hidden layers represent the most fundamental ANN structures. With more than one hidden layer, ANN models transition into deep models, enabling the learning of multiple representation levels

and enhancing their capacity to model complex real-world data.

Given the intricate nature of the data handled by ANNs, introducing non-linearity into the model is crucial, which is achieved through activation functions. These functions facilitate the neural network in emphasizing pertinent information, while disregarding irrelevant data points. Various sigmoid activation functions, including TanH, linear, and Gaussian, can be utilized in developing ANN models. TanH non-linearity is commonly favored, particularly when the data structure is entirely unknown. In the present study, ANN has been utilized to estimate the speed of the traffic stream at different traffic volumes, based on the categories of vehicles and the percentage of vehicles following 3Ws. This in turn can accurately determine how LOS is being affected due to the presence of slow-moving 3Ws.

#### 4 Results and analysis

The study revolves around the assessment of operational effects of 3-wheelers on the flow of traffic on urban roads. To examine this effect, first the classified traffic volume along with speeds of various motorised category of vehicles have been extracted as mentioned in section 3. The data has been knowingly collected during the working hours of 8 AM to 8 PM, when the most of the public is active to ascertain the true effect of 3-wheelers. During this time, the lowest volume on the studied locations has been found to be around 1500-2000 v/h, which can reach up to 5000 v/h. The consolidated data of average speeds of various categories of vehicles during different traffic volumes is presented in Table 1.

The data provided in Table 1 is a compilation of more than 20000 vehicles across various traffic volumes at different times of the day. It can be observed that the average speeds remain statistically the same up to 3500-4000 v/h ( $p > 0.05$  for speed values from 1500-4000 v/h in t-tests comparison). However, at traffic volumes above 4000 v/h, the road is moving towards congestion, therefore the average speeds decrease suddenly in the range of 25-37%. The t-test comparing speeds of vehicles within 1500-4000 v/h and >4000 v/h also gave similar results as the p-value was obtained to be  $<0.05$ . The effect of traffic congestion is seen more in the case of cars, jeeps, and HV as compared to 2W and 3W due to the dimensions of vehicles. From Table 1 can be observed that the 3-W and HVs have lesser speed as compared to

other 2 categories of vehicles, which is in similar lines with the objective of the present study. The proportion of HVs is much lesser (0.5-1% of total traffic), as compared to other categories and HVs mostly comprises city buses and school buses in the present study. However, out of every 100 vehicles on the studied road, 11-12 vehicles are 3Ws, and therefore they affect the flow of other vehicles more, as compared to HVs due to their inherent lesser operating speed and higher traffic composition. Secondly, it is observed that due to bigger dimensions, buses are visible from a distance and that is why other road users take appropriate measures while driving, from a distance (like lane changing manoeuvres, or overtaking manoeuvres) based on the traffic condition. The same does not apply in the case of vehicles following the 3Ws. Moreover, due to their design of 1 wheel in front, they suddenly change their lane towards the curb side for picking up passengers or drop them off. Before divulging that assessment, Table 2 showcases the average change in speed as compared to 3W for various categories of vehicles across different volumes.

The positive values in Table 2 represent an increase in speed over 3Ws, while a negative value represents a decrease in speed. As can be seen from Table 2, the 2W and cars and jeeps have higher speeds as compared to 3Ws at any traffic volume. The difference in speeds is bigger at lower traffic volumes. As the traffic goes towards higher volumes and congestion, the difference in speed decreases. Although the 3Ws are the slowest vehicles on the road, in 3 instances, HVs have shown

**Table 1** Descriptive statistics of classified speeds at different traffic volume levels

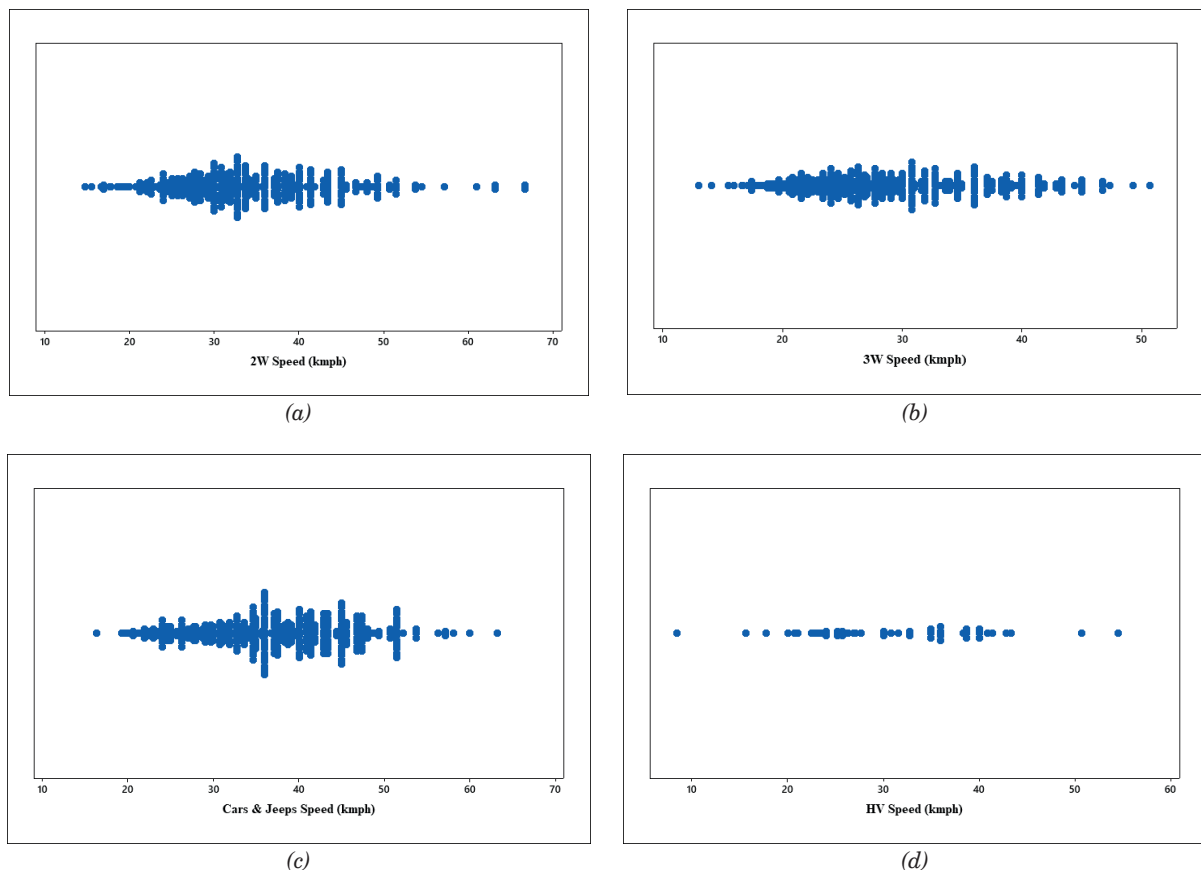
Volume (v/h)	Average Speeds (km/h)			
	2W	3W	Cars and Jeeps	HV
1500-2000	34	27	40	27
2000-2500	33	26	39	26
2500-3000	35	28	40	27
3000-3500	35	30	41	30
3500-4000	36	32	41	27
4000-4500	29	24	29	23
4500-5000	27	24	26	23

**Table 2** Percentage increase of operating speeds as compared to 3W

Volume (v/h)	% of increase/decrease of speed as compared to 3W		
	2W	Cars and Jeeps	HV
1500-2000	25.93	48.15	0
2000-2500	26.92	50	0
2500-3000	25.00	42.86	-3.57
3000-3500	16.67	36.67	0
3500-4000	12.50	28.13	15.63
4000-4500	20.83	20.83	-4.17
4500-5000	12.50	8.33	-4.17

**Table 3** Grubb's test to determine outlier speed values for different categories of vehicles

	Mean Speed (km/h)	Std. Deviation	Min.	Max.	G	P
2W	34.05	9.80	14.75	80.00	4.69	0.001
3W	28.50	7.28	13.00	50.70	3.05	0.703
Cars and Jeeps	36.55	8.72	16.36	63.16	3.05	0.746
HV	31.11	9.22	8.43	54.55	2.54	0.406
2W (post outlier removal)	33.70	8.98	14.75	66.67	3.67	0.073



**Figure 3** Outlier charts for speeds of different categories of vehicles

smaller speeds than 3Ws. However, this speed decrease of 3-4% as compared to 3W is statistically insignificant at 5% significance level. Moreover, the number of these HVs is very small due to which this observed smaller speeds can be analysed to be the same as that of 3Ws' speeds. Post this initial analysis, Grubb's outlier tests were performed to delete outliers (if any) present in the data. It is observed that only one speed variable in 2W (a speed of 80 km/h) was an outlier. Table 3 showcases the results of Grubb's test where it can be observed that the p value > 0.05 for all the other categories except for 2W. The result for the 2W after, removing the outlier, is also shown in Table 3. The outlier charts, based on Grubb's test, are shown in Figure 3.

Since the present study has attempted to examine the effect of slow-moving vehicle (SMV) i.e., 3W, the data was extracted to calculate the speeds of vehicles,

which follow the 3W, and are not able to overtake them. The speeds of various category of vehicles, which are exclusively following the 3W, at different traffic volumes, are presented in Table 4.

It is obvious that every category of vehicle shall move at a speed near to or slower than the average speed of 3W, for any specific traffic volume, and this is evident from Table 4. For example, at 2000-2500 v/h, the average speed of 3W was found to be 26 km/h and therefore the vehicles following 3W are observed to be moving at similar average speeds i.e., between 25-28 km/h. Now, if we see the average speed of a regular car (From Table 1) is found to be 39 km/h at 2000-2500 v/h. Thus, the average reduction in speed of cars is around 11 km/h (39-28 km/h), which amounts to a reduction of 28.2%. The reduction in speeds of each category of vehicles due to following a 3W is provided in Tables 5-8.

**Table 4** Average speeds of vehicles exclusively following 3W

Volume (v/h)	Average Speeds (km/h) while following 3W			
	2W	3W	Cars and Jeeps	HV
1500-2000	28	26	29	25
2000-2500	28	25	28	26
2500-3000	26	28	29	27
3000-3500	28	28	29	26
3500-4000	27	30	31	26
4000-4500	22	23	23	23
4500-5000	21	23	22	22

**Table 5** Comparison between speeds of regular 2W and 2W following 3W

Volume (v/h)	Average Speeds (km/h)		
	2W regular speed	2W following 3W	% reduction in speed
1500-2000	34	28	17.64
2000-2500	33	28	15.15
2500-3000	35	26	25.71
3000-3500	35	28	20.00
3500-4000	36	27	25.00
4000-4500	29	22	24.14
4500-5000	27	21	22.22

**Table 6** Comparison between speeds of regular 3W and 3W following 3W

Volume (v/h)	Average Speeds (km/h)		
	3W regular speed	3W following 3W	% reduction in speed
1500-2000	27	26	3.70
2000-2500	26	25	3.84
2500-3000	28	28	0.00
3000-3500	30	28	6.67
3500-4000	32	30	6.25
4000-4500	24	23	4.17
4500-5000	24	23	4.17

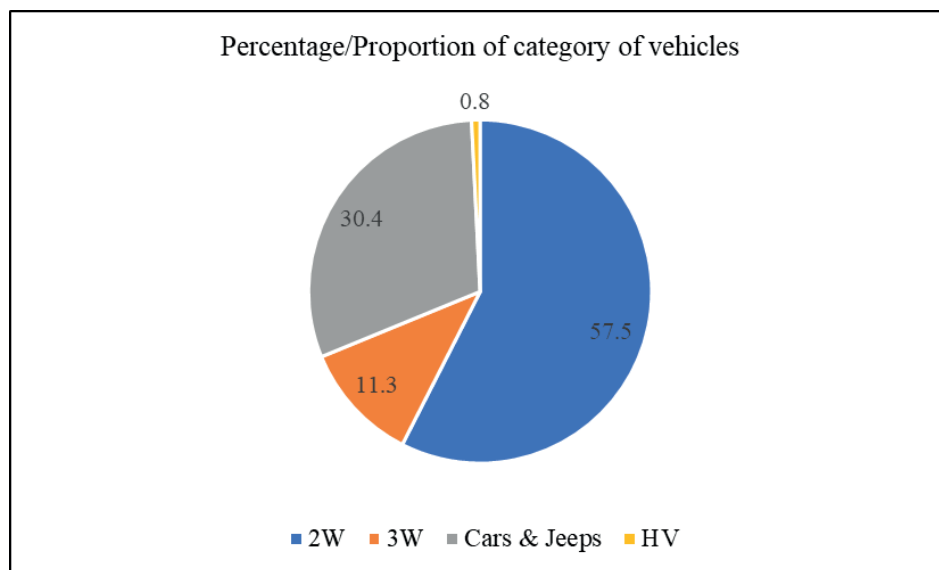
**Table 7** Comparison between speeds of regular cars and jeeps and those following 3W

Volume (v/h)	Average Speeds (km/h)		
	Cars and Jeeps regular speed	Cars and Jeeps following 3W	% reduction in speed
1500-2000	40	29	27.50
2000-2500	39	28	28.21
2500-3000	40	29	27.50
3000-3500	41	29	29.27
3500-4000	41	31	24.39
4000-4500	29	23	20.69
4500-5000	26	22	15.38



**Table 8** Comparison between speeds of regular HVs and those following 3W

Volume (v/h)	Average Speeds (km/h)		
	HV regular speed	HV following 3W	% reduction in speed
1500-2000	27	25	7.41
2000-2500	26	26	0.00
2500-3000	27	27	0.00
3000-3500	30	26	13.33
3500-4000	27	26	3.70
4000-4500	23	23	0.00
4500-5000	23	22	4.35

**Figure 4** Proportion of various category of vehicles**Table 9** Proportion of vehicles affected by 3-Wheelers (forcibly following 3W)

Traffic volume (v/h)	Percentage of vehicles affected (%)			
	2W	3W	Cars and Jeeps	HV
1500-2000	17.5	13.3	20.2	10
2000-2500	22.6	17.6	22.8	-
2500-3000	23.8	22.4	23.4	-
3000-3500	23.6	28.6	24.6	16.6
3500-4000	21.2	30.9	25.1	14.4
4000-4500	20.5	30.8	25.3	-
4500-5000	20.2	31.1	25.2	15.6
Average	21.3	25.0	23.8	8.1

NB - Since number of HVs are too small on the studied road, the percentage values of HVs affected by 3W is on a higher side.

As can be seen from Tables 5-8, the vehicles are forced to slowdown when following a 3W. The cars and jeeps, being the fastest are affected the most, followed by 2W. While the cars and jeeps are forced to reduce their speeds in the range of 15-29% while following a 3W forcibly, 2W have to reduce their speeds in the range of 15-26%. It is also observed that since the regular speeds

of 2W do not change much with increase in volume, therefore, the higher reduction in speeds is observed at higher volumes. However, due to bigger size, the regular speeds of cars and jeeps decrease with increase in volume. Therefore, their forced reduction is higher at lower traffic volumes. The HVs are usually not seen to be following the 3W. Even when the HVs follow 3W, due

to their regular speeds being smaller, they do not usually get affected by them. Similar is the case of 3W following 3W. The present study is conducted on an urban arterial road where the highest allowable speed is marked at 50 km/h for cars and jeeps, and 40 km/h for motorised 2W. For urban arterials, the LOS can be determined based on operating speeds (OS) as percentage of free flow speeds (FFS) [40-41].

It is evident from Tables 5 to 8 that due to the prevalence of 3W, the 2W, 3W, cars and jeeps are forced to reduce their speed to an extent, which will certainly cause a reduction in LOS leading to undesirable delays and congestion. However, the magnitude of the effect of this forced reduction on traffic flow completely depends on the number of vehicles that are getting affected/ have to forcefully follow 3W. If more vehicles are getting affected by 3Ws, then the regular speeds of 2W and cars and jeeps will also increase if 3W are removed from road or are provided a special lane. Therefore, the composition of traffic, the unaffected percentage, and the affected percentage (following 3W) must be obtained. Figure 4 showcases the average proportion of vehicles on the road. Next, Table 9 shows the percentage of affected vehicles, which forcibly follow 3W.

Table 9 provides an insight that on an average 20-25% of vehicles across all categories of vehicles (except HV) are getting affected by 3Ws. For 3W and cars and jeeps, general trend can be observed

that with increase in traffic volume, the proportion of affected vehicles increases, as well. For 2W, this number increases with volume, but up to a certain extent. Thereafter, the number marginally decreases and remains constant. Since, the vehicles who follow the 3W also affect the regular speeds and their proportion is not less, therefore, it can be noted that without 3W on the road, or the vehicles that are not following the 3W, the average speeds of the vehicles shall increase, which can be calculated based on the available data. If the average regular speed of  $i^{\text{th}}$  category of vehicle is  $V_i^r$ , the average forced reduced speed of same category of vehicle is  $V_i^f$ , and the proportion of affected vehicles is  $P_i$ , then the average unaffected speed of the  $i^{\text{th}}$  category of vehicle ( $V_i^u$ ) can be obtained by applying:

$$V_i^u = \left( \frac{V_i^r - P_i \cdot V_i^f}{1 - P_i} \right) \quad (1)$$

The regular and forced reduction in speed is already provided in Tables 5 to 8. Tables 10 to 13 provide an addition to the above data where the unaffected average speeds of each category of vehicles are also presented.

From Tables 10 to 13 can be observed that the average speed of each category of vehicles is affected by the presence of 3W. The speeds of 2Ws and cars and jeeps reduce in the range of 18% to 35% and are the

**Table 10** Comparison of speeds for regular 2W, unaffected 2W, and 2W following 3W

Volume (v/h)	Average Speeds (km/h)			
	2W regular speed	2W following 3W	2W unaffected	% Reduction in unaffected speed percentage as compared to following 3W speed
1500-2000	34	28	35.3	20.68
2000-2500	33	28	34.5	18.84
2500-3000	35	26	37.8	31.22
3000-3500	35	28	37.2	24.73
3500-4000	36	27	38.4	29.69
4000-4500	29	22	30.8	28.57
4500-5000	27	21	28.5	26.32

**Table 11** Comparison of speeds for regular 3W, unaffected 3W, and 3W following 3W

Volume (v/h)	Average Speeds (km/h)			
	3W regular speed	3W following 3W	3W unaffected	% Reduction in unaffected speed percentage as compared to following 3W speed
1500-2000	27	26	27.2	4.41
2000-2500	26	25	26.2	4.58
2500-3000	28	28	28	0.00
3000-3500	30	28	30.8	9.10
3500-4000	32	30	32.9	8.81
4000-4500	24	23	24.5	6.12
4500-5000	24	23	24.5	6.12

**Table 12** Comparison of speeds for regular Cars and Jeeps, unaffected Cars and Jeeps, and Cars and Jeeps following 3W

Volume (v/h)	Average Speeds (km/h)			% Reduction in unaffected speed percentage as compared to following 3W speed
	Cars and Jeeps regular speed	Cars and Jeeps following 3W	Cars and Jeeps unaffected	
1500-2000	40	29	42.8	32.24
2000-2500	39	28	42.3	33.81
2500-3000	40	29	43.4	33.18
3000-3500	41	29	44.9	35.41
3500-4000	41	31	44.4	30.18
4000-4500	29	23	31.0	25.81
4500-5000	26	22	27.4	19.71

**Table 13** Comparison of speeds for regular HV, unaffected HV, and HV following 3W

Volume (v/h)	Average Speeds (km/h)			% Reduction in unaffected speed percentage as compared to following 3W speed
	HV regular speed	HV following 3W	HV unaffected	
1500-2000	27	25	27.2	8.09
2000-2500	26	26	26	0.00
2500-3000	27	27	27	0.00
3000-3500	30	26	30.8	15.58
3500-4000	27	26	27.2	4.41
4000-4500	23	23	23	0.00
4500-5000	23	22	23.2	5.17

most affected by the presence/movement of 3Ws on road. Even other 3Ws and HVs on the road also get affected by the slow moving 3Ws on few instances where they are forced to reduce their speeds to 15% for HVs following 3Ws and 9% for 3Ws following 3Ws. The speeds of cars and 2W are drastically reduced as they usually travel faster on roads, while 3W and HV are affected less. This phenomenon not only affects their travel times and contribute to congestion, but also decreases the overall LOS of the road. Further, the results obtained are only for the present study area and will differ from place to place, with different proportions of 3W on the road.

To present this reduction in speed via a model, Artificial Neural Network (ANN) has been used, where percentage reduction in speed for any category of vehicles can be predicted by knowing the average traffic volume on the road and how much percentage of that category of vehicles are affected by 3W (or following 3W). The JMP SAS software has been used to conduct the ANN. For the analysis, 3 hidden layers were considered. Shallow networks were not considered, since 3 independent variables, where one of them is nominal (category of vehicle), have been used for prediction. TanH activation function, which is the default activation function in the software has been directly employed. This is because the TanH provided very good prediction accuracies in the first attempt, and secondly TanH is usually preferred over other activation functions, like Sigmoid, as it gives

better performance for multi-layer neural networks [42-43]. Random Holdback validation technique is used for the validation. Figure 5 showcases the general ANN framework followed by the statistics for training and validation in Table 14.

Values from Table 14 show how good the model is at predicting the reduction in speed. The R-square values are more than 0.95 for both training and validation. Similarly, the values of Root Average Squared Error (RASE) and mean absolute deviation are in the range of 1 and 2. While calculating the average percentage reduction in speed, the calculated error, as compared to the field data, is in the range of 1-2% only. Figure 6 shows a screenshot of the profiler for determining the percentage reduction in speed utilising the independent variables. The vertical red lines can be adjusted dynamically to get the speed reduction values. The figure also shows how Cars and Jeeps is the category that are forced to reduce their speed by a higher margin as compared to other categories. The first graph shows that at lower volumes the speed reduction is high since the regular vehicular speeds are high at low traffic volumes. The regular speed decreases with increase in volume, which reflects in the graph that the speed reduction also decreases. For example, a car travels at 45-50 km/h at 2000-2500 v/h whereas it travels at around 40 km/h at 3000 v/h. Thus, when following 3W in both volumes, if the car's speed reduces to 30 km/h,

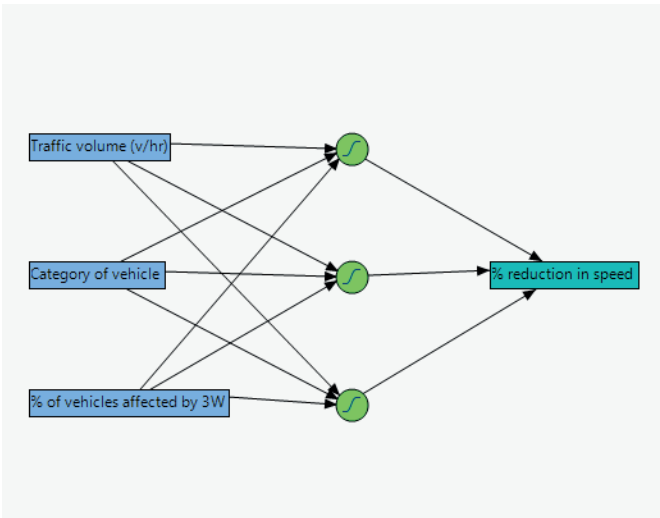


Figure 5 ANN architecture for predicting percentage reduction in speed

Table 14 Statistical values for ANN training and validation

Training (70 % data)		Validation (30 % data)	
Measures	Value	Measures	Value
R-Square	0.954	R-Square	0.968
RASE	2.262	RASE	2.150
Mean Absolute Deviation	1.861	Mean Absolute Deviation	1.332

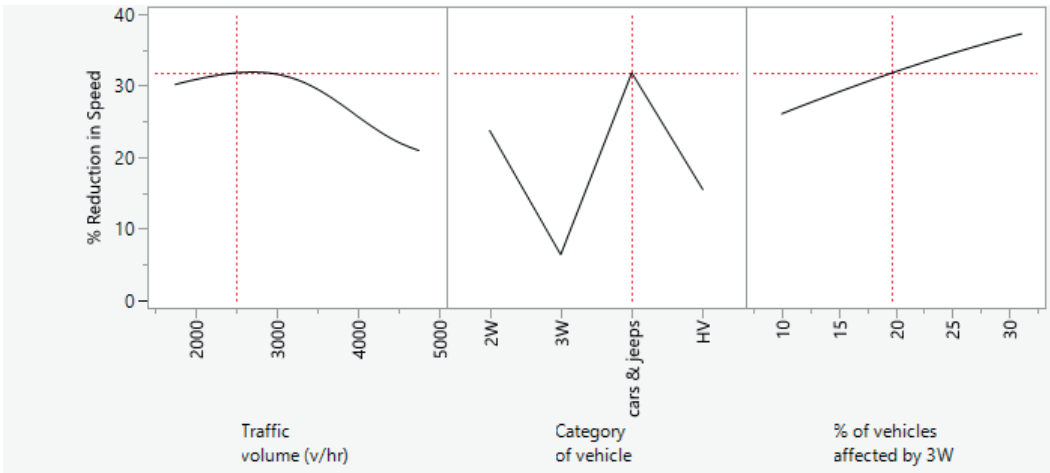


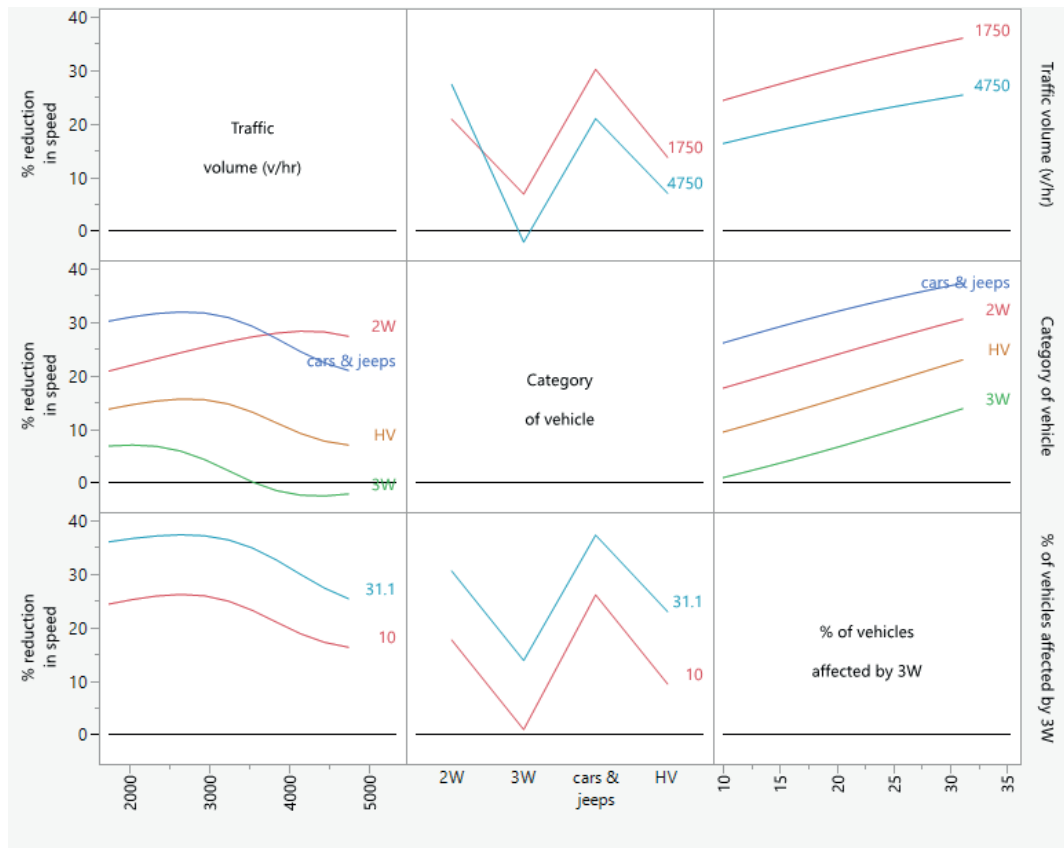
Figure 6 Profilers to determine the reduction in speed

the reduction is higher at lower traffic volume. The last graph tells the major point that higher the vehicles that get affected by 3W, higher is the reduction in speed. Indirectly, it hints towards the fact that, higher the number of 3W on road, more vehicles will get affected by them, ultimately leading to higher reduction in overall speed of traffic.

Figure 7 shows the interaction profilers, representing the trends in a very clear way. The figure shows the trends for 2 extremes of traffic volumes and percentage of vehicles getting affected by 3W/following 3W. As can be seen from the first row of Figure 7, at lower volumes (1750 v/h), speed reduction for vehicles is high

as compared to higher volumes (4750 v/h). Similarly, though cars and jeeps are the ones whose speed reduces the highest, however at higher volumes, speed of 2W is reduced more as opposed to other category of vehicles. This is because of the flexibility to change lanes while manoeuvring is high for 2W, which significantly decreases with an increase in traffic volume. The same phenomenon is observed in the first graph of the second row of Figure 7.

The ANN can be used effectively to determine the average reduction in speed for each category, at different traffic volumes and the percentage of vehicles getting affected by 3W. Utilising this speed, and proportion of



**Figure 7** Interaction Profilers to determine the reduction in speed

**Table 15** LOS for urban roads

LOS	Percentage of free flow speed
A	> 84
B	83-76
C	75-59
D	58-41
E	40-22
F	< 22

**Table 16** Average LOS at different traffic volumes

Average Traffic Volume (v/h)	Average operating speed (km/h)	% of free flow speed (60 km/h)	Designated LOS
1500-2000	36.9	0.62	C
2000-2500	35.9	0.60	C
2500-3000	37.6	0.63	C
3000-3500	38.4	0.64	C
3500-4000	38.9	0.65	C
4000-4500	30.0	0.50	D
4500-5000	28.0	0.47	D

vehicles, the overall average reduction in speed on any road stretch, at any time of the day can be obtained by a simple equation as provided in:

$$ORS = (P_{2W} \cdot RS_{2W}^{ANN}) + (P_{3W} \cdot RS_{3W}^{ANN}) + (P_{Cars\&Jeeps} \cdot RS_{Cars\&Jeeps}^{ANN}) + (P_{HV} \cdot RS_{HV}^{ANN}) \quad (2)$$

where:

$ORS$  = Overall percentage reduction in speed of traffic flow,

$P_i$  = Proportion of  $i^{th}$  category of vehicle in the traffic,  
 $RS_i^{ANN}$  = Percentage reduction in speed for  $i^{th}$  category of the vehicle obtained from ANN model.

This reduction in speed due to 3W shall cause

a decrease in the Level of Service of the road leading to congestion and undesirable delay. According to [40], the LOS for urban roads can be determined using the operating speed as a percentage of free flow speed. Table 15 presents the LOS levels for urban roads.

On the studied road, the safe speed limit or the 85<sup>th</sup> percentile speed is 50 km/h. The observed free-flow speed on the road is around 60 km/h. Based on those numbers, it can be said that the road usually remains under LOS C for most traffic volumes, which slowly goes towards LOS D at very high traffic volumes. Details about the same is provided in Table 16.

Applying the unaffected speed data, it is observed that the traffic stream naturally goes to LOS C, but not worse, like up to LOS D, which proves the fact that 3Ws decrease the speed of whole traffic, thereby decreasing the overall LOS of the road.

## 5 Discussion

The focus of the present study lies in evaluating the operational impact of the three-wheelers on urban road traffic flow. To investigate this impact, the study initially extracted data concerning the classified traffic volume and the speeds of various categories of motorized vehicles across weekdays during the active hours of 8 AM to 8 PM, when the public is most engaged. Observations reveal that the average speeds exhibit consistency up to traffic volumes ranging from 1500 to 4000 vehicles per hour (v/h), with minor fluctuations likely attributed to the diversity of vehicles and varying times of the day. However, beyond the 4000 v/h threshold, as traffic congestion becomes more apparent, average speeds undergo a sudden decline within the range of 25% to 37%. Notably, it becomes evident that three-wheelers (3Ws) and heavy vehicles (HVs) tend to operate at much lower speeds, compared to the other vehicle categories.

It was observed that when vehicles follow a three-wheeler, they are compelled to reduce their speeds forming a queue in the process if a lateral gap for overtaking is not available. Cars and jeeps, which are the fastest category, experience the most significant impact, with speed reductions ranging from 15% to 29% when tailing a 3W. Similarly, two-wheelers (2W) need to reduce their speeds by approximately 15% to 26% when following a 3W. These reductions inevitably result in a decrease in the Level of Service (LOS), causing undesirable delays and congestion. Artificial Neural Network (ANN) has been employed to model and quantify this speed reduction. The ANN model predicts the percentage reduction in speed for any vehicle category, based on knowledge of the average traffic volume on the road and the proportion of that category affected by 3W, with high accuracy (R-square > 0.95 for both training and validation). It is worth noting that as the number of 3Ws on the road increases, a larger

number of vehicles are affected by them, resulting in a more substantial overall reduction in traffic speed. This reduction in speed, attributable to the presence of 3Ws, invariably leads to a decrease in the Level of Service (LOS) of the road, resulting in congestion and undesirable delays. It is noted that the road typically operates at LOS C for most traffic volumes, gradually transitioning to LOS D at peak traffic volumes. Had there been less 3Ws on the road, the other categories could also have travelled at higher speeds (4-35% higher than forced reduced speeds), and LOS levels would not have gone down so much.

## 6 Conclusion

The presence of three-wheelers in urban traffic systems is a phenomenon that warrants careful examination due to its multifaceted impact on traffic flow. The presented study explored the dynamic influence of three-wheelers on traffic flow, encompassing both the positive and negative repercussions of their integration into urban transportation networks. Three-wheelers often provide essential last-mile connectivity, reducing the need for private car usage for short trips and thereby potentially easing congestion. Additionally, their smaller footprint demands less parking space, which can alleviate the burden on urban parking infrastructure. However, a surge in the number of three-wheelers in certain regions can contribute to traffic congestion and safety concerns due to their lower engine capacities leading them to travel at a lower speed as compared to other categories.

The present study has illustrated several key findings that shed light on the effect of 3W on the traffic ecosystem. The analysis, based on data collected at various traffic volumes and proportions of vehicles affected by 3W, has revealed substantial reductions in average speeds, ranging from 4% to 35% for the vehicles following 3W, which are unable to change their lanes. Notably, vehicles like cars and two-wheelers experience the most significant speed declines due to their typically higher speeds on the road. This phenomenon has been effectively modelled using the Artificial Neural Networks (ANN), exhibiting the high levels of prediction accuracy. By quantifying these speed reductions, it becomes possible to ascertain the broader implications on the on-road performance. The decrease in speed instigated by the presence of 3Ws invariably results in a degradation of the Level of Service (LOS), leading to congestion and delays.

These findings carry critical implications for the traffic management and urban planning. Recognizing the significant role of 3Ws in shaping the traffic dynamics enables policymakers to devise strategies that enhance the road efficiency, mitigate congestion, and improve overall transportation systems. As urban areas continue to evolve, understanding and addressing the



complexities introduced by 3Ws will be instrumental in fostering efficient and sustainable mobility solutions for the future. Introducing more public buses can reduce the number of 3Ws on the road, which should help in improving road traffic conditions. Similarly, 3W can be given a specific lane towards the kerb side for their manoeuvres, so that they do not interfere with the general flow of traffic. Although the study has assessed all the vehicles following a 3W, which are not able to overtake the vehicle, the study has not talked about the queues, which might form because of more than one vehicle where the leader might not be a 3W but may be a direct follower is a 3W. Similarly, the congestion due to the presence of 3Ws is not directly measured and can be determined in future studies. Lane changing behaviour of 3Ws can also be studied in the future, which should provide more insights into their movement on the

road. Further, the studies can be expanded to include the results for rural roads and roads with other lane configurations.

### Acknowledgment

The authors received no financial support for the research, authorship and/or publication of this article.

### Conflicts of interest

The authors declare that they have no known competing financial interests or personal relationships that could have appeared to influence the work reported in this paper.

### References

- [1] WEN, L., KENWORTHY, J., MARINOVA, D. Higher density environments and the critical role of city streets as public open spaces. *Sustainability* [online]. 2020, **12**(21), 8896. eISSN 2071-1050. Available from: <https://doi.org/10.3390/su12218896>
- [2] ABDULAMER, S. H., EEDAN, H. A. Effect of three-wheeled vehicles on the capacity of a traffic stream. *Journal of Engineering and Sustainable Development (JEASD)* [online]. 2021, **25**(Special\_ Issue\_2021), p. 3-165-3-173. ISSN 2520-0917, eISSN 2520-0925. Available from: <https://doi.org/10.31272/jeasd.conf.2.3.16>
- [3] MOHANTY, M., SARKAR, B., PATTANAIK, M. L., SAMAL, S. R., GORZELANCZYK, P. Development of congestion severity index for uncontrolled median openings utilising fundamental traffic parameters and clustering technique: a case study in India. *International Journal of Intelligent Transportation Systems Research* [online]. 2023, **21**, p. 461-472. ISSN 1348-8503, eISSN 1868-8659. Available from: <https://doi.org/10.1007/s13177-023-00365-1>
- [4] MOHAPATRA, S. S., DEY, P. P. Application of cluster analysis to define the level of service criteria of U-turns at median openings. *European Transport* [online]. 2021, **81**, p. 1-17. ISSN 1825-3997. Available from: <https://doi.org/10.48295/ET.2021.81.3>
- [5] XU, P., LI, W., HU, X., WU, H., LI, J. Spatiotemporal analysis of urban road congestion during and post COVID-19 pandemic in Shanghai, China. *Transportation Research Interdisciplinary Perspectives* [online]. 2022, **13**, 100555. eISSN 2590-1982. Available from: <https://doi.org/10.1016/j.trip.2022.100555>
- [6] MOHANTY, M., DEY, P. P. Operational effects of U-turns at median opening. *Transportation Letters* [online]. 2022, **14**(6), p. 565-577. ISSN 1942-7867, eISSN 1942-7875. Available from: <https://doi.org/10.1080/19427867.2021.1908491>
- [7] SAMAL, S. R., MOHANTY, M., SELVARAJ, M. S. Assessment of traffic congestion under Indian environment - a case study. *Communications - Scientific Letters of the University of Zilina* [online]. 2022, **24**(4), p. D174-D182. ISSN 1335-4205, eISSN 2585-7878. Available from: <https://doi.org/10.26552/com.C.2022.4.D174-D182>
- [8] SAMAL, S. R., MOHANTY, M., SANTHAKUMAR, S. M. Adverse effect of congestion on economy, health and environment under mixed traffic scenario. *Transportation in Developing Economies* [online]. 2021, **7**(2), 15. ISSN 2199-9287, eISSN 2199-9295. Available from: <https://doi.org/10.1007/s40890-021-00125-4>
- [9] Morth Annual Report [online]. 2023. Available from: <https://morth.nic.in/annual-report-2022-23>
- [10] SAMAL, S. R., MOHANTY, M., GORZELANCZYK, P. Exploring the traffic congestion and improving travel time reliability measures in heterogeneous traffic environments: a focus on developing countries. *Communications - Scientific Letters of the University of Zilina* [online]. 2023, **25**(4), p. D91-D102. ISSN 1335-4205, eISSN 2585-7878. Available from: <https://doi.org/10.26552/com.C.2023.074>
- [11] PANDEY, A., SHARMA, M., BISWAS, S. Concept of heterogeneity index for urban mixed traffic. *International Journal of Transportation Science and Technology* [online]. 2023, **12**(2), p. 354-372. ISSN 2046-0430, eISSN 2046-0449. Available from: <https://doi.org/10.1016/j.ijtst.2022.02.008>
- [12] MOHANTY, M., DEY, P. P., OJHA, A. K. Assessment of lane changing behaviour due to U-turns using Markov process. (No. 17-01905). 2017.

- [13] BOKARE, P. S., MAURYA, A. K. Study of acceleration behaviour of motorized three-wheeler in India. *Transportation Research Procedia* [online]. 2016, **17**, p. 244-252. ISSN 2352-1457, eISSN 2352-1465. Available from: <https://doi.org/10.1016/j.trpro.2016.11.088>
- [14] PINZKE, S., LUNDQVIST, P. Slow-moving vehicles in Swedish traffic. *Journal of Agricultural Safety and Health* [online]. 2004, **10**(2), 121. ISSN 1074-7583, eISSN 1943-7846. Available from: <https://doi.org/10.13031/2013.16071>
- [15] SAMAL, S. R., DAS, A. K. Evaluation of traffic congestion parameters under heterogeneous traffic condition: A case study on Bhubaneswar city. In: *Transportation Research: Proceedings of CTRG 2017: proceedings* [online]. Springer. 2020. ISBN 978-981-32-9041-9, eISBN 978-981-32-9042-6, p. 675-684. Available from: [https://doi.org/10.1007/978-981-32-9042-6\\_53](https://doi.org/10.1007/978-981-32-9042-6_53)
- [16] SAMAL, S. R., KUMAR, P. G., SANTHOSH, J. C., SANTHAKUMAR, M. Analysis of traffic congestion impacts of urban road network under Indian condition. *IOP Conference Series: Materials Science and Engineering* [online]. 2020, **1006**(1), 012002. ISSN 1757-899X. Available from: <https://doi.org/10.1088/1757-899X/1006/1/012002>
- [17] CHANDRA, S., SINHA, S. Effect of directional split and slow-moving vehicles on two lane capacity. *Road and Transport Research*. 2001, **10**(4), p. 33-41. ISSN 1037-5783.
- [18] JAYASOORIYA, S. A. C. S., BANDARA, Y. M. M. S. Measuring the economic costs of traffic congestion. In: *2017 Moratuwa Engineering Research Conference MERCon: proceedings* [online]. IEEE. 2017. eISBN 978-1-5090-6491-5, p. 141-146. Available from: <https://doi.org/10.1109/MERCon.2017.7980471>
- [19] KERNER, B. S., KLENOV, S. L. A theory of traffic congestion at moving bottlenecks. *Journal of Physics A: Mathematical and Theoretical* [online]. 2010, **43**(42), 425101. ISSN 1751-8121. Available from: <https://doi.org/10.1088/1751-8121/43/42/425101>
- [20] BOTMA, H. Effects on traffic operation of a slow moving vehicle on two lane rural roads. In: *14th Australian Road Research Board (ARRB) Conference: proceedings*. 1988. Vol. 14, No. 2, p. 48-55.
- [21] WICKES JR, H. G., NELSON, G. S. Collisions with slow-moving vehicles. *Professional Safety*. 2000, **45**(8), p. 39-44. ISSN 0099-0027.
- [22] DEL SERRONE, G., CANTISANI, G., GRILLI, R., PELUSO, P. Effectiveness of climbing lanes for slow-moving vehicles when riding uphill: a microsimulation study. *Vehicles* [online]. 2023, **5**(3), p. 744-760. eISSN 2624-8921. Available from: <https://doi.org/10.3390/vehicles5030041>
- [23] JAARSMA, C. F., BOTMA, H., BEUNEN, R. Passing bays for slow moving vehicles on rural two lane roads. *Transport Reviews* [online]. 2005, **25**(4), p. 491-509. ISSN 0144-1647, eISSN 1464-5327. Available from: <https://doi.org/10.1080/01441640500038805>
- [24] GARVEY, P. M. Motorist comprehension of the Slow-Moving Vehicle (SMV) emblem. *Journal of Agricultural Safety and Health* [online]. 2003, **9**(2), 159. ISSN 1074-7583, eISSN 1943-7846. Available from: <https://doi.org/10.13031/2013.13005>
- [25] SYLLA, A. Influence of a slow moving vehicle on traffic: well-posedness and approximation for a mildly nonlocal model. *Networks and Heterogeneous Media* [online]. 2021, **16**, p. 221-256. ISSN 1556-1801, eISSN 1556-181X. Available from: <https://doi.org/10.3934/nhm.2021005>
- [26] GAUR, P., SACHDEVA, S. N. Effect of shoulder and slow moving vehicles on capacity of a road. *International Journal of Engineering Applied Sciences and Technology* [online]. 2022, **4**(10), p. 377-380. ISSN 2455-2143. Available from: <https://doi.org/10.33564/IJEAST.2020.v04i10.068>
- [27] YUSOF, N. M., KARJANTO, J., HASSAN, M. Z., SULAIMAN, S., AB RASHID, A. A., JAWI, Z. M., KASSIM, K. A. A. Effect of road darkness on young driver behaviour when approaching parked or slow-moving vehicles in Malaysia. *Automotive Experiences* [online]. 2023, **6**(2), p. 216-233. eISSN 2615-6636. Available from: <https://doi.org/10.31603/ae.8206>
- [28] KALASOVA, A., SKRIVANEK KUBIKOVA, S., CULIK, K., PALUCH, J. Comparison of traffic flow characteristics of signal controlled intersection and turbo roundabout. *The Archives of Automotive Engineering - Archiwum Motoryzacji* [online]. 2020, **88**(2), p. 19-36. eISSN 2084-476X. Available from: <https://doi.org/10.14669/AM.VOL88.ART2>
- [29] LIZBETIN, J., STOPKA, O. Proposal of a roundabout solution within a particular traffic operation. *Open Engineering* [online]. 2016, **6**(1), p. 441-445. eISSN 2391-5439. Available from: <https://doi.org/10.1515/eng-2016-0066>
- [30] GORZELANCZYK, P., TYLICKI, H. Forecasting the number of road accidents in Poland depending on the day of the week using neural networks. *LOGI-Scientific Journal on Transport and Logistics* [online]. 2023, **14**(1), p. 35-42. eISSN 2336-3037. Available from: <https://doi.org/10.2478/logi-2023-0004>
- [31] AKCELIK, R., MAHER, M. J. Route control of traffic in urban road networks: review and principles. *Transportation Research* [online]. 1977, **11**(1), p. 15-24. ISSN 0041-1647. Available from: [https://doi.org/10.1016/0041-1647\(77\)90062-4](https://doi.org/10.1016/0041-1647(77)90062-4)



- [32] TANIMOTO, J., NAKAMURA, K. Social dilemma structure hidden behind traffic flow with route selection. *Physica A: Statistical Mechanics and its Applications* [online]. 2016, **459**, p. 92-99. ISSN 0378-4371, eISSN 1873-2119. Available from: <https://doi.org/10.1016/j.physa.2016.04.023>
- [33] METELSKI, A. Analysis of selected methodological problems regarding the examination of traffic events at road intersections. *The Archives of Automotive Engineering - Archiwum Motoryzacji* [online]. 2018, **82**(4), p. 75-85. eISSN 2084-476X. Available from: <https://doi.org/10.14669/AM.VOL82.ART6>
- [34] JEREB, B., STOPKA, O., SKRUCANY, T. Methodology for estimating the effect of traffic flow management on fuel consumption and CO2 production: a case study of Celje, Slovenia. *Energies* [online]. 2021, **14**(6), 1673. eISSN 1996-1073. Available from: <https://doi.org/10.3390/en14061673>
- [35] WITT, A. Determination of the number of required charging stations on a German motorway based on real traffic data and discrete event-based simulation. *LOGI-Scientific Journal on Transport and Logistics* [online]. 2023, **14**(1), p. 1-11. eISSN 2336-3037. Available from: <https://doi.org/10.2478/logi-2023-0001>
- [36] AHMED S, A., ELKATATNY, S., ALI, A. Z., ABDULRAHEEM, A., MAHMOUD, M. Artificial neural network ANN approach to predict fracture pressure. In: SPE Middle East Oil and Gas Show and Conference: proceedings [online]. 2019. ISBN 978-1-61399-639-3. Available from: <https://doi.org/10.2118/194852-MS>
- [37] SABIR, Z., BALEANU, D., SHOAIB, M., RAJA, M. A. Z. Design of stochastic numerical solver for the solution of singular three-point second-order boundary value problems. *Neural Computing and Applications* [online]. 2021, **33**(7), p. 2427-2443. ISSN 0941-0643, eISSN 1433-3058. Available from: <https://doi.org/10.1007/s00521-020-05143-8>
- [38] ILLIAS, H. A., CHAI, X. R., ABU BAKAR, A. H., MOKHLIS, H. Transformer incipient fault prediction using combined artificial neural network and various particle swarm optimisation techniques. *PLoS One* [online]. 2015, **10**(6), e0129363. eISSN 1932-6203. Available from: <https://doi.org/10.1371/journal.pone.0129363>
- [39] YU, B., WANG, Y. T., YAO, J. B., WANG, J. Y. A comparison of the performance of ANN and SVM for the prediction of traffic accident duration. *Neural Network World* [online]. 2016, **26**(3), p. 271-287. ISSN 1210-0522. Available from: <https://doi.org/10.14311/NNW.2016.26.015>
- [40] Indian highway capacity manual (Indo-HCM). New Delhi: CSIR-Central Road Research Institute, 2017.
- [41] National Research Council. Highway capacity manual 2000. Transportation Research Board Special Report, 209, 16-9. 2000.
- [42] LEWIS, P., PEREZ, E., PIKTUS, A., PETRONI, F., KARPUKHIN, V., GOYAL, N., KUTTLER, H., LEWIS, M., YIH, W.-T., ROCKTASCHEL, T., RIEDEL, S., KIELA, D. Retrieval-augmented generation for knowledge-intensive NLP tasks. *Advances in Neural Information Processing Systems*. 2020, **33**, p. 9459-9474. ISSN 1049-5258.
- [43] LIU, C., CHEN, L. C., SCHROFF, F., ADAM, H., HUA, W., YUILLE, A. L., FEI-FEI, L. Auto-deeplab: hierarchical neural architecture search for semantic image segmentation. In: IEEE/CVF Conference on Computer Vision and Pattern Recognition: proceedings [online]. IEEE. 2019. eISSN 2575-7075, eISBN 978-1-7281-3293-8, p. 82-92. Available from: <https://doi.org/10.1109/CVPR.2019.00017>



This is an open access article distributed under the terms of the Creative Commons Attribution 4.0 International License (CC BY 4.0), which permits use, distribution, and reproduction in any medium, provided the original publication is properly cited. No use, distribution or reproduction is permitted which does not comply with these terms.

# THE TE33A SERIES DIESEL LOCOMOTIVE BRAKE EQUIPMENT TESTS

Seidulla Abdullayev

Satbayev University, Almaty, Republic of Kazakhstan

E-mail of corresponding author: seidulla@mail.ru

Seidulla Abdullayev  0000-0001-5028-8143

## Resume

The purpose of the article was to present the results of braking equipment testing and determination of the adequacy of compressed air production of the braking system when the train is loaded. Experimental tests of the braking system of TE33A diesel locomotive in a goods train are performed. According to the initial data the main parameters of the braking system in the empty and loaded train were evaluated. As a result of tests, and according to the calculated data, the dependences of the volume of the main reservoirs, and the dependences of the required compressor capacity, on the number of axles have been obtained. It has been established that the braking system operation in release modes for a 400-axle train corresponds to the operating conditions and the main requirements of the normative documents.

## Article info

Received 5 March 2024

Accepted 2 May 2024

Online 14 May 2024

## Keywords:

rolling stock brakes  
measuring instruments of control  
the system is a complex  
of locomotive safety devices  
traction tracks

Available online: <https://doi.org/10.26552/com.C.2024.029>

ISSN 1335-4205 (print version)

ISSN 2585-7878 (online version)

## 1 Introduction

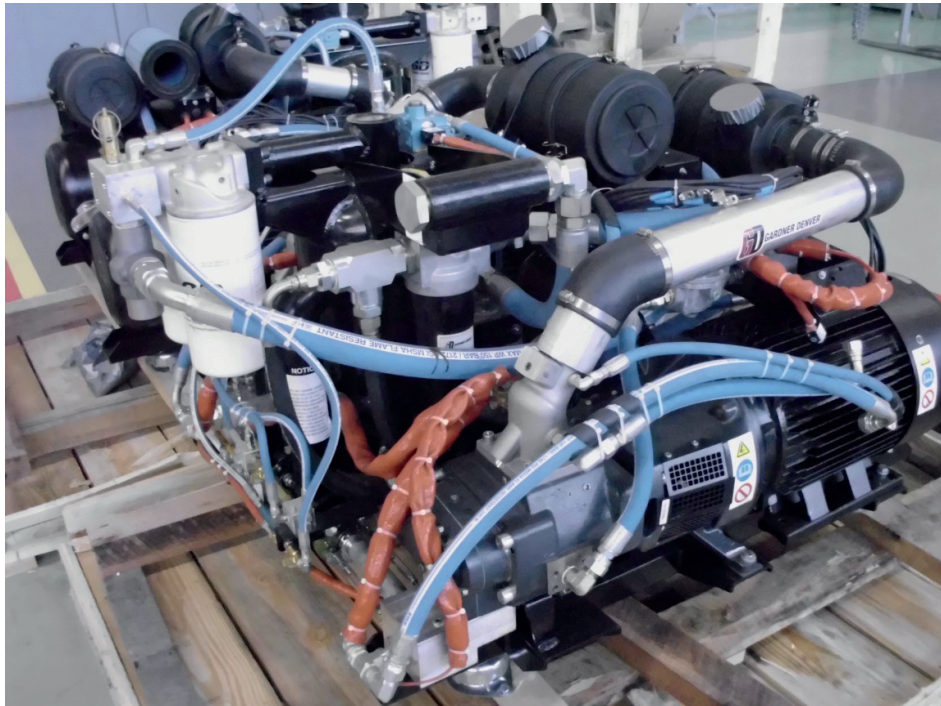
According to the Rules for the technical operation of railways of the Republic of Kazakhstan [1], one of the main duties of railway transport workers is to meet the needs for the transportation of passengers and goods with unconditional provision of traffic safety and safety of transported goods. To fulfill this requirement, one needs not only powerful locomotives, but the advanced braking systems of the rolling stock, as well.

The rolling stock brakes should have good controllability and operate reliably in different operating conditions. The braking systems must ensure smooth braking, and the slowing force of each unit of the rolling stock must be proportional to its mass.

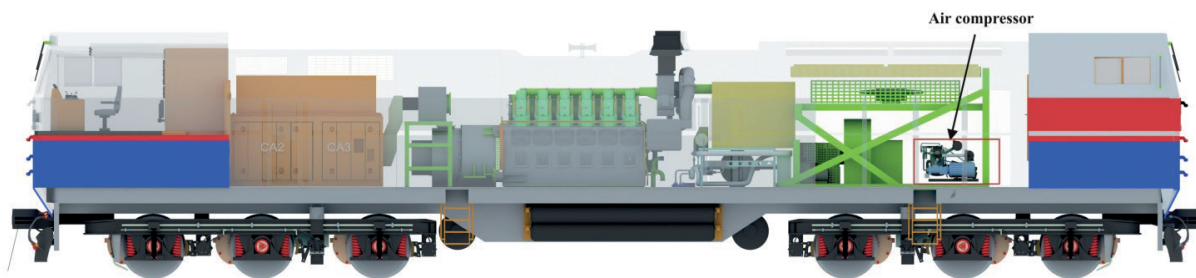
With pneumatic braking of trains, problems arise related to the non-timeliness of switching the braking devices of the rolling stock from the release mode to the braking mode, due to the delay of this process on cars remote from the locomotive [2].

The braking equipment of the rolling stock operates under conditions of complex processes occurring in the moving train (dry friction of the brake pads of the friction shoe brake with the conversion of mechanical energy into thermal, gas-dynamic processes in the brake

line during the charging, braking, when releasing the brakes; rolling of the brake wheel on the rails under conditions of use of the wheel-rail coupling forces; interaction of rolling stock with each other with the occurrence of significant longitudinal forces in conditions of unsteady braking force, etc.). The combination of high reliability, brake safety with good controllability will increase passenger train speeds to 200-250 km/h in the near future, and freight trains to 140-160 km/h with an axial load of 18-20 tons (high-speed shuttle trains for container cargo transportation), and increase the weight of freight trains to 10-12 thousand tons, to increase transportation productivity. To successfully solve these problems, it is necessary to fully expand and strengthen the creative cooperation of engineering and technical workers of the brakes of construction plants, linear enterprises of the carriage industry, as well as researchers related to calculation and design of the braking equipment, in particular the pneumatic and mechanical parts of the rolling stock brakes. It is also necessary to comprehensively and critically study the modern experience of railways of foreign countries to enable and expediently use it on the railways of Kazakhstan, considering the modern conditions of their operation [3-4].



**Figure 1** General view of the Gardner Denver air compressor



**Figure 2** Location of the air compressors on the locomotive

## 2 Main components of diesel locomotive brake system TE33A

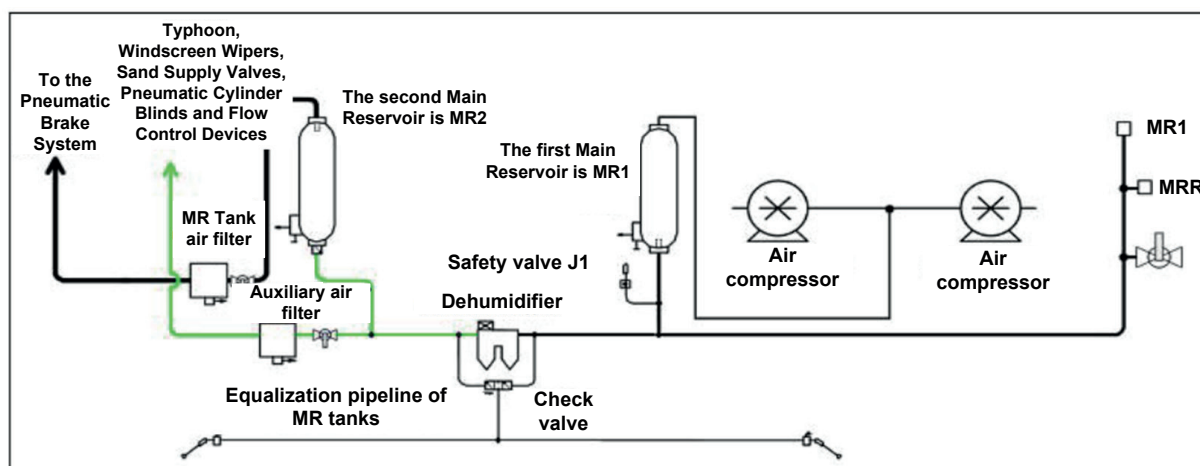
The main component for compressed air compression in the compressed air system is a twin-screw compressor manufactured by Gardner Denver (Figure 1). Each compressor head has one AC motor to drive the screw rotor. For each locomotive 2 such units are installed. The location of the air compressors on the locomotive is shown in Figure 2.

Figure 3 shows a schematic diagram of the location of the main elements of the TE33A diesel locomotive braking system. To cool the air, compressed air coolers are used, which are activated after the compressed air temperature reaches 115 °C. One of the coolers is located on the compressor frame, the second in the refrigeration chamber. Cooling is due to convection, or due to the combined influence of convection and the operation of the fan of the diesel cooling system. After the compressor, the compressed air enters the first main tank, where the air is cooled by the moisture

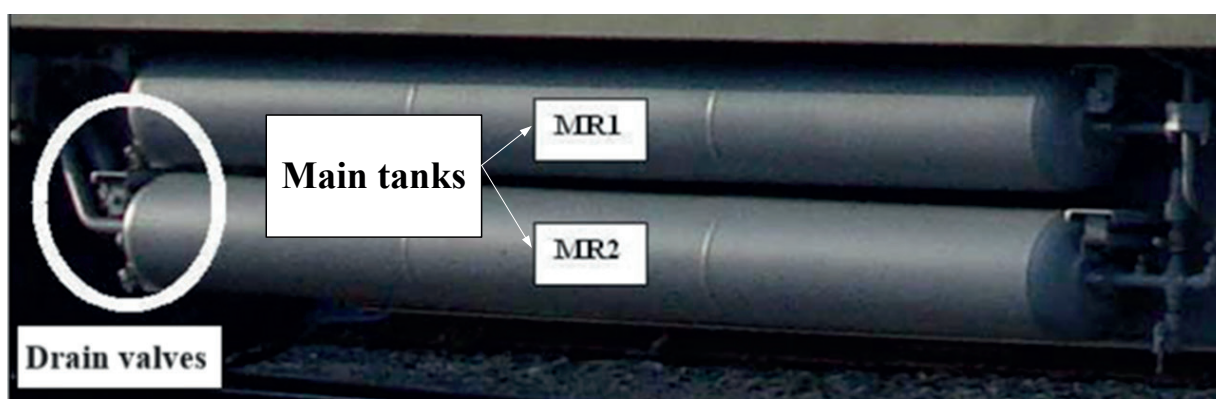
condensation. The Main Reservoir (Main Reservoir, MR) is tilted, so moisture flows to one of the ends (from where it is drained through the drain valve). Each MR tank has a separate drain valve, which is activated by a drain valve solenoid (Drain Valve Magnet Valve, DVMV) [4].

The safety valve is installed on outlet branch pipe of the first main tank. This valve is designed to protect the compressor and other components of the compressed air system from overpressure. The compressed air flow from the first main tank is divided into two parts. One part of the flow is supplied to the main tank pressure sensor (MR1), which provides a feedback signal on the compressed air pressure to the locomotive control system. The second part of the flow enters the air dryer, in which the compressed air is further purified from moisture. After the dryer, the air enters the second main tank and the auxiliary air filter. A reverse throttling valve with a diaphragm of about 8mm (5/16 inch) is used to limit the air flow into the auxiliary equipment pipeline and to ensure priority filling of the MR2 tank.





*Figure 3 Schematic diagram of the location of the braking system main elements*



*Figure 4 Main tanks (MR1 and MR2) typical arrangement*

The valve is installed between the outlet of the first main tank and the equalizing pipeline of the MR tanks [5-6].

The second check valve is installed between the outlet of the air dryer and the equalizing pipeline of the tanks MR. This check valve is designed to supply air to the second locomotive of the coupler. This arrangement allows air to enter the compressed air system of the second coupling locomotive only through the air dryer. Air passing into the second tank MR2 through the check valve enters the air filter of the main tanks. The presence of a check valve prevents the return movement of air into the first main reservoir. This is done in the case of air leakage from the first main tank. In such a situation, the air remaining in the second tank will be sufficient to provide emergency braking. The MR air filter and auxiliary air filter are also referred to as final air filters. These devices are used to filter air before it enters the pneumatic brake system and auxiliary equipment. Each filter is equipped with a drain valve. The valves serve to drain moisture from the filters. Filtered air from the auxiliary equipment air filter (auxiliary supply air) is supplied to the typhon, windshield wipers and sand supply valves [6].

Filtered air from the MR tank air filter (make-up air

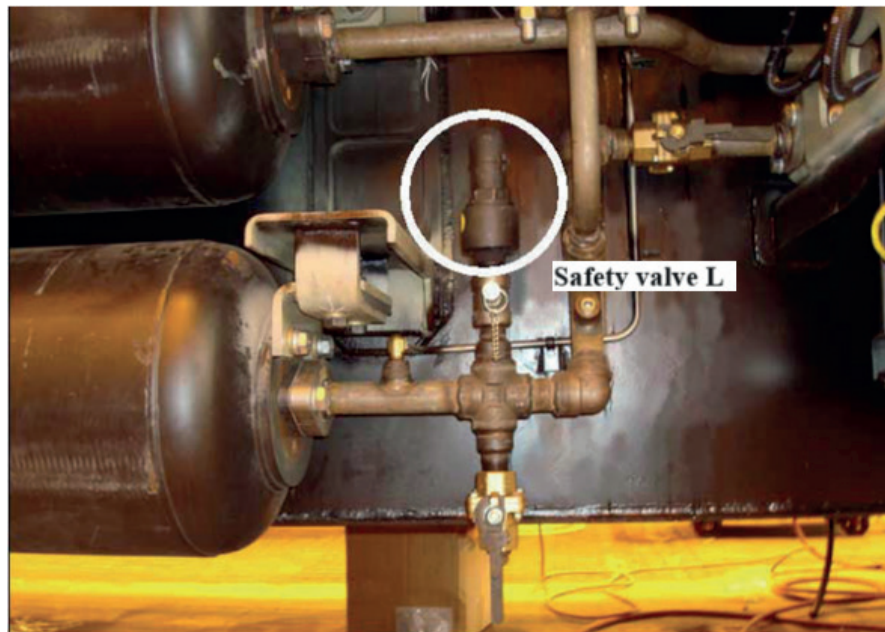
from MR tanks) is distributed among the components of the pneumatic brake system.

## 2.1 Main tanks of the compressed air system

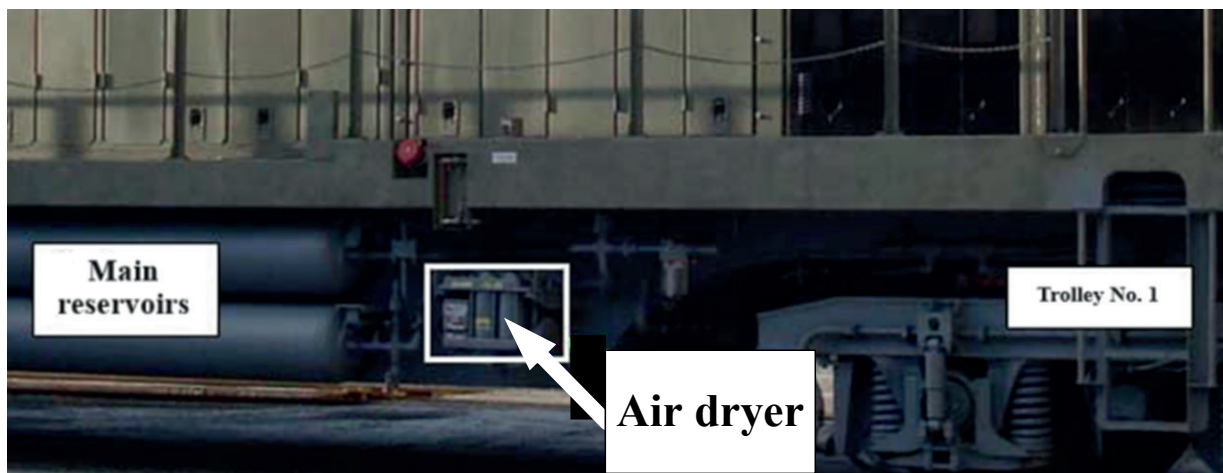
The main tanks (Figure 4) serve to store compressed air intended for use in a locomotive. The locomotive has two tanks of a diameter of 394 mm and a length of 3950 mm. Two tanks contain 960 liters of air under the pressure of the main tanks 10 MPa. The main tanks are fixed on the locomotive at a slight inclination, which ensures the drainage of moisture to one of the ends of the tank. Automatic blowdown devices (drain valves) are installed at the lower end of each tank to drain the moisture.

## 2.2 Safety valve L

Valve L is designed to protect the compressor and other components of the compressed air system from overpressure (Figure 5). If the air pressure exceeds 1.05 MPa, the valve opens and releases excess air to the atmosphere. Safety valve is arranged between the two main tanks on locomotive A side [3].



*Figure 5 Safety valve L*



*Figure 6 Air dryer*

### 2.3 Air dryer

Dryer is designed to separate the compressed air from moisture. When frozen, moisture can damage pneumatically controlled devices (Figure 6). The air dryer is located on the A side of the locomotive between the main tanks and trolley No. 1.

### 2.4 Main Tank Pressure Transmitter (MR1)

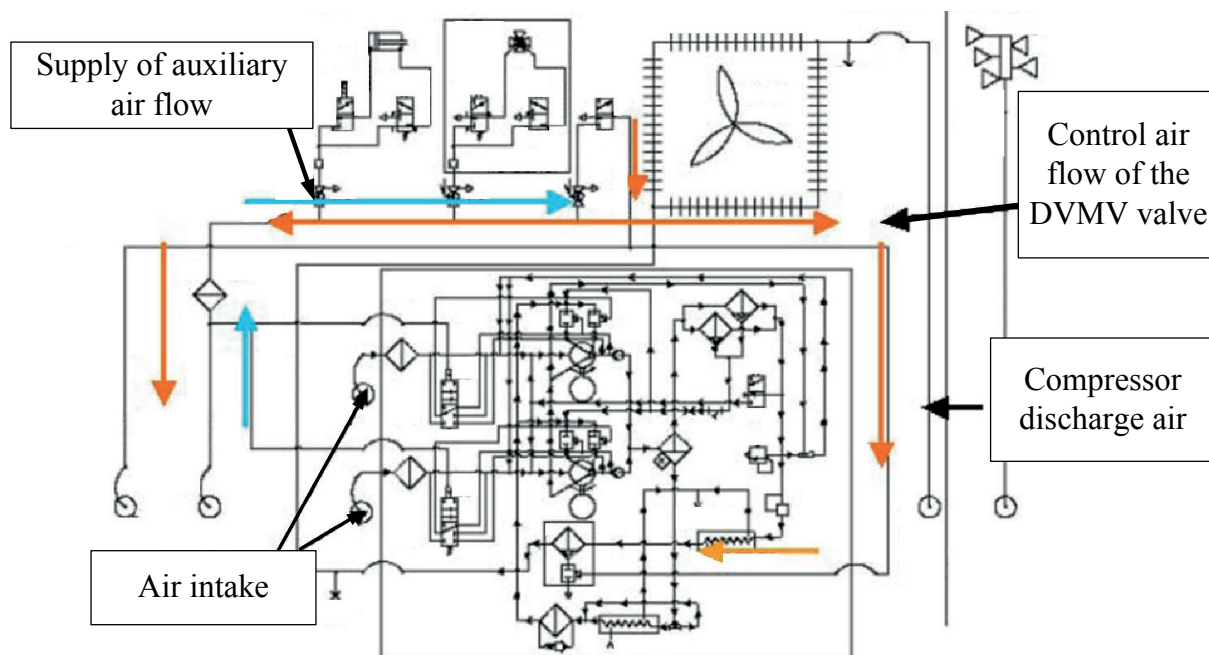
MR1 is used to measure the air pressure at the outlet of the main tank of the compressed air system. In the locomotive control system, this data is used to calculate the moment when the compressor motors are turned on and off, and to monitor its load. The ultimate goal of such monitoring is to maintain a constant pressure in the compressed air system. Pressure information is

also displayed on programmable displays to inform the driver [7].

The sensor MR1 is located on the inner wall of the CA9 zone in the refrigeration chamber.

### 2.5 Principle of the braking system operation

The air discharged from the air compressor enters the main tank No. 1 (MR No. 1). At the exit of MR No. 1, the air flows are separated: one air flow goes to the safety valve L, the other goes through the air dryer, and the third goes to the MR1 sensor. The safety valve L protects equipment located downstream of MR tank No. 1. The MR1 is used in the feedback loop to control the pressure in the main tanks. The air downstream of the dehumidifier passes through a 2" check valve with a 0.312" bypass [5]. This air is then routed to the



**Figure 7** DVMV and DVMV pneumatic signals for MR drain valves

main tank outlets located at the four corners of the locomotive (MRE air connections) and enters the main tank No.2 (MR No.2) via a 2» check valve. Each MR tank is provided with a drain valve, which opens to remove moisture at each on/off cycle of the air compressor (Figure 7).

These drain valves are automatically controlled by the DVMV valve located in the compartment above the compressor. (The drain valves in “automatic” mode are opened to remove the moisture or they can be turned to “off” position when they do not perform this function). The normal operation of the locomotive is to work in the “auto” mode to remove moisture from the tanks. When the drain valves move from the “auto” position to the “off” position, or from the “off” position to the “auto” position at increased pressure MR, compressed air is released and a sharp sound is heard. Be careful and protect your eyes and ears when doing this.

The air injected from the main tank No. 1, after the air dryer, has a different path. This is an auxiliary airflow. There is a shut-off valve for venting air to the valve if work is needed, and a built-in filter for further removal of dirt and moisture [8].

The POU, or pneumatic control module, is located in the brake compartment on the A-side of the locomotive. The module consists of control components (electrical, pneumatic, mechanical and electronic) for adjusting the pressure in the brake line pipelines. The POU module is a central device for connecting the air ducts and electrical wiring to the locomotive. It consists of the following replaceable units: brake line control assembly, MC-13 control valve, quick-acting valve assembly, brake cylinder control assembly, idle (cold) towing assembly, and power supply.

Brake main line control unit. Designed to control the brake line pressure, when the automatic brakes are activated in the CUT-IN full control mode, it allows one to adjust the CUT-IN/CUT-OUT full/partial control modes of the automatic brake application via SDIS and provides the possibility of emergency discharge of the brake line.

MC-13 control valve. It is a backup and allows braking in such situations when there is a complete lack of power supply, computers fail, the locomotive is hauled in an inoperative (cold) state in a coupling or as part of a train.

Quick-acting valve assembly. Ensures proper brake cylinder pressure in any automatic brake operation mode.

Brake cylinder control assembly. Provides control of air supply from the main reservoir No.2 to the brake cylinders and release of air from the brake cylinders to the atmosphere in all braking and release modes.

Idle (cold) towing assembly. Used when hauling a completely inoperable locomotive.

Power supply. Provides redundant power supply for the FastBrake controller logic circuits and solenoid valve driver circuits, and is two separate 74 VDC power supplies.

### 3 Stationary test of a single diesel locomotive TE33A series brake equipment No. 0120

To check for compliance with the requirements of the Instruction on Operation of Rolling Stock Brakes of the Closed Joint Stock Company “National Company Kazakhstan tem r zholy” the condition and operation of



**Table 1** Check of the condition and operation of the braking equipment of the diesel locomotive TE33A No. 0120

No.	Measured parameter	Actual		Standard	
		P	T	P	T
		MPa	s	MPa	s
1.	Brake line density	0.55	75	0.02	>60
2.	Feed line density	0.8-0.78	200	0.02	>150
3.	Capacity of 2 compressors	0.7-0.8	21	0.7-0.8	<45
4.	Turning on the compressor	0.75-0.76		0.75	
5.	Compressor shutdown	0.99-1.0		0.9	
6.	Overpressure in the equalization tank IV position (overlap with the power supply of the brake line) after the first stage of braking	0.45	standard	Not allowed	
7.	Overestimation of pressure in the equalization tank to the IV position (overlap with the power supply of the brake line) after the full-service braking	0.39	standard		
8.	Service discharge rate	0.5-0.4	5.27	0.5-0.4	4-6
9.	Rate of elimination of supercharge pressure	0.6-0.58	87	0.6-0.58	80-120

**Table 2** Check of the condition and operation of the braking equipment of the diesel locomotive 2TE10M No. 3628

No.	Measured parameter	Actual		Standard	
		P	T	P	T
		MPa	s	MPa	s
1.	Brake line density	0.55	72	0.02	>60
2.	Feed line density	0.8-0.78	190	0.02	>150
3.	Capacity of 2 compressors	0.7-0.8	46	0.7-0.8	<50
4.	Turning on the compressor	0.74		0.75	
5.	Compressor shutdown	0.84		0.9	
6.	Overpressure in the equalization tank IV position (overlap with the power supply of the brake line) after the first stage of braking	0.45	standard	Not allowed	
7.	Overestimation of pressure in the equalization tank to the IV position (overlap with the power supply of the brake line) after the full-service braking	0.39	standard		
8.	Service discharge rate	0.5-0.4	5.01	0.5-0.4	4-6
9.	Rate of elimination of supercharge pressure	0.6-0.58	92	0.6-0.58	80-120

the braking equipment of the locomotive was checked [9]. The results of the inspection of the braking equipment of the TE33A locomotive No. 0120 are given in Table 1. Results of the braking equipment check of 2TE10M locomotive No. 3628 are given in Table 2.

### 3.1 Stationary tests of operation of the locomotive TE33A braking equipment

To carry out the functional tests of braking equipment during the stationary tests, a test train of 100 units of rolling stock (400 axles) was formed on the receiving tracks of station Almaty 1 according to the scheme in Figure 8.

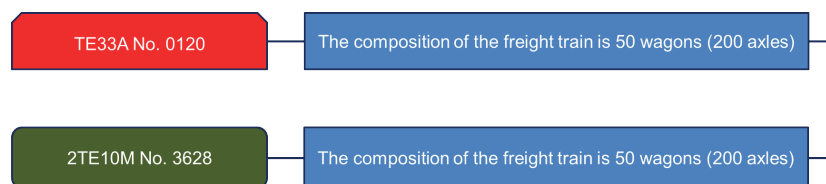
Diesel locomotives TE33A No. 0120 and 2TE10M No. 3628 were delivered from both ends of the train, for testing the braking equipment and for recording the

braking processes and pressure in the brake line at the rear of the train.

During the stationary tests, the pressure in the brake cylinders of the diesel locomotive, the spare tank and the brake cylinder of the tail freight car (portable pressure gauges) was checked in various braking modes (brake line discharge stages, full service and emergency braking) [10].

According to the functioning tests of the TE33A locomotive No. 120 braking system - the volume of the main tank is 1900 liters, with a train consisting of 100 units of rolling stock - 400 axles release of tailgate brakes:

1. after the step braking occurs in 1-3 minutes - the train is prepared to turn on the traction with no danger of breaking the train, and charging of spare tanks up to 95% of the charging one (and according to the air flow meter reading on the TE33A) occurs



**Figure 8** Test diagram when forming a train of 100 rolling stock (400 axles)

- in 4-5 minutes - readiness of the braking system (95%) for subsequent effective braking;
- after the full-service braking and deep discharges of the brake line, the decompression takes 1-3 minutes. Even faster than with small stages, since the decompression is carried out with overpressure above the train line - the train is prepared to turn on traction with no danger of breaking the train, and charging spare tanks up to 95% of the charging (and according to the air flowmeter reading on the TE33A) occurs during 5-7 minutes - the brake system is ready (95%) for subsequent effective braking;
  - after the emergency braking, the decompression takes 2-3 minutes. The train is prepared to turn on the traction with no danger of breaking the train, and the spare tanks are charged up to 95% of the charging tank (and according to the air flowmeter reading on the TE33A) takes 8-14 minutes. - the brake system is ready (95%) for subsequent effective braking.
- Brake control at train pressure in the brake line 0.50.52 MPa is considerably improved [11]:
- increasing the density of the brake line (reducing the intensity of leaks);
  - the pressure difference between the head and the tail of the train decreases;
  - reducing the time for releasing the brakes and charging spare tanks.

#### 4 Calculation of diesel locomotive braking system TE33A

The braking system must have high reliability and ensure the safety of train traffic. Automatic brakes of the railway rolling stock should be maintained according to the established standards and have controllability and reliability of action in various operating conditions, provide smooth braking. To determine the performance of the braking system according to the results of the tests performed, it is necessary to assess the braking system. To perform the calculation of the brake system, the main parameters of the main elements of the braking equipment were obtained from the passport data of TE33A series diesel locomotives [12]. The value of barometric pressure in normal conditions is taken as 0.103 MPa. The compressor's capacity and main reservoir's capacity are obtained by measuring the indicators on the control panel instruments in empty

and loaded states of diesel locomotives, for the cases of brake release and charging after the full-service braking. To perform the calculation of the main devices, the main parameters of the braking equipment of TE33A diesel locomotive are given in Table 3 [9].

#### 4.1 Compressor unit calculation

Calculation is carried out for the most unfavorable operating conditions of the locomotive (presence of the largest permissible air leaks and air flow rate).

The train braking network volume is determined according to Equation (1). Train Brake Network Volume  $\Sigma V_{BN.T}$  consists of the volumes of the brake network of the locomotive  $V_{BN.L}$  and rolling stock  $V_{BN.RS}$  [13]:

$$\Sigma V_{BN.T} = V_{BN.L} + V_{BN.RS}, \quad (1)$$

60 rolling stock -  $\Sigma V_{BN.T} = 20 + 103.5 \times 60 = 6230$  liter,

71 rolling stock -  $\Sigma V_{BN.T} = 20 + 103.5 \times 70 = 7265$  liter,

90 rolling stock -  $\Sigma V_{BN.T} = 20 + 103.5 \times 90 = 9335$  liter,

100 rolling stock -  $\Sigma V_{BN.T} = 20 + 103.5 \times 100 = 10370$  liter.

For one wagon unit the volume of the braking network is equal to:

$$V_{BN} = V_{LINE} + V_{ST} + V_{OT} = 13.5 + 78 + 12 = 103.5 \text{ liters}, \quad (2)$$

where:  $V_{LINE}$  - brake line volume, 13.5 liter,

$V_{ST}$  - spare tank volume, 78 liters,

$V_{OT}$  - volume of operating tanks, 12 liters.

##### 4.1.1 Determination of the total hourly air flow rate

The total hourly air flow rate in the train at frequent adjustment braking is determined by the equation:

$$Q_{GENT} = Q_{L.T} + Q_{BRAKE} + Q_{O.L}, \quad (3)$$

where:  $Q_{L.T}$  - consumption of compressed air to replenish leaks from the brake line and braking devices in the train, l/h,

$Q_{BRAKE}$  - air flow rate for braking, l/h,

$Q_{O.L}$  - other air consumption, for electric locomotives and diesel locomotives can be accepted  $Q_{O.L} = 12000$  l/h,

60 rolling stock:

$$Q_{GENT} = 72\,583 + 48\,388 + 12\,000 = 132\,971 \text{ l/h};$$



**Table 3** Initial data for calculation

Basic parameters	Empty	Loaded	Empty	Loaded
Number of rolling stocks, units	100	90	70	60
Locomotive main line volume, l	20.0	20.0	20.0	20.0
Car main line volume, l	13.5	13.5	13.5	13.5
Spare tank volume, l	78.0	78.0	78.0	78.0
Volume of working tanks of air distributors, l	12.0	12.0	12.0	12.0
Barometric pressure, MPa	0.103	0.103	0.103	0.103
Allowable pressure decrease in the brake line, MPa per minute (leak)	0.02	0.02	0.02	0.02
Required compressor capacity, m <sup>3</sup> /min	4.80	4.36	3.49	3.06
Required minimum volume of the main tank, l.	1688	1909	1181	1273
Selected volume of the main tank, l	1900	1900	1000	1000
Checking the performance of the compressor and the capacity of the main tank for cases of release and charging of brakes after the full-service braking				
Decompression time, min	3.0	3.0	3.0	3.0
Pressure drop in working tanks, MPa	0.15	0.15	0.15	0.15
Charging pressure in the reserve tank, MPa	0.49	0.54	0.49	0.54
Pressure in the reserve tank after braking, MPa	0.34	0.39	0.34	0.39
Value of pressure decrease in TM (full-service pressure), MPa	0.15	0.15	0.15	0.15
Permissible pressure drop in the main tank	2.5	2.0	2.5	2.0
Selected compressor capacity, m <sup>3</sup> /min	5.8	5.8	5.8	5.8
Required compressor capacity, m <sup>3</sup> /min	5.0	4.7	3.8	3.3

70 rolling stock:

$$Q_{GEN.T} = 84\,641 + 56\,427 + 12\,000 = 153\,068 \text{ l/h;}$$

90 rolling stock:

$$Q_{GEN.T} = 108\,757 + 72\,505 + 12\,000 = 193\,262 \text{ l/h;}$$

100 rolling stock:

$$Q_{GEN.T} = 120\,816 + 80\,544 + 12\,000 = 213\,359 \text{ l/h.}$$

The air flow rate in the main air duct is determined according to the Equation (4):

$$Q_{MAD} = \frac{60 \cdot \Delta P_{MAD} \cdot V_{TBN}}{P_{BAR}} \quad (4)$$

where:  $\Delta P_{MAD}$  - permissible pressure reduction in the main air duct in 1 minute through leaks in the absence of its supply (0.02 MPa is accepted),

$\Sigma V_{TBN}$  - the volume of the train's braking network, l,

$P_{BAR}$  - barometric atmospheric pressure,  $P_{BAR} = 0.103$  MPa,

60 rolling stock:

$$Q_{MAD} = \frac{60 \cdot 0.02 \cdot 6230}{0.103} = 72583$$

l/hour,

70 rolling stock:

$$Q_{MAD} = \frac{60 \cdot 0.02 \cdot 7265}{0.103} = 84641$$

l/hour,

90 rolling stock:

$$Q_{MAD} = \frac{60 \cdot 0.02 \cdot 9335}{0.103} = 108757$$

l/hour,

100 rolling stock:

$$Q_{MAD} = \frac{60 \cdot 0.02 \cdot 10370}{0.103} = 120816$$

l/hour,

The air consumption for braking is determined by the equation:

$$Q_{BRAKE} = \frac{\Delta P_{BRL} \cdot \Sigma V_{TBN} \cdot K}{P_{BAR}}, \quad (5)$$

$\Delta P_{BRL}$  - reduction of air pressure in the brake line during braking (in the case of adjustment braking, it is accepted

$\Delta P_{BRL} = 0.08$  MPa),

$K$  - the number of adjustment brakes per 1 hour (in the most unfavorable case for a mountainous area with long descents  $K = 10$ /h),

60 rolling stock:

$$Q_{MAD} = \frac{0.08 \cdot 6230 \cdot 10}{0.103} = 48388$$

l/hour,

70 rolling stock:

$$Q_{MAD} = \frac{0.08 \cdot 7265 \cdot 10}{0.103} = 56427$$

l/hour,

90 rolling stock:

$$Q_{MAD} = \frac{0.08 \cdot 9335 \cdot 10}{0.103} = 72505$$

l/hour,  
100 rolling stock:

$$Q_{MAD} = \frac{0.08 \cdot 10370 \cdot 10}{0.103} = 80544$$

l/hour.

#### 4.1.2 Determination of the compressor performance

The compressor performance is determined by the equation:

$$Q_{COM} = 1.3 \cdot \left( \frac{Q_{GENT}}{60} + Q_{LOKL} \right), \quad (6)$$

where: 1.3 - a coefficient that takes into account the need to turn off the compressor for cooling,

$Q_{LOKL}$  - air consumption to compensate for locomotive leaks (take 135 l/min),

60 rolling stock:

$$Q_{COM} = 1.3 \cdot \left( \frac{132971}{60} + 135 \right) = 3060$$

l/min,  
70 rolling stock:

$$Q_{COM} = 1.3 \cdot \left( \frac{153068}{70} + 135 \right) = 3490$$

l/min,  
90 rolling stock:

$$Q_{COM} = 1.3 \cdot \left( \frac{193262}{90} + 135 \right) = 4360$$

l/min,  
100 rolling stock:

$$Q_{COM} = 1.3 \cdot \left( \frac{213359}{100} + 135 \right) = 4800$$

l/min.

The performance of the Garden Denver compressor is 5800 l/min, it satisfies the calculation results.

#### 4.1.3 Determination of the volume of the main reservoirs

The approximate volume of the main tanks is determined from the filling condition of the main air pipeline (without powering the spare tanks) after emergency braking [11].

$$V_{MT} \frac{\Delta P_{BRL} \cdot V_{BRL}}{\Delta P_{MT}}, \quad (7)$$

where:  $\Delta P_{MT}$  - permissible pressure drop in the main reservoirs during the emergency braking in accordance with the Instructions for operation of railway rolling stock brakes [9]:

for loaded rolling stock  $\Delta P_{MT} = 0.9 - 0.55 = 0.35$  MPa,

for empty rolling stock  $\Delta P_{MT} = 0.9 - 0.5 = 0.4$  MPa,

$V_{BRL}$  - the volume of the train's brake line, l,

$\Delta P_{BRL}$  - reduction of air pressure in the brake line from charging to 0 MPa,

60 rolling stock (loaded):

$$V_{MT} = \frac{0.55 \cdot 60 \cdot 13.5}{0.35} = 1273$$

liters,

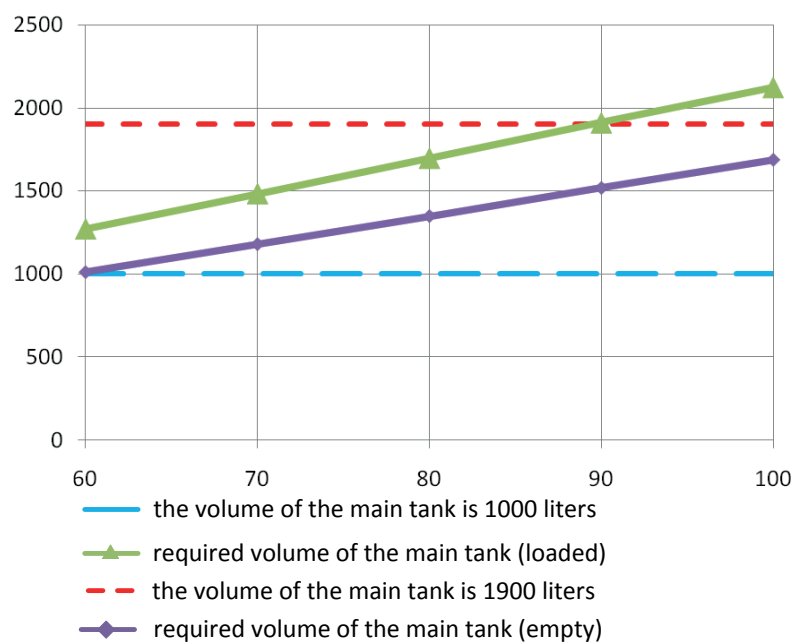


Figure 9 Dependence of the volume of the main reservoirs on the number of axes

70 rolling stock (empty):

$$V_{MT} = \frac{0.5 \cdot 70 \cdot 13.5}{0.4} = 1181$$

liters,

90 rolling stock (loaded):

$$V_{MT} = \frac{0.55 \cdot 90 \cdot 13.5}{0.35} = 1909$$

liters,

100 rolling stock (empty):

$$V_{MT} = \frac{0.5 \cdot 100 \cdot 13.5}{0.4} = 1688$$

liters.

The volume of the main tanks on locomotive TE33A No. 120 is 1,900 liters, which satisfies the calculation results for both loaded and empty trains with a length of up to 400 axles, whereas the serial locomotives with a volume of 1000 liters of main tanks (Figure 9) do not satisfy even for trains with a length of 280 axles (70 rolling stock) [8, 14].

#### 4.2 Checking the compressor performance and the capacity of the main tanks

The calculated values of the compressor capacity and the volume of the main tanks must be checked for the cases of release and charging of the brakes after the full-service braking (FSB) [10]. The check is performed based on the compressed air flow balance equation according to:

$$Q_{COM}^I \cdot t_{R.BR} + \frac{\Delta P_{MT}}{P_{BAR}} \cdot V_{MT} = \frac{\Delta P_{BR.L}}{P_{BAR}} \cdot \sum V_{LINE} + \frac{\Delta P_{WT}}{P_{BAR}} \cdot \sum V_{ST} + \frac{\Delta P_{ST} - \Delta P_{ST}^I}{P_{BAR}} \cdot \sum V_{ST} + \frac{\Delta P_{MAD}}{P_{BAR}} \cdot \sum V_{ST} \cdot t_{R.BR},$$

where:  $t_{R.BR}$  - estimated time to release the brakes and recharge the reserve tank to full charging pressure.

In calculating, the following values were taken:

for trains with a length of less than 200 axles  $t_{R.BR} = 1.5$  min,

for trains with a length of more than 200 axles  $t_{R.BR} = 3.0$  min,

$V_{MR}$  - the total volume of the selected main reservoirs,  $V_{MR} = 1900$  liters,

$\Delta P_{WT}$  - pressure drop in the working tanks (for FSB with air distributors, conl. No. 483-000-  $\Delta P_{WT} = 0.15$  MPa,

$P_{ST}$  - pressure in the spare tanks (freight train  $P_{ST} = 0.54$  MPa),

$P_{ST}$  - pressure in the spare tanks after braking (freight train -  $P_{ST} = 0.39$  MPa),

$\Delta P_{BR.L}$  - the amount of pressure reduction in the brake line (with full service braking),  $\Delta P_{BR.L} = 0.15$  MPa,

$\Delta P_{MT}$  - permissible pressure drop in the main tanks (with full service braking  $\Delta P_{MT} = 0.75 - 0.55 = 0.2$  MPa).

Solving Equation (8) with respect to  $Q_{COM}$ , the compressor performance is determined [15]:

60 rolling stock:

$$Q_{COM} = 1.3 \cdot \left( \frac{132971}{60} + 135 \right) = 3300$$

l/min,

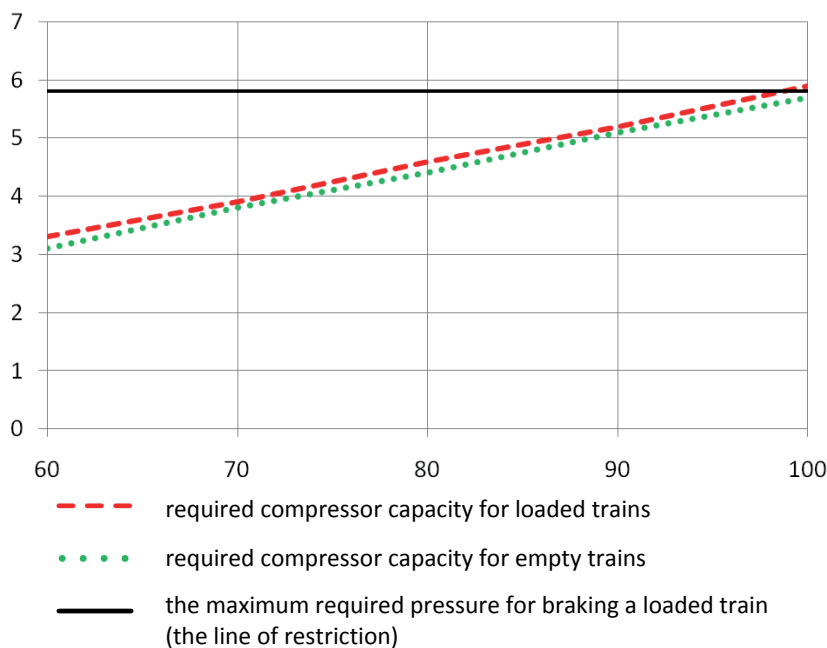


Figure 10 Curve of required compressor capacity versus number of axes

70 rolling stock:

$$Q_{COM} = 1.3 \cdot \left( \frac{153068}{70} + 135 \right) = 3800$$

l/min,

90 rolling stock:

$$Q_{COM} = 1.3 \cdot \left( \frac{193262}{90} + 135 \right) = 4700$$

l/min,

100 rolling stock:

$$Q_{COM} = 1.3 \cdot \left( \frac{213359}{100} + 135 \right) = 5000$$

l/min.

Compressor capacity on a locomotive is  $5.8 \text{ m}^3/\text{min} = 5800 \text{ l/min}$ . The resulting dependences of the required compressor capacity on the number of axles are shown in Figure 10.

## 5 Discussion of results

On Western European railways, slow-acting brakes are used on freight cars with a weak screw coupling in short trains, which can switch to accelerated braking in passenger trains. The design and research (study) of brakes are mainly carried out by the companies Knorr-Bremse (Germany) and Oerlikon (Switzerland), DACO (Czech Republic). The highly sensitive braking systems developed by them with valve-diaphragm design air distributors with stepped release and with a braking wave speed of 250-280 m/s, have been adopted by the UIC as uniform on all the railways in Western Europe [16-17].

The braking devices and equipment manufactured in the USA are characterized by the lower braking efficiency and a longer braking distance compared to the braking devices of Western European railways. In the USA, Westinghouse brakes are used, which supplies brakes to all countries of North and South America and has branches in England, Germany, Italy, Spain and France [17]. These brakes have an air distributor that provides stepless accelerated release in long-length freight trains formed from the rolling stock with a powerful automatic coupling. The most common non-direct exhaust air distributors are air distributors of types AB, ABD, ABDW [18].

In the high-speed passenger trains, the creation of which is currently receiving the great attention in Kazakhstan and abroad, disc and magnetic rail brakes in combination with pad brakes, as well as electronic anti-skid devices to protect the wheels of wheelsets

from damage (the appearance of sliders, metal shear on the surface of the wheels) are widely used in sections railway tracks with a low coefficient of wheel-to-rail coupling [18].

## 6 Conclusions

1. According to the results of the brake tests, it was established that the modifications carried out to increase the volume of the main tanks to 1900 liters showed the operation of the brake system in accordance with the standards of the "Instructions for the operation of rolling stock brakes, National Company, Kazakhstan temir Zholy" dated 17.10.2002 No. 120-TsZ.
2. According to the results of stationary tests with trains on the site, it was revealed:
  - a. The operation of the brake system in braking modes complies with the operating conditions and the standards of the "Instructions for operating the brakes of rolling stock of the Closed Joint Stock Company, National Company, Kazakhstan temir Zholy" dated 17.10.2002 No. 120-TsZ.
  - b. The operation of the brake system in the release modes for a train of 400 axles (flat mode) complies with the operating conditions and standards of paragraph 19.2.7 "Instructions for operating the brakes of rolling stock of the Closed Joint-Stock Company, National Company, Kazakhstan temir Zholy" dated 17.10.2002 No. 120-TsZ. With a decompression time rate of 80 seconds, the actual tail car decompression time was 57-60 seconds.
  - c. Comparative stationary brake tests for the release of the train brakes in 400 axles by control from the diesel locomotive of the 2TE10M series No. 3628AB showed that at a rate of 80 seconds, the actual time of the tail car release was 75-80 seconds (volume GR 2000 L), and with the diesel locomotive TE33A (volume GR 1900 L) 57-60 seconds.

## Acknowledgements

The authors received no financial support for the research, authorship and/or publication of this article.

## Conflicts of interest

The authors declare that they have no known competing financial interests or personal relationships that could have appeared to influence the work reported in this paper.

## References

- [1] Rules of technical operation of railway transport of the Republic of Kazakhstan. Approved by the Order of the Minister of Investment and Development of the Republic of Kazakhstan dated 30 April 2015 No. 544 [online]. Available from: <https://adilet.zan.kz/rus/docs/V1500011897>
- [2] LANIGAN, J., KRIER, P., LEWIS, R. Field trials of a methodology for locomotive brake testing to assess friction enhancement in the wheel/rail interface using a representative leaf layer. *Proceedings of the Institution of Mechanical Engineers, Part F: Journal of Rail and Rapid Transit* [online]. 2020, **235**(9), p. 1053-1064. ISSN 0954-4097, eISSN 2041-3017. Available from: <https://doi.org/10.1177/0954409720973135>
- [3] ABDULLAYEV, S., BAKYT, G., KAMZINA, A., SANSANBEKOV, K., ABDULLAYEVA, A. Interaction of the TE33a diesel locomotive and the railway track on curved section with radius 290 m. *Communications - Scientific Letters of the University of Zilina* [online]. 2023, **25**(4), p. B315-326. ISSN 1335-4205, eISSN 2585-7878. Available from: <https://doi.org/10.26552/com.C.2023.069>
- [4] WHITE, B. T., NILSSON, R., OLOFSSON, U., ARNALL, A. D., EVANS, M. D., ARMITAGE, T., FISK, J., FLETCHER, D. I., LEWIS, R. Effect of the presence of moisture at the wheel-rail interface during dew and damp conditions. *Proceedings of the Institution of Mechanical Engineers, Part F: Journal of Rail and Rapid Transit* [online]. 2018, **232**(4), p. 979-989. ISSN 0954-4097, eISSN 2041-3017. Available from: <https://doi.org/10.1177/0954409717706251>
- [5] PFAFF, R., ENNING, M., SUTTER, S. A risk-based approach to automatic brake tests for rail freight service: incident analysis and realisation concept. *SN Applied Sciences* [online]. 2022, **115**(4), p. 1-14. eISSN 3004-9261. Available from: <https://doi.org/10.1007/s42452-022-05007-x>
- [6] SUCHANEK, A., KURCIK, P., STASTNIAK, P. Design of a testing equipment for experimental research of railway brake systems. *AIP Conference Proceedings* [online]. 2019, **2198**(1), 020015. ISSN 0094-243X, eISSN 1551-7616. Available from: <https://doi.org/10.1063/1.5140876>
- [7] GERLICI, J., LACK, T., RAILBCOT test stand dynamics properties analysis. In: 22nd International Conference Current Problems in Rail Vehicles - PRORAIL 2015: proceedings. Part I. 2015. p. 329-343.
- [8] ABDULLAYEV, S., BAKYT, G., ABDULLAYEVA, A., DUSEMBAYEVA, B., ASKENOV, Y., ASHIRBAYEV, G., BESEKENOV, R. Testing of railway equipment for the impact on the track and turnouts. *Communications - Scientific Letters of the University of Zilina* [online]. 2024, **26**(2), p. B99-B107. ISSN 1335-4205, eISSN 2585-7878. Available from: <https://doi.org/10.26552/com.C.2024.020>
- [9] Instructions on operation of brakes of rolling stock of the Closed Joint Stock Company "National Company Kazakhstan Temirzholy". Approved by the order of the President of the Closed Joint Stock Company "National Company Kazakhstan Temir zholy" from 17.10. 2002 No. 120-TsZ.
- [10] STRAZOVEC, P., GERLICI, J., LACK, T., HARUSINEC, J. Innovative solution for experimental research of phenomena resulting from the wheel and rail rolling. *Transportation Research Procedia* [online]. 2019, **40**, p. 906-911. ISSN 2352-1457, eISSN 2352-1465. Available from: <https://doi.org/10.1016/j.trpro.2019.07.127>
- [11] MUSSABEKOV, M., BAKYT, G., OMIRBEK, A., BRUMERCIKOVA, E., BUKOVA, B. Shunting locomotives fuel and power resources decrease. *MATEC Web of Conferences* [online]. 2017, **134**, 00041. eISSN 2261-236X. Available from: <https://doi.org/10.1051/mateconf/201713400041>
- [12] KUANYSHEV, B. M., ABDULLAYEV, S. S., BAKYT, G. B. Diesel locomotive TE33A produced by JSC "Locomotive Kurastyru Zauyty". Device, purpose of units and assemblies: manual. Almaty: KazATC, 2015.
- [13] HAUSER, V., NOZHENKO, O., KRAVCHENKO, K., LOULOVA, M., GERLICI, J., LACK, T. Impact of three axle boxes bogie to the tram behavior when passing curved track. *Procedia Engineering* [online]. 2017, **192**, p. 295-300. ISSN 1877-7058. Available from: <https://doi.org/10.1016/j.proeng.2017.06.051>
- [14] DIZO, J., BLATNICKY, M., STEISUNAS, S., SKOCILASOVA, B. Assessment of a rail vehicle running with the damaged wheel on a ride comfort for passengers. *MATEC Web of Conferences* [online]. 2018, **157**, 03004. eISSN 2261-236X. Available from: <https://doi.org/10.1051/mateconf/201815703004>
- [15] AZILKIYASHEVA, M. M., SHAYAKHMETOV, S. B., BAKYT, G. B., KOPENOV, B. T., BAUBEKOV, Y. Y., ZHAUYT, A. Development of a method for calculating the degree of use of the plasticity resource (Dupr) when rolling on a new continuous mill. *Metalurgiya-Metallurgy*. 2021, **60**(3-4), p. 362-364. ISSN 0543-5846.
- [16] RAKIPOVSKI, E., MILCIC, D. Validation testing of an innovative braking system for freight wagons. *Transactions of Famena* [online]. 2020, **44**(3), p. 81-92. ISSN 1333-1124, eISSN 1849-1391. Available from: <https://doi.org/10.21278/TOF.44307>
- [17] SMILESKEI, T., VRTANOSKI, G. Development of innovative brake system for rolling stock. *Mechanical Engineering Scientific Journal* [online]. 2019, **37**(1-2), p. 17-27. ISSN 1857-5293, eISSN 1857-9191. Available from: <https://doi.org/10.55302/MESJ19371-2614017s>

- [18] GUNAY, M., ERDI KORKMAZ, M., OZMEN, R. An investigation on braking systems used in railway vehicles. *Engineering Science and Technology, an International Journal* [online]. 2020, **23**(2), p. 421-431. eISSN 2215-0986. Available from: <https://doi.org/10.1016/j.jestch.2020.01.009>





This is an open access article distributed under the terms of the Creative Commons Attribution 4.0 International License (CC BY 4.0), which permits use, distribution, and reproduction in any medium, provided the original publication is properly cited. No use, distribution or reproduction is permitted which does not comply with these terms.

# ASSESSMENT OF THE QUALITY INDICATORS OF THE CARRIAGE MOVEMENT BY DIRECTLY MEASURING THE FORCES OF INTERACTION BETWEEN THE WHEELS AND RAILS

Oleksij Fomin<sup>1,\*</sup>, Pavlo Prokopenko<sup>2</sup>

<sup>1</sup>Department of Cars and Carriage Facilities, State University of Infrastructure and Technologies, Kyiv, Ukraine

<sup>2</sup>Branch "Scientific-Research and Design and Technological Institute of Railway Transport JSC Ukrainian Railways", Kyiv, Ukraine

E-mail of corresponding author: fomin\_ov@gsuite.duit.edu.ua

Oleksij Fomin 0000-0003-2387-9946,

Pavlo Prokopenko 0000-0002-1631-6590

## Resume

This work describes the features and methods of measuring the forces of interaction between the wheel pairs and rails by measuring wheel deformations at control points. The work also contains recommendations for direct measurements of the forces of interaction between the wheels and rails to determine the actual margin of stability of wheel pairs from derailment. The result of the work is general requirements for the system of direct measurement of the strength of interaction of the high-speed rolling stock wheel pairs with rails and scientifically based recommendations for direct measurement of the interaction forces of wheels and rails. The problems of interaction between the wheel pairs and rails do not significantly depend on the track width and are general in nature for different countries of the world.

## Article info

Received 19 March 2024

Accepted 5 May 2024

Online 28 May 2024

## Keywords:

contact of wheels with rails  
control  
interaction indicators  
rolling stock  
traffic safety

Available online: <https://doi.org/10.26552/com.C.2024.030>

ISSN 1335-4205 (print version)

ISSN 2585-7878 (online version)

## 1 Introduction

The task of increasing the speed of passenger rolling stock requires new approaches to the assessment of the safety indicators of train movement and the smoothness of carriages. The conditions of stability on the track of rolling stock can be defined as the ratio of forces acting upon contact of the wheel with the rail. Determining these forces is an extremely difficult task, since the contact zone is constantly moving along the rolling surfaces of the wheels and rails. In addition, to assess the stability of the wheel against rolling onto the rail, it is necessary to constantly calculate the ratio of horizontal and vertical contact forces over a certain period of time, because even isolated cases of exceeding the permissible values of this ratio can cause a violation of traffic safety conditions.

It should be noted that the existing methods of the full-scale tests of rolling stock provide for the determination of traffic safety indicators based on the ratio of forces acting on the wheel pairs from the

frame structures of the running parts, the so-called "frame forces". That is, the values of the forces of direct interaction between the wheels and rails, which depend on the ratio of the stability of the wheel pair in the rail track, are essentially not used. In addition, this method of determining the dynamic forces acting on the wheels at the points of contact with the rails, based on deformations of the side frames of the bogies, due to a number of assumptions, does not have high accuracy.

Therefore, this work substantiates recommendations regarding direct measurements of the forces of interaction between the wheels and rails to determine the actual margin of stability of wheelsets from derailment. This approach will improve the level of safety of train traffic and increase the effectiveness of forecasted evaluations of dynamic indicators of the rolling stock, which will generally improve the conditions for the prevention of traffic events associated with derailment of wheelsets.

Problems of interaction between the wheelsets and rails do not depend significantly on the width of the

track and are of a general nature for different countries of the world.

## 2 Literature review

Railway transport is rapidly developing and is a component of the high-speed transport system. The safety of train operation is becoming a more acute issue. To assess the safety quality of the movement of wagons, locomotives and other types of rails rolling stock, there are various approaches to assessing the safety conditions and solving this problem.

The study [1] describes the development of a finite element model for simulating the descent of trains moving in a curved section of the track located on a bridge during earthquakes. The simulation results showed that the risk of derailment of trains moving on curved bridges is greater than that of trains moving on straight bridges. But this study does not take into account and does not describe determination of performance of the wheelset with rails along the entire train tracking route.

The work [2] gives the results of studying and establishing the mechanism of interaction between the railway wheel and a rail. The modeling is based on the fundamental theory of circular motion kinematics. The proposed method makes it possible to determine the characteristic of the interaction kinematics criteria of the wheel pairs tire cross-section of the rolling stock with the lateral sides of the rail heads. However, the work does not describe the process of interaction between the railway wheel and rail from the point of view of traffic safety.

In document [3], the authors propose a new strategy for improving the dynamics of railway cars and reducing the energy consumption during the transportation, by optimizing the position of the center of gravity of the car during the cargo loading. However, the authors do not indicate how the optimized center of gravity affects the general indicators of the safety of railway carriages.

The paper [4] presents a theoretical basis for modeling the interaction of a railway car and a track, in which the dynamic equations of motion of car-track systems are composed by effectively connecting linear and nonlinear dynamic characteristics. The result of this study is determination of the critical speed of a railway train and the localization of track irregularities through the effective integration of a dynamic modeling model, a probabilistic model of track irregularities and a time-frequency analysis method. However, the work does not consider the possibility of developing a mobile system for determining the indicators of the interaction of a railway car and the track based on the conducted research.

The authors of the work [5] investigate the longitudinal forces acting on a railway car for different loading conditions of the cars in the train. Three different types of wagons are considered in the work,

namely fully loaded, partially loaded and empty wagons. The purpose of this work is to determine the best place for their location in a freight train where the smallest longitudinal forces occur, regardless of the wagon loading scheme. However, the work does not assess the influence of horizontal forces on the railway car, which significantly affect the safety of the movement of railway cars.

The article [6] presents a study of the freight wagons derailment in symmetrical turnouts. A dynamic model of the open wagon and a model of a flexible turnout, which undergoes derailment when the wheel flange is lifted, was created. In addition, a full-scale wheel-rail interaction test was conducted to verify the dynamic model. As a result of the simulation of derailment during the lifting, the wheels are consistent with the research data, and the safety of the bogie depends on the condition of both the front and rear wheels.

In the article [7], the authors describe the concept of a smart wagon consisting of various components. This concept meets the safety requirements of a modern railway system. Self-diagnosis functions in a wagon significantly reduce the risk of accidents. This paper also presents the concept and functional model of this railway wagon and illustrates the utility of this concept based on investigated railway accidents.

Research [8] describes the behavior of dynamic derailment caused by the failure of rail connections of a railway switch, as well as the assessment of the impact of such parameters on the safety of train operation. The developed model takes into account the transverse difference between the sections of the rail connection, which directly cause the lifting of the wheel. The conducted research indicates that the proposed derailment model is able to effectively evaluate operational safety as a result of various wheels and track defects, and thus provide a basis for providing a cost-effective platform for future optimization of railway track and rolling stock parameters.

In [9], the authors study the effect of gaps between the blocks, changes in the wheel-rail friction coefficient, and the radius of the track curve on the nonlinear critical speed of a railway vehicle. The influence of the gaps between the axle boxes on the wear of the wheels and the interaction of the wheels with the railway track was also investigated.

The paper [10] describes the dynamic behavior of the wheel-rail interaction under various surface contaminations of the rail track, using the methodology of experimental and numerical modelling. The results of the study showed that the wheel-rail creep force drops sharply when the wheel enters the low adhesion zone, and when the adhesion is restored, there is a sudden increase in the creep force, which negatively affects the dynamics of the railway car.

In the study [11], a refined wheel-rail contact formula was proposed for analysis of the nonlinear train-track interaction, which takes into account the geometry



of the wheel and rail. While most of the existing methods consider contact forces as external forces, the work uses modeling of the behavior of the contact surface based on Hertz's theory and Kalker's laws. The proposed refined mathematical model is confirmed by experimental data.

In the article [12] three-dimensional numerical modelling of the moving load of the wheel-rail interaction for high-speed and heavy trains is investigated. Simulations were performed in ANSYS with a hybrid model involving a flexible wheelset moving on a pair of rigid rails, which helped in estimating the frictional stresses at the wheel-rail interface during the train motion. As a result of the work, it was found that contact pressure and frictional stress increase quadratically with increasing train speed.

In the article [13], the authors proposed a three-dimensional (3-D) model of train-track interaction. As a result of the study of the developed dynamic model, it was found that this model demonstrates high computational stability, accuracy and efficiency in comparison to traditional solutions; in addition to some key parameters, such as bridge element length, the length of the track and bridge section in numerical integration can be conveniently refined using this model.

In work [14], the authors developed a dynamic model for studying the vertical interaction of a rail track and a system of cars. The developed model is verified using several test data and other numerical models.

In the article [15], the authors presented an analysis of the influence of creep paths on the contact forces of the wheel and rail. The simulation results showed that the maximum normal wheel-rail contact stresses are less than 1600 MPa in the range of typical conditions of normal operation.

The article [16] presents the features and results of the cataloging of the supporting system of semi-cars, the application of this approach for the end wall of one of the basic models of wagons.

In [17], the authors described the problem of various deformations at all the stages of operation of freight wagons. The main type of these deformations are residual deformations that occur during welding as a result of thermal exposure.

The authors of the article [18] describe the process of conducting the control tests of tank wagons for dangerous goods. The testing methodology described in this work was used during the research.

In the article [19], the author highlights the results of work on determining ways to increase the degree of ideality of freight wagons and forecasting the evolution of the chassis of new generation wagons. A review of examples of the idealistic strategy of improving the undercarriage of railway universal freight open wagons.

In the studies [20-21], the authors elucidate a method to enhance the efficiency of the braking system by regulating the cooling of friction surfaces through adaptive air supply. A mathematical model has been

devised to govern the air pressure supply to the brake's frictional interface, determining the optimal diameters of friction lining holes and the velocity of air delivery.

According to the findings from the examination of literary sources [1-21], it can be inferred that the exploration of directly measuring the forces of interaction between the wheel pairs and rails through assessing the wheel deformations at specified control points is pertinent and necessitates further investigation.

### 3 Methodology

#### 3.1 Systems for measuring the forces acting on the running parts of the rolling stock

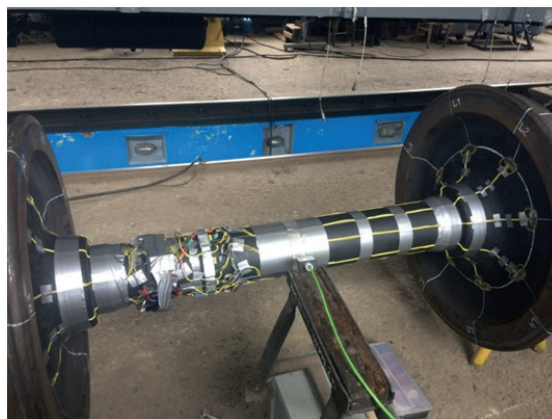
As traffic intensity continues to rise and the inclination to increase the speed of passenger trains persists, there is a growing need to experimentally assess the power modes of wheel pair elements and the proportions of vertical and lateral forces at the points where wheels make contact with rails. These factors determine the resistance to rolling of the wheel on the rail head, a crucial aspect for ensuring traffic safety.

Measuring tools, currently used in testing the rolling stock, there are no standard systems suitable for determining the forces directly in contact between the wheels and rails. Instead, the force responses of the rail crew to the interaction of wheels and rails in the form of mechanical stresses are measured in the elements of the load-bearing structures, that is, in the rails, wheels, axles or axle assemblies.

There are two ways of measuring the interaction forces between the wheels and rails:

- 1 - due to deformations of the elements of the upper structure of the track;
- 2 - due to deformations of elements of running parts.

The first method is used mainly in tests regarding the effect of rolling stock on the track and consists in equipping a certain section of the rail track with measuring devices. That is, the measurements are carried out on a limited section of the track. A significant drawback of this method is the difficulty of ensuring sufficiently high insulation of measuring circuits, especially when they are used for a long time on sections of operating railway lines. However, this method has been improved in recent years. It became possible to continuously measure the vertical forces acting on the rail on a certain section of the track. It is successfully used to detect defects on the rolling surface of the wheels, which cause an increased effect of dynamic forces on the track and axle assemblies of cars. Thus, the localization of stationary means of measuring force action on the track is, in a certain sense, useful from the point of view of detecting defects on the rolling surfaces of the wheels, to evaluate them and make decisions regarding the removal, of wagons from trains for repair if necessary.



**Figure 1** General view of the tensometric wheelset

In contrast to measurements by stationary devices, which are carried out on a fixed section of the track at the same time, systems for measuring force actions by deformations (tensions) of the load-bearing elements of the running parts provide for the current collection of data on dynamic processes accompanying the movement of the crew.

### 3.2 Measurement of data of elements of load-bearing structures

To measure the mechanical stresses in the surface layers of the elements of the load-bearing structures of the rolling stock, the methods and means of tensometry are used, that is, strain gauges and registration equipment. The operation of the strain gauge is based on the tensile effect of the conductor or semiconductor, which is attached to the surface of the supporting element of the structure with a special glue. Thus, deforming together with the metal element when it is loaded, the strain gauge changes its electrical resistance.

The change in resistance of the strain gauge during deformation is very small, usually of the order of several hundreds of  $\Omega$ . One of the most convenient means of measuring such changes is the Wheatstone bridge. It includes four resistors connected to a DC power supply.

### 3.3 Direct measurements of the interaction forces between the wheels and rails

From the point of view of determining the dynamic properties of some researched rail crew and assessing the conditions of its safe operation, the most effective is the use of measuring wheel pairs, that is, wheel pairs equipped with devices for direct measurement of the interaction forces between wheels and rails. According to this method, the forces of interaction between the wheel and a rail are measured with the help of strain gauges installed on the elements of the wheel pair and combined in the corresponding strain gauge schemes.

The use of measuring wheel pairs gives a number of advantages. Such instrumentation provides direct measurement of instantaneous values of contact forces in the wheel-rail system. Direct measurement is opposed to indirect or approximate, which involves determining the forces of interaction of wheels with rails due to deformations of the supporting structures of the running parts.

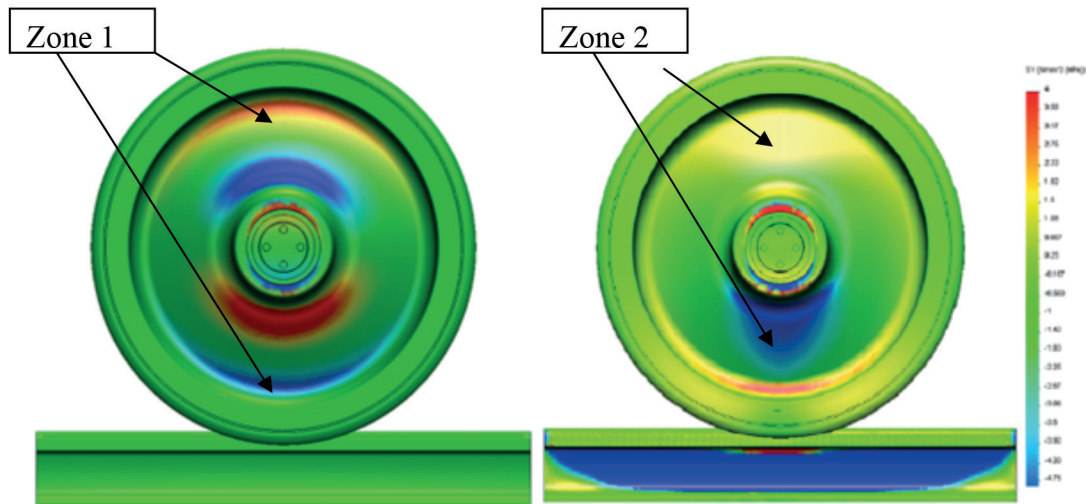
Methods of measuring the forces of interaction of wheels with rails by wheel deformations can be divided into two technologies:

- 1 - measurement of stresses in spokes of spoked wheels;
- 2 - measurement of stresses in the wheel disc, i.e. between the axle and the rim.

The method associated with the equipment of tensometric schemes of spoked wheels is not used often, mainly due to the need to manufacture wheels of a special design. At the same time, with proper design, manufacture and appropriate calibration, strain gauge wheel pairs with spoked wheels provide high measurement accuracy.

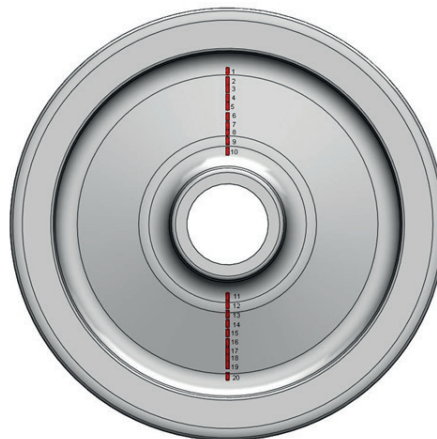
Among the methods of experimental determination of the wheel-rail interaction forces, the method based on the deformation measurements of the wheel discs is nowadays gaining widespread use. There are a number of different projects within this method. The basic principle is measurement of stresses in specific places on the wheels.

An important problem of force-measuring wheel pairs is the need to compensate for "parasitic" effects and to prevent mutual influences between forces acting in different directions. Parasitic effects include the influence of wheel rotation, temperature, and the position of forces on the wheels. It is also necessary to take into account the influence of magnetoelectric phenomena, since the very strong currents (1000-2000 A) sometimes pass only at a distance of 50-100 mm from the wheels and cable lines. In addition, the effects of humidity, temperature and mechanical impact of a shock nature should be taken into account. Thus, the ultimate goal is to achieve output signals proportional to



**Figure 2** Chart of wheel surface stresses under vertical load

**Figure 3** Chart of wheel surface stresses under vertical load and under the simultaneous action of vertical and lateral forces



**Figure 4** Schematics of stress gauge placement on the wheel disc

the applied load with a minimum of mutual influences and parasitic effects.

The main advantage of this method is that it provides an opportunity to measure horizontal (Y) and vertical (Q) forces continuously and close to the wheel-rail interface. It is also possible to measure fairly high-frequency force processes (at least up to 100 Hz). The accuracy of measurements can be quite high (at least within 5-10%).

Figure 1 shows the general view of the tensometric wheelset for measuring miles of interaction between wheel pairs and rails.

### 3.4 Determination of zones of deformation sensitivity of the wheel disc to force load

Places of tensor resistors on wheel disks and ways of including them in the measuring scheme should be such that, with sufficient sensitivity of the scheme to the action of the measured force, the influence of

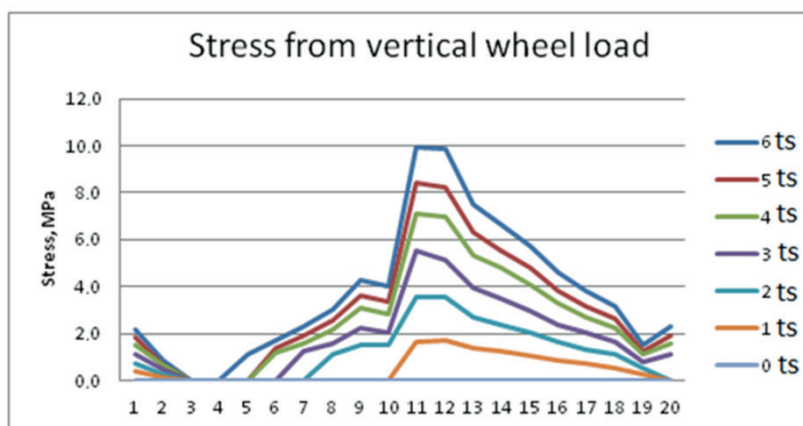
the force in the other direction is as small as possible. Therefore, studies on the determination of the zones on the surface of the wheel disk, the deformations of which are caused by the action of purely vertical and horizontal contact forces, are necessary to substantiate the recommendations for equipment with strain gauge schemes.

To carry out calculations of the stress-strain state of the wheelset using the finite element method, 3D models of individual elements of the wagon wheelset and rails of the R65 type were created, from which a general 3D model of the wheelset installed on the rails was made.

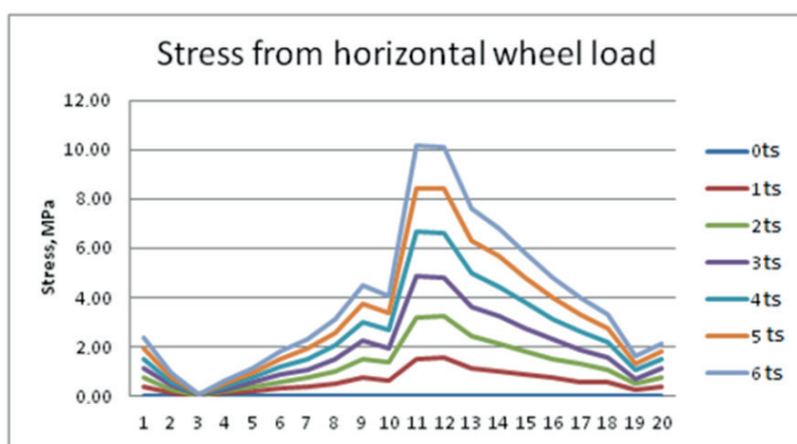
The determination of the zones of deformation sensitivity of the wheel disc is carried out according to the following calculated cases of the wheel pair load:

- vertical load;
- loading by vertical forces and forces from the action of the tare system (horizontal load).

The vertical loads were set based on the mass of the wagon of 52 tons. The lateral load scheme simulated the application of horizontally directed forces from the tare



**Figure 5** Distribution of stresses from the vertical load of the wheel



**Figure 6** Stress distribution from horizontal wheel load

device to the outer face of the wheel above the contact with the rail. In the calculations, the value of the lateral force was set at the level of 50 kN.

The results of the calculation of the surface stresses distribution of the wheel under vertical load (Figure 2) and simultaneous action of vertical and lateral forces (Figure 3) are presented. As can be seen, the greatest stresses in the wheel disc under vertical load occur in the transition zone of the disc to the rim (zone I), as well as in the place adjacent to the hub (zone III). In the case of lateral loading, deformations spread to the middle part of the disk (zone II) near the area of attachment to the hub.

Thus, according to the results of VAT calculations of the wheel disc, zone III was the most sensitive in terms of deformations to both vertical and lateral loads. Therefore, for the lateral load measurement, zone II should be chosen, which is practically sensitive only to lateral forces, and zone I should be chosen for vertical load measurement.

Places of tensor resistors on the disc of a wheel pair and methods of their inclusion in the measuring scheme should be such that, with sufficient sensitivity of the scheme to the measured force, influence on the

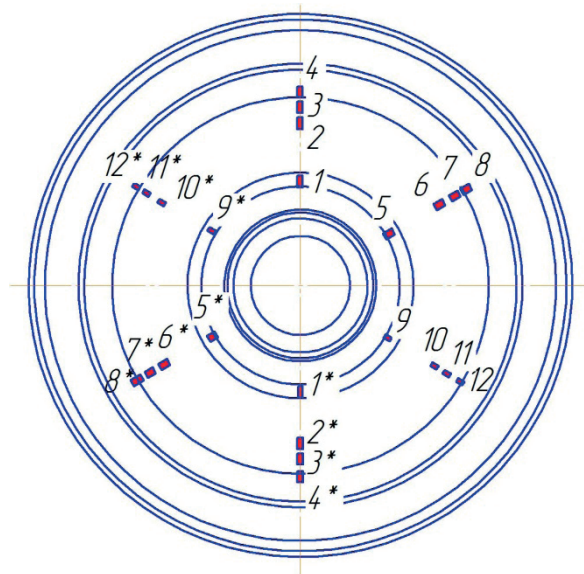
scheme of the force of the other direction is excluded. To clarify the locations on the wheel disk of the points of sensitive zones to the action of vertical and lateral loads, appropriate experimental studies were conducted. Tensor resistors were placed on the wheel disc in the radial direction with a step equal to the base of the tensor resistor. The diagram of placing tensor resistors on the wheel disk is presented in Figure 4. A total of 20 tensor resistors were installed along the diametrical direction of the wheel.

The vertical load of the wheel was created by the weight of the wagon body. Figure 5 shows the stress distribution from the vertical load of the wheel, measured at the placement points of each tensor. As can be seen, in this case the greatest stresses occur at points 9-12.

The results of stress measurements, when the wheel is loaded with lateral forces, are presented in Figure 6. Here, the stress distribution graphs correspond to the power-level values of the forces. As with vertical loading, points 9 to 12 turned out to be the most sensitive in this case.

The obtained experimental data allow to identify the zones of maximum stress that occur on the wheel





**Figure 7** The diagram of placement of tensor resistors for determining the forces of interaction of wheels and rails



**Figure 8** Measuring scheme on the experimental wheel pair

disc under the action of lateral (horizontal) and vertical loads. Experimental data, taking into account the results of computer modelling of the wheel load, provide the basis for the development of a refined tensometric scheme for direct measurements of the interaction forces between wheels and rails.

Based on the calculations and experimental data for determining the zones of deformation sensitivity of the disk of a standard wagon wheel to vertical and lateral loads, a scheme for placing strain gauges for determining the contact forces of the interaction of wheels and rails is recommended, which is shown in Figure 7.

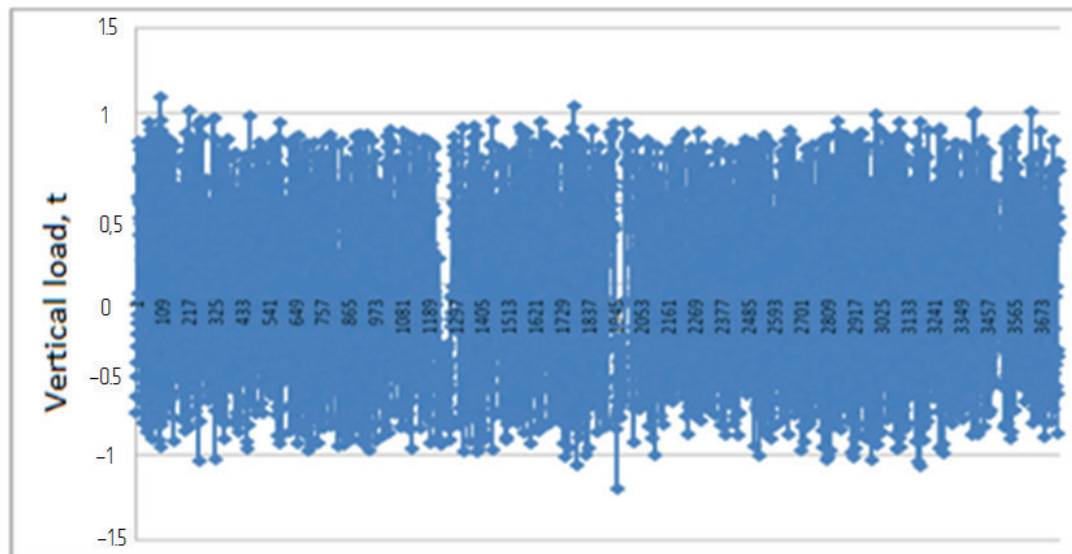
Points 1-1\*, 5-5\*, 9-9\* indicate the places where the greatest stresses occur. Points 2-2\*, 6-6\*, 10-10\* are selected for measuring lateral forces, and 3-3\*, 7-7\*, 11-11\* for vertical ones. Measurement of deformations at points 4-4\*, 8-8\*, 12-12\* is intended to determine the momentary position of the wheel during the carriage movement.

### 3.5 An experimental study on measuring the interaction forces of a wheel pair with rails

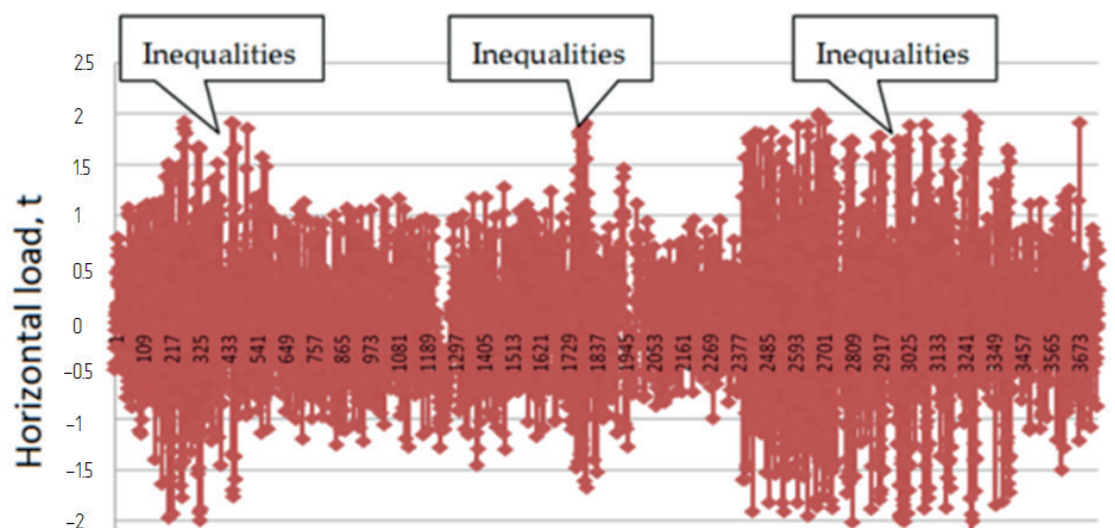
Experimental studies on the direct measurement of forces in the wheel-rail system were carried out on the carriage of a passenger car. Stress gauges were installed on the wheel pair of the experimental cart according to the proposed scheme (Figure 7). After installing the strain gauges on the wheel disc, measuring circuits were installed (Figure 8). The measuring equipment and batteries were mounted on the axle of the wheel pair using a special mount.

To establish the relationship between the readings of the strain gauges and the load in the vertical direction, the measurement system was calibrated.

The test trip was conducted on a section of the track with a length of about 20 km. The position of the wagon on the site and the speed of its movement were



*Figure 9 Recording of vertical forces*



*Figure 10 Recording of horizontal forces*

determined with the help of a GPS-Logger. The GPS survey was conducted once per second.

Strain measurement data was recorded using a software-hardware complex, which consists of a hardware part based on the NI cRIO 9012 controller, an eight-slot NI cRIO 9104 chassis with NI9237 modules, and a software-virtual recorder developed in the LabView software shell.

The software of the complex performs the following functions:

- configuration of measuring channels;
- selection of the strain gauge connection scheme;
- autonomous registration of signals on the internal FLASH storage device;
- data recording in a text file (for further processing).

Signals were recorded on a local FLASH drive. Figure 9 and Figure 10 provide a complete record of the forces that occurred during the test ride.

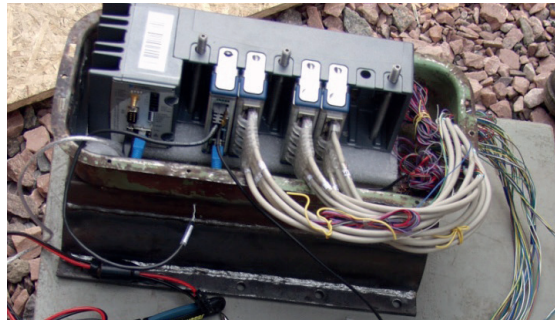
## 4 Results and discussion

### 4.1 General requirements for the system of direct measurement of the interaction forces of wheel pairs of high-speed rolling stock with rails

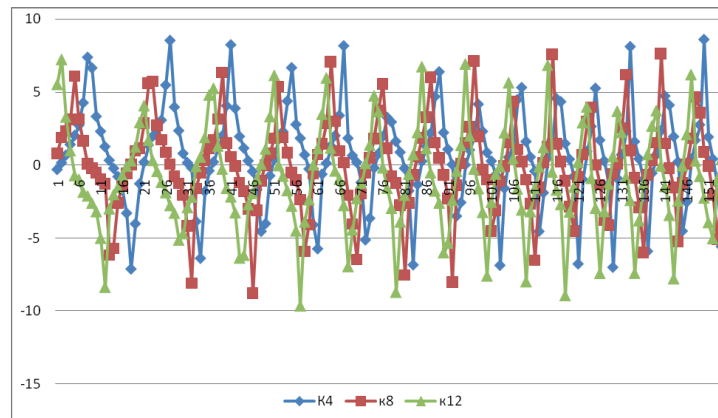
A mobile system for measuring the interaction forces of wheel pairs of high-speed rolling stock with rails should include:

- sensors primary converters;
- GPS receiver;
- cables for signal transmission;
- system of collection and registration of measurement indicators;
- transfer of data about the location and status of the system to the server;
- determination and assessment of traffic quality and safety indicators in the mode express processing.

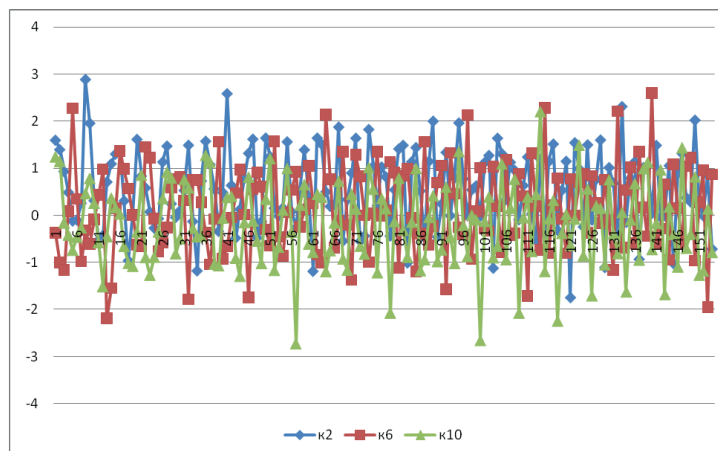




**Figure 11** The direct measurement system for assessing the forces involved in the interaction between the wheel pairs and rails



**Figure 12** A fragment of the vertical load record



**Figure 13** A fragment of the lateral load record

The mobile system for measuring the interaction forces of wheel pairs of high-speed rolling stock with rails based on National Instruments CompactRIO solves a wide list of tasks aimed at monitoring the technical condition of rolling stock during tests and in normal operation.

The software of the software-hardware logger is developed in the LabView FPGA software shell.

The application software is designed to read measurement data from channels selected by the user at the hardware level with a specified sampling frequency, select the type of connection of the outputs of the primary measuring transducers, and set the voltage measurement limits.

The NI 9012 controller application software consists of two parts. The first part reads data from NI 9237 and NI 9205 ADC modules, performs data processing and writes to the non-volatile memory of the controller. The second part transmits data using the Transmission Control Protocol (TCP) to an external computer.

The general view of the system for the system of direct measurement of the forces of interaction of wheel pairs of high-speed rolling stock with rails is shown in Figure 11.

Results of the study are now analyzed in more details on measuring the forces of interaction between the wheel pair and the rails. Figures 12 and 13 show

**Table 1** Results of statistical processing of contact force values

Estimation of magnitude	Q (ton-force)	Y (ton-force)
Mean square deviation	0.47	0.33
Maximum value	9.77	0.99

fragments of vertical and lateral load processes at a speed of 36 km/h, respectively.

Based on the results of taring, calculations and experimental research of the stress-strain state of the wheel disks, the actual value of the interaction forces was determined by the readings of those sensors that were in a vertical position relative to the track plane.

Representative parts of the records of dynamic processes at  $v = 36$  km/h were subjected to statistical processing. The results of this processing are shown in Table 1. Here, the maximum values of the studied quantity are determined by the expression:

$$\bar{x}_{\max} = \bar{x} + ks,$$

(1)

where:

- $\bar{x}$  - arithmetic mean (mathematical expectation),
- $s$  - root mean square deviation (RMS),
- $k$  - is a coefficient that depends on the given level of reliability.

For values  $\Sigma Y$  and  $Y/Q$ , which are important for evaluation of the traffic safety,  $k = 3$ , for other calculated quantities,  $k = 2.2$ , except for quasi-static, for which  $k = 0$ . Since the values of contact forces are important for evaluation of the traffic safety, then  $k$  is taken equal to three.

5 Conclusions

The outcomes of the research focused on directly measuring the forces between the wheel pairs and rails, support the following scientifically grounded conclusions:

1. The approach to measuring the forces involved in the interaction between the wheels and rails, which relies on the deformation of elements in the upper track structure, is constrained to short track sections. Consequently, it does not facilitate continuous monitoring of the force exertion on the moving parts of rolling stock when traversing track sections that exhibit heterogeneity in terms of plan, profile, and condition. At the same time, this method is becoming widely used to identify wagons in trains with deviations in the technical condition of elements of running parts.
2. Theoretically and experimentally, the zones of dependence of the occurrence of stresses on the disk of a standard wagon wheel under the action of vertical and horizontal force load have been determined, which provide grounds for the

development of a refined tensometric scheme for direct measurements of the interaction forces between wheels and rails.

3. A scheme for placement of tensoresistors is proposed for determining the contact forces of the interaction of wheels and rails to determine the actual margin of stability of wheel pairs from derailment in a direct way.
4. A comparison of the values of rms deviations obtained by computer simulation and from the experiment was carried out and it was established that the discrepancy in the lateral load is 0.22%, and in the vertical - 9.34%. Thus, these data confirm, on the one hand, the reliability of the developed computer model, and on the other, the effectiveness of the method of direct measurement of the contact forces of the interaction of wheels and rails.
5. The developed general requirements for the system of direct measurement of the interaction forces of wheels with rails provide for the following:
  - 5.1. For the high-speed passenger wagons, it is mandatory to assess the interaction forces using wheel pairs equipped with strain gauges;
  - 5.2. Determining the locations of the strain gauges on the wheel discs must be accompanied by calculations of the stress-strain state of the wheel pairs under the complex loading by forces that correspond to the operating conditions in terms of magnitude and points of application;
  - 5.3. Specialized devices should be used to calibrate the strain gauges placed on the wheels of the measuring wheel pairs - to implement the lateral load of the wheel in the part that is as close as possible to the zone of its contact with the rail, and to apply the vertical load.

Acknowledgment

The authors received no financial support for the research, authorship and/or publication of this article.

Conflicts of interest

The authors declare that they have no known competing financial interests or personal relationships that could have appeared to influence the work reported in this paper.

## References

- [1] SHEN-HAW, J. Derailment of high-speed trains moving on curved and cant rails under seismic loads. *Soil Dynamics and Earthquake Engineering* [online]. 2023, 166, 107757. ISSN 0267-7261, eISSN 1879-341X. Available from: <https://doi.org/10.1016/j.soildyn.2023.107757>
- [2] NOVACHUK, Y., KOBLOV, R., TEPLYAKOV, A., EGOROV, P. Innovative method of determination of speed of interaction of wheels with rails. *Procedia Engineering* [online]. 2016, 165, p. 1503-1511. ISSN 1877-7058. Available from: <https://doi.org/10.1016/j.proeng.2016.11.886>
- [3] ZHANG, D., ZHOU, F., TANG, Y., TAO, Z., PENG, Q. Optimization of the loading plan for a railway wagon from the perspectives of running safety and energy conservation. *Energy* [online]. 2023, 280, 128229. ISSN 0360-5442, eISSN 1873-6785. Available from: <https://doi.org/10.1016/j.energy.2023.128229>
- [4] XU, L., CHEN, X., LI, X., HE, X. Development of a railway wagon-track interaction model: case studies on excited tracks. *Mechanical Systems and Signal Processing* [online]. 2018, 100, p. 877-898. eISSN 1096-1216. Available from: <https://doi.org/10.1016/j.ymssp.2017.08.008>
- [5] RAKSHIT, U., MALAKAR, B., ROY, B. K. Study on longitudinal forces of a freight train for different types of wagon connectors. *IFAC-PapersOnLine* [online]. 2018, 51(1), p. 283-288. ISSN 2405-8971, eISSN 2405-8963. Available from: <https://doi.org/10.1016/j.ifacol.2018.05.074>
- [6] LAI, J., XU, J., WANG, P., YAN, Z., WANG, S., CHEN, R., SUN, J. Numerical investigation of dynamic derailment behavior of railway vehicle when passing through a turnout. *Engineering Failure Analysis* [online]. 2021, 121, 105123. ISSN 1350-6307, eISSN 1873-1961. Available from: <https://doi.org/10.1016/j.engfailanal.2020.105132>
- [7] CLARHAUT, J., HAYAT, S., CONRAD, B., COQUEMPOT, V. The concept of the smart wagon for improving the safety of a railroad transportation system. *IFAC Proceeding* [online]. 2010, 43(8), p. 638-643. eISSN 1474-6670. Available from: <https://doi.org/10.3182/20100712-3-FR-2020.00102>
- [8] LAI, J., XU, J., LIAO, T., ZHENG, Z., CHEN, R., WANG, P. Investigation on train dynamic derailment in railway turnouts caused by track failure. *Engineering Failure Analysis* [online]. 2022, 134, 106050. ISSN 1350-6307, eISSN 1873-1961. Available from: <https://doi.org/10.1016/j.engfailanal.2022.106050>
- [9] REZVANI, M., MAZRAEH, A. Dynamics and stability analysis of a freight wagon subjective to the railway track and wheelset operational conditions. *European Journal of Mechanics - A/Solids* [online]. 2017, 61, p. 22-34. ISSN 0997-7538, eISSN 1873-7285. Available from: <https://doi.org/10.1016/j.euromechsol.2016.08.011>
- [10] WU, B., XIAO, G., AN, B., WU, T., SHEN, Q. Numerical study of wheel/rail dynamic interactions for high-speed rail vehicles under low adhesion conditions during traction. *Engineering Failure Analysis* [online]. 2022, 137, 106266. ISSN 1350-6307, eISSN 1873-1961. Available from: <https://doi.org/10.1016/j.engfailanal.2022.106266>
- [11] MONTENEGRO, P. A., NEVES, S. G. M., CALCADA, R., TANABE, M., SOGABE, M. Wheel rail contact formulation for analyzing the lateral train structure dynamic interaction. *Computers and Structures* [online]. 2015, 152, p. 200-214. ISSN 0045-7949, eISSN 1879-2243. Available from: <https://doi.org/10.1016/j.compstruc.2015.01.004>
- [12] KHAN, M. R., DASAKA, S. M. Wheel-rail interactions in high speed railway networks during rapid train transit. *Materials Today: Proceedings* [online]. 2018, 5(11), p. 25450-25457. eISSN 2214-7853. Available from: <https://doi.org/10.1016/j.matpr.2018.10.350>
- [13] XU, L., ZHAI W. A three dimensional model for train-track-bridge dynamic interactions with hypothesis of wheel-rail rigid contact. *Mechanical Systems and Signal Processing* [online]. 2019, 132(1), p. 471-489. eISSN 1096-1216. Available from: <https://doi.org/10.1016/j.ymssp.2019.04.025>
- [14] SUN, Y. Q., DHANASEKAR, M. A dynamic model for the vertical interaction of the rail track and wagon system. *International Journal of Solids and Structures* [online]. 2002, 39(5), p. 1337-1359. ISSN 0020-7683, eISSN 1879-2146. Available from: [https://doi.org/10.1016/S0020-7683\(01\)00224-4](https://doi.org/10.1016/S0020-7683(01)00224-4)
- [15] XIA, F., COLE, C., WOLFS, P. The dynamic wheel-rail contact stresses for wagons on various tracks. *Wear* [online]. 2008, 265(9-10), p. 1545-1555. Available from: <https://doi.org/10.1016/j.wear.2008.01.035>
- [16] FOMIN, O., BURLUTSKY, O., FOMINA, Y. Development and application of cataloging in structural design of freight car building. *Metallurgical and Mining Industry* [online]. 2015, 2, p. 250-256. ISSN 2078-8312. Available from: [https://www.metaljournal.com.ua/assets/Journal/english-edition/MMI\\_2015\\_2/039Fomin.pdf](https://www.metaljournal.com.ua/assets/Journal/english-edition/MMI_2015_2/039Fomin.pdf)
- [17] FOMIN, O., LOGVINENKO, O., BURLUTSKY, O., RYBIN, A. Scientific substantiation of thermal leveling for deformations in the car structure. *International Journal of Engineering and Technology* [online]. 2018, 7(4.3), p. 125-129. eISSN 2227-524X. Available from: <https://doi.org/10.14419/ijet.v7i4.3.19721>
- [18] KELRYKH, M., FOMIN, O., GERLICI, J., PROKOPENKO, P., KRAVCHENKO, K., LACK, T. Features of tank car testing for dangerous cargoes transportation. *IOP Conference Series: Materials Science and Engineering* [online]. 2019, 659, 012055. ISSN 1757-899X. Available from: <https://iopscience.iop.org/article/10.1088/1757-899X/659/1/012055/pdf>

- [19] FOMIN, O. Increase of the freight wagons ideality degree and prognostication of their evolution stages. *Scientific Bulletin of the National Mining University. Ukraine, Dnipro* [online]. 2015, 2, p. 68-76. ISSN 2071-2227, eISSN 2223-2362. Available from: <http://nvngu.in.ua/index.php/en/monographs-and-innovations/monographs/1078-engcat/archive/2015/contents-no-3-2015/geotechnical-and-mining-mechanical-engineering-machine-building/3040-increase-of-the-freight-wagons-ideality-degree-and-prognostication-of-their-evolution-stages>
- [20] GORBUNOV, M., FOMIN, O., PROSVIROVA, O., PROKOPENKO, P. Conceptual basis of thermo-controllability in railways braking tribopairs. *Scientific Bulletin of the National Mining University. Dnipro, Ukraine*. [online]. 2019, 2, p. 58-66. ISSN 2071-2227, eISSN 2223-2362. Available from: <https://doi.org/10.29202/nvngu/2019-2/5>
- [21] FOMIN, O., LOVSKA, A., RADKEVYCH, V., HORBAN, A., SKLIARENKO, I., GURENKOVA, O. The dynamic loading analysis of containers placed on a flat wagon during shunting collisions. *ARPN Journal of Engineering and Applied Sciences* [online]. 2019, 14(21), p. 3747-3752. ISSN 1819-6608. Available from: [http://www.arpnjournals.org/jeas/research\\_papers/rp\\_2019/jeas\\_1119\\_7989.pdf](http://www.arpnjournals.org/jeas/research_papers/rp_2019/jeas_1119_7989.pdf)



This is an open access article distributed under the terms of the Creative Commons Attribution 4.0 International License (CC BY 4.0), which permits use, distribution, and reproduction in any medium, provided the original publication is properly cited. No use, distribution or reproduction is permitted which does not comply with these terms.

# INCREASING THE TRAFFIC SAFETY LEVEL OF ROLLING STOCK BY WHEEL CONDITION MONITORING USING AN AUTOMATED MEASURING COMPLEX

Sergii Kliuiev<sup>1</sup>, Stanislav Semenov<sup>1</sup>, Evgeny Mikhailov<sup>1</sup>, Ján Dižo<sup>2,\*</sup>, Miroslav Blatnický<sup>2</sup>, Vadym Ishchuk<sup>2</sup>

<sup>1</sup>Department of Logistics and Transport Safety, Volodymyr Dahl East Ukrainian National University, Kyiv, Ukraine

<sup>2</sup>Department of Transport and Handling Machines, Faculty of Mechanical Engineering, University of Zilina, Zilina, Slovak Republic

\*E-mail of corresponding author: jan.dizo@fstroj.uniza.sk

Sergii Kliuiev 0000-0003-3698-9917,  
Evgeny Mikhailov 0000-0002-6667-5348,  
Miroslav Blatnický 0000-0003-3936-7507,

Stanislav Semenov 0000-0002-5236-4557,  
Ján Dižo 0000-0001-9433-392X,  
Vadym Ishchuk 0000-0003-2024-382X

## Resume

The rail rolling stock undercarriage condition monitoring is proposed by using an automated measuring system, located on the railway track and measuring the specified parameters of the wheels directly, while the train is moving. Regular undercarriage condition monitoring reduces the costs of preventive maintenance of rolling stock without compromising the traffic safety. An algorithm has been developed for the operation of a special software package for visualizing and assessing monitoring data on the condition of the undercarriage of rail rolling stock. The software package consists of separate software modules that can be used independently of each other. It is possible to make short- or long-term predictions of the behavior of any of the monitored parameters using an proposed automated measuring system.

## Article info

Received 12 February 2024

Accepted 4 May 2024

Online 23 May 2024

## Keywords:

rolling stock  
carriage part  
wheel  
rail  
measurements  
defect  
measurement accuracy  
traffic safety

Available online: <https://doi.org/10.26552/com.C.2024.031>

ISSN 1335-4205 (print version)

ISSN 2585-7878 (online version)

## 1 Introduction

With the increase in the speed of rail vehicles, the demands for the quality of both the track and rolling stock are growing. However, the situation in the transportation services market does not allow for a significant increase in expenses for the technical maintenance of rolling stock. Therefore, it is necessary to ensure optimal utilization of funding without compromising the safety level of transportation [1-4].

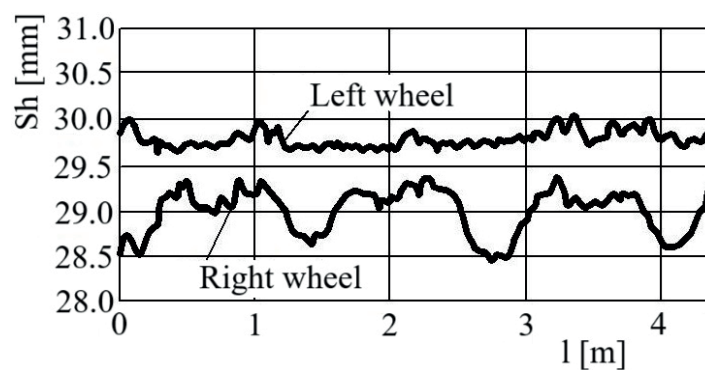
Increasing the traffic volumes and train speeds require greater attention to monitoring the condition of the rail rolling stock. To solve this problem, measuring devices are created that are located on or near the railway track and are capable to measure the necessary parameters directly while the train is moving, by their dimensions, weight and other parameters [5-8].

## 2 Presentation of basic materials

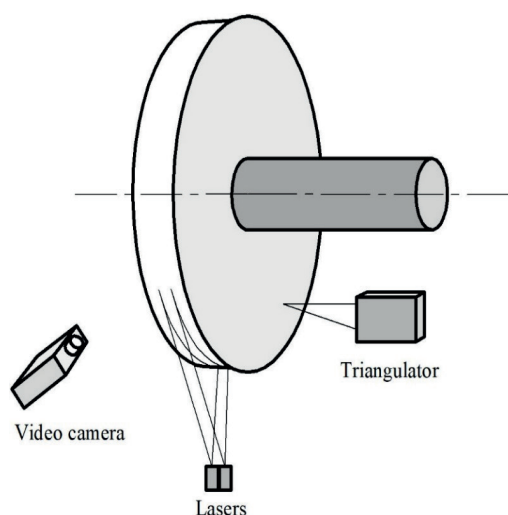
The operation of the wheel-rail system is associated with significant wear of both components interacting in it [9-12]. This specially applies to wheels. The parameters of wheel pairs, controlled in operation, are the distance between the inner edges of the railway wheel flanges, rolling surfaces, thickness and vertical undercut of the wheel flanges [13-14]. To ensure the high reliability, measurements of these parameters are carried out at four points on the circumference of each wheel [15-17].

Manual measurements, using special templates, are associated with significant labour costs, as well as downtime of the rolling stock. Automation makes these measurements faster. This ensures the necessary measurement accuracy.





**Figure 1** Changing the flange height



**Figure 2** Measuring the wheel diameter and the distance between the inner edges

Monitoring wheels to detect out-of-roundness and sliders is a basic condition for ensuring the traffic safety [18-20], especially for high-speed trains. Having accepted that the wheel flange apex has a sufficiently accurate circularity and concentricity with respect to the axis of rotation, it is supposed that the deviation from the nominal wheel flange height is identical to the deviation of the rolling circle from the ideal circle and carries information about the size of non-roundness and the depth of the sliders. In the proposed automated measuring complex, to control this parameter, a measuring beam is used, the lowering of which, when pressed with the top of the flange, is counteracted by the pressure of compressed air [21-22]. When the wheel rolls, the vertical stroke of the beam is measured using an electromechanical sensor. The signal from the sensor is transmitted to the micro-processor of the module, where it is processed and recorded as a change in the beam stroke for at least one wheel revolution [23-24]. Using the curve of changes in the height of the flange per revolution, the presence of non-roundness or a slider is determined (Figure 1). The error of sliders depth, or the size of out-of-roundness measuring, do not exceed 0.2 mm.

The wheel diameter is determined by the radius of one wheel segment curvature using the laser beams. To

do this (Figure 2), two lasers, with the V-shaped beams diverging in one plane, are placed beneath the wheel under the study. These rays are recorded by a digital video camera located on the side.

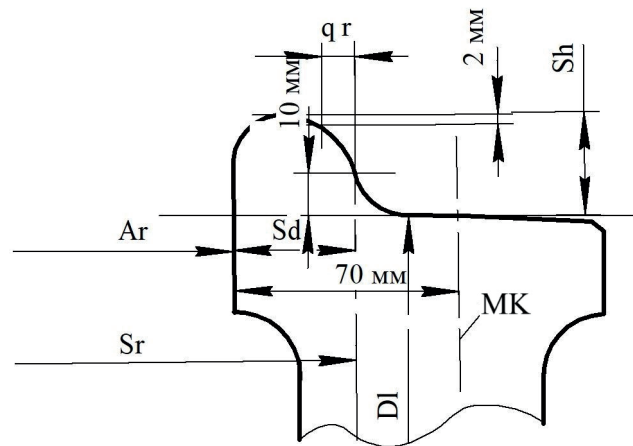
Images of pictures are transferred to the microprocessor module using appropriate transformation. For this process to be carried out without disturbing the scale, the transformation parameters are calibrated on a wheel segment of known diameter [25-26]. Guaranteed accuracy of the wheel diameter measurements with a range from 600 to 1300 mm is 0.6 mm.

The distance between the inner edges of the wheelset wheels flanges is determined using an optical measuring system. The triangulation device used for measurements sends a laser beam to the inner edge of the wheel flange, where the beam trace is observed as a luminous point. An optical system, mounted on the side, records the location of this point. The error, when measuring the distance between the inner edges of the wheel flanges, can reach the value of 0.4 mm.

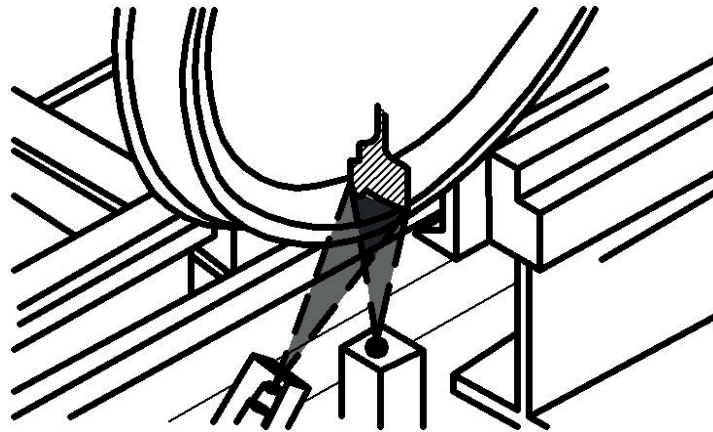
To use an automated measuring complex for other types of rail vehicles (subway cars, trams, etc.), it is necessary to select the diameter of the probing laser beam experimentally, and adapt the location of the complex measuring elements.

The change of the wheel profile is caused by its wear

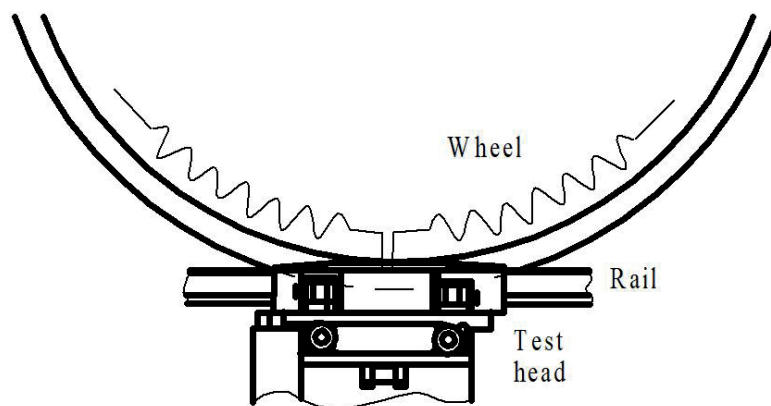




**Figure 3** Parameters of the measured wheel profile: Ar - the distance between the inner edges of the wheel flanges; Sr - track width; Sd - flange thickness; Sh - flange height; DI - diameter of the rolling circle; MK - surface of the measuring circle; qr - transverse dimension used to calculate the amount of flange trimming



**Figure 4** Measurement of the wheel tread surface profile



**Figure 5** Propagation of pulses in a wheel during the ultrasonic flaw detection

due to the loss of material from the tread surface [27-30]. The quality of a wheelset is determined by the following main parameters: height and thickness of the flange, transverse size (qr) used as the basis for calculating the amount of flange trimming, the distance between the inner edges of the wheel flanges and the equivalent conicity (Figure 3).

Measurement of a wheel tread surface profile is performed using the same method as measuring its

diameter (Figure 4). To do this, one laser with a flat V-shaped beam is installed below the rolling wheel such that the plane of the beam is strictly perpendicular to the direction of the wheel movement. All the specified parameters that determine the profile are measured with an accuracy of 0.2 mm. For repeated measurements of the same parameter, the accuracy is 0.1 mm.

The condition of the metal adjacent to the wheel tread is examined using ultrasonic pulses of a frequency

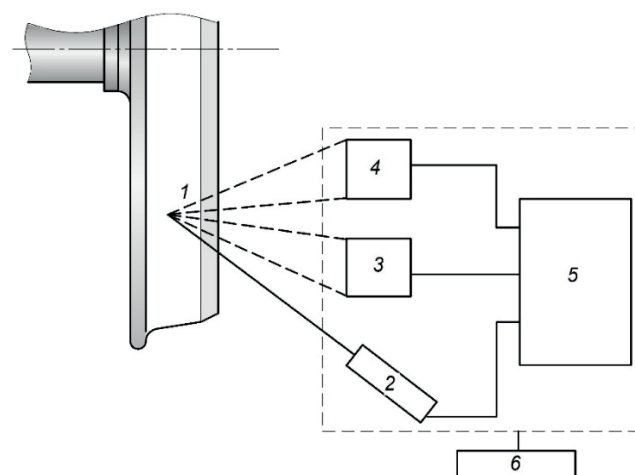
of 400 kHz, which are sent to the wheel tread by the transceiver head. The impulse is being propagated in the wheel in the form of surface waves, which repeatedly circle the wheel in both directions (Figure 5). A defect in the wheel generates a reflected echo.

A crack located perpendicularly to the direction of the ultrasonic pulse propagation causes the signal to be reflected. The echo signal, reflected from the defect, and the so-called bottom signals that run around a full circle, are recorded by the transceiver head. In this case, the useful signal is amplified, passes through an electronic filter, and then enters the micro-processor of the module [31-32]. Here it is assessed according to various criteria, and the ratio of the amplitudes of the signals reflected from the defect and the bottom signals serves as a measure for assessing the depth of the crack in the metal layer adjacent to the wheel tread (Figures 4 and 5).

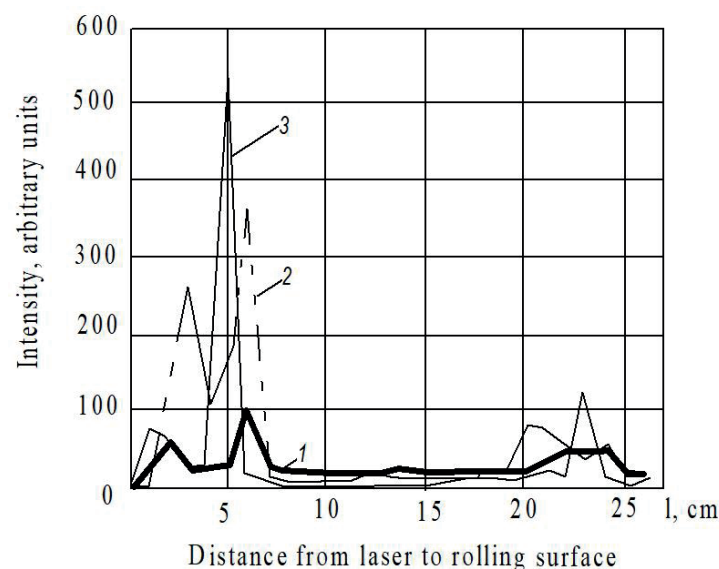
To ensure the high reliability of the presented method, wheel parameters are measured at four points on the circumference of each wheel. To check the measurement accuracy of the automated measuring system, they are compared to manual measurements using special templates. Errors were determined and possible deviations were investigated.

### 3 Findings and discussion

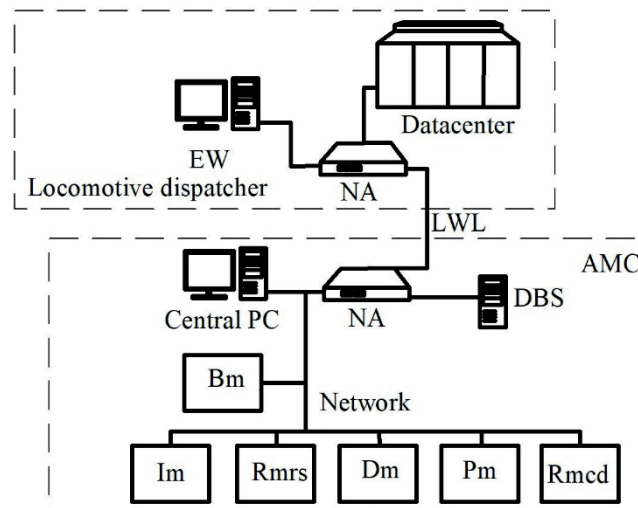
Based on the assigned tasks, the structure of the automated measuring complex was determined. Measuring sensors consist of 16 units installed evenly at the  $\frac{1}{4}$  distance of the wheel circumference on both sides of a rail. The operating principle of the sensors is laser triangulation. The functional diagram of the automated measuring complex is shown in Figure 6.



**Figure 6** A functional diagram of an automated measuring complex with feedback on radiation intensity: 1 - wheel, 2 - laser, 3 - photodetector, 4 - measuring cell, 5 - computing module, 6 - controller



**Figure 7** Dependence of the reflected signal intensity on the position of the laser beam on the rolling surface: 1 - laser beam with a diameter of 0.7 mm; 2 - laser beam with a diameter of 3.5 mm; 3 - laser beam with a diameter of 5 mm



**Figure 8** Networking of measuring and testing modules, base module and operator workstations:  
*EW* - external workplace; *NA* - network device; *LWL* - fiber optic cable; *Central PC* - central PC;  
*DBS* - Database server; *AMC* - Automated measuring complex; *Bm* - basic module;  
*Im* - identification module; *Rmrs* - module for detecting non-roundness and sliders;  
*Dm* - wheel diameter measurement module; *Pm* - profile measurement module;  
*Rmcd* - crack detection module

As the wheel moves, it crosses a beam of laser radiation, and the wheel tire is scanned. The image of the radiation spot on the rolling surface is projected through the lens onto a matrix of linear photosensors.

The position of the spot on the matrix corresponds to the distance from the sensor to a certain point on the rolling surface.

Due to the large inertia of the train, the movement of the wheel during measurement can be considered uniform. The running speed is determined using an inductive axle number sensor. Based on the known values of the distance from the wheel tread to the sensor and the train running speed, the controller calculates the profile and other parameters of the wheel.

The optimal diameter of the probing laser beam for the average wheel tread surface roughness was experimentally selected. The results of measurements performed at different laser beam diameters are shown in Figure 7. Analysis shows that the maximum dynamic range and maximum intensity burst occur with focused laser beam radiation. Increasing the beam diameter from 3 mm to 4 mm does not lead to a decrease in dynamic range. Therefore, the optimal beam diameter value can be considered in the range from 3 mm to 4 mm.

The introduction of a second feedback channel made it possible to increase the accuracy and speed of measurements, as well as to expand the range of applicability of sensors under external illumination conditions.

The automated measuring system is designed for installation directly on the railway track in the area of the entrance to the technical inspection point (TIP). This arrangement of the complex makes it possible

to check the wheels of all the passing trains without significantly reducing the speed of movement. In this case, the entire measurement cycle, together with the delivery of information to the operator's console of the TIP, occurs in real time. All measurements of train's wheelsets with the length of 400 m, which moves at a speed of about 10 km/h are performed within 3 minutes. All the measurement results, which provide complete information about the condition of each wheel and wheel pairs, are stored in the digital media.

All elements of the automated measuring complex are combined into a network (Figure 8). The measurement results make it possible to identify wheelsets for wheel turning or replacement of wheelsets. Having the data on the condition of the profile of each wheel, the mode of turning it on a wheel lathe can be preset.

A special software package is used to visualize and analyze the obtained data. It consists of individual software modules that can also be used independently of each other. The main mandatory data showing the train configuration, maximum dimensions and types of measurements are contained in the database. To obtain the necessary information, the computer connects the system database via a network. All the measurement results stored in the database can be quickly accessed using this software package.

Reducing the railway transport maintenance costs (percentage or quantity) depends on the specific car fleet, the availability of equipment for maintenance and repair and many other factors. The main costs of servicing the railway transport are associated with a reduction in labour costs, downtime of rail vehicles and other factors. Specific figures for costs reduction may vary depending on operating conditions and several other factors. The

idea of the presented method is to show that the use of an automated measuring system can reduce the servicing railway transport costs by several percent.

#### 4 Conclusions

Regular registration of critical vehicle parameters with their subsequent assessment and analysis is the basis for organizing the reliable and cost-effective condition-based maintenance. Similar technologies are already widely used in air transport. Under operating conditions of rail rolling stock, regular parameters monitoring of wheel pairs, reduces the costs of preventive maintenance work without compromising traffic safety. Of course, the potential for savings in operating costs with increased the traffic safety can only be achieved with regular monitoring of the bogie parameters.

When using the proposed automated measuring system, a short- or long-term prediction of the behavior of any monitored parameters can be performed, which

are, e.g. changes in the flange height of a certain wheelset within two weeks. The prediction makes it possible to determine the remaining service life of each wheel pair and plan measures for its repair.

#### Acknowledgment

This research was supported by the project VEGA 1/0305/23: The research of dynamic properties of mechanical systems of railway vehicles with flexible structural components when running on a track and by the project KEGA No. 031ZU-4/2023: Development of key competencies of the graduate of the study program Vehicles and Engines.

#### Conflicts of interest

The authors declare that they have no known competing financial interests or personal relationships that could have appeared to influence the work reported in this paper.

#### References

- [1] ROSIC, S., STAMENKOVIC, D., BANIC, M., SIMONOVIC, M., RISTIC-DURRANT, D., ULIANOV, C. Analysis of the safety level of obstacle detection in autonomous railway vehicles. *Acta Polytechnica Hungarica* [online]. 2022, **19**(3), p. 187-205. ISSN 1785-8860, eISSN 2064-2687. Available from: <https://doi.org/10.12700/APH.19.3.2022.3.15>
- [2] KAGRAMANIAN, A., AULIN, D., TRUBCHANINOVA, K., CABAN, J., VORONIN, A., BASOV, A. Perspectives of multifunctional integrated suburban-urban rail transport development. *Scientific Journal of Silesian University of Technology. Series Transport* [online]. 2023, **120**, p. 105-115. ISSN 0209-3324, eISSN 2450-1549. Available from: <https://doi.org/10.20858/sjsutst.2023.120.7>
- [3] LOVSKA, A., FOMIN, O., PISTEK, V., KUCERA, P. Dynamic load and strength determination of carrying structure of wagons transported by ferries. *Journal of Marine Science and Engineering* [online]. 2020, **8**(11), p. 1-14. eISSN 2077-1312. Available from: <https://doi.org/10.3390/jmse8110902>
- [4] FOMIN, O., LOVSKA, A., MASILYEV, V., TSYMBALIUK, A., BURLUTSKI, O. Determining strength indicators for the bearing structure of a covered wagon's body made from round pipes when transported by a railroad ferry. *Eastern-European Journal of Enterprise Technologies* [online]. 2019, **1**(1-97), p. 33-40. ISSN 1729-3774, eISSN 1729-4061. Available from: <https://doi.org/10.15587/1729-4061.2019.154282>
- [5] LYOVIN, B. Integrated monitoring of transport infrastructure. *Science and Technology of Railways*. 2017, **1**, p. 14-21, ISSN 2587-5752.
- [6] MORAIS, P., MORAIS, J., SANTOS, C., PAIXAO, A., FORTUNATO, E., ASSEICEIRO, F., ALVARENGA, P., GOMES, L. Continuous monitoring and evaluation of railway tracks: proof of concept. *Procedia Structural Integrity* [online]. 2019, **17**, p. 419-426. eISSN 2452-3216. Available from: <https://doi.org/10.1016/j.prostr.2019.08.055>
- [7] KLIUIEV, S., MEDVEDIEV, I., KHALIPOVA, N. Study of railway traffic safety based on the railway track condition monitoring system. *IOP Conference Series: Materials Science and Engineering* [online]. 2020, **985**, 012012. ISSN 1757-899X. Available from: <https://doi.org/10.1088/1757-899X/985/1/012012>
- [8] KLIUIEV, S. O. Ensuring the safety of railway transport in conditions of digitalization (in Ukrainian). *Bulletin of the SNU named after V. Dulya*. 2020, **5**(261), p. 14-18, ISSN 1998-7927.
- [9] PAPAELIAS, M., AMINI, A., HUANG, Z., VALLELY, P., DIAS, D. C., KERKYRAS, S. Online condition monitoring of rolling stock wheels and axle bearings. *Proceedings of the Institution of Mechanical Engineers, Part F: Journal of Rail and Rapid Transit* [online], 2014, **230**(3), p. 709-723. ISSN 0954-4097, eISSN 2041-3017. Available from: <https://doi.org/10.1177/0954409714559758>
- [10] HAUSER, V., NOZHENKO, O., KRAVCHENKO, K., LOULOVA, M., GERLICI, J., LACK, T. Impact of wheelset steering and wheel profile geometry to the vehicle behavior when passing curved track. *Manufacturing Technology* [online]. 2017, **17**(3), p. 306-312. ISSN 1213-2489, eISSN 2787-9402. Available from: <https://doi.org/10.21062/ujep/x.2017/a/1213-2489/MT/17/3/306>



- [11] GERLICI, J., LACK, T., HARUSINEC, J. Development of test stand prototype for rail vehicles brake components testing. *Communications - Scientific Letters of the University of Zilina* [online]. 2014, **16**(3a), p. 27-32. ISSN 1335-4205, eISSN 2585-7878. Available from: <https://doi.org/10.26552/com.C.2014.3A.27-32>
- [12] KARDAS-CINAL, E. Statistical analysis of dynamical quantities related to running safety and ride comfort of a railway vehicle. *Scientific Journal of Silesian University of Technology. Series Transport* [online]. 2020, **106**, p. 63-72. ISSN 0209-3324, eISSN 2450-1549. Available from: <https://doi.org/10.20858/sjsutst.2020.106.5>
- [13] TURABIMANA, P., NKUNDINEZA, C. Development of an on-board measurement system for railway vehicle wheel flange wear. *Sensors* [online]. 2020, **20**(1), 303. eISSN 1424-8220. Available from: <https://doi.org/10.3390/s20010303>
- [14] ASKEROV, H., VAKULENKO, I., GRISCHENKO, N. Insights into factors of damage of surface rolling of railway wheels during operation. *Scientific Journal of Silesian University of Technology. Series Transport* [online]. 2019, **105**, p. 27-33. ISSN 0209-3324, eISSN 2450-1549. Available from: <https://doi.org/10.20858/sjsutst.2019.105.3>
- [15] ENTEZAMI, M., ROBERTS, C., WESTON, P., STEWART, E., AMINI, A., PAPAELIAS, M. Perspectives on railway axle bearing condition monitoring. *Proceedings of the Institution of Mechanical Engineers, Part F: Journal of Rail and Rapid Transit* [online]. 2020, **234**(1), p. 17-31. ISSN 0954-4097, eISSN 2041-3017. Available from: <https://doi.org/10.1177/0954409719831822>
- [16] Transportation Research Board. Rail safety IDEAS programme annual report. Washington, DC: The National Academy of Science, 2018.
- [17] DUTTA, S., HARRISON, T. J., SARMIENTO-CARNEVALI, M. L., WARD, C. P., DIXON, R. Modelling and controller design for self-adjusting railway track switch system. In: 7th Transport Research Arena TRA: proceedings [online]. 2018. Available from: <https://hdl.handle.net/2134/32959>
- [18] GIANG, K. L. E. Enhancing traffic safety: a comprehensive approach through real-time data and intelligent transportation systems. *Scientific Journal of Silesian University of Technology. Series Transport* [online]. 2024, **122**, p. 129-149. ISSN 0209-3324, eISSN 2450-1549. Available from: <https://doi.org/10.20858/sjsutst.2024.122.8>
- [19] MACIOSZEK, E. Analysis of the rail cargo transport volume in Poland in 2010-2021. *Scientific Journal of Silesian University of Technology. Series Transport* [online]. 2023, **119**, p. 125-140. ISSN 0209-3324, eISSN 2450-1549. Available from: <https://doi.org/10.20858/sjsutst.2023.119.7>
- [20] LOVSKAYA, A. Assessment of dynamic efforts to bodies of wagons at transportation with railway ferries. *Eastern-European Journal of Enterprise Technologies* [online]. 2014, **3**(4), p. 36-41. ISSN 1729-3774, eISSN 1729-4061. Available from: <https://doi.org/10.15587/1729-4061.2014.24997>
- [21] AMINI, A., ENTEZAMI, M., PAPAELIAS, M. Onboard detection of railway axle bearing defects using envelope analysis of high frequency acoustic emission signals. *Case Studies in Nondestructive Testing and Evaluation* [online]. 2016, **6**(Part A), p. 8-16. ISSN 2214-6571. Available from: <https://doi.org/10.1016/j.csndt.2016.06.002>
- [22] LUBNA, M., MEHDI, G., ZIED, B. Smart gas sensors: materials, technologies, practical applications, and use of machine learning - a review. *Journal of Applied and Computational Mechanics* [online]. 2023, **9**(3), p. 775-803. eISSN 2383-4536. Available from: <https://doi.org/10.22055/JACM.2023.41985.3851>
- [23] KUMAR, S., GOYAL, D., DHAMI, S. S. Statistical and frequency analysis of acoustic signals for condition monitoring of ball bearing. *Materials Today: Proceedings* [online]. 2018, **5**(2), p. 5186-5194. eISSN 2214-7853. Available from: <https://doi.org/10.1016/j.matpr.2017.12.100>
- [24] YANG, T., DU, C., ZHOU, S. Study on reverberation suppression method combined with prewhitening and wavelet transform. *Acoustic Technique* [online]. 2021, **40**, p. 110-116, ISSN 1819-2408.
- [25] SUN, R.-B., YANG, Z.-B., ZHAI, Z., CHEN, X.-F. Sparse representation based on parametric impulsive dictionary design for bearing fault diagnosis. *Mechanical Systems and Signal Processing* [online]. 2019, **122**, p. 737-753. eISSN 1096-1216. Available from: <https://doi.org/10.1016/j.ymssp.2018.12.054>
- [26] CHEN, Y., NING, P., FAN, T. An improved fast spectral kurtosis algorithm in bearing fault diagnosis for a motor drive system. In: IEEE 6th International Electrical and Energy Conference CIEEC: proceedings [online]. IEEE. 2023. eISBN 979-8-3503-4667-1. Available from: <https://doi.org/10.1109/CIEEC58067.2023.10166214>
- [27] FISCHER, S., SZURKE, S. K. Detection process on energy loss in electric railway vehicles. *Facta Universitatis, Series: Mechanical Engineering* [online]. 2023, **21**(1), p. 81-99. ISSN 0354-2025, eISSN 2335-0164. Available from: <https://doi.org/10.22190/FUME221104046F>
- [28] SEMENOV, S., MIKHAILOV, E., DIZO, J., BLATNICKY, M. The research of running resistance of a railway wagon with various wheel designs. In: Transportation Science and Technology Lecture Notes in Intelligent Transportation and Infrastructure TRANSBALICA XII: proceedings [online]. 2022. ISBN 978-3-030-94776-7, eISSN 2523-3459, p. 110-119. Available from: [https://doi.org/10.1007/978-3-030-94774-3\\_11](https://doi.org/10.1007/978-3-030-94774-3_11)
- [29] SEMENOV, S., MIKHAILOV, E., KLIUIEV, S., DIZO, J., BLATNICKY, M., ISHCHUK, V. Improving the energy efficiency of a tram's running gear. *Acta Polytechnica* [online]. 2023, **63**(3), p. 216-226. ISSN 1210-2709, eISSN 1805-2363. Available from: <https://doi.org/10.14311/AP.2023.63.0216>



- [30] VATULIA, G., LOVSKA, A., PAVLIUCHENKOV, M., NERUBATSKYI, V., OKOROKOV, A., HORDIIENKO, D., VERNIGORA, R., ZHURAVEL, I. Determining patterns of vertical load on the prototype of a removable module for long-size cargoes. *Eastern-European Journal of Enterprise Technologies* [online]. 2022, **6**(7), p. 21-29. ISSN 1729-3774, eISSN 1729-4061. Available from: <https://doi.org/10.15587/1729-4061.2022.266855>
- [31] DAI, W., MO, Z., LUO, CH., JIANG, J., MIAO, Q. Bearing fault diagnosis based on reinforcement learning and kurtosis. In: 2019 Prognostics and System Health Management Conference PHM-Qingdao: proceedings [online]. IEEE. 2019. eISBN 978-1-7281-0861-2. Available from: <https://doi.org/10.1109/PHM-Qingdao46334.2019.8942977>
- [32] OSORIO SANTANDER, E. J., NETO, S., VAZ, L.V., MONTEIRO, U. A. Using spectral kurtosis for selection of the frequency bandwidth containing the fault signature in rolling bearings. *Marine Systems and Ocean Technology* [online]. 2020, **15**, p. 243-252. ISSN 1679-396X, eISSN 2199-4749. Available from: <https://doi.org/10.1007/s40868-020-00084-2>



This is an open access article distributed under the terms of the Creative Commons Attribution 4.0 International License (CC BY 4.0), which permits use, distribution, and reproduction in any medium, provided the original publication is properly cited. No use, distribution or reproduction is permitted which does not comply with these terms.

# EXEMPLARY DETERMINATION OF THE ADHESION ELLIPSES BASED ON SIMULATION OF AN ACCELERATING MOTOR VEHICLE

Jarosław Zalewski

Warsaw University of Technology, Warsaw, Poland

E-mail of corresponding author: jaroslaw.zalewski@pw.edu.pl

Jarosław Zalewski 0000-0002-7559-0119

## Resume

In the paper, some selected results concerning the ellipses of adhesion for various conditions of motion of a vehicle model, have been presented. The analysis, regarding the phenomena between the road and the wheels of the given motor vehicle's model, was previously carried out in the earlier paper by the author. However, they proved useful for the second part of research based on determination of the ellipses of adhesion. This can enable answering the question whether the road conditions may affect the maximum longitudinal and lateral forces combining such ellipses in the contact plane between the road and the wheels. The analysis has been presented based on the previously obtained results.

## Article info

Received 22 March 2024

Accepted 15 May 2024

Online 28 May 2024

## Keywords:

ellipses of adhesion  
contact forces between a wheel and  
a road

Available online: <https://doi.org/10.26552/com.C.2024.032>

ISSN 1335-4205 (print version)

ISSN 2585-7878 (online version)

## 1 Introduction

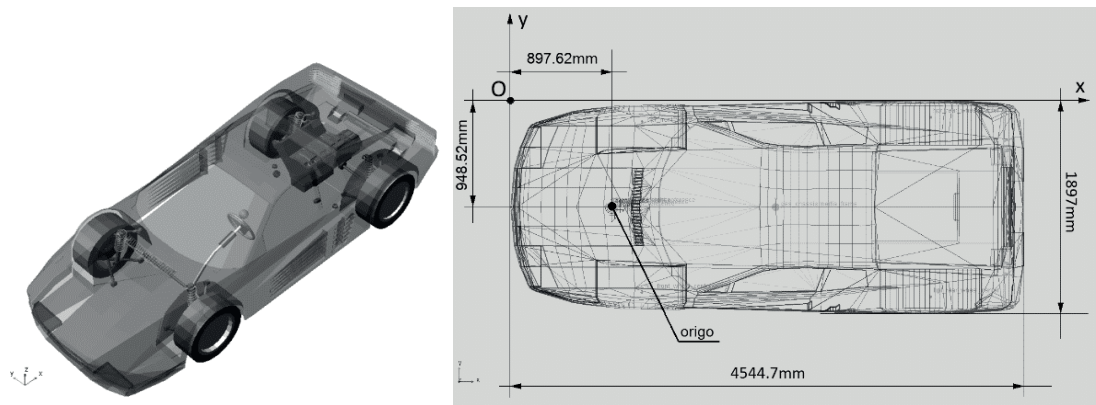
The ability of a motor vehicle to develop a full adhesion between its wheels and the road is one of the most crucial feature, among others in terms of the road traffic safety. One of the maneuvers requiring the adhesion is accelerating when, depending on the road conditions, it may not be fully developed and the wheels may either slip or partially lose contact with the road, especially with the random irregularities occurring. Multiple researches on the adhesion between the wheels and the road have so far been conducted, both from the point of view of the rubber ingredients, e.g. in [1-2] and the road conditions, e.g. in [3-5].

However, research on the adhesion does not consider only the above mentioned aspects. Determining the characteristics useful for further research also plays an important role which has been presented, e.g. in [6-8]. Moreover, determination of the adhesion coefficient in various conditions of motion of road vehicles can give answers, e.g., which road conditions tend to be the least beneficial for safe driving. This has been undertaken, among others in [9-12] up to the wheel blocking conditions [13] and analysis of the discussed phenomena for the electric vehicles [14]. One of the

considered problems was the influence of the icy road on the friction between the tire and a surface.

Of course, it seems important to be acquainted with the problems of road irregularities, especially when the randomness is taken into account. Some works, including, e.g., [15-17], have been devoted to these problems. Some papers have been devoted to more specific aspects, such as determining the road conditions via a signal obtained from the vehicle [18], using measurements for vehicle dynamics simulations [19], or nonlinearity included in the problem of the wheel - road contact phenomena on a randomly uneven road [20].

The aim of this paper was to present the possibility of determining the ellipses of adhesion between the wheels and the road with the use of results obtained for a specific maneuver of vehicle's acceleration simulated in MSC/Adams environment. The selected results of the simulations have previously been presented in [21] by the author and were used as a basis to determine the ellipses of adhesion between the wheels and the road for various adopted conditions of motion. The paper [21] is a source for the research presented here and the main question is whether the longitudinal and the lateral forces, occurring between the wheels and the road, can combine to produce such ellipses and whether the



**Figure 1** The vehicle's model used in simulations and the location of the "origo" point [based on MSC Adams / Car]

**Table 1** Mass - inertia parameters of the unladen simulated vehicle model [21]

	Unladen vehicle	Laden vehicle
Mass	1528kg	1686kg
Center of mass location relative to the "origo"	$x_c = 1.75\text{m},$ $y_c = -0.0014\text{m}, z_c = 0.43\text{m}$	$x_c = 1.73\text{m},$ $y_c = -0.007\text{m}, z_c = 0.435\text{m}$
Moment of inertia ( $I_x$ ) relative to the X axis	583kg·m <sup>2</sup>	618kg·m <sup>2</sup>
Moment of inertia ( $I_y$ ) relative to the Y axis	6129kg·m <sup>2</sup>	6550kg·m <sup>2</sup>
Moment of inertia ( $I_z$ ) relative to the Z axis	6022kg·m <sup>2</sup>	6409kg·m <sup>2</sup>
Moment of deviation ( $I_{xy}$ ) versus the XY axes	-1.9kg·m <sup>2</sup>	1.95kg·m <sup>2</sup>
Moment of deviation ( $I_{xz}$ ) versus the XZ axes	1160kg·m <sup>2</sup>	1276kg·m <sup>2</sup>
Moment of deviation ( $I_{yz}$ ) versus the YZ axes	-1.3kg·m <sup>2</sup>	0.51kg·m <sup>2</sup>

random irregularities and the icy road surface have any influence on these ellipses.

The significance of research presented below is focused on understanding if the lateral and the longitudinal forces in the area of a mutual contact between the road and the wheels can compose an ellipse of adhesion and if such an ellipse can be a factor determining the nature of the wheel - road cooperation, as well as to what degree it could be a feature specifying the road traffic safety.

## 2 Assumptions for the adopted maneuver

In order to present the discussed problem in a proper way it is fair to recall the basic assumptions made in [21] so that determination of the adhesion ellipses would be presented for the specific conditions of motion and the specific maneuver.

A double seater model was used (Figure 1) in the simulations performed in Adams/Car. This model has previously been used in several works by the author for various maneuvers. Although the general assumptions remained the same, e.g., as in [21] the whole mass of a vehicle was changed by adding different masses representing a driver, a passenger, and a baggage. In [21] they were altered as in Table 1. The new coordinates of the center of mass and the moments of inertia and

deviation after loading were calculated by Adams/Car in relation to the so-called "origo" point (Figure 1), which is a point moving along with the vehicle but located on the road.

The vehicle's double seater model used in [21] had the FTIRE (flexible) tires because they allowed running the simulations on the randomly uneven road. This means that a single irregularity can be shorter than the length of the contact area between the wheel and a road. The springs in the MacPherson columns in the vehicle's suspension was linear and the dampers were non-linear. The vehicle's body was assumed rigid to provide the analysis of a multibody without any deformations or micro deformations within its structure.

The simulations in [21] were run for various road conditions with the initial speed 20 km·h<sup>-1</sup> and the road conditions adopted as configurations presented in Table 2, mainly regarding the road surface (dry or icy) and the maximum amplitudes of the random irregularities, which were specified by the intensity parameter. Moreover, the difference between the road profiles for the left and the right wheels was specified by the  $cor_n$  parameter, which, in this case, provided almost different profiles for both sides of the vehicle enabling greater reality. The most difficult conditions of motion were adopted for the configurations 7 and 8 as in Table 2, which was more exactly discussed in [21].

The road was randomly uneven in each configuration,

**Table 2** The configurations of the road conditions adopted for the simulations [21]

	Road	Road condition	Intensity	Corrl	Initial V [km · h <sup>-1</sup> ]
Configuration 1	flat	dry	-	-	20
Configuration 2	flat	icy	-	-	20
Configuration 3	uneven	dry	0.5	0.2	20
Configuration 4	uneven	icy	0.5	0.2	20
Configuration 5	uneven	dry	1.0	0.2	20
Configuration 6	uneven	icy	1.0	0.2	20
Configuration 7	uneven	dry	1.5	0.2	20
Configuration 8	uneven	icy	1.5	0.2	20

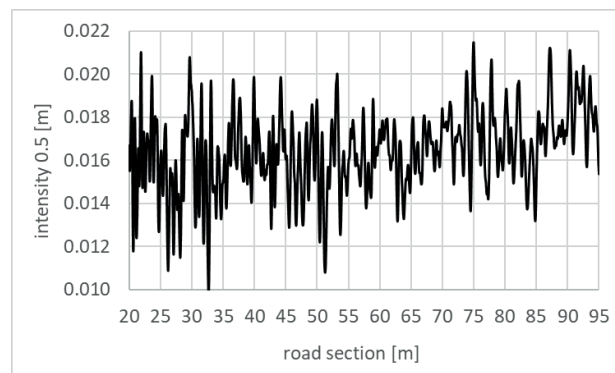
except for 1 and 2. Moreover, the icy road means that the coefficient of adhesion between the wheels and the road was set to 0.3 and the dry road had its value set at 0.8. In all the configurations it was the same for each wheel. The assumed values reflect the average coefficient on a dry and an icy road.

Although the acceleration maneuver was performed for the initial speed of 20 km h<sup>-1</sup>, the vehicle started accelerating after the first 2 s of the simulation (which lasted for 10 s) as if it was moving with the initial speed for the first 2 s. After the next 0.5 s the vehicle had the full throttle on, and it meant only a short period to start fully accelerating.

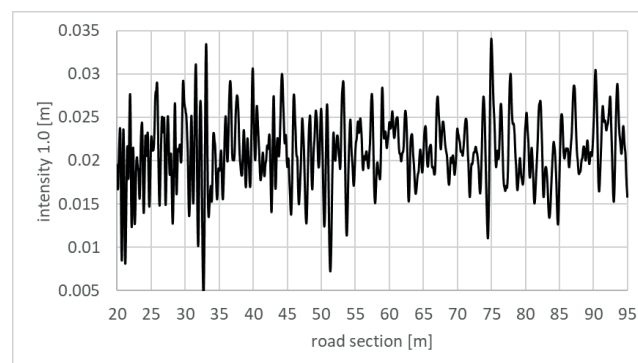
The intensity parameter used specifically in MSC/Adams Car is a coefficient determining the amplitudes of the road irregularities in the random profiles. To

mark the differences caused in the profiles by intensity, three exemplary road profiles were presented in [21] and repeated here in Figures 2, 3 and 4 for three values of intensity, 0.5, 1 and 1.5, respectively. Although it is not clearly specified how the intensity is related to the road profile in MSC/Adams Car, in several tutorials it has been marked that these profiles are prepared in accordance with the ISO standards. One of the aims of this paper was to examine whether the greater intensity would alter the ellipses of adhesion and that is why it was increased even to 1.5, given that [21] is a background for the analyses presented here.

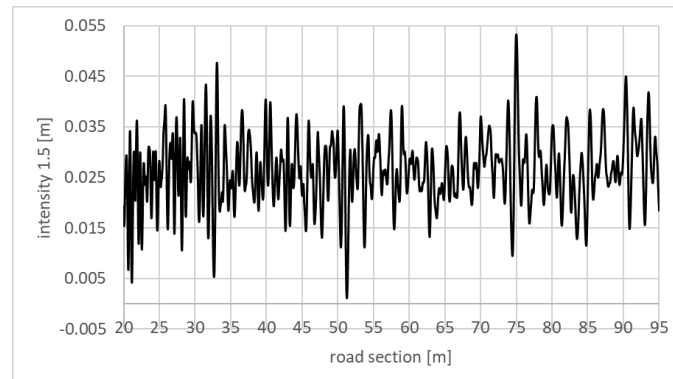
As for the random irregularities in a stochastic uneven road, their generation has been described in many MSC/Adams tutorials (e.g. [22]). These irregularities are easily dealt with by Adams/Car thanks to the FTIRE



**Figure 2** Road profile for the selected road section between 20th and 95th meter at the intensity = 0.5 [21], based on Adams/Car



**Figure 3** Road profile for the selected road section between 20th and 95th meter at the intensity = 1 [21], based on Adams/Car



**Figure 4** Road profile for the selected road section between 20th and 95th meter at the intensity = 1.5 [21], based on Adams/Car

(flexible tire) model, also described in, e.g. [22], which allows recognition of the holes and bumps in the road, which are up to twice shorter than the length of the area of the mutual contact between the wheels and the road (let us call it the contact patch as, e.g. in [22]). For the purpose of this paper it was assumed that the holes shorter than half of this contact patch can be omitted in the analysis, but the bumps can influence the vehicle's behavior.

More on the intensity and its relation to the maximum amplitudes of the irregularities of the road profiles used for the purposes of this paper, one can read, e.g., in [21].

In [21] it was also stressed that the discussed example of the acceleration maneuver was performed for the steering wheel locked to maintain the straightforward direction, which seems obvious when driving on a straight part of a road. However, another possibility taken into account for further research may involve free (no handling) motion with the acting disturbances causing the vehicle to deviate from the assumed straightforward direction.

### 3 Analysis of results related to the road - wheel adhesion

During each simulation one of the components calculated by Adams/Car were the contact forces between the wheels and the road. The measurement was conducted with the use of the virtual sensors, which are located at various points in the vehicle's model. Hence, the maximum absolute values of these contact forces were determined based on the internal measuring system of Adams.

To draw some necessary conclusions, some simple formulas should be introduced at first. The ellipse of adhesion should be based on the maximum values of the coefficient of adhesion in two directions: longitudinal and lateral in relation to the direction of motion of the vehicle's model. Therefore, the first formula used here allows determination of these coefficients. This formula is ok, typical for each book on motor vehicle dynamics.

$$\mu_{ix} = \frac{F_{ix}}{G_i}, \quad \mu_{iy} = \frac{F_{iy}}{G_i}, \quad (1)$$

where:

$\mu_{ix}$  - the coefficient of adhesion in the longitudinal direction (along the direction of motion of a vehicle) for the i-th wheel,

$\mu_{iy}$  - the coefficient of adhesion in the lateral direction (perpendicular to the direction of motion of a vehicle) for the i-th wheel,

$F_{ix}$  - the maximum absolute contact force in the longitudinal direction (along the direction of motion of a vehicle) for the i-th wheel,

$F_{iy}$  - the maximum absolute contact force in the lateral direction (perpendicular the direction of motion of a vehicle) for the i-th wheel,

$G_i$  - the force loading the i-th wheel and normal to the contact plane between this wheel and the road.

The second formula was used to specify the equation of each ellipse of adhesion to use the obtained coefficient to calculate this ellipse, e.g., in Excel. It is also simply used to build an ellipse based on the maximum values of its axes only. It is worth noticing that the paper presents the ellipses of adhesion as a maximum available areas of a contact between the wheels and the road for various conditions of motion.

$$x_i = \mu_{ix} \cos \alpha, \quad y_i = \mu_{iy} \sin \alpha, \quad (2)$$

where:

$\mu_{ix}$  - the coefficient of adhesion in the longitudinal direction (along the direction of motion of a vehicle) for the i-th wheel,

$\mu_{iy}$  - the coefficient of adhesion in the lateral direction (perpendicular to the direction of motion of a vehicle) for the i-th wheel,

$x_i$  - the values along the longitudinal axis of the ellipse of adhesion for the i-th wheel,

$y_i$  - the values along the lateral axis of the ellipse of adhesion for the i-th wheel,

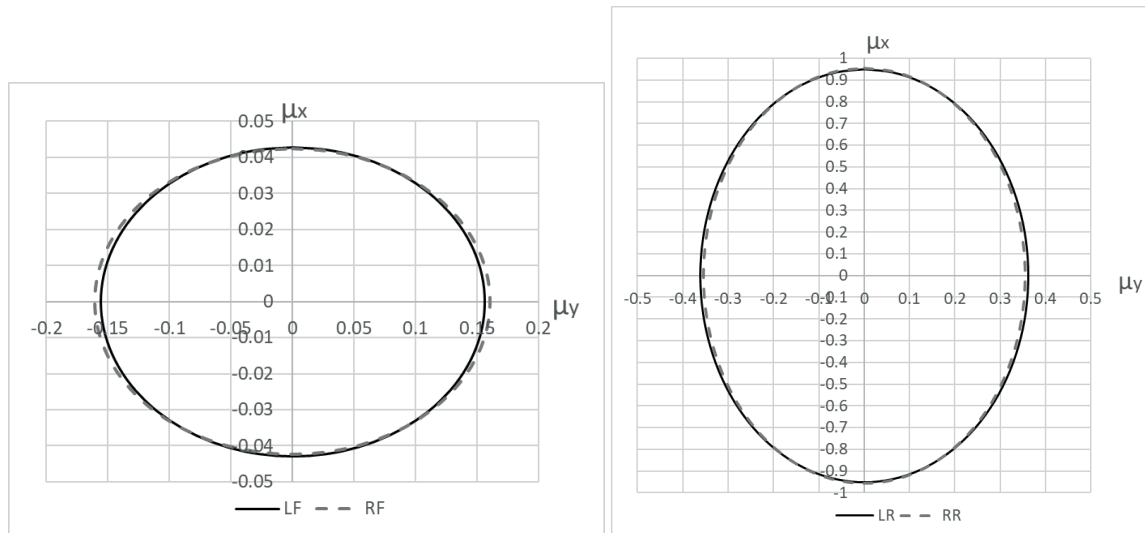
$\alpha$  - the angle used in specifying the ellipses of adhesion, ranging from  $0^\circ$  to  $360^\circ$ .

The first set of results was related to braking on a flat and dry road (configuration 1). In Table 3 the



**Table 3** The forces between the road and the wheels for configuration 1 [21]

	Left front wheel (LF)			Right front wheel (RF)		
	$F_{Xmax}$ [N]	$F_{Ymax}$ [N]	$F_{Zmax}$ [N]	$F_{Xmax}$ [N]	$F_{Ymax}$ [N]	$F_{Zmax}$ [N]
Max absolute	166.08	604.31	3874.66	167.57	634.3	3946.36
	Left rear wheel (LR)			Right rear wheel (RR)		
	$F_{Xmax}$ [N]	$F_{Ymax}$ [N]	$F_{Zmax}$ [N]	$F_{Xmax}$ [N]	$F_{Ymax}$ [N]	$F_{Zmax}$ [N]
Max absolute	5289.13	2010.29	5564.94	5400.4	2003.81	5653.86

**Figure 5** Ellipses of adhesion between the wheels and the road for configuration 1**Table 4** The forces between the road and the wheels for configuration 2 [21]

	Left front wheel (LF)			Right front wheel (RF)		
	$F_{Xmax}$ [N]	$F_{Ymax}$ [N]	$F_{Zmax}$ [N]	$F_{Xmax}$ [N]	$F_{Ymax}$ [N]	$F_{Zmax}$ [N]
Max absolute	317.05	481.68	3734.42	325.09	488.95	3827.46
	Left rear wheel (LR)			Right rear wheel (RR)		
	$F_{Xmax}$ [N]	$F_{Ymax}$ [N]	$F_{Zmax}$ [N]	$F_{Xmax}$ [N]	$F_{Ymax}$ [N]	$F_{Zmax}$ [N]
Max absolute	3357.03	1060.93	5783.71	3434.92	1148.62	5856.73

maximum absolute values of the forces acting on each wheel are presented based on the results obtained in [21], whereas in Figure 5 is shown the ellipse of adhesion based on the determined coefficients in Equation (1) and the Equation (2).

The markings in Table 1 denote the selected wheels for which the ellipses were determined, i.e., LF - left front, RF - right front, LR - left rear and RR - right rear. These markings were also used in Figure 5. The rest of the presented results have been marked in the same way.

It is important to stress that the calculated ellipses presented in this part of the paper, have been obtained for the maximum absolute values of the forces tangential and normal versus the plane of a mutual contact between the wheels and the road.

As it can be observed in Figure 5 the ellipse of adhesion has greater values of its axes for the rear wheels as the engine is located at the back of a vehicle. Despite braking, where usually the front wheels are

extra loaded, the maximum coefficient  $\mu_x$  here was only about 0.04 with about 0.95 for the rear wheels. The  $\mu_y$  coefficient was also more than twice the magnitude for the rear (about 0.35) than for the front wheels (about 0.15).

The maximum absolute forces for configuration 2 are presented in Table 4, while in Figure 6 are shown the ellipses for this configuration. Here the ellipses for the front wheels show that the  $\mu_x$  coefficient was twice greater than in the case of configuration 1, despite braking on the icy road. However, the  $\mu_y$  coefficient was about 0.12, which is less than in the case of configuration 1. For the rear wheels the maximum  $\mu_x$  coefficient was about 0.6, which is far less than in the case of configuration 1, whereas the  $\mu_y$  coefficient was about 0.2, also less than for the dry road. It can be seen that braking on the icy road worsened the effectiveness for the rear wheels. Of course, both configurations (1 and 2) were adopted for a flat road surface.

The differences between the left and the right

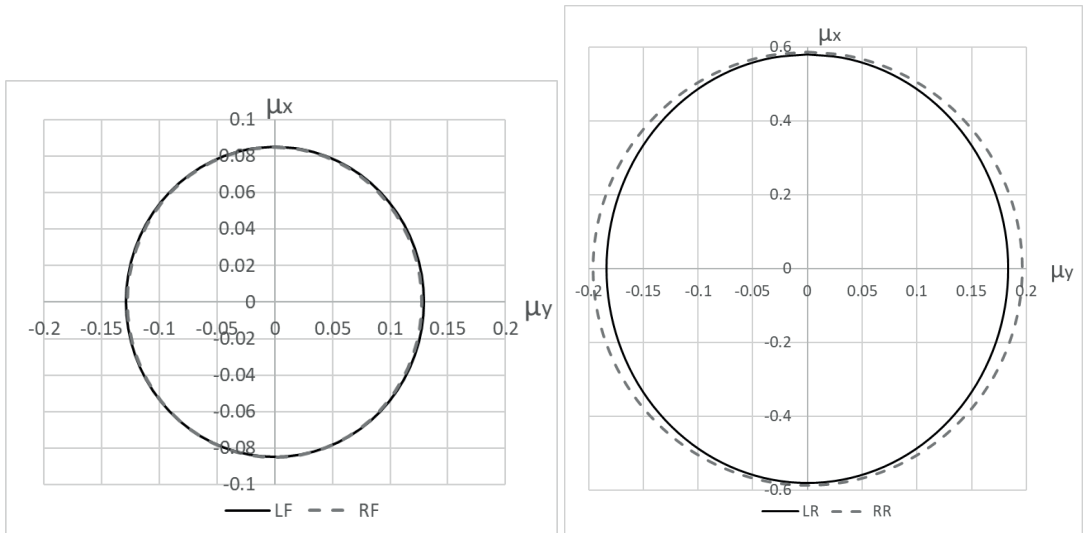


Figure 6 Ellipses of adhesion between the wheels and the road for configuration 2

Table 5 The forces between the road and the wheels for configuration 3 [21]

Left front wheel (LF)				Right front wheel (RF)		
	$F_{x_{max}}$ [N]	$F_{y_{max}}$ [N]	$F_{z_{max}}$ [N]	$F_{x_{max}}$ [N]	$F_{y_{max}}$ [N]	$F_{z_{max}}$ [N]
Max absolute	995.51	723.65	4816.76	1051.4	452.45	5134.61
Left rear wheel (LR)				Right rear wheel (RR)		
	$F_{x_{max}}$ [N]	$F_{y_{max}}$ [N]	$F_{z_{max}}$ [N]	$F_{x_{max}}$ [N]	$F_{y_{max}}$ [N]	$F_{z_{max}}$ [N]
Max absolute	7141.09	1296.05	7615.85	6474.63	1223.14	7636.4

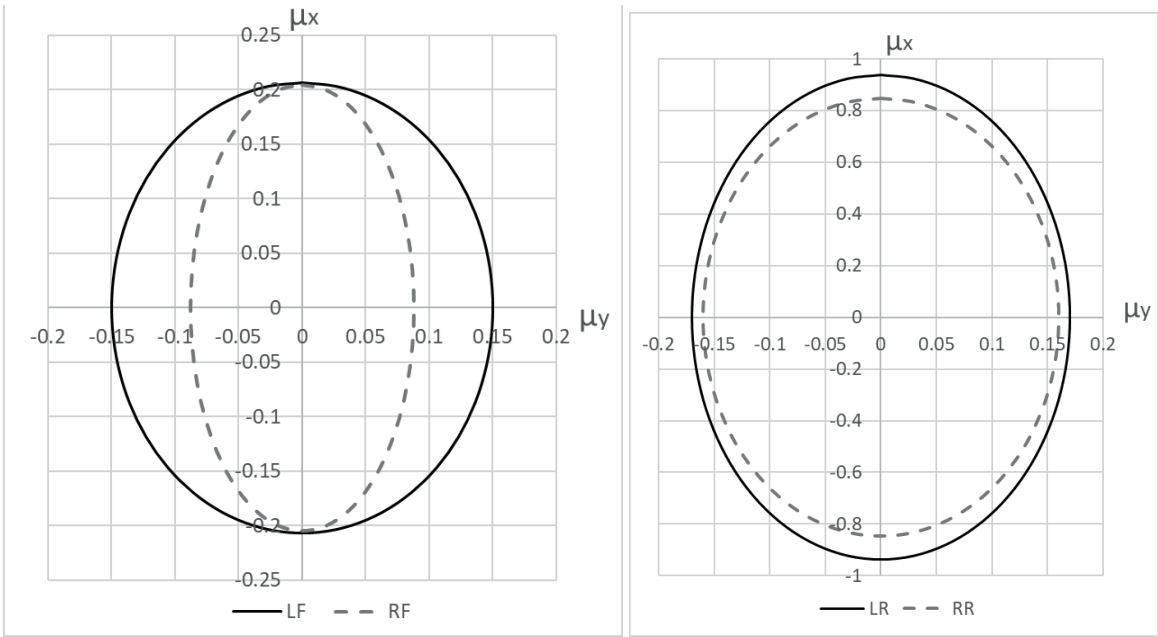


Figure 7 Ellipses of adhesion between the wheels and the road for configuration 3

wheels were marginal for the both configurations.

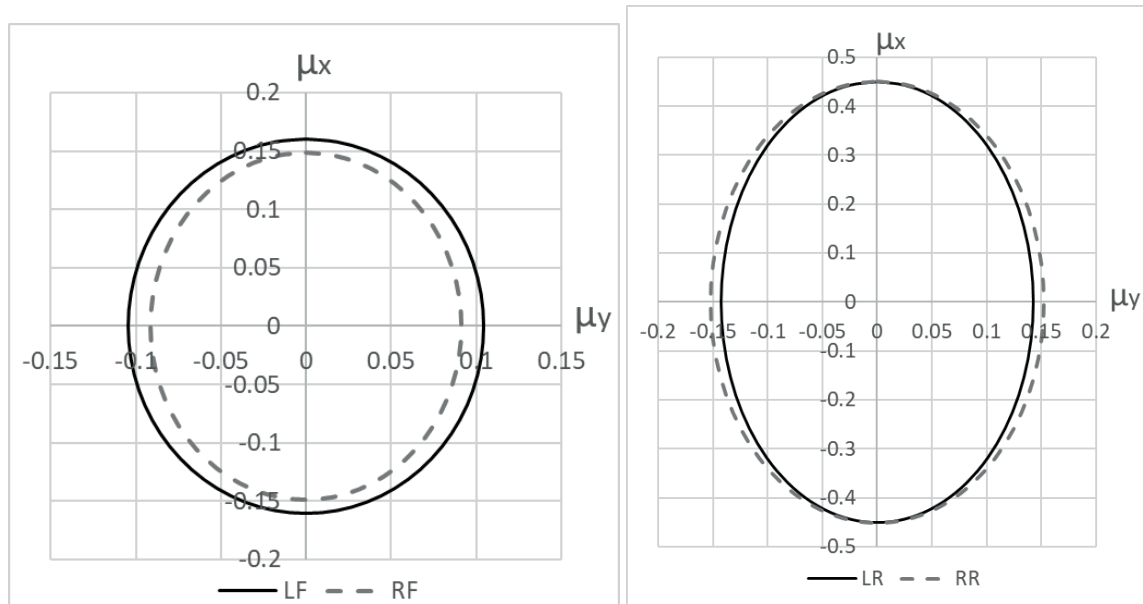
Let now analyze what effect the low amplitude irregularities (Figure 2, intensity 0.5) may cause in terms of the ellipses of adhesion. In Table 5 the results for the configuration 3 have been presented with the respective ellipses shown in Figure 7.

The ellipses for the front wheels show that the maximum  $\mu_x$  coefficient was greater for both the left

and the right wheels than in the case of configurations 1 and 2. However, the  $\mu_y$  coefficient was different for the front wheels by about 0.05, which can be explained by the almost different road profiles adopted with the use of the  $cor_{ri}$  coefficient (Table 2). For the rear wheels the difference in the  $\mu_x$  and  $\mu_y$  coefficients was marginal and both wheels of the rear axis had almost the same maximum values (about 0.9 with little differences). This

**Table 6** The forces between the road and the wheels for configuration 4 [21]

Left front wheel (LF)			Right front wheel (RF)			
	F <sub>Xmax</sub> [N]	F <sub>Ymax</sub> [N]	F <sub>Zmax</sub> [N]	F <sub>Xmax</sub> [N]	F <sub>Ymax</sub> [N]	F <sub>Zmax</sub> [N]
Max absolute	867.39	565	5413.73	840.36	514.98	5653.29
Left rear wheel (LR)			Right rear wheel (RR)			
	F <sub>Xmax</sub> [N]	F <sub>Ymax</sub> [N]	F <sub>Zmax</sub> [N]	F <sub>Xmax</sub> [N]	F <sub>Ymax</sub> [N]	F <sub>Zmax</sub> [N]
Max absolute	3156.29	1000.58	7009.33	3440.19	1157.3	7624

**Figure 8** Ellipses of adhesion between the wheels and the road for configuration 4**Table 7** The forces between the road and the wheels for configuration 5 [21]

Left front wheel (LF)			Right front wheel (RF)			
	F <sub>Xmax</sub> [N]	F <sub>Ymax</sub> [N]	F <sub>Zmax</sub> [N]	F <sub>Xmax</sub> [N]	F <sub>Ymax</sub> [N]	F <sub>Zmax</sub> [N]
Max absolute	1470	768	6700	1430.18	597.07	6868
Left rear wheel (LR)			Right rear wheel (RR)			
	F <sub>Xmax</sub> [N]	F <sub>Ymax</sub> [N]	F <sub>Zmax</sub> [N]	F <sub>Xmax</sub> [N]	F <sub>Ymax</sub> [N]	F <sub>Zmax</sub> [N]
Max absolute	5761.58	1135.63	8935.27	7167.79	1146.32	9400

can be understood such that the engine acts as a mass loading the rear axle, which in these circumstances provided the understeering nature of a vehicle.

It is also necessary to mention that the motion during the braking, according to configuration 3, was performed on the dry road surface.

As for configuration 4 the additional factor was the icy road. The maximum values of the selected forces are presented in Table 6 and the ellipses of adhesion in Figure 8.

The  $\mu_x$  coefficient for the front wheels was about 0.15 which is lower than in the case of configuration 3, with little differences between the left and the right wheels. The  $\mu_y$  coefficient was about 0.1 and there were also some marginal differences between the left and the right wheel. It seems that in this case the icy road had also reduced the influence of the almost different road profiles.

As for the rear wheels, the maximum  $\mu_x$  coefficient was about 0.45, which was twice less than for the dry road in configuration 3, and about 0.05 less than for the icy road in configuration 2. The  $\mu_y$  coefficient was about 0.15 with almost no differences between the left and the right wheel, which means that the icy road, in combination with the low amplitude irregularities, had reduced the adhesion even more than in the case of configuration 2.

As for the motion on the more randomly uneven road, let move to the next results, i.e. configurations 5 and 6, where some additional observations can be made. In Table 7 the maximum forces between the wheels and the road have been shown, along with the ellipses of adhesion (Figure 9) obtained for them.

The  $\mu_x$  coefficient for the front wheels was similar to that in configuration 3 on the dry road, i.e., about 0.2 with marginal differences between the left and the right

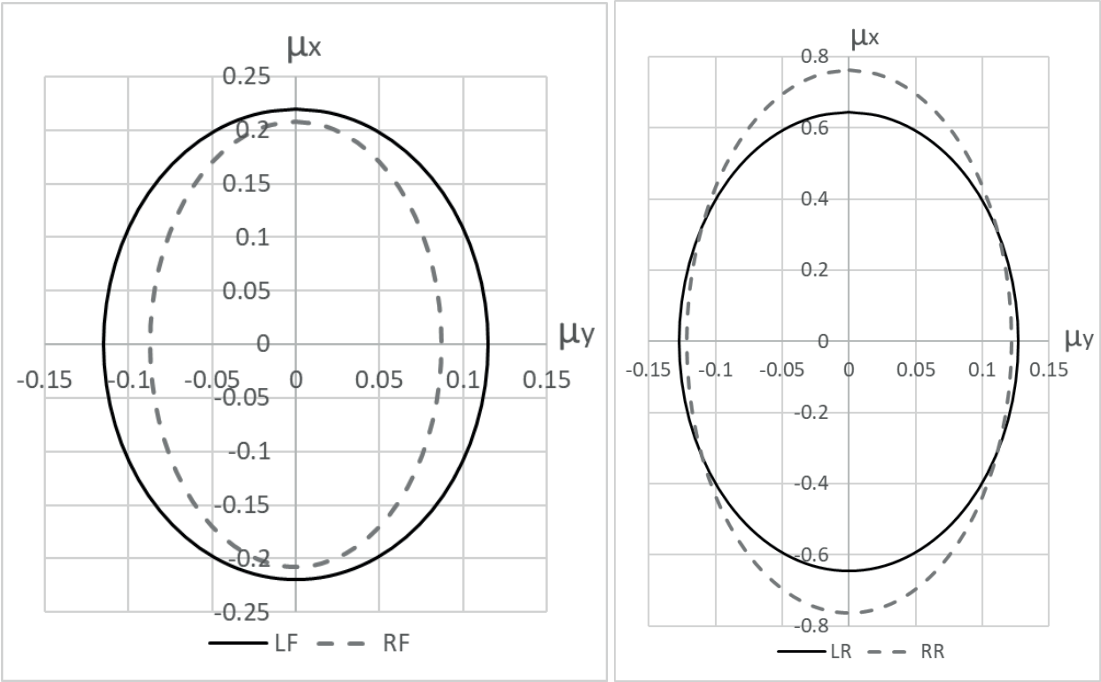


Figure 9 Ellipses of adhesion between the wheels and the road for configuration 5

Table 8 The forces between the road and the wheels for configuration 6 [21]

	Left front wheel (LF)			Right front wheel (RF)		
	$F_{Xmax}$ [N]	$F_{Ymax}$ [N]	$F_{Zmax}$ [N]	$F_{Xmax}$ [N]	$F_{Ymax}$ [N]	$F_{Zmax}$ [N]
Max absolute	1151.32	677.93	6703.52	1244	562.24	7218.32
	Left rear wheel (LR)			Right rear wheel (RR)		
	$F_{Xmax}$ [N]	$F_{Ymax}$ [N]	$F_{Zmax}$ [N]	$F_{Xmax}$ [N]	$F_{Ymax}$ [N]	$F_{Zmax}$ [N]
Max absolute	3012.9	1051.38	8560.18	2927.14	1036.44	8487.15

wheels. As for the differences in the  $\mu_y$  coefficient, they were also marginal and amounted to about 0.12 for the left and 0.09 for the right wheel.

As for the rear wheels, the maximum  $\mu_x$  coefficient was about 0.6 for the left and almost 0.8 for the right wheel, which seems strange when considering the motion on a dry, yet randomly uneven road. However, the almost different road profiles may have affected the vehicle’s motion along with the slightly disturbed center of mass affected by loading the vehicle with a driver, a passenger and a baggage. The  $\mu_y$  coefficient was almost the same for the left and the right wheel (about 0.12).

In Table 8 the maximum absolute forces for configuration 6 are presented, while the corresponding ellipses are presented in Figure 10. In this case the random irregularities of higher amplitudes (Figure 3) were covered with ice as an additional factor, which may have caused the disturbances of the vehicle’s motion.

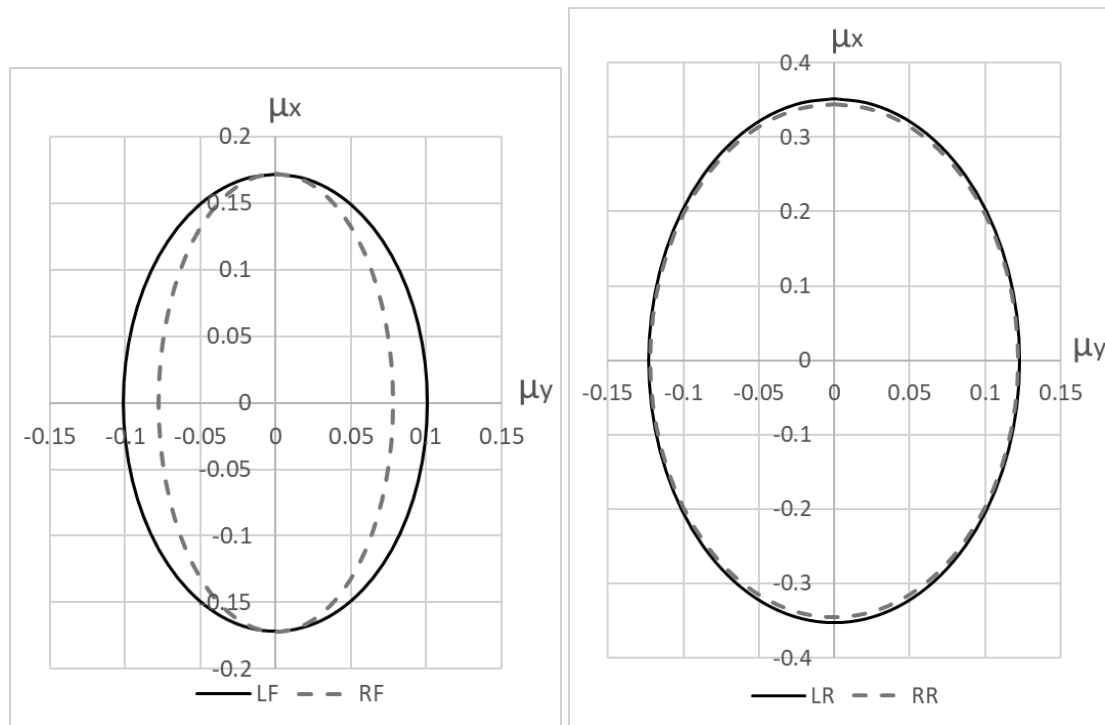
The ellipse for the front wheels shows that the  $\mu_x$  coefficient was about 0.17, which was lower than for the dry road (configuration 5), and the  $\mu_y$  coefficient 0.1 for the left and 0.08 for the right wheel. As for the rear wheels the  $\mu_x$  coefficient was about 0.35, which was twice lower than in configuration 5, indicating the influence of both the icy road and the irregularities with

higher amplitudes (intensity = 1.0). The maximum  $\mu_x$  coefficient was about 0.12 for both rear wheels, similar as in configuration 5.

The last pair of results is presented in Tables 9 and 10, where the maximum absolute forces between the wheel and the road have been shown for configurations 7 and 8, respectively. The road conditions included the highest adopted amplitudes of the irregularities (Figure 4) in configuration 7 with the additional icy road in configuration 8.

The ellipses of adhesion for both configurations are presented in Figures 11 and 12 and discussed below.

The last set of results corresponds with the harshest of the adopted road conditions with the intensity of the road irregularities 1.5. Taking into account the almost different road profiles for the left and the right wheels, the  $\mu_x$  coefficient in Figure 11 was about 0.22 for the left front and 0.26 for the right front wheel, which is similar to the values obtained for configuration 5, also on a dry road. The  $\mu_y$  coefficient was about 0.11, which is also similar to the results for configuration 5. For the rear wheels, however, the maximum  $\mu_x$  coefficient was almost 0.8 for the left and almost 1 for the rear wheels, which is higher than in the case of configuration 5. The  $\mu_y$  coefficient was similar to that obtained for configuration



**Figure 10** Ellipses of adhesion between the wheels and the road for configuration 6

**Table 9** The forces between the road and the wheels for configuration 7 [21]

Left front wheel (LF)				Right front wheel (RF)		
	$F_{Xmax}$ [N]	$F_{Ymax}$ [N]	$F_{Zmax}$ [N]	$F_{Xmax}$ [N]	$F_{Ymax}$ [N]	$F_{Zmax}$ [N]
Max absolute	1708.59	848.5	7734.13	2062.91	862.01	7878.1
Left rear wheel (LR)				Right rear wheel (RR)		
	$F_{Xmax}$ [N]	$F_{Ymax}$ [N]	$F_{Zmax}$ [N]	$F_{Xmax}$ [N]	$F_{Ymax}$ [N]	$F_{Zmax}$ [N]
Max absolute	8049.54	1408.92	10251.4	9764.48	1149.82	10013.7

**Table 10** The forces between the road and the wheels for configuration 8 [21]

Left front wheel (LF)				Right front wheel (RF)		
	$F_{Xmax}$ [N]	$F_{Ymax}$ [N]	$F_{Zmax}$ [N]	$F_{Xmax}$ [N]	$F_{Ymax}$ [N]	$F_{Zmax}$ [N]
Max absolute	1629.48	717.01	7679.95	1822.09	722.8	7863.34
Left rear wheel (LR)				Right rear wheel (RR)		
	$F_{Xmax}$ [N]	$F_{Ymax}$ [N]	$F_{Zmax}$ [N]	$F_{Xmax}$ [N]	$F_{Ymax}$ [N]	$F_{Zmax}$ [N]
Max absolute	3678.81	1111.65	10318.8	3525.51	1062.44	11779.8

5 (about 0.14 for the left and about 0.11 for the right wheel).

As for configuration 8 (the icy road included with the same intensity of the irregularities), the  $\mu_x$  coefficient in the ellipse of adhesion (Figure 12) was about 0.21 for the left front and 0.23 for the right front wheel, which is greater than in the case of configuration 6 (lower amplitudes of the road irregularities). The  $\mu_y$  coefficient was about 0.09, which is also similar to the results for configuration 6.

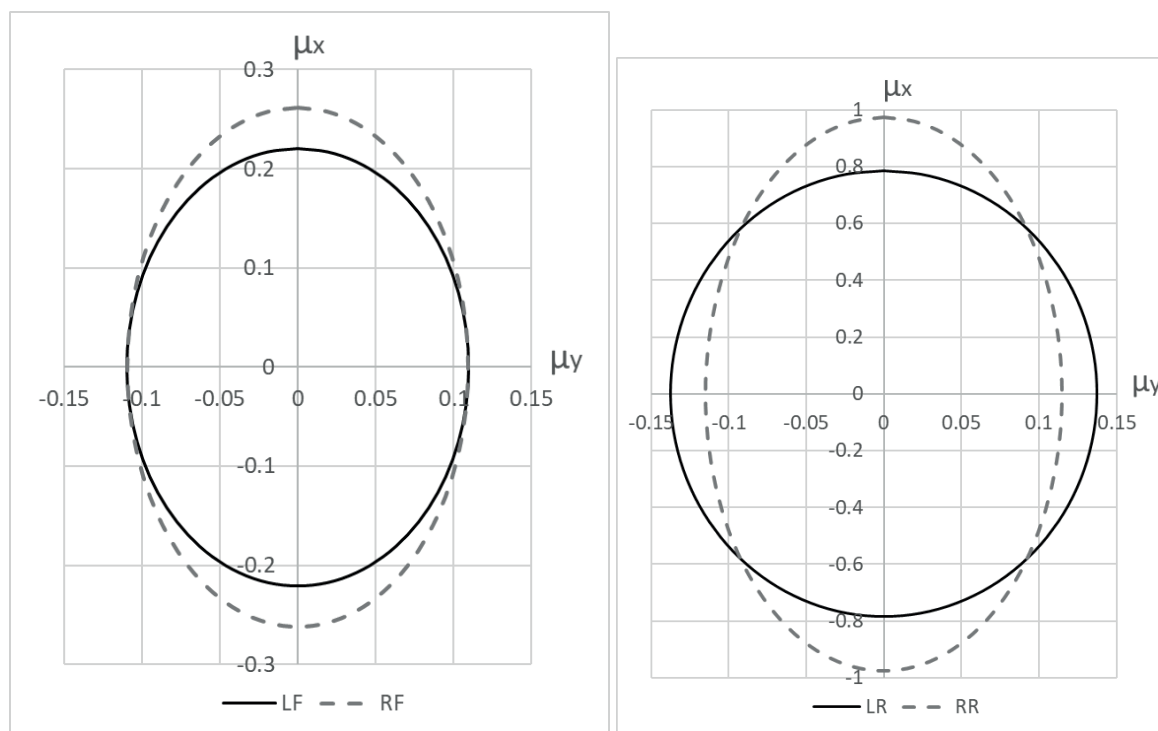
As for the rear wheels, the maximum  $\mu_x$  coefficient was about 0.35 for the left and 0.3 for the right wheel, which is not entirely similar to configuration 6. The  $\mu_y$

coefficient for the rear wheels was close to 0.11 for the left and about 0.09 for the right one. This was less than in the case of configuration 6.

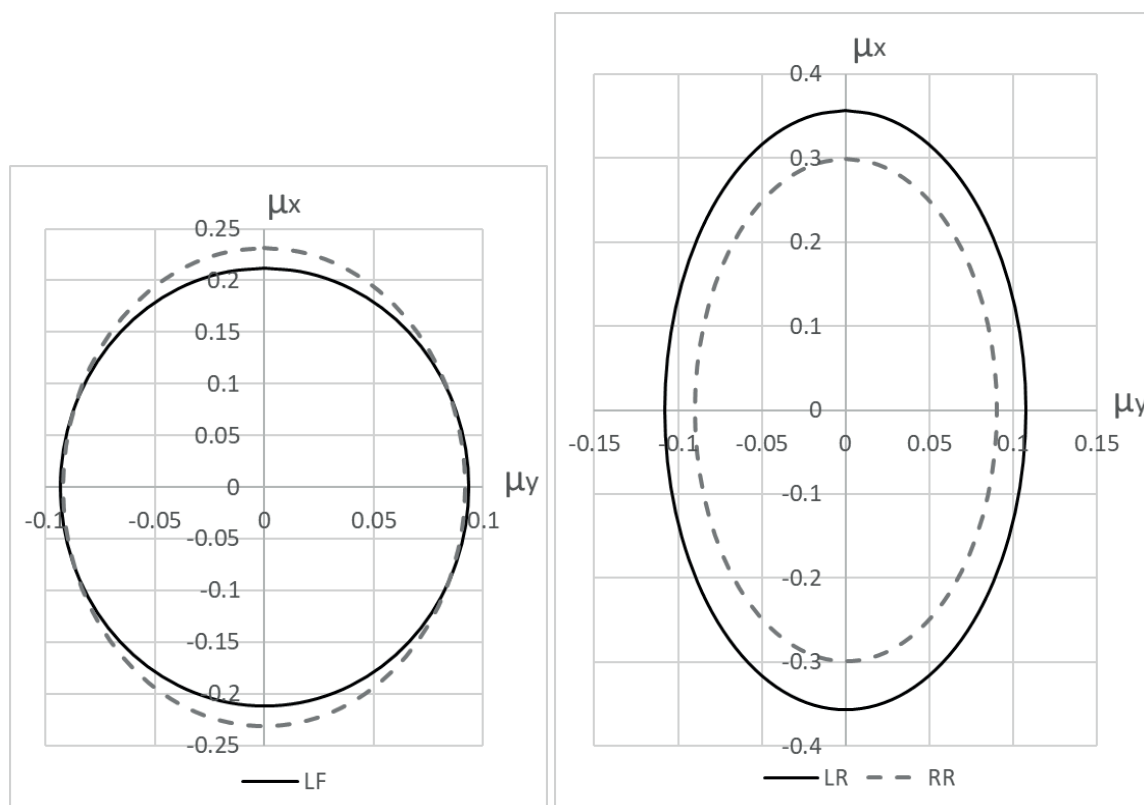
#### 4 Conclusions

From the presented results it can be concluded that the adopted road conditions, used in all the simulations, did not affect the lateral phenomena between the wheels and the road to any significant extent. However, when it comes to analyzing their influence on the longitudinal coefficient of adhesion the differences are





**Figure 11** Ellipses of adhesion between the wheels and the road for configuration 7



**Figure 12** Ellipses of adhesion between the wheels and the road for configuration 8

visible, especially for the rear wheels.

The low values of the coefficient of adhesion for the front wheels of a vehicle, despite the braking maneuver, indicate that the front of a vehicle was too light and laden too poorly, versus the rear where the engine is located to generate the greater adhesion.

The rear wheels however, tended to lose their adhesion for the more harsh road conditions, especially when the icy road was included. On the dry road the highest amplitudes of the irregularities provided the increase in the maximum coefficient of longitudinal adhesion ( $\mu_x$ ), which seems weird when one thinks of

the potential tendency to lose contact between the road and the wheels. However, maybe the higher amplitudes caused the increase of adhesion, when the contact between the road and the wheels was regained, and the normal force increased rapidly.

The higher amplitude of the random irregularities (up to 0.022m for the intensity 0.5, up to 0.035m for the intensity 1 and up to 0.055m for the intensity 1.5) along with the icy road caused the maximum values of the coefficient of adhesion decrease significantly, especially for the rear wheels of the vehicle. This was also caused by the uneven spread of mass in the vehicle's model.

One of the important indicators in such analyses seems to be the  $cor_n$  coefficient, providing almost similar or almost different road profiles.

Further research will include some other maneuvers

and other loading of a vehicle, along with different values of the intensity parameter.

### Acknowledgements

The authors received no financial support for the research, authorship and/or publication of this article.

### Conflicts of interest

The authors declare that they have no known competing financial interests or personal relationships that could have appeared to influence the work reported in this paper.

### References

- [1] SHAHDEHI, I. A., ALIMARDANI, M., RAZZAGHI-KASHANI, M., ROSHANAIEI, H. Adhesion and hysteretic friction of tire tread rubbers having process oils with different aromatic content. *Rubber Chemistry and Technology* [online]. 2022, **95** (4), p. 656-670. ISSN 0035-9475. Available from: <https://doi.org/10.5254/rct.22.77937>
- [2] TOLPEKINA, T. V., PERSSON, B. N. J. Adhesion and friction for three tire tread compounds. *Lubricants* [online]. 2019, **7**(3), 20. ISSN 2075-4442. Available from: <https://doi.org/10.3390/lubricants7030020>
- [3] ZHENG, B., HUANG, X., ZHANG, W., ZHAO, R., ZHU, S. Adhesion characteristics of tire-asphalt pavement interface based on a proposed tire hydroplaning model. *Advances in Materials Science and Engineering* [online]. 2018, **2018**, 5916180. ISSN 1687-8442. Available from: <https://doi.org/10.1155/2018/5916180>
- [4] ZHENG, B., TANG, J., CHEN, J., ZHAO, R., HUANG, X. Investigation of adhesion properties of tire-asphalt pavement interface considering hydrodynamic lubrication action of water film on road surface. *Materials* [online]. 2022, **15**(12), 4173. ISSN 1996-1944. Available from: <https://doi.org/10.3390/ma15124173>
- [5] ZHANG, Y., GAO, J., LI, Q. Experimental study on friction coefficients between tire tread rubber and ice. *AIP Advances* [online]. 2018, **8**(7), 075005. ISSN 2158-3226. Available from: <https://doi.org/10.1063/1.5041049>
- [6] CABRERA, J. A., CASTILLO, J. J., PEREZ, J., VELASCO, J. M., GUERRA, A. J., HERNANDEZ, P. A. Procedure for determining tire-road friction characteristics using a modification of the magic formula based on experimental results. *Sensors* [online]. 2018, **18**(3), 896, p. 1-17. ISSN 1424-8220. Available from: <https://doi.org/10.3390/s18030896>
- [7] MA, T., TANG, J., ZHENG, B., HUANG, X. Adhesion characteristics of vehicle tire and asphalt pavement under rainy conditions. *Journal of Beijing University of Technology* [online]. 2022, **48**(6), p. 635-643. ISSN 0254-0037. Available from: <https://doi.org/10.11936/bjtxb2021090024>
- [8] OH, Y., LEE, H. Characteristics of a tire friction and performances of a braking in a high speed driving. *Advances in Mechanical Engineering* [online]. 2014, **6**. ISSN 1687-8140. Available from: <https://doi.org/10.1155/2014/260428>
- [9] KHALEGHIAN, S., EMAMI, A., TAHERI, S. A technical survey on tire-road friction estimation. *Friction* [online]. 2017, **5**, p. 123-146. ISSN 2223-7690. Available from: <https://doi.org/10.1007/s40544-017-0151-0>
- [10] ZHAO, L., ZHAO, H., CAI, J. Tire-pavement friction modeling considering pavement texture and water film, *International Journal of Transportation Science and Technology* [online]. 2023, in press. ISSN 2046-0430. Available from: <https://doi.org/10.1016/j.ijtst.2023.04.001>
- [11] SHAOYI, B., BO, L., YANYAN, Z. Adhesion state estimation based on improved tire brush model. *Advances in Mechanical Engineering* [online]. 2018, **10**(1). ISSN 1687-8132. Available from: <https://doi.org/10.1177/1687814017747706>
- [12] WANG, Y., HU, J., WANG, F., DONG, H., YAN, Y., REN, Y., ZHOU, CH., YIN, G. Tire road friction coefficient estimation: review and research perspectives. *Chinese Journal of Mechanical Engineering* [online]. 2022, **35**, 6. ISSN 2192-8258. Available from: <https://doi.org/10.1186/s10033-021-00675-z>
- [13] WU, J., WANG, Y., SU, B., LIU, Q. Experimental and numerical studies on tire tread block friction characteristics based on a new test device. *Advances in Materials Science and Engineering* [online]. 2014, **2014**, 816204. ISSN 1687-8434. Available from: <http://dx.doi.org/10.1155/2014/816204>

- [14] LENG, B., JIN, D., XIONG, L., YANG, X., YU, Z. Estimation of tire-road peak adhesion coefficient for intelligent electric vehicles based on camera and tire dynamics information fusion. *Mechanical Systems and Signal Processing* [online]. 2021, **150**, 107275. ISSN 0888-3270. Available from: <https://doi.org/10.1016/j.ymssp.2020.107275>
- [15] HAIGERMOSER, A., LUBER, B., RAUH, J., GRAFE, G. Road and track irregularities: measurement, assessment and simulation. *Vehicle System Dynamics* [online]. 2015, **53**(7), p. 878-957. ISSN 1744-5159. Available from: <https://doi.org/10.1080/00423114.2015.1037312>
- [16] KORTIS, J., DANIEL, L., DURATNY, M., The simulation of the influence of surface irregularities in road pavements on the response of the bridge to moving vehicle. *Procedia Engineering* [online]. 2017, **199**, p. 2991-2996. ISSN 1877-7058. Available from: <https://doi.org/10.1016/j.proeng.2017.09.545>
- [17] NGUYEN, T., LECHNER, B., WONG, Y.D. Response-based methods to measure road surface irregularity: a state-of-the-art review. *European Transport Research Review* [online]. 2019, **11**, 43. ISSN 1866-8887. Available from: <https://doi.org/10.1186/s12544-019-0380-6>
- [18] PRAZNOWSKI, K., MAMALA, J., SMIEJA, M., KUPINA, M. Assessment of the road surface condition with longitudinal acceleration signal of the car body. *Sensors* [online]. 2020, **20**(21), 5987. ISSN 1424-8220. Available from: <https://doi.org/10.3390/s20215987>
- [19] RAPINO, L., LA PAGLIA, I., RIPAMONTI, F., CORRADI, R., DI LIONE, R., BARO, S. Measurement and processing of road irregularity for surface generation and tyre dynamics simulation in NVH context. *International Journal of Pavement Research and Technology* [online]. 2023. ISSN 1997-1400. Available from: <https://doi.org/10.1007/s42947-023-00277-z>
- [20] ZHANG, J., YANG, S., LI, S., LU, Y., DING, H. Influence of vehicle-road coupled vibration on tire adhesion based on nonlinear foundation. *Applied Mathematics and Mechanics* [online]. 2021, **42**, p. 607-624. ISSN 1573-2754. Available from: <https://doi.org/10.1007/s10483-021-2724-6>
- [21] ZALEWSKI, J. The Impact of Road Irregularities on the Motion of a Motor Vehicle during Acceleration. *Communications - Scientific Letters of the University of Zilina* [online]. 2022, **24**(2), p. 135-147. ISSN 1335-4205. Available from: doi: 10.26552/com.C.2022.2.B135-B147
- [22] Adams/Tire User's Guide, MSC Software.



This is an open access article distributed under the terms of the Creative Commons Attribution 4.0 International License (CC BY 4.0), which permits use, distribution, and reproduction in any medium, provided the original publication is properly cited. No use, distribution or reproduction is permitted which does not comply with these terms.

# TRANSPORT EFFICIENCY STRATEGIES IN ASSEMBLY WORKPLACE: A CASE STUDY

Dariusz Plinta<sup>1</sup>, Luboslav Dulina<sup>1</sup>, Beáta Furmannová<sup>2</sup>, Ján Zuzik<sup>2,\*</sup>

<sup>1</sup>Department of Industrial Engineering, Faculty of Mechanical Engineering and Computer Science, University of Bielsko-Biala, Bielsko-Biala, Poland

<sup>2</sup>Department of Industrial Engineering, Faculty of Mechanical Engineering, University of Zilina, Zilina, Slovakia

\*E-mail of corresponding author: jan.zuzik@fstroj.uniza.sk

Dariusz Plinta 0000-0002-4638-5319,  
Beáta Furmannová 0000-0001-5355-2464,

Luboslav Dulina 00000-0002-5385-7476,  
Ján Zuzik 0000-0003-2992-7064

## Resume

In this article, improvements in assembly workplace layouts in an industrial context are investigated to enhance productivity and efficiency. The installation of the Cleaner M300 device is focused on, existing layout challenges are identified, and targeted improvements are proposed. Data collection, analysis, and real-world experimentation are employed to evaluate current workplace conditions and potential enhancements, including material flow dynamics and transport cart utilization. Proposed solutions are aimed at streamlining assembly processes, minimizing material transportation time, and boosting operational efficiency. The effectiveness of these improvements is validated through qualitative feedback from workers and supervisors. The importance of improving workplace design to enhance manufacturing operations, increase productivity, and improve transport efficiency is underscored by the study.

## Article info

Received 11 April 2024

Accepted 28 May 2024

Online 21 June 2024

## Keywords:

mechanical engineering  
industrial engineering  
transport  
design  
assembly  
improved layout

Available online: <https://doi.org/10.26552/com.C.2024.035>

ISSN 1335-4205 (print version)

ISSN 2585-7878 (online version)

## 1 Introduction

Efficient workplace design is crucial for maximizing productivity and improving operational performance in various industries, particularly in manufacturing environments [1-3]. The layout of assembly workplaces significantly influences workflow efficiency, material handling, and overall productivity [4-6]. This scientific article is focused on the comprehensive evaluation and proposed enhancements of assembly workplace layouts within an industrial context.

A thorough analysis of the current state of a selected workplace is entailed by the study, with a specific focus on the installation of the Cleaner M300 device.

Through meticulous examination, existing layout challenges and inefficiencies are identified, providing the groundwork for targeted improvement measures.

The proposed solutions aim to streamline assembly processes, minimize material transportation time, and enhance the overall ergonomic design of the workplace. Key aspects of the proposed measures include a detailed

overview of the current workplace layout and strategies for reducing the number of transport carts required for efficient operations [7-10].

Specific subtopics outlined in subsequent sections, such as the current and proposed layout of the assembly workplace, and the reduction in the number of transport carts with material, are explored in this study to offer valuable insights and actionable recommendations for improving assembly workplace layouts and enhancing operational efficiency.

A combination of data analysis, software utilization, and real-world experimentation is employed in this research to provide practical solutions for enhancing workplace productivity and performance. [11-13].

## 2 Material and methods

This section presents an outline of the methodology employed in workplace design aimed at enhancing transportation, workplace layout, material flows,

and productivity augmentation. The study employed a blend of data collection, analysis, software utilization, and real-world data obtained from an industrial entity.

The current state of the workplace and subsequent proposals for their enhancement were determined through material flow analysis using the assessments delineated in the third section and the fourth case study.

The company for the investigation was selected due to its alignment with the research goals and feasibility of collaboration. Data acquisition encompassed the compilation of data concerning the current workplace arrangement and manufacturing procedures via onsite observations, interviews, and document scrutiny.

The AutoCAD and Delmia software packages were employed for evaluating the existing conditions and suggesting remedies. Those aided in generating visual representations of the workplace and production system, as well as assessing various solution alternatives. Data visualization was utilized for result interpretation and trend identification.

The investigation yielded a notable decrease in transportation duration, underscoring the efficacy of the recommended layout enhancements. Substantive input from employees and supervisors offered insightful perspectives on the usability and feasibility of the novel layout proposals.

In essence, the significance of refining workplace design to improve material flows and elevate operational efficiency, particularly concerning transportation, is underscored by the study.

### 3 Case study

The primary aim of this investigation was to suggest enhancements to the configuration of the working environment. The arrangement of the workplace has been addressed within the chosen organization, which specializes in the manufacturing of components.

The sub-objectives of the case study include:

- Research the company from the manufacturing sector and examine the range of activities and services provided by the company.
- Analyze the current state of the selected company, in which the case study is being implemented, in the field of production system deployment.
- Examine the layout of the equipment assembly workplace.
- Analyze transportation and transport of material within the production system.

A production process encompasses a series of orchestrated activities involving human resources, production facilities, and physical operations, necessitating one or more forms of inputs to yield an output of value to the consumer. Such activities involve the conversion of raw materials into a finished product or the fulfillment of a customer service request [14-16].

To optimize the operational efficiency of the

production system, particular facets of the production process were scrutinized in this investigation, with a specific focus on the flow of production and layout within the company. The objective was to enhance the transformation of inputs into valuable outputs for the clientele. Considering that customers typically have restricted insight into the realization of these outputs, their paramount interest lies in the end product or service [17-20].

#### 3.1 Revealing the analyzed firm: comprehensive company overview

The establishment located in Slovakia, established in December 1995, sustains an employee count of approximately 270 individuals. Its primary objective entails the fabrication and processing of comprehensive systems for the global semiconductor and electrotechnical sectors. Its product portfolio encompasses solar energy resources and the assembly of machinery for solar cell manufacturing. The engineering division has spearheaded numerous projects upon the request of client enterprises, inclusive of developmental initiatives and structural designs tailored for the electrical industry. The organization has delineated objectives for each division annually, with the overarching aim of attaining a preeminent stance within the energy-solar industry domain by delivering high-caliber output at a competitive pricing tier. Presently, the focus of the company lies in the production and assembly of diverse equipment varieties tailored for both the electrotechnical sector and the burgeoning energy solar market.

In Figure 1, one can see selected production equipment that is manufactured by the company. The M 600 Cleaner device is used to clean or maintain certain components or parts in the production process. The Cleanroom 10'000 device is designed to protect sensitive processes and products from contamination from the environment. A wafer sorter is a device used in semiconductor manufacturing to sort and arrange silicon wafers, also called "wafers", according to specified criteria.

#### 3.2 Description of the investigated selected device

The configuration of the assembly environment dedicated to fabricating the Cleaner M 300 apparatus is endeavored to be enhanced by the research. This device can be seen in Figure 2. This semi-automated device is integral to the "wet" process, specifically designed for cleansing wafer transport enclosures utilized in board carrier manipulation. Board carriers serve as conduits for silicon boards (wafers), fundamental components in semiconductor manufacturing employed across diverse electronic sectors, including computer





**Figure 1** Crafted precision: Company's cutting-edge production equipment



**Figure 2** Visual Representation of Engineered Machinery Cleaner M 300

technology, consumer electronics, telecommunications, and automotive industries, among others.

The transportation of this material necessitates a highly pristine and dust-free environment. The company's apparatus undergoes a rigorous cleaning process utilizing pressurized deionized water, coupled with rotational motion and subsequent drying, ensuring

the thorough cleansing of transport containers, rendering them impeccably prepared for the conveyance of compatible materials. These devices are fabricated to exacting standards of quality, representing some of the most widely utilized and distinctive machinery within this domain.

The intricately structured device comprises

numerous components, necessitating its categorization into five primary segments, specifically:

- Structural Component,
- Electrical and Propulsion Components,
- Process Component,
- Pneumatic and Water Components,
- Complete Encasement.

### 3.3 Description of the selected workplace: comprehensive overview

Presently, the majority of products encompass intricate mechatronic apparatuses, such as the Cleaner M300 device. Consequently, the assembly process encompasses not only mechanical component integration, but the interconnection of electrical, hydraulic, or pneumatic circuits, as well. The equipment is incorporated into piece (small-batch) production, characterized by a diverse range of products, each manufactured in quantities ranging from 1 to 50 pieces (e.g., Cleaner M204, Wafer sorter M20, Reticle stocker M1990). The assembly process adheres to stationary assembly principles, characterized by:

- Assembly conducted at a single location by one or more workers,
- Adherence to established assembly protocols with predefined time constraints (time standards), dictating the sequence of assembly operations.

The primary advantage of this assembly approach lies in its adaptability to changes in the production schedule. The mounting system for the Cleaner M300 is classified as a nest mounting system, distinguished by its solitary or partially isolated placement from other nests. Installation of this equipment typically involves 2 or 3 highly skilled workers, responsible for overseeing all aspects of the work. Worker roles are specialized in two professions: electrical assembly and mechanical assembly.

The cumulative assembly duration amounted to 588 hours, delineated across various stages. Foundry and welding operations accounted for 207 hours, while electrical assembly required 168 hours. Mechanical and pneumatic assembly tasks consumed 201 hours, with an additional 27 hours dedicated to IBN (In-Bonded Inspection) inspection and testing procedures.

Figure 3 illustrates the layout of the assembly facility within the company premises using the AutoCAD software.

Figure 3 provides an overview of the complete configuration of the production system, with a focused depiction delineated within the green circumscription, offering detailed elucidation of the assembly workspace dedicated to the Cleaner M 300 apparatus, inclusive of comprehensive annotations regarding its constituent devices. The assembly workplace, as can be seen explained in the lower part of the picture, contains the device Cleaner M300, assembly table, side table,

cart with material, small cart with material, trash and chair.

## 4 Proposal for assembly workplace layout improvement

In the process of design, it is imperative to consider all facets comprehensively to mitigate the time losses, diminish the risk of material degradation during the transportation, and curtail material costs. Consequently, two prospective configurations for the workplace layout have been proposed.

In response to the requirements, the following principles, governing material flow and workplace arrangement in assembly have been delineated:

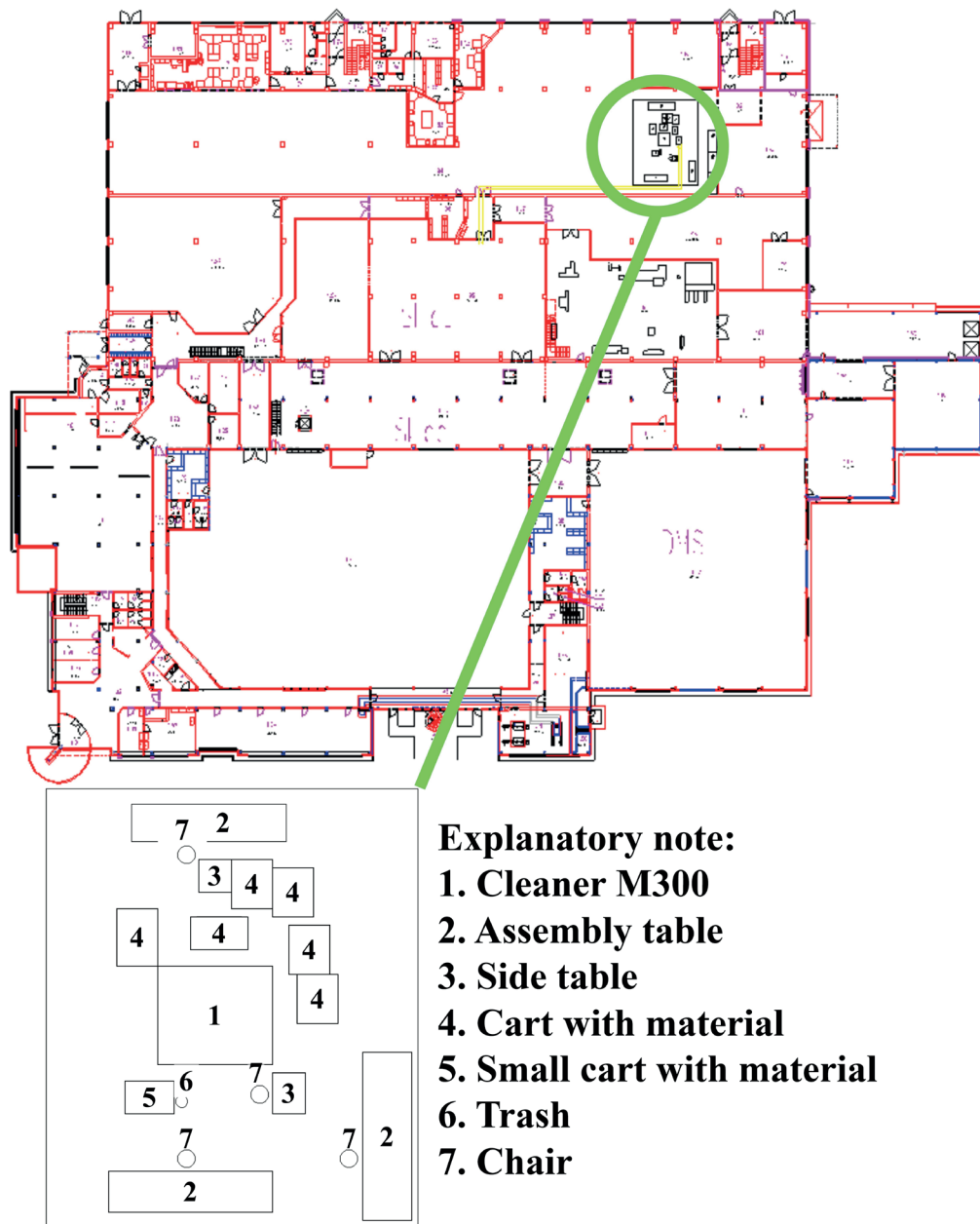
- Proximity of the warehouse to the assembly, workplace is essential,
- Assembly workstations should be configured to minimize material transit distances and prevent crossflow,
- For mobile assembly setups, ensuring the timely supply of input materials to workstations and facilitating inter-operational transport is paramount,
- Concluding operations such as inspection, testing, surface treatment, packaging, and shipping should follow the final assembly operation,
- The improved layout of mounting points is contingent upon factors including the type, complexity, and dimensions of assembled products and the seriality and repeatability of the production processes,
- Spatial arrangement considerations may commence concerning a catalog of standard assembly locations, which addresses mounting site allocation, access to assembly units, equipment handling, and worker positioning.

Additionally, an ergonomic approach is integral to the design of manual assembly workstations:

- Tools should be organized based on the sequence of assembly tasks,
- Tools and aids should be stored according to their frequency of use and weight,
- Storage of tools should be so oriented to accommodate right or left-handed workers,
- Dedicated fixed locations should be designated for the storage of tools and aids,
- Tools and aids should consistently be stored within the worker's reach zone.

### 4.1 Proposal of measures leading to an improved layout of the assembly workplace

This section provides a detailed description of both the existing and proposed arrangements of the Cleaner M300 assembly workspace. Subsequently, an alternative approach, aimed at minimizing the quantity of material



**Figure 3** Graphic representation of the workplace layout

transport carts, is delineated, including an analysis of both the current status and the proposed design.

In the process of layout design, it is imperative to consider spatial dimensions meticulously to ensure optimal placement of the workplace. This entails providing adequate distances between assembly tables, equipment, and material carts to facilitate efficient workflow. Material transport carts are utilized for the conveyance of materials and constitute integral components in material flow management.

#### 4.1.1 Current layout of the workplace for the installation of the Cleaner M300 device

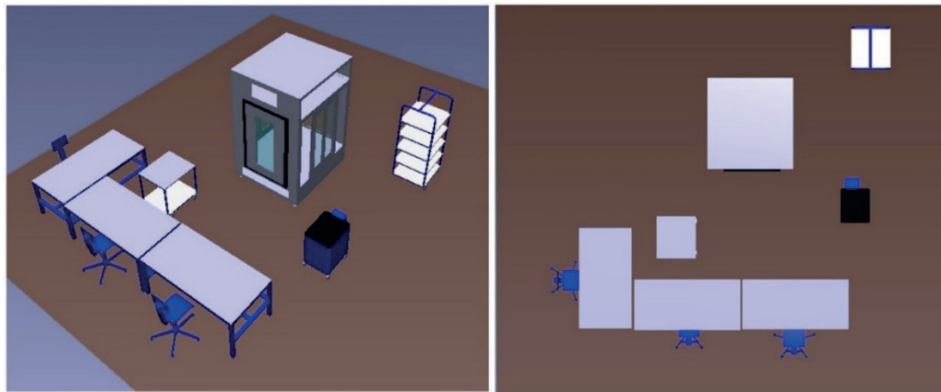
The layout of the assembly workplace is currently placed in an inappropriate way, which results in:

- Difficult access to the used material (carts are lined up tightly),
- Inappropriate arrangement of pre-assembly parts,
- The carts are located at an inappropriate distance from the equipment, which forces the employee to move away from the assembly workplace and thus leads to time losses that could have been used more efficiently for work on the given operation,
- Improper arrangement of carts with material results in limited movement of workers around the equipment,
- There is material at the workplace that is not necessary for assembly in the current state of development of the device.

Figure 4 shows the current layout of the workplace. The design of the workplace also took into account the storage and subsequent inspection of



**Figure 4** Current layout of the assembly workplace



**Figure 5** The first variant of the L-shaped arrangement of assembly trolleys

the Cleaner M300 device. These two aspects were not of much importance, since the warehouse and control have well-defined areas that are conveniently located.

Particular attention was paid to the arrangement of the assembly workplace itself. The dimensional arrangement according to the catalog of typical mounting points was taken into account. Important is the used space, which will be created in this design by rearrangement. In this way, the free capacity would be created for the assembly of a second device of the same type, which would increase production. By suitably organizing the workplace, the accident rate at the workplace would be reduced and sufficient spaces will be created for the movement of the worker around the equipment. Appropriate arrangement of the tools and used material according to the principles of ergonomic design would facilitate and speed up the assembly of the device, thereby reducing the overall assembly time.

#### 4.1.2 Design layout of the workplace for installation of the cleaner M300 device

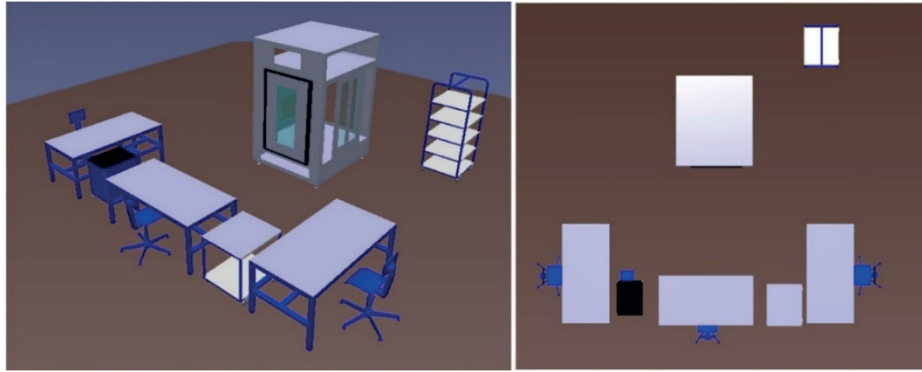
Upon thorough review of pertinent documentation, regarding layout alternatives and appropriate workplace dimensions, two layout variants were proposed for the company.

The first proposed variant entails an L-shaped configuration of assembly trolleys, occupying minimal space and arranged around the device at an appropriate distance. This setup features two carts - a supplementary cart and a smaller cart housing materials - both maneuvering around the device without designated fixed locations. The number of material carts has been reduced from six to either one or two, contingent upon the requirements of the assembly operator. The first variant can be seen in Figure 5.

In the second variant, assembly tables were arranged in a U-shaped configuration, with the intervening spaces filled by mobile carts (auxiliary cart, small cart with material). This positioning ensures unimpeded movement for workers around the equipment, thereby enhancing workplace safety. Through the reduction of material carts and consequent space savings, additional room was made available for the installation of another Cleaner M300 device. The second variant can be seen in Figure 6.

Upon presentation of the proposals to the company, it was assessed that the optimal arrangement for the new layout would be the first variant. This decision was reached based on the rationale that the small mobile carts, being in constant motion around the facility, do not require dedicated permanent space. Consequently, the allocation of space for them in the second variant unnecessarily occupies valuable space that could be utilized more efficiently. Therefore, the first variant



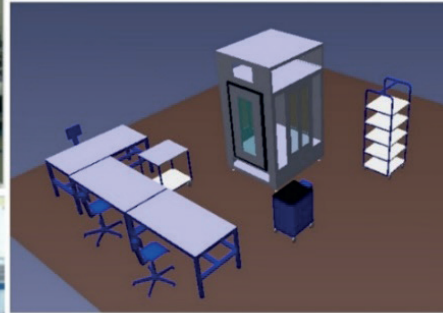


**Figure 6** The second variant of the U-shaped arrangement of assembly trolleys

## BEFORE



## AFTER



**Figure 7** View of the workplace before the new layout and after processing the design of the new layout

stands as an enhanced solution and recommendation for the company.

### 4.2 Reduction in the number of transport carts with material

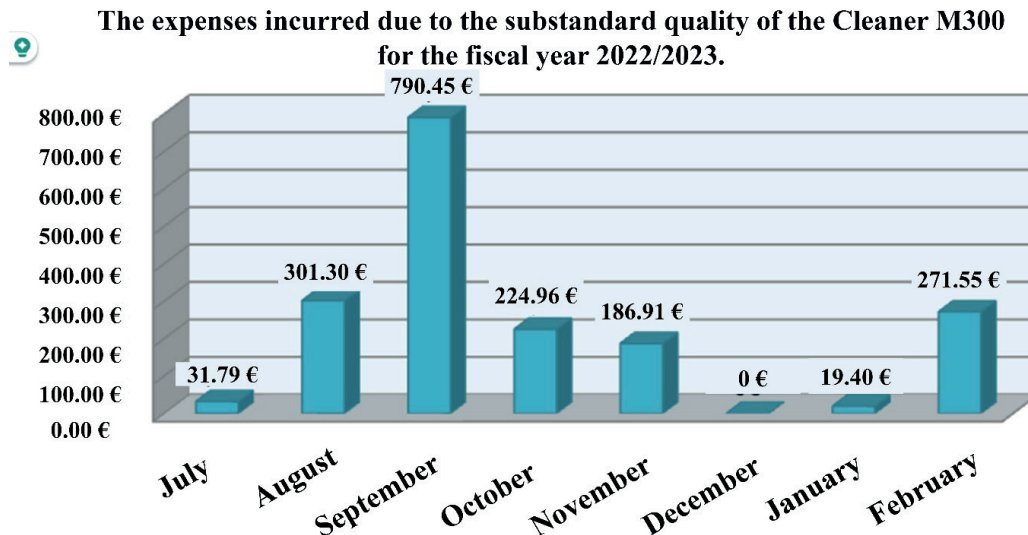
The basic task of material handling is the temporal and spatial connection of the production process and material consumption. It was decided to reduce the number of carts, which will reduce the area of the entire assembly workplace and thus create space for the assembly of a second device of the same type, increase the quality of the material, and shorten the time of transporting the material and the time of the overall assembly of the Cleaner M300 device. View of the workplace before the new layout and after processing the design of the new layout can be seen in Figure 7.

#### 4.2.1 The current state of transport trucks with material

Presently, a defined sequence of individual operations is lacking, necessitating the simultaneous movement of 6 material carts from the warehouse to the workplace by the worker. Additional carts are consistently in stock, as carts for other equipment are also being retrieved. The worker is obliged to seek out suitable carts for assembly, resulting in time losses that could otherwise be allocated to the assembly process on the designated equipment.

Currently, during the initial phase of assembly, the worker transports 6 material carts to the device, consuming approximately 15 minutes. The carts, being relatively heavy, necessitate careful transportation, requiring approximately 2.5 minutes per cart to traverse the 100-meter distance from the warehouse to the





**Figure 8** Figure of costs for the poor quality of the Cleaner M300 device

workplace. Following the completion of equipment assembly, the carts must be returned to the warehouse, a process taking approximately 9 minutes. Notably, this duration is shorter since the carts being empty, allowing for the transportation of two carts simultaneously. The cumulative time for transporting material carts to and from the warehouse totals 24 minutes. Most of the worker's time is spent selecting a suitable cart from the warehouse, a duration included in the cart transportation time. Six carts are present at the workplace, constraining the movement of the worker or workers currently engaged in assembling the respective component. Furthermore, these carts occupy valuable workspace.

Material retrieval occurs at the initiation of Cleaner M300 assembly, requiring 0.25 hours, and after assembly, when carts are returned to the warehouse, necessitating 0.15 hours.

The materials required for assembling the polished parts of the device (carousels) must remain undamaged and flawless throughout the transportation. Damage to the materials often arises due to prolonged stationary positioning and frequent manipulation around them, or when materials intended for other operations are extracted from the cart. Given the considerable expense associated with these materials, any damage incurred leads to significant losses, subsequently elevating costs and compromising quality. Moreover, the necessity to replace the damaged materials further exacerbates time and cost burdens.

The company provided data related to the cost of poor quality. Figure 8 shows the current state of the costs of poor quality. The fluctuations shown in Figure 8 were caused by the changing volume of production in individual months. Figure 8 demonstrates a notable fluctuation in the cost of poor quality across the examined months. Specifically, in July, the cost was €31.79. This figure escalated significantly in August,

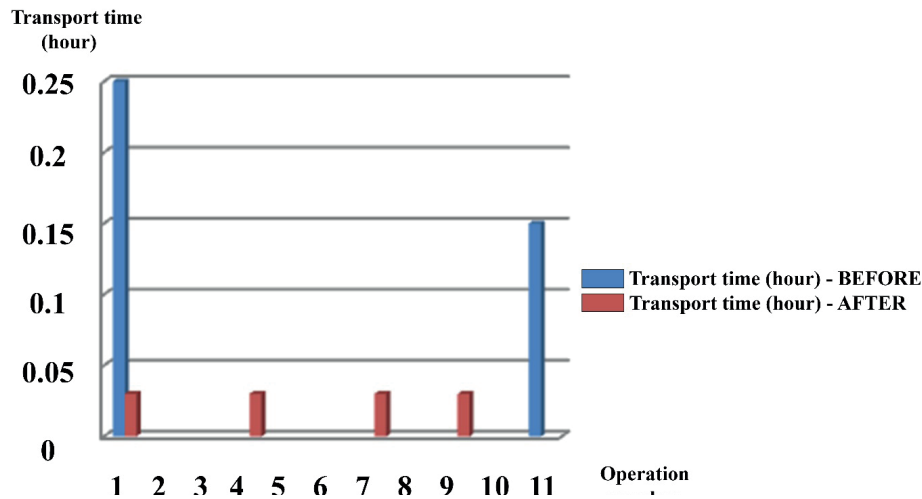
reaching €301.30. The highest cost was recorded in September, amounting to €790.45. In October, the cost decreased to €224.96, followed by a further reduction to €186.91 in November. Remarkably, December exhibited optimal conditions with no cost of poor quality reported, amounting to €0. The cost in January was €19.40, which then increased to €271.55 in February.

#### 4.2.2 The design state of transport trucks with material

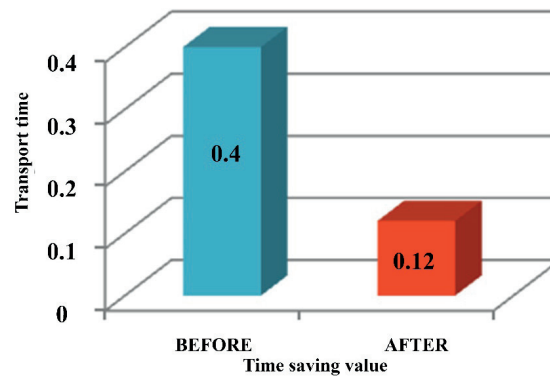
By implementing an appropriate technological procedure, it is feasible to reduce the number of original 6 trolleys to 1-2 trolleys.

With the assistance of the company's personnel, we conducted an in-depth examination of the entire procedure, which was previously established but lacked a specified sequence. The procedure underwent meticulous analysis, inclusive of individual operation times, leading to the development of a new material-picking technological procedure with the requisite sequence. Subsequently, it was segmented into four main groups based on material retrieval from the warehouse. The picking procedure was ultimately partitioned into a technological framework, utilized for designing an enhanced layout in DELMIA Process Engineer. By implementing the new picking procedure, material carts would be selected based on the component of the equipment being assembled, enabling employees to select a cart labeled with the appropriate number (1 to 4) without wasting time searching for a suitable cart.

This approach ensures that the material required for assembly at any given moment consistently arrives at the workplace, thereby reducing the truck transport time and the time spent selecting suitable trucks. Whereas the original technological procedure involved



**Figure 9** Comparison of material transport before and after the modification of the technological procedure



**Figure 10** Representation of time savings for material transport

the simultaneous retrieval of all the carts by the employee, the modified approach involved carts being retrieved one at a time and prepared in the warehouse for the employee according to numerical order. Consequently, the employee retrieves a single cart without the need for a search, reducing retrieval time from 2.5 minutes to 1.8 minutes. Upon completing the installation of relevant materials on the device, the employee returns with an empty cart to the warehouse and immediately retrieves another pre-prepared cart. This process repeats until the final assembly of the device.

This method reduced material transport time by up to 70% and a 6% decrease in total assembly time, while reducing the transportation time for a single truck by 25%. The distribution of individual cart transport and the color-coded cart picking can be observed in Table 1.

In Figure 9, is shown the comparison of a material transport before and after the modification of the technological procedure, distinguished by colors. Before the creation of the new picking procedure, the material was transported at the beginning of the assembly of the device, which took 0.25 hours (15 minutes), and at the end of the assembly with a time of 0.15 hours (9 minutes), which together makes up a time of 0.40 hours (24 minutes).

After the introduction of the new procedure, the transportation of the material was divided 4 times, while the cart with the material was brought to the workplace only when the material was mounted on the equipment at that moment. The possible time saving is calculated for one cart from the original 2.5 minutes to 1.8 minutes, where 0.7 minutes were saved.

Figure 10 illustrates the reduction in material transportation time from the warehouse to the workplace, where the time was decreased from the original 0.40 hours (24 minutes) to 0.12 hours (7.2 minutes), resulting in a savings of 0.28 hours (16.8 minutes).

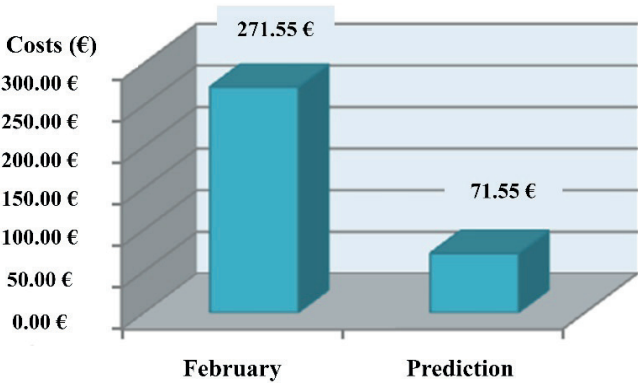
Thanks to the new picking procedure, it is possible to mitigate the material degradation, particularly for polished parts. The material cart will only be dispatched from the warehouse to the workplace when the specific part is being assembled on the device.

Figure 11 illustrates the costs associated with poor quality for February 2023, amounting to € 271.55, with € 200 attributed to the cost of damaged polished material. This damage occurred due to prolonged storage in one location and constant manipulation, or when the material was removed from the cart for other operations.

Therefore, cost savings can be achieved if the cart is prepared for the job site when the relevant part is

**Table 1** Modified technological procedure for assembling the device with new transport times

Operation number	Description of the operation	Transport - current state (h)	Transport - design state (h)	Type of trolley for design state
1	Bringing the supporting part	0.25	0.03	Trolley
2	Preparation of electric plate			
3	Installation of electric plate			
4	Preparation of pneumatic plate		0.03	Trolley
5	Installation of a pneumatic plate			
6	Installation of moving parts of the door			
7	Assembly of the chemical part		0.03	Trolley
8	Installation of water nozzles and heating elements			
9	Pre-assembly of polished parts		0.03	
10	Installation of polished parts			Trolley
11	Carousel and door installation	0.15		
12	Casing assembly			
Total transport time		0.40 h = 24 min	0.12 h = 7.2 min	



**Figure 11** Cost of poor quality for February and estimated cost savings

promptly mounted on the equipment. The estimated cost savings amount to approximately € 200, leading to a reduction in material costs by 73.65 %.

**5 Conclusion**

In conclusion, the layout of the Cleaner M300 assembly workplace is endeavored to be enhanced through a meticulous analysis of its current state. Comprehensive documentation was meticulously prepared to facilitate the design of improved variants. To facilitate comprehension, the assembly workplace was succinctly depicted using the AutoCAD graphics program, subsequently integrated into the broader company layout. This integration allowed for a gradual examination of problematic areas within the workplace, which served as the focal point of this case study. Identified issues encompassed challenging material

access, suboptimal arrangement of pre-assembly tables, improper cart positioning about equipment, restricted worker mobility, surplus material accumulation, and protracted material transport times.

Moreover, this study introduces partial digitization of the company, leveraging Delmia software to craft visualizations of proposed solutions. In response to identified challenges, various strategies were proposed. These include adopting improved methods for material storage to mitigate damage risks, expanding space around the assembly workplace to enhance safety, optimizing cart placement to streamline assembly processes, and rationalizing material distribution to minimize worker movement.

A key proposal involves reducing the number of material carts from six to one or two, affording several advantages. This reduction optimizes space utilization, potentially accommodating additional equipment while curbing material damage and associated

costs. Additionally, it promises to expedite material transportation, thereby augmenting overall efficiency.

Anticipated benefits of these interventions encompass diminished material damage and costs, heightened workplace safety, reduced spatial requirements for assembly, shorter transport durations, heightened productivity, and enhanced operational efficiency. Through meticulous analysis and strategic proposals, the Cleaner M300 assembly workplace is endeavored to be improved, offering a pathway to enhanced performance and resource utilization within the company's operational framework.

## Acknowledgments

This work was supported by the KEGA Agency under the contract 001ZU-4/2024.

## Conflicts of interest

The authors declare that they have no known competing financial interests or personal relationships that could have appeared to influence the work reported in this paper.

## References

- [1] BESTVINOVA, V., PRAJ, F., CAMBAL, M. Identification of sustainability risks and their quantification in the conditions of small and medium-sized industrial enterprises. *MM Science Journal* [online]. 2022, **11**(2022), p. 6086-6090 [accessed 2024-03-10]. ISSN 1803-1269. Available from: [https://doi.org/10.17973/MMSJ.2022\\_11\\_2022137](https://doi.org/10.17973/MMSJ.2022_11_2022137)
- [2] PEKARCIKOVA, M., TREBUNA, P., KLIMENT, M., KRAL, S., DIC, M. Modelling and simulation of the value stream mapping - case study. *Management and Production Engineering Review* [online]. 2021, **12**(2), p. 107-114 [accessed 2024-03-12]. ISSN 2080-8208. Available from: <https://doi.org/10.24425/mper.2021.137683>
- [3] PEKARCIKOVA, M., TREBUNA, P., KLIMENT, M., TROJAN, J., KOPEC, J., DIC, M., KRONOVA, J. Case study: testing the overall efficiency of equipment in the production process in TX plant simulation software. *Management and Production Engineering Review* [online]. 2023, **14**(1), p. 34-42 [accessed 2024-03-12]. ISSN 2080-8208. Available from: <https://doi.org/10.24425/mper.2023.145364>
- [4] PLINTA, D., RADWAN, K. Implementation of technological innovation in a manufacturing company. *Applied Sciences* [online]. 2023, **13**(10), 6068 [accessed 2024-03-14]. ISSN 2076-3417. Available from: <https://doi.org/10.3390/app13106068>
- [5] MICIETA, B., BINASOVA, V., MARCAN, P., GASO, M. Interfacing the control systems of enterprise-level process equipment with a robot operating system. *Electronics* [online]. 2023, **12**(18), 3871 [accessed 2024-03-14]. ISSN 2079-9292. Available from: <https://doi.org/10.3390/electronics12183871>
- [6] BUCKOVA, M., KRAJCOVIC, M., JERMAN, B. Impact of digital factory tools on designing of warehouses. *Journal of Applied Engineering Science*, [online]. 2017, **15**(2), p. 173-180 [accessed 2024-03-12]. ISSN 1451-4117. Available from: <https://doi.org/10.5937/jaes15-13245>
- [7] KOVAC, J., MALEGA, P., RUDY, V., SVETLIK, J. Vumark's method of production layout designing. *Applied Sciences* [online]. 2023, **13**(3), 1496 [accessed 2024-03-14]. ISSN 2076-3417. Available from: <https://doi.org/10.3390/app13031496>
- [8] RAKYTA, M., BUBENIK, P., BINASOVA, V., MICIETA, B., STAFFENOVA, K. Advanced logistics strategy of a company to create sustainable development in the industrial area. *Sustainability* [online]. 2022, **14**(19), 12659 [accessed 2024-03-14]. ISSN 2071-1050. Available from: <https://doi.org/10.3390/su141912659>
- [9] MOZOLOVA, L., GRZNAR, P., MOZOL, S., KRAJCOVIC, M. Streamlining utilisation of the assembly line using computer simulation. *Acta Logistica* [online]. 2023, **10**(2), p. 165-173 [accessed 2024-03-14]. ISSN 1339-5629. Available from: <https://doi.org/10.22306/al.v10i2.365>
- [10] MICIETA, B., STASZEWSKA, J., KOVALSKY, M., KRAJCOVIC, M., BINASOVA, V., PAPANEK, L., ANTONIUK, I. Innovative system for scheduling production using a combination of parametric simulation models. *Sustainability* [online]. 2021, **13**(17), 9518 [accessed 2024-03-14]. ISSN 2071-1050. Available from: <https://doi.org/10.3390/su13179518>
- [11] KLIMENT, M., TREBUNA, P., PEKARCIKOVA, M., STRAKA, M., TROJAN, J., DUDA, R. Production efficiency evaluation and products' quality improvement using simulation. *International Journal of Simulation Modelling* [online]. 2020, **19**(3), p. 470-481 [accessed 2024-03-14]. ISSN 1726-4529. Available from: <https://doi.org/10.2507/IJSIMM19-3-528>
- [12] LORINCOVA, S., CAMBAL, M., MIKLOSIK, A., BALAZOVA, Z., BABELOVA, Z. G., HITKA, M. Sustainability in business process management as an important strategic challenge in human resource management. *Sustainability* [online]. 2020, **12**(15), 5941 [accessed 2024-03-17]. ISSN 2071-1050. Available from: <https://doi.org/10.3390/SU12155941>

- [13] SZABO, P., MLKVA, M., MARKOVA, P., SAMAKOVA, J., JANIK, S. Change of competences in the context of industry 4.0 implementation. *Applied Sciences* [online]. 2023, **13**(14), 8547 [accessed 2024-03-14]. ISSN 2076-3417. Available from: <https://doi.org/10.3390/app13148547>
- [14] KRALIK, M., JERZ, V., PASTEKA, M. Optimization of the machine and device layout solution in a specific company production. *Lecture Notes in Mechanical Engineering*, [online]. 2020, **10**(2020), p. 91-103 [accessed 2024-03-14]. ISSN 2195-4356. Available from: [https://doi.org/10.1007/978-3-030-31343-2\\_8](https://doi.org/10.1007/978-3-030-31343-2_8)
- [15] GRZNAR, P., BURGANOVA, N., MOZOL, S., MOZOLOVA, L. A Comprehensive digital model approach for adaptive manufacturing systems. *Applied Sciences* [online]. 2023, **13**(19), 10706 [accessed 2024-03-14]. ISSN 2076-3417. Available from: <https://doi.org/10.3390/app131910706>
- [16] GRZNAR, P., KRAJCOVIC, M., GOLA, A., DULINA, L., FURMANNOVA, B., MOZOL, S., PLINTA, D., BURGANOVA, N., DANILCZUK, W., SVITEK, R. The use of a genetic algorithm for sorting warehouse optimisation. *Processes* [online]. 2021, **9**(7), 1197 [accessed 2024-03-14]. ISSN 2227-9717. Available from: <https://doi.org/10.3390/pr9071197>
- [17] ANTONIUK, I., SVITEK, R., KRAJCOVIC, M., FURMANNOVA, B. Methodology of design and optimization of internal logistics in the concept of industry 4.0. *Transportation Research Procedia* [online]. 2021, **55**(2021), p. 503-509 [accessed 2024-03-12]. ISSN 2352-1465. Available from: <https://doi.org/10.1016/j.trpro.2021.07.093>
- [18] KRAJCOVIC, M., BASTIUCHENKO, V., FURMANNOVA, B., BOTKA, M., KOMACKA, D. New approach to the analysis of manufacturing processes with the support of data science. *Processes* [online]. 2024, **12**(3), 449 [accessed 2024-04-09]. ISSN 2227-9717. Available from: <https://doi.org/10.3390/pr12030449>
- [19] TOMANICOVA, M. Design of the optimal layout of the assembly workplace in the selected company. Diploma thesis. Zilina: University of Zilina, Faculty of Mechanical Engineering, Department of Industrial Engineering, 2010.
- [20] FURJELOVA, D. Optimization of material flows within the selected company. Bachelor's thesis. Zilina: University of Zilina, Faculty of Mechanical Engineering, Department of Industrial Engineering. 2020.





This is an open access article distributed under the terms of the Creative Commons Attribution 4.0 International License (CC BY 4.0), which permits use, distribution, and reproduction in any medium, provided the original publication is properly cited. No use, distribution or reproduction is permitted which does not comply with these terms.

# STRUCTURAL ANALYSIS OF DESIGNED TUBES UNDER AXIAL COMPRESSION: VARIATIONS OF APPLIED TEMPERATURE, MATERIAL TYPE, AND GEOMETRY DESIGN

Hensa Akbar Al Kautsar<sup>1</sup>, Anandito Adam Pratama<sup>1</sup>, Suryanto Suryanto<sup>1</sup>, Aditya Rio Prabowo<sup>1,\*</sup>, Ristiyo Adiputra<sup>2</sup>, Heru Sukanto<sup>1</sup>, Bambang Kusharjanta<sup>1</sup>, Hermes Carvalho<sup>3,4</sup>

<sup>1</sup>Department of Mechanical Engineering, Sebelas Maret University, Surakarta, Indonesia

<sup>2</sup>Research Center for Hydrodynamics Technology, National Research and Innovation Agency (BRIN), Surabaya, Indonesia

<sup>3</sup>Department of Structural Engineering, Federal University of Minas Gerais, Minas Gerais, Brazil

<sup>4</sup>Department of Structural Engineering and Geotechnical, University of Sao Paulo, Sao Paulo, Brazil

\*E-mail of corresponding author: aditya@ft.uns.ac.id

Aditya Rio Prabowo 0000-0001-5217-5943,  
Heru Sukanto 0009-0008-3719-3607,  
Hermes Carvalho 0000-0002-4652-8068

Ristiyo Adiputra 0000-0003-3630-9432,  
Bambang Kusharjanta 0000-0002-0194-3268,

## Resume

The research presented in this article consisted of analysis of the ship structural accidents at low temperatures and the effect of carbon percentage in various classifications of carbon steel, compared to the high tensile strength steel materials. The objective of this research was to fill the knowledge gap by expanding the understanding of the influence of low temperature, material, and structure on the axial compression test of tubes. The simulations as idealization of the compression test were conducted with variations in temperature, material carbon percentage, and geometry shape, using Finite Element Analysis (FEA). The results showed that at -100 °C, the material had the best ability to resist compression energy; high carbon steel had the highest strength at various carbon percentages, and the square geometry showed the best ability to absorb energy before failure.

## Article info

Received 17 March 2024

Accepted 3 June 2024

Online 27 June 2024

## Keywords:

axial compression  
low temperature  
carbon steel  
tube geometry  
finite element analysis

Available online: <https://doi.org/10.26552/com.C.2024.036>

ISSN 1335-4205 (print version)

ISSN 2585-7878 (online version)

## 1 Introduction

Throughout history, people and goods have moved between continents and across oceans. Ocean transportation effectively and efficiently moves almost all goods across a wide range of expedition needs [1]. Ocean transportation is responsible for moving thousands of goods daily, contributing to global trade [2]. Media and scientists predict that an increase in ship traffic will occur [3]. Results introduced by scholars in [4-5] indicate that the consequences of large volumes of global ocean transportation are also associated with negative environmental impacts on the marine environment. In pioneer researches, such as [6-7], it is also stated that accidents at sea pose significant risks to individuals and society in various fields, and ship collisions are one of the main contributors to frequent

maritime traffic accidents. Figure 1 shows the high frequency and severe consequences of collisions, both practitioners and researchers have paid attention to related research, and various types of techniques aimed at preventing accidents and reducing the risks resulting from accidents have been developed [8-11].

For the safety of ship structures, predicting the load-carrying capacity of these types of members is crucial. There are several methods to estimate the collapse behavior of ship structures, including experiments, numerical analysis, analytical methods, and so on [13-15]. Huhne et al. [16] conducted 4000 tests; the test results and numerical analysis showed that the approach used has the potential to provide better and less conservative designs. This approach is used in designs that show that imperfect buckling loads must be maximized to determine a realistic optimal

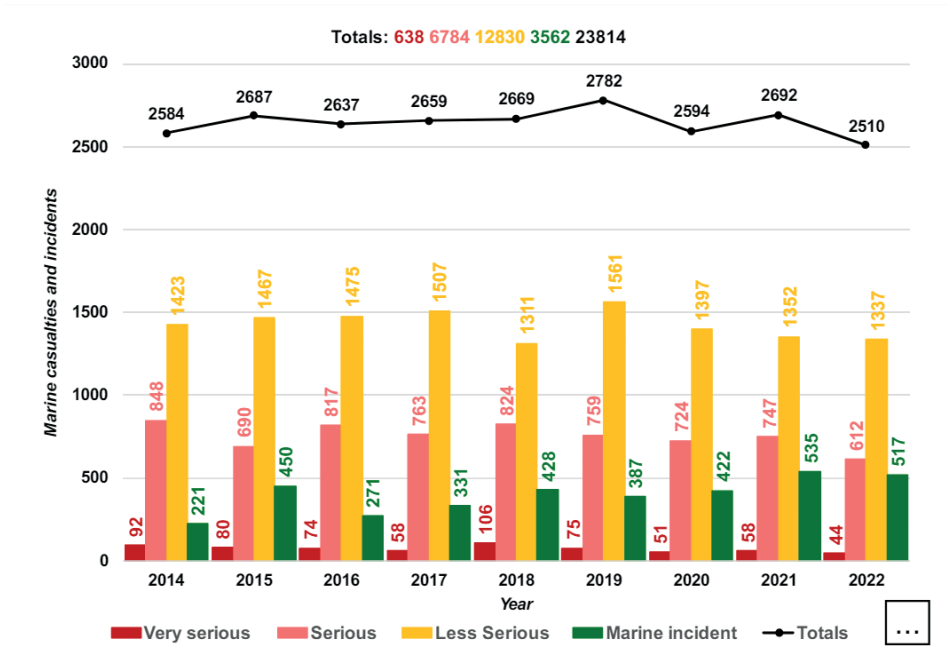


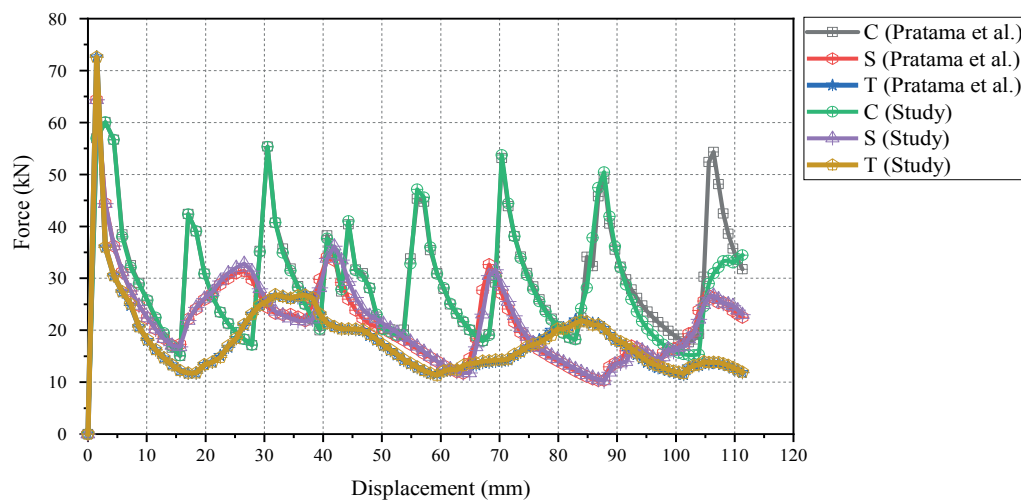
Figure 1 Number of marine casualties and incidents [12]

Table 1 Material parameters of the mild steel

Parameter	Notation, unit	Mild Steel
Density	$\rho$ (kg/m <sup>3</sup> )	7850
Modulus of elasticity	$E$ (N/m <sup>2</sup> )	203 x 10 <sup>9</sup>
Poisson's ratio	$\nu$	0.33
Johnson-Cook flow stress parameters		
Initial yield stress	$A$ (N/m <sup>2</sup> )	304.33 x 10 <sup>6</sup>
Hardening coefficient	$B$ (N/m <sup>2</sup> )	422 x 10 <sup>6</sup>
Hardening exponent	$n$	0.345
Strain rate constant	$C$	0.0156
Thermal softening constant	$m$	0.87
Reference strain rate	$\dot{\epsilon}_0$ (s <sup>-1</sup> )	0.0001
Melting temperature	$T_{melt}$ (K)	1800
Transition temperature	$T_0$ (K)	293
Johnson-Cook fracture strain parameters		
Fracture strain constant	$D_1$	0.1152
	$D_2$	1.0116
	$D_3$	- 1.7684
	$D_4$	- 0.05279
	$D_5$	0.5262

design. Another study, conducted by McGregor et al. [17], showed the success of modelling in numerical simulation helps in the achievement of good design for future integration of composites into collision-resistant structures, good calculations contribute to the design objectives of the parts safely and efficiently for final integration into collision structures. Another study, was presented by Greiner et al. [18], which discussed the interaction of bending and axial compression. The study

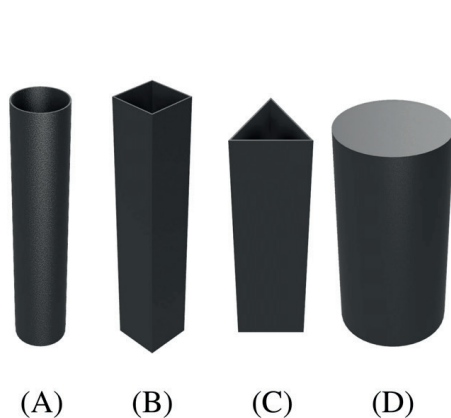
results showed that the interaction behavior of stainless steel under the load can be represented by interaction testing of the same structure as for carbon steel. The study conducted in [18] covers a wide range of practical sections. However, a number of other parameters have not been investigated, which suggests that further research is needed to compare the interaction behavior of carbon steel to other types of steel. In axial compression testing, low-carbon steels tend to have lower strength



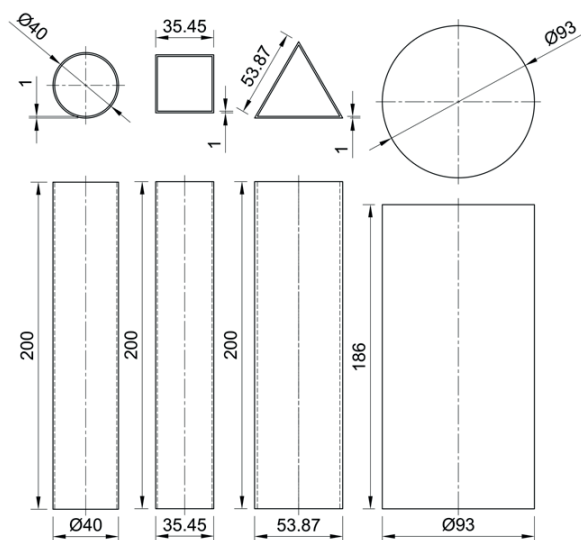
**Figure 2** Force-Displacement comparison diagram to Pratama et al. [24]; C = Cylinder, S = Square, and T = Triangle

**Table 2** Error percentage comparison to research of Pratama et al. [24]

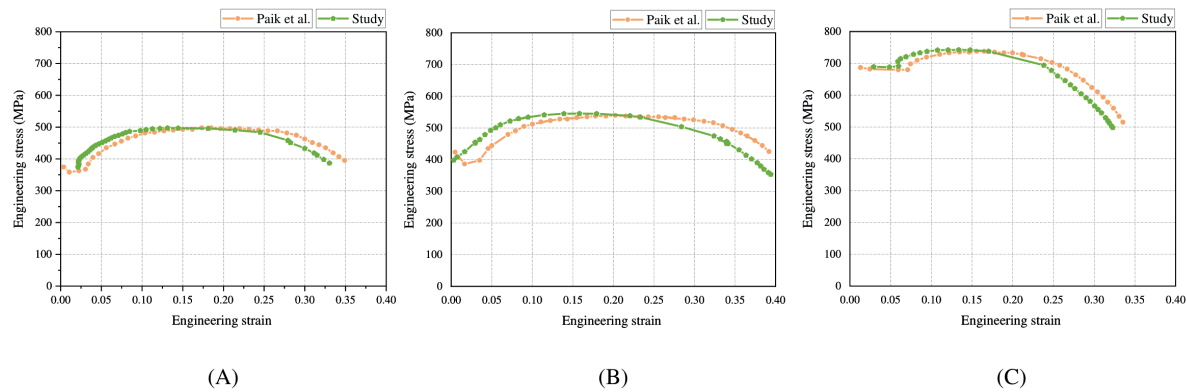
Output	Geometry	Pratama et al. [24]	Current Study	Error (%)
Maximum Displacement (mm)	Cylinder	90.53	91.00	0.519165
	Square	103.54	103.14	0.386324
	Triangle	111.39	111.32	0.062842
Total Energy Absorption (J)	Cylinder	2707.64	2665.86	1.543041
	Square	2271.06	2285.92	0.65432
	Triangle	2031.69	2036.89	0.255945
Peak Force (kN)	Cylinder	60.09	60.10	0.016642
	Square	64.40	64.40	0
	Triangle	72.62	72.58	0.055081
Average Force (kN)	Cylinder	29.66	28.48	3.978422
	Square	21.10	21.29	0.900474
	Triangle	17.62	17.68	0.340522
Average				0.726



**Figure 3** Geometrical design; (A) Cylindrical Tube, (B) Square Tube, (C) Triangular Tube, and (D) Impactor



**Figure 4** Dimensions of geometrical design; in (mm)



**Figure 5** Comparison of engineering stress-strain curve to results introduced by Paik et al. [19]; (A) at 20 °C, (B) at -40 °C, and (C) at -160 °C

**Table 3** Variation of the AH32 input parameters at low temperature [19]

Property	Temperature (°C)					
	20	-40	-80	-100	-130	-160
Yield strength, $\sigma_y$ (MPa)	359.65	369.06	381.01	386.22	387.20	411.51
Fracture strain, $\epsilon_f$	0.376	0.423	0.430	0.448	0.409	0.336

**Table 4** Material parameter of used steels ASTM A36 [31-33]; AISI 1045 [34-36] and AISI 52100 [34, 36]

Parameter	Notation	ASTM A36	AISI 1045	AISI 52100
Density	$\rho$ (kg/m <sup>3</sup> )	7850	7850	7810
Modulus of elasticity	$E$ (N/m <sup>2</sup> )	200 x 10 <sup>9</sup>	205 x 10 <sup>9</sup>	200 x 10 <sup>9</sup>
Poisson's ratio	$\nu$	0.26	0.29	0.3
Johnson-Cook flow stress parameters				
Initial yield stress	$A$ (N/m <sup>2</sup> )	250 x 10 <sup>6</sup>	506 x 10 <sup>6</sup>	774.48 x 10 <sup>6</sup>
Hardening coefficient	$B$ (N/m <sup>2</sup> )	477 x 10 <sup>6</sup>	320 x 10 <sup>6</sup>	134 x 10 <sup>6</sup>
Hardening exponent	$n$	0.18	0.28	0.37
Strain rate constant	$C$	0.012	0.064	0.018
Thermal softening constant	$m$	1	1.06	3.171
Reference strain rate	$\dot{\epsilon}_0$ (s <sup>-1</sup> )	0.0001	0.0001	0.0001
Melting temperature	$T_{melt}$ (K)	1811	1733	1424
Transition temperature	$T_0$ (K)	300	300	300
Johnson-Cook fracture strain parameters				
Fracture strain constant	$D_1$	0.403	0.1	0.0368
	$D_2$	1.107	0.76	2.34
	$D_3$	- 1.899	- 1.57	- 1.484
	$D_4$	0.00961	0.005	0.0035
	$D_5$	0.3	-0.84	0.411

with good ductility; medium-carbon steels balance the strength and ductility, while the high-carbon steels have high strength but may lack ductility. Paik et al. in 2020 conducted tests experimentally for ship structural requirements, the test database developed in

this study can be used to validate computational models for structural accident analysis under low temperature conditions, [19]. The researchers recommended further studies in computational models for structural accident analysis at low temperatures, since then the high tensile

strength steel materials tend to decrease in strength and elastic modulus, which can affect the increase in material stress at low temperatures. At low temperatures, ship structures need to be designed, taking into account the material's potential fragility, dimensional changes, and the need for thermal insulation to ensure optimal safety and performance.

The Northern Sea Route (NSR) is one of the sea trade routes connecting Asia and Europe. According to studies, for examples [20-21], the NSR cuts emissions, fuel consumption by around 40 %, and shipping distances. The location is unsuitable for maritime transit due to the exceptionally low temperatures, which also pose a hazard to ships [22-23]. Consequently, a more thorough analysis of ship structural mishaps at low temperatures is required. The impact of low temperatures on the strength of materials suitable for use in ship structures is explored in this study. Furthermore, the authors delved into the impact of carbon percentage on every carbon steel classification, drawing comparisons to high tensile strength steel material.

In the available literature, there is limited research on the effect of low temperature, material, and structure on the axial compression test of tubes. So far, several studies have focused on the effect of low temperature but on tensile testing, as well as studies focusing on axial compression tests but with different test variations such as corrosion and test angle. Therefore, there is still a significant lack of information on the reaction of tubes when exposed to axial compression loads. Thus, the objective of this research was to fill the testing gap by expanding the understanding of the effect of temperature, material composition, and geometry on the strength of a structure.

## 2 Benchmark particulars

### 2.1 Model references

Before conducting research using numerical analysis, it is necessary to conduct methodology verification to ensure the fidelity of the deployed numerical method. Therefore, benchmark analysis is performed with an objective to obtain numerical method that results similar output compared to the benchmark reference. In this study, numerical model was built by adopting same methodology as in the reference, i.e., model size, FEA configuration, and loading conditions. The research geometry variation was equalized with the study conducted in [24], namely cylinder of a diameter of 40 mm, square of a length of each side of 35.45 mm, and triangle of a length of each side of 53.87 mm, each tube has the same height of 200 mm, using the direction of the impactor load angle adjusted to 0 ° as an illustration of deformation caused by ship collisions. The use of a mesh was also adjusted to a value of 1 mm. Table 1 shows that in this study were used the material parameters adapted

to [24], as well. The research aim was to comprehend how the mild steel materials, which are frequently used in shipbuilding, behave when subjected to compression. The computational methods were employed to investigate thin-walled metal tubes response to static and dynamic loads. The three-dimensional computational models were used to examine the thin-walled metal tubes with varying sizes and forms, under the static and dynamic loads. The ABAQUS software was employed to create the model, and the impact response of the tube was examined in terms of its diameter and form. Simulations were run to comprehend the tube's deformation and energy absorption under varied load situations. The research method was carried out using the design of empty tube structure, validation of the numerical method, variation of tube design, and explicit dynamic simulation. The parametric study was conducted by varying the geometric shape of the tube, load angle, and corrosion location to understand the axial deformation and energy absorption. Results showed that round tubes had the best resistance.

The Johnson-Cook model [25] can be used to characterize the material of the model to be used in the simulation. In this model the material flow is made as a combination of the linear thermo-elasticity, von Mises yield criterion, isotropic strain hardening, strain rate hardening, and softening due to adiabatic effects. The equivalent von Mises stress  $\sigma$  of the Johnson-Cook model is expressed as:

$$\bar{\sigma}(\bar{\epsilon}^{bl}, \dot{\bar{\epsilon}}^{bl}, \hat{T}) = [A + B(\bar{\epsilon}^{bl})^n] \left[ 1 + C \ln\left(\frac{\dot{\bar{\epsilon}}^{bl}}{\dot{\epsilon}_0}\right) \right] \cdot [1 - T^m], \quad (1)$$

where,  $A, B, n, C$  and  $m$  are material parameters obtained from various tensile tests.  $\dot{\epsilon}_0$  is the reference strain rate,  $\bar{\epsilon}^{bl}$  is equivalent plastic strain,  $\dot{\bar{\epsilon}}^{bl}$  is equivalent to plastic strain rate, and  $\hat{T}$  is dimensionless parameter. The equivalent fracture strain in the Johnson-Cook model is given as:

$$\bar{\epsilon}_f^{bl}\left(\frac{\sigma_m}{\bar{\sigma}}, \dot{\bar{\epsilon}}^{bl}, \hat{T}\right) = \left[ D_1 + D_2 \exp\left(D_3 \frac{\sigma_m}{\bar{\sigma}}\right) \right] \left[ 1 + D_4 \ln\left(\frac{\dot{\bar{\epsilon}}^{bl}}{\dot{\epsilon}_0}\right) \right] [1 + D_5 \hat{T}], \quad (2)$$

where  $D_1, D_2$ , and  $D_3$  represent the stress triaxiality parameters,  $D_4$  is the parameter of strain rate-dependent damage,  $D_5$  is temperature-dependent fracture strain

parameter,  $\frac{\sigma_m}{\bar{\sigma}}$  is the stress triaxiality ratio,  $\sigma_m$  is the mean stress, and  $\bar{\sigma}$  is the equivalent von Mises stress.

### 2.2 Benchmark results

As validation was needed in this research, the results conducted by [24] on the output of maximum displacement, peak force, average force, and total energy



absorption, were compared. The result comparisons, as a validation step, are shown in Figure 2 where the comparison of the Force-Displacement diagram had conformity with the reference, and Table 2 shows a comparison of output values with an average percentage error of 0.72 %.

### 3 Methodology

#### 3.1 Geometrical model

In this numerical analysis-based research, the component design consists of two parts, namely the tube and the impactor. Shown in Figures 3 and 4, the tube used had three geometry variations: Cylinder, Square, and Triangle, with their respective dimensions, equated with those of reference. In this research, the three geometries used the same material properties; the variation was conducted to analyze the effect of tube geometry on material strength. The impactor is defined as a rigid object that would not deform.

#### 3.2 Applied material

##### 3.2.1 Low variations

In this study, validation of applied material in numerical analysis with previous testing was also carried out by comparing the output of the last experimental testing results to production of the results in the numerical analysis corresponding to this test. Specifically, as shown in Figure 5, a comparison was made between the Engineering Stress-Strain output of the experimental test conducted in study by Paik et al. [19] and the output obtained from this numerical analysis. Comparisons were made between several tests since they were considered representative of the numerical analysis results. Temperature variations were performed on the AH32 Steel material by adjusting the experimental testing of reference, namely 20 °C, -40 °C, -80 °C, -100 °C, -130 °C, and -160 °C. Table 3 shows that for each temperature variation performed, the difference in parameter input is adjusted to experimental testing, as well, namely in the yield strength and fracture strain.

##### 3.2.2 Carbon steel classifications

The American Iron and Steel Institute (AISI) defines carbon steel as a steel that has no specified minimum content or requirements for chromium, cobalt, niobium, molybdenum, nickel, titanium, tungsten, vanadium, or zirconium, or special requirements for other elements. The low-carbon steel contains up to 0.30 % carbon; it has high formability due to its shallow carbon content. The medium carbon steels are similar to low carbon

steels except that they contain from 0.30 % to 0.60 % carbon, and the increase in carbon content allows medium carbon steels to be used in quenched and tempered conditions. The high-carbon steel contains carbon from 0.60 % to 1.00 %; it is used for some hand tools, spring materials, high-strength wires, etc. The high-strength low-alloyed (HSLA) is a micro-alloyed steel designed to improve mechanical properties. It may also have more excellent resistance to atmospheric corrosion and low temperatures than the conventional carbon steels. The HSLA steels have low carbon content (0.05 % - 0.25 %) to produce adequate formability and weldability [26].

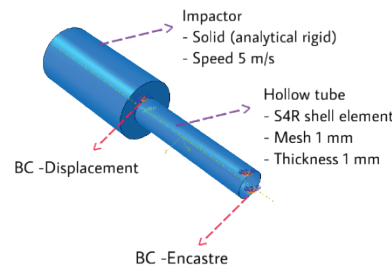
In this study, the ASTM A36 steel was used as the applied material in the low-carbon steel classification, because it has a carbon content of 0.25 %, as stated by [27]. The AISI 1045 steel is in the medium carbon steel classification because it has a carbon content of around 0.312 %, as stated by [28]. The AISI 52100 steel is in the high carbon steel classification because it has a carbon content of around 0.95 %, as [29] stated. The AH32 steel is in the HSLA steel classification because it has material characteristics by this classification and has a carbon content of around 0.12 %, as stated by [30]. Table 4 shows the used material parameters.

#### 3.3 Finite element setting

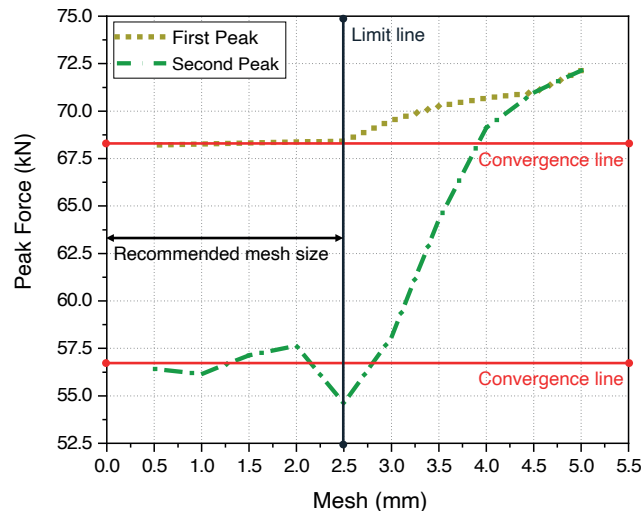
In this study, the placement and setting of boundary conditions were critical to ensure the reproduction of physical test conditions, prevent unwanted wave reflections, maintain the numerical stability, enable correlation with experimental data, and support structural design optimization. Displacement/rotation and encastre boundary conditions were the boundary conditions used. Encastre boundary conditions were placed on the side of the hollow tube that had no contact with the impactor. Displacement/rotation boundary conditions were placed on the side of the tube that contacted with the impactor. Figure 6 shows the boundary condition setup. The loading is carried out using an impactor in an axial direction towards the tube.

The mesh arrangement in the hollow tube model uses the S4R shell element settings in the ABAQUS software. The mesh used in the simulation is 1 mm. As presented in Figure 7, the first and second major peaks are shown in the convergence study starting from mesh size 2.5 mm and larger, which is noted by the limit line. Based on stability criteria for the mesh convergence, i.e., (1) the fluctuation between two closest mesh sizes is less than 10%, and (2) no rise or decline on the results more than one mesh size; it can be concluded that the recommended mesh sizes are in the range of 0 - 2.5 mm. The indication of the recommended mesh is highlighted by red lines in Figure 7.

The displacement/rotation boundary condition restricts the movement of the selected degrees of



**Figure 6** Boundary conditions setting



**Figure 7** Mesh convergence diagram

**Table 5** Scenario of simulations

Material	Temperature (°C)	Geometrical
Low carbon (ASTM A36)	20	Cylinder, square, and triangle
Medium carbon (AISI 1045)	20	Cylinder, square, and triangle
High carbon (AISI 52100)	20	Cylinder, square, and triangle
HSLA (AH32)	20	Cylinder, square, and triangle
	-40	Cylinder, square, and triangle
	-80	Cylinder, square, and triangle
	-100	Cylinder, square, and triangle
	-130	Cylinder, square, and triangle
	-160	Cylinder, square, and triangle

freedom. The degrees of freedom are in the Y-axis direction and parallel to the impact axis direction. The encase boundary condition allows structural degrees of freedom on the side of the tube without contact with the impactor to be considered fixed. The interaction between the tube and the impactor is constrained and coupled at one geometric point. The contact between the impactor and the tube is modelled with a friction coefficient of 0.05, as shown by previous research conducted in [37]. The impact velocity was set with a constant velocity value of 5 m/s since in [38] was mentioned that ship collisions can be assumed with this value. Table 5 shows the finite element simulation variations

were conducted on tube geometry, temperature, and material.

#### 4 Results and discussion

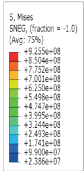
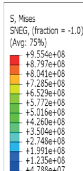
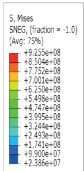
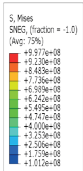
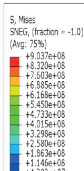
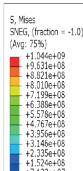
The content of this research discusses the effect of different shapes and material compositions on axial compression testing as a numerical analysis intended as a ship structure material. The research is also intended to determine the effect of temperature on the material. The output of numerical analysis results in the form of maximum displacement, total energy absorption, peak

**Table 6** Finite element simulation output with temperature variations; *C* = Cylinder, *S* = Square, *T* = Triangle, and *Av* = Average

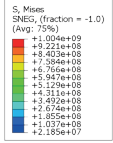
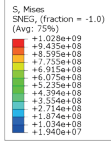
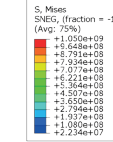
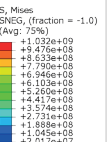
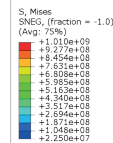
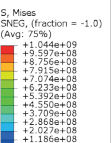
Temp. (°C)	Maximum displacement (mm)				Total energy absorption (J)			
	<i>C</i>	<i>S</i>	<i>T</i>	<i>Av</i>	<i>C</i>	<i>S</i>	<i>T</i>	<i>Av</i>
20	84.10	97.33	92.16	91.20	2731.89	2394.67	2582.49	2569.68
-40	82.79	98.49	93.55	91.61	2799.91	2382.42	2545.22	2575.85
-80	81.11	97.35	92.97	90.48	2798.40	2399.74	2567.45	2588.53
-100	82.08	97.33	86.81	88.74	2785.68	2413.91	2642.51	2614.03
-130	82.61	96.98	87.08	88.89	2776.13	2404.35	2586.82	2589.10
-160	79.73	94.94	87.14	87.27	2826.91	2455.39	2658.75	2647.01
Av	82.07	97.07	89.95		2786.49	2408.41	2597.21	

Temp. (°C)	Peak force (kN)				Average force (kN)			
	<i>C</i>	<i>S</i>	<i>T</i>	<i>Av</i>	<i>C</i>	<i>S</i>	<i>T</i>	<i>Av</i>
20	68.27	73.36	85.03	75.55	31.37	23.03	26.93	27.11
-40	69.65	74.85	86.85	77.17	32.67	22.93	26.04	27.21
-80	71.56	76.89	89.37	79.27	33.45	23.21	26.54	27.73
-100	72.18	77.55	90.18	79.97	32.65	23.36	28.33	28.11
-130	72.32	77.71	90.37	80.13	32.29	23.30	27.41	27.67
-160	75.88	81.57	95.09	84.18	33.99	24.09	29.14	29.07
Av	71.64	76.99	89.48		32.74	23.32	27.40	

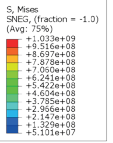
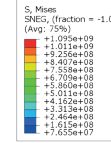
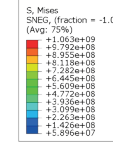
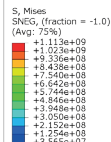
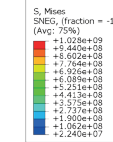
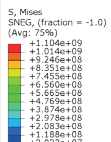
**Table 7** Tube deformation contour of cylindrical geometry at several temperatures

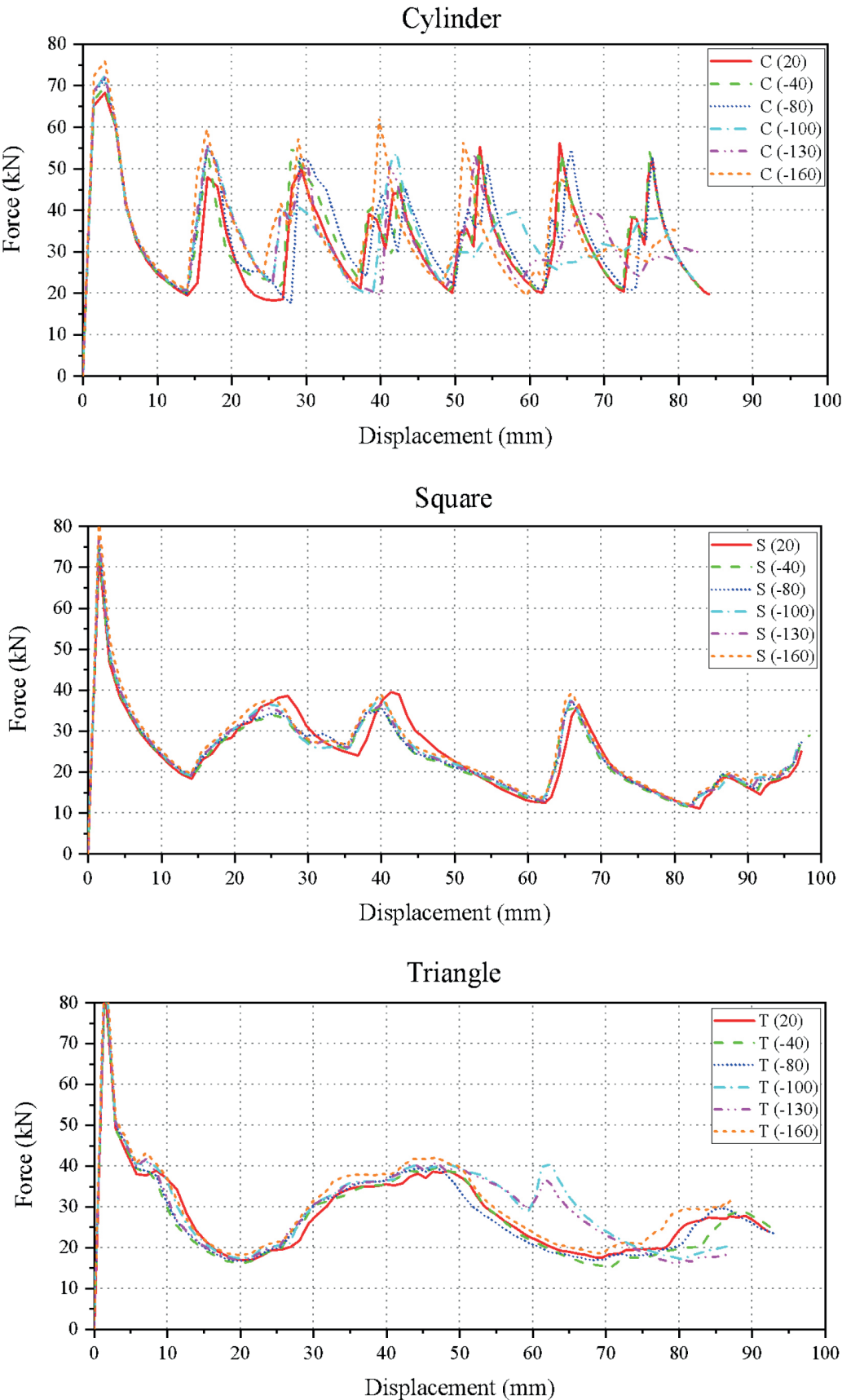
Temp. (°C)	Cylinder Geometry	Temp. (°C)	Cylinder Geometry
20		-100	
-40		-130	
-80		-160	

**Table 8** Tube deformation contour of square geometry at several temperatures

Temp. (°C)	Square Geometry	Temp. (°C)	Square Geometry
20		-100	
-40		-130	
-80		-160	

**Table 9** Tube deformation contour of triangle geometry at several temperatures

Temp. (°C)	Triangle Geometry	Temp. (°C)	Triangle Geometry
20		-100	
-40		-130	
-80		-160	



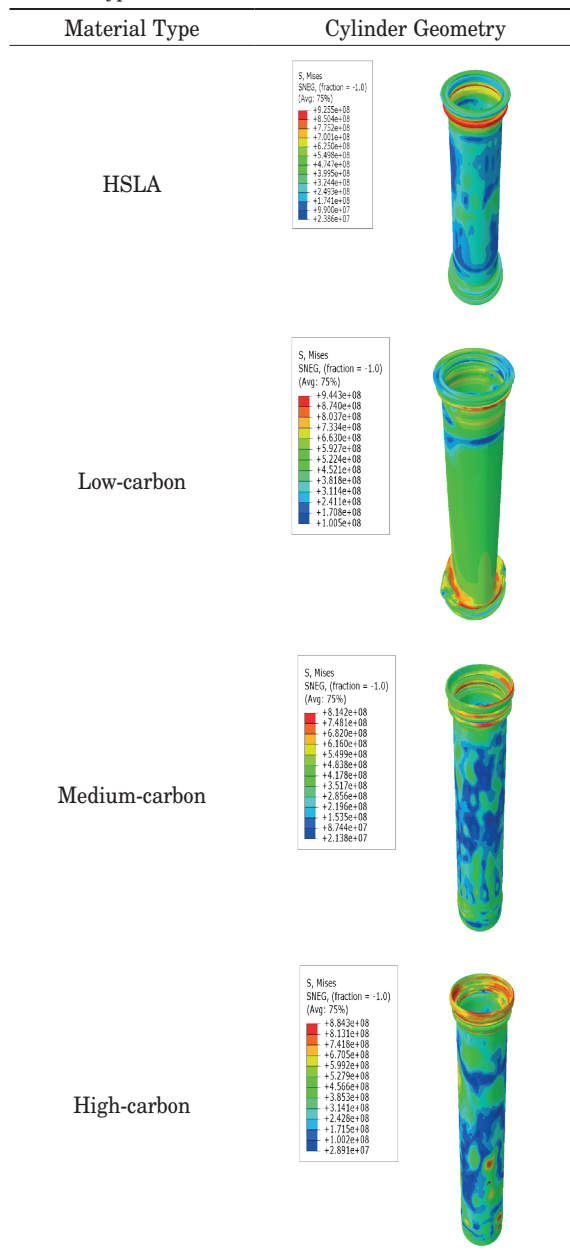
**Figure 8** Force-displacement diagram of finite element simulation results with temperature and geometry variations



**Table 10** Finite element simulation output with carbon content variations; *C* = Cylinder, *S* = Square, *T* = Triangle, and *Av* = Average

Class	Maximum displacement (mm)				Total energy absorption (J)			
	<i>C</i>	<i>S</i>	<i>T</i>	<i>Av</i>	<i>C</i>	<i>S</i>	<i>T</i>	<i>Av</i>
HSLA	84.10	97.33	92.16	91.20	2731.89	2394.67	2582.49	2569.68
Low	81.60	90.50	103.02	91.71	2782.38	2597.08	2354.95	2578.14
Medium	55.56	67.64	80.29	67.83	2824.38	2823.34	2722.20	2789.97
High	44.49	46.16	62.39	51.01	2818.60	2772.72	2785.53	2792.28
Av	66.44	75.41	84.46		2789.31	2646.95	2611.29	
Class	Peak force (kN)				Average force (kN)			
	<i>C</i>	<i>S</i>	<i>T</i>	<i>Av</i>	<i>C</i>	<i>S</i>	<i>T</i>	<i>Av</i>
HSLA	68.27	73.36	85.03	75.55	31.37	23.03	26.93	27.11
Low	70.98	74.12	83.89	76.33	32.67	26.97	22.20	27.28
Medium	91.44	100.01	114.08	101.84	37.48	38.41	31.61	35.83
High	120.21	135.78	153.24	136.41	37.73	38.08	38.59	38.13
Av	87.72	95.82	109.06		34.81	31.62	29.83	

**Table 11** Tube deformation contour of cylinder geometry at material types



**Table 12** Tube deformation contour of square geometry at material types

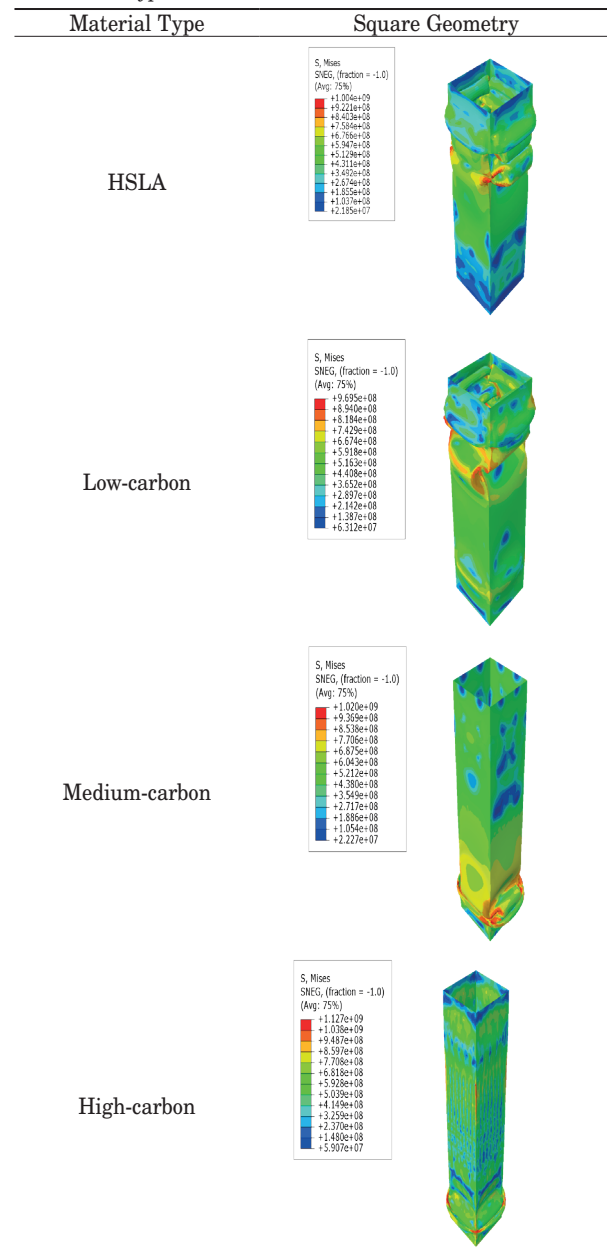

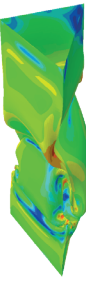




Table 13 Tube deformation contour of triangle geometry at material types

Material Type	Triangle Geometry
HSLA	<div><div><div>S, Mises SNEG, (fraction = -1.0) (Avg: 75%) +1.039e+09 +8.516e+08 +8.097e+08 +7.878e+08 +7.803e+08 +6.241e+08 +5.422e+08 +4.806e+08 +3.789e+08 +2.968e+08 +2.147e+08 +1.029e+08 +5.101e+07</div></div></div>
Low-carbon	<div><div><div>S, Mises SNEG, (fraction = -1.0) (Avg: 75%) +9.844e+08 +9.078e+08 +8.313e+08 +7.540e+08 +6.782e+08 +6.017e+08 +5.251e+08 +4.486e+08 +3.727e+08 +2.955e+08 +2.130e+08 +1.424e+08 +6.588e+07</div></div></div>
Medium-carbon	<div><div><div>S, Mises SNEG, (fraction = -1.0) (Avg: 75%) +1.094e+09 +1.006e+09 +9.182e+08 +8.304e+08 +7.427e+08 +6.549e+08 +5.672e+08 +4.794e+08 +3.916e+08 +3.039e+08 +2.161e+08 +1.283e+08 +4.057e+07</div></div></div>
High-carbon	<div><div><div>S, Mises SNEG, (fraction = -1.0) (Avg: 75%) +1.117e+09 +1.029e+09 +9.407e+08 +8.526e+08 +7.645e+08 +6.764e+08 +5.883e+08 +5.002e+08 +4.121e+08 +3.239e+08 +2.358e+08 +1.477e+08 +5.961e+07</div></div></div>

force, and average force are obtained in each simulation variation performed.

4.1 The effect of low temperatures

In this numerical analysis, the material selected in the test with low temperature variation was AH32 steel, because such is considered in accordance with previous study conducted by Suryanto et al. [39]. The numerical

simulation was varied by inputting different material characteristics according to the material characteristics when subjected to temperatures of 20 °C, -40 °C, -80 °C, -100 °C, -130 °C, and -160 °C. This test was also validated on different geometries. As shown in Figure 8, it is found that at -100 °C, there are the most peaks and valleys in the force-displacement graph, which can be interpreted that the material can withstand greater compression energy at that temperature. Table 6 shows the output of the finite element simulation results,

where at Maximum Displacement the highest value was at  $-40^{\circ}\text{C}$  namely 91.61 mm, which indicates that at that temperature the specimen can absorb more energy before reaching the failure point. The Total Energy Absorption had the highest value at  $-160^{\circ}\text{C}$  namely 2647.01 J, indicating that at that temperature the material had good resistance to deformation and failure. The Peak Force highest value was at  $-160^{\circ}\text{C}$  namely 84.18 kN, which indicates that at that temperature the material had good strength and can withstand significant external loads before failure. The Average Force highest value was at  $-160^{\circ}\text{C}$  namely 29.07 kN, which indicates that at that temperature the material underwent consistent deformation. Table 7 to 9 shows a comparison of the final deformation contour shape of the tube with temperature variations.

#### 4.2 The effect of carbon content

In this research, the materials used in the finite element simulation were ASTM AH32 in HSLA classification, ASTM A36 in low carbon steel classification, AISI 1045 in medium carbon steel classification, and 52100 in high carbon steel. The simulation was also validated using several geometries. Figure 9 shows that it was found that the HSLA steel had the most peaks and valleys in the force-displacement graph, which can be interpreted that at that temperature the material is able to withstand greater compression energy. In Table 10, one can see the output of the simulation results, where the highest Maximum Displacement value was found in the low carbon steel, namely 91.71 mm, indicating that the simulation specimen was able to absorb more energy before reaching the failure point. The highest Total Energy Absorption value was found in the high carbon steel, namely 2792.28 J, indicating that the material had good resistance to deformation and failure. The highest Peak Force value was found in the high carbon steel, namely 136.41 kN, indicating that the material had good strength and can withstand significant external loads before failure, and the highest Average Force value was found in the high carbon steel 38.13 kN, indicating that the material underwent consistent deformation. Tables 11 to 13 shows a comparison of the final deformation contour shape of the tube with temperature variations.

#### 4.3 The effect of geometry

In this research, the geometries used in the numerical simulation were cylinder, square, and triangle. Figures 8 and 9 show that the cylinder geometry had the most peaks and valleys on the force-displacement graph, which can be interpreted that at that temperature the material can withstand greater compression energy. Table 14 shows the output of the numerical simulation

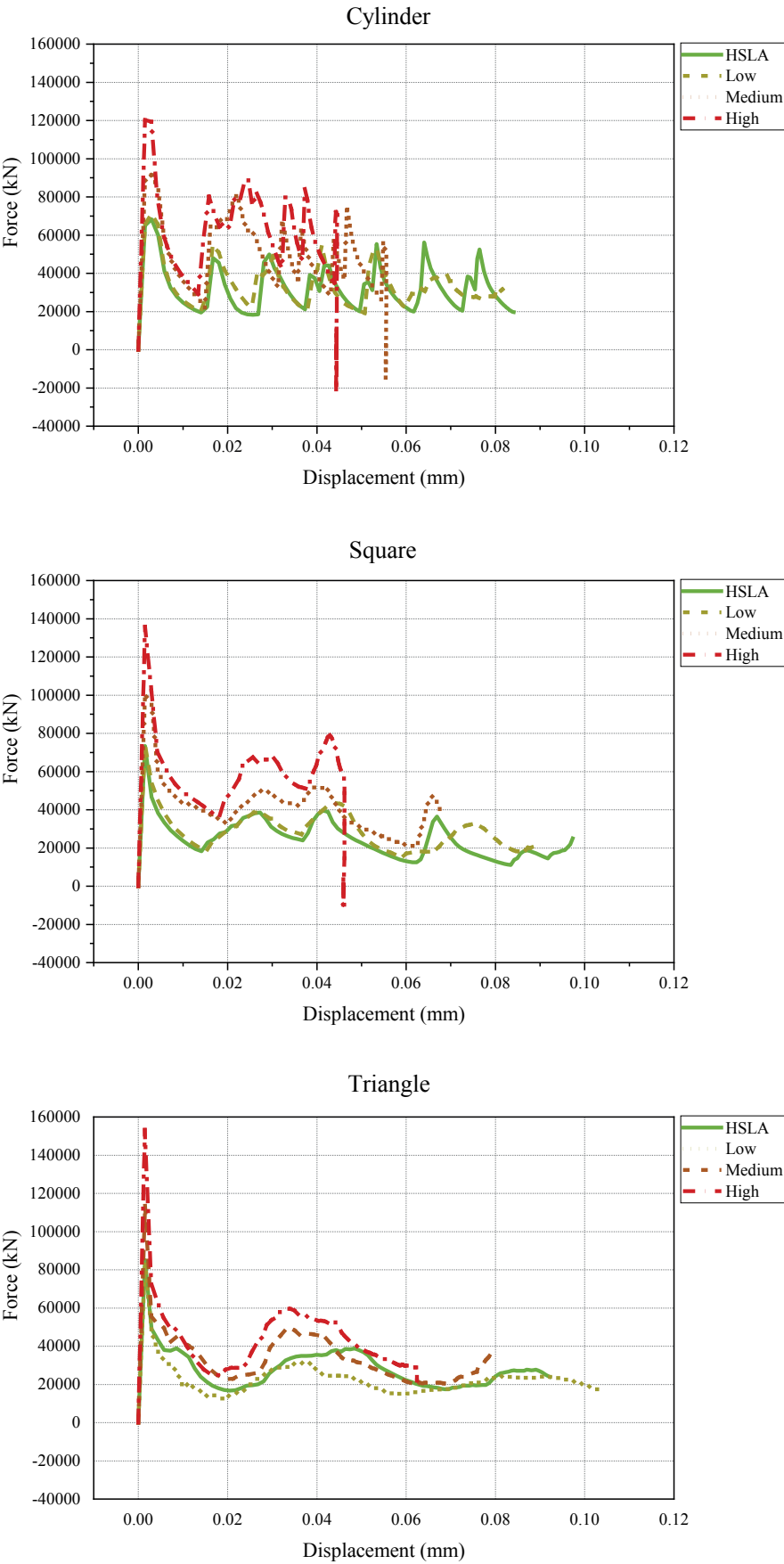
results, where in Maximum Displacement the highest value was in Triangle geometry, namely 87.2 mm, which indicates that in that geometry the simulation object was able to absorb more energy before reaching the point of failure. The Total Energy Absorption highest value was in Cylinder geometry, namely 2787.9 J, which indicates that in that geometry the material had good resistance to deformation and failure. The highest Peak Force value was found in the Triangle geometry namely 99.27 kN, which indicated that in that geometry the material had good strength and can withstand significant external loads before failure, and the highest Average Force value was found in the Cylinder geometry, namely 33.77 kN, which indicates that in that geometry the material was consistently deformed. Tables 7 and 9 show the comparison of the contour shape of the final deformation of the tube with geometry variations.

### 5 Conclusions

In this research, the authors examined the impact of low temperature and carbon percentage, validated by geometry variation, on the strength of materials used in ship structures, focusing on numerical idealization and analysis of axial compression testing. Then, investigations were conducted using a numerical approach to understand how low temperature, carbon percentage variation, and geometry shape affect the material's response to axial compression. Based on this understanding, this study could contribute to development of knowledge about material behaviour and helps to formulate safer and more efficient design strategies for future ship structures.

The results of this study using a numerical approach through ABAQUS software found that overall, in terms of the effect of low temperature effects, the displacement value decreases with decreasing temperature. In these terms, it means that the lower the temperature or the closer to the low temperature ( $-160^{\circ}\text{C}$ ) will cause an increase in the strength of the material used. On the other hand, this results in an insignificant increase in total energy absorption, peak force, and average force. Then, regarding the effect of the percentage of carbon content, the HSLA-type material is the least strong. This is indicated by the many peaks and valleys produced in the force-displacement graph. Meanwhile, the more robust materials are high, medium, and low-carbon steels. In addition, the effect of the compression numerical specimen's geometric shape was also examined in this study. The square shape was the least strong because it experienced the most considerable deformation, followed by the triangular and cylindrical shapes.

This study has limitations related to the simplified representation of the mathematical model and factors that may occur in actual experimental testing, such as temperature changes during the testing process



**Figure 9** Force-displacement diagram of finite element simulation results with carbon content and geometry variations

**Table 14** Finite element simulation output with geometry variations; C = Cylinder, S = Square, and T = Triangle

	Maximum displacement (mm)			Total energy absorption (J)		
	C	S	T	C	S	T
Temperature	82.07	97.07	89.95	2786.49	2408.41	2597.21
Carbon	66.44	75.41	84.46	2789.31	2646.95	2611.29
Average	74.25	86.24	87.20	2787.90	2527.68	2604.25
	Peak force (kN)			Average force (kN)		
	C	S	T	C	S	T
Temperature	71.64	76.99	89.48	32.74	23.32	27.40
Carbon	87.72	95.82	109.06	34.81	31.62	29.83
Average	79.68	86.40	99.27	33.77	27.47	28.61

and dimensional changes due to temperature changes. Although the various factors affecting the test were taken into account, this study remains an idealistic representation, hence, the results need to be verified with real experiments. However, this study provides important insights into the response of the system to variations in temperature, material composition, and geometry in axial compression tests. To improve the safety and effectiveness of marine transportation in the future, this study is expected to contribute greatly to our understanding of the safety challenges faced by ship structures in harsh environments.

### Acknowledgements

The authors received no financial support for the research, authorship and/or publication of this article.

### Conflicts of interest

The authors declare that they have no known competing financial interests or personal relationships that could have appeared to influence the work reported in this paper.

### References

- [1] SCHNURR, R. E. J., WALKER, T. R. *Marine transportation and energy use*. In: *Reference Module in Earth Systems and Environmental Sciences*. Amsterdam: Elsevier, 2019. ISBN 9780124095489.
- [2] WALKER, T. R. Green marine: an environmental program to establish sustainability in marine transportation. *Marine Pollution Bulletin* [online]. 2016, **105**(1), p. 199-207. ISSN 0025-326X. Available from: <https://doi.org/10.1016/j.marpolbul.2016.02.029>
- [3] LASSERRE, F., PELLETIER, S. Polar super seaways? Maritime transport in the Arctic: an analysis of shipowners' intentions. *Journal Transportation Geography* [online]. 2011, **19**(6), p. 1465-1473. ISSN 0966-6923. Available from: <https://doi.org/10.1016/j.jtrangeo.2011.08.006>
- [4] WALKER, T. R., ADEBAMBO, O., FEIJOO, M. C. D. A., ELHAIMER, E., HOSSAIN, T., EDWARDS, S. J., MORRISON, C. E., ROMO, J., SHARMA, N., TAYLOR, S., ZOMORODI, S. Chapter 27 - Environmental effects of marine transportation [online]. In: *World seas: an environmental evaluation*. Cambridge: SHEPPARD, CH. (Ed.). Academic Press, 2019. ISBN 9780128050521. Available from: <https://doi.org/10.1016/B978-0-12-805052-1.00030-9>
- [5] BRYNOLF, S., LINDGREN, J. F., ANDERSSON, K., WILEWSKA-BIEN, M., BALDI, F., GRANHAG, L., JOHNSON, H., LINNE, P., SVENSSON, E., ZETTERDAHL, M. Improving environmental performance in shipping. In: *Shipping and the environment* [online]. ANDERSSON, K., BRYNOLF, S., LINDGREN, J. F., WILEWSKA-BIEN, M. (Eds.). 1. ed. Berlin, Heidelberg: Springer, 2016. ISBN 9783662490457. Available from: <https://doi.org/10.1007/978-3-662-49045-7>
- [6] Annual overview of marine casualties and incidents 2017 - European Maritime Safety Agency (EMSA) [online] [accessed 2024-02-07]. Available from: <http://emsa.europa.eu/emsa-documents/latest/item/3156-annual-overview-of-marine-casualties-and-incidents-2017.html>
- [7] CHEN, P., HUANG, Y., MOU, J., van Gelder, P. H. A. J. M. Probabilistic risk analysis for ship-ship collision: State-of-the-art. *Safety Science* [online]. 2019, **117**, p. 108-122. ISSN 0925-7535. Available from: <https://doi.org/10.1016/j.ssci.2019.04.014>
- [8] HUANG, Y. CHEN, L., CHEN, P., NEGENBORN, R. R., VAN GELDER, P. H. A. J. M. Ship collision avoidance methods: state-of-the-art. *Safety Science* [online]. 2020, **121**, p. 451-473. ISSN 0925-7535. Available from: <https://doi.org/10.1016/j.ssci.2019.09.018>



- [9] PRABOWO, A. R., RIDWAN, R., TUSWAN, T., SMARADHANA, D.F., CAO, B., BAEK, S. J. Crushing resistance on the metal-based plate under impact loading: a systematic study on the indenter radius influence in grounding accident. *Applications in Engineering Science* [online]. 2024, **18**(4), 100177. ISSN 2666-4968. Available from: <https://doi.org/10.1016/j.apples.2024.100177>
- [10] FAQIH, I., ADIPUTRA, R., PRABOWO, A. R., MUHAYAT, N., EHLERS, S., BRAUN, M. Hull girder ultimate strength of bulk carrier (HGUS-BC) evaluation: structural performances subjected to true inclination conditions of stiffened panel members. *Results in Engineering* [online]. 2023, **18**, 101076. ISSN 2590-1230. Available from: <https://doi.org/10.1016/j.rineng.2023.101076>
- [11] LUTFI, Y. M., ADIPUTRA, R., PRABOWO, A. R., UTSUNOMIYA, T., ERWANDI, E., MUHAYAT, N. Assessment of the stiffened panel performance in the OTEC seawater tank design: parametric study and sensitivity analysis. *Theoretical Application Mechanics Letters* [online]. 2023, **13**(4), 100452. ISSN 2095-0349. Available from: <https://doi.org/10.1016/j.taml.2023.100452>
- [12] Annual overview of marine casualties and incidents 2023 - European Maritime Safety Agency (EMSA) [online] [accessed 2024-05-05]. Available from: <https://www.emsa.europa.eu/component/flexicontent/download/7639/5055/23.html>
- [13] XU, M. C., SONG, Z. J., ZHANG, B. W., PAN, J. Empirical formula for predicting ultimate strength of stiffened panel of ship structure under combined longitudinal compression and lateral loads. *Ocean Engineering* [online]. 2018, **162**, p. 161-175. ISSN 0029-8018. <https://doi.org/10.1016/j.oceaneng.2018.05.015>
- [14] HABIB, M. I., ADIPUTRA, R., PRABOWO, A. R., ERWANDI, E., MUHAYAT, N., YASUNAGA, T., EHLERS, S., BRAUN, M. Internal flow effects in OTEC cold water pipe: finite element modelling in frequency and time domain approaches. *Ocean Engineering* [online]. 2023, **288**(1), 116056. ISSN 0029-8018. Available from: <https://doi.org/10.1016/j.oceaneng.2023.116056>
- [15] HANIF, M. I., ADIPUTRA, R., PRABOWO, A. R., YAMADA, Y., FIRDAUS, N. Assessment of the ultimate strength of stiffened panels of ships considering uncertainties in geometrical aspects: finite element approach and simplified formula. *Ocean Engineering* [online]. 2023, **286**(1), 115522. ISSN 0029-801. Available from: <https://doi.org/10.1016/j.oceaneng.2023.115522>
- [16] HUHNE, C., ROFLES, R., BREITBACH, E., TESSMER, J. Robust design of composite cylindrical shells under axial compression - simulation and validation. *Thin-Walled Structure* [online]. 2008, **46**(7-9), p. 947-962. ISSN 0263-8231. Available from: <https://doi.org/10.1016/j.tws.2008.01.043>
- [17] MCGREGOR, C. J., VAZIRI, R., POURSAITIP, A., XIAO, X. Simulation of progressive damage development in braided composite tubes under axial compression. *Composite Part A: Application Science and Manufacturing* [online]. 2007, **38**(11), p. 2247-2259. ISSN 1359-835X. Available from: <https://doi.org/10.1016/j.compositesa.2006.10.007>
- [18] GREINER, R., KETTLER, M. Interaction of bending and axial compression of stainless steel members. *Journal of Construction Steel Research* [online]. 2008, **64**(11), p. 1217-1224. ISSN 0143-974X. Available from: <https://doi.org/10.1016/j.jcsr.2008.05.008>
- [19] PAIK, J. K., LEE, D. H., NOH, S. H., PARK, D. K., RINGSBERG, J. W. Full-scale collapse testing of a steel stiffened plate structure under axial-compressive loading triggered by brittle fracture at cryogenic condition. *Ships and Offshore Structures* [online]. 2020, **15**(sup1), p. S29-S45 ISSN 1744-5302. Available from: <https://doi.org/10.1080/17445302.2020.1787930>
- [20] SCHOYEN, H., BRATHEN, S. The northern sea route versus the Suez Canal: cases from bulk shipping. *Journal of Transportation Geography* [online]. 2011, **19**(4), p. 977-983 [accessed 2024-02-12]. ISSN 0966-6923. Available from: <https://doi.org/10.1016/j.jtrangeo.2011.03.003>
- [21] KITAGAWA, H. Arctic routing: challenges and opportunities. *WMU Journal of Maritime Affairs* [online]. 2008, **7**(2), p. 485-503 ISSN 1651-436X. Available from: <https://doi.org/10.1007/BF03195147>
- [22] Arctic marine shipping assessment 2009 report - Protection of Arctic Marine Environment (PAME) [online] [accessed 2024-02-14]. Available from: [https://www.pmel.noaa.gov/arctic-zone/detect/documents/AMSA\\_2009\\_Report\\_2nd\\_print.pdf](https://www.pmel.noaa.gov/arctic-zone/detect/documents/AMSA_2009_Report_2nd_print.pdf)
- [23] BAKSH, A. A., ABBASSI, R., GARANIYA, V., KHAN, F. Marine transportation risk assessment using Bayesian Network: application to Arctic waters. *Ocean Engineering* [online]. 2018, **159**, p. 422-436. ISSN 0029-8018. Available from: <https://doi.org/10.1016/j.oceaneng.2018.04.024>
- [24] PRATAMA, A. A., PRABOWO, A. R., MUTTAQIE, T., MUHAYAT, N., RIDWAN, R., CAO, B., LAKSONO, F. B. Hollow tube structures subjected to compressive loading: implementation of the pitting corrosion effect in nonlinear FE analysis. *Journal of the Brazilian Society of Mechanical Sciences and Engineering* [online]. 2023, **45**(3), 143. ISSN 1678-5878. Available from: <https://doi.org/10.1007/s40430-023-04067-3>
- [25] JOHNSON, G. R., COOK, W. H. Fracture characteristics of three metals subjected to various strains, strain rates, temperatures and pressures. *Engineering Fracture Mechanics* [online]. 1985, **21**(1), p. 31-48. ISSN 0013-7944. Available from: [https://doi.org/10.1016/0013-7944\(85\)90052-9](https://doi.org/10.1016/0013-7944(85)90052-9)
- [26] SINGH, R. *Applied welding engineering*. Oxford: Butterworth-Heinemann, 2020. ISBN 9780123919175.

- [27] UTAMI, N. P. E., ELLYANIE, E., NASUTION, J. D. The effect of lead (Pb) hot dipping on seawater corrosion rate in ASTM A36 steel. *IOP Conference Series: Materials Science and Engineering* [online]. 2019, **620**, 012108. ISSN 1757-899X. Available from: <https://doi.org/10.1088/1757-899X/620/1/012108>
- [28] SENTHILKUMAR, N., TAMIZHARASAN, T. Effect of tool geometry in turning AISI 1045 steel: experimental investigation and FEM analysis. *Arabian Journal for Science and Engineering* [online]. 2014, **39**(6), p. 4963-4975. ISSN 2191-4281. Available from: <https://doi.org/10.1007/s13369-014-1054-2>
- [29] HUSSAIN, A., PODGURSKY, V., GOLJANDIN, D., ANTONOV, M., BASIT, M. A., AHMAD, T. Mild steel tribology for circular economy of textile industries. *Tribology in Industry* [online]. 2021, **43**(4), p. 552-560. ISSN 0354-8996. Available from: <http://dx.doi.org/10.24874/ti.1050.02.21.04>
- [30] ZHOU, C. YE, Q., YAN, L. Effect of ultra and fast cooling on microstructure and properties of high strength steel for shipbuilding [online]. In: *HSLA steels 2015, microalloying 2015 and offshore engineering steels 2015*. The Chinese Society for Metals (CSM), Chinese Academy of Engineering (CAE) (Eds.). Cham: Springer, 2015. ISBN 978-3-319-48614-7. Available from: [https://doi.org/10.1007/978-3-319-48767-0\\_147](https://doi.org/10.1007/978-3-319-48767-0_147)
- [31] AGARANA, M. C., AKINLABI, E. T. Modelling of A36 steel plate dynamic response to uniform partially distributed moving iron load using differential transform method. *IOP Conference Series: Materials Science and Engineering* [online]. 2018, **413**, 012011. ISSN 1757-899X. Available from: <https://doi.org/10.1088/1757-899X/413/1/012011>
- [32] ELSHENAWY, T., LI, Q. M. Influences of target strength and confinement on the penetration depth of an oil well perforator. *International Journal of Impact Engineering* [online]. 2013, **54**, p. 130-137 [accessed 2024-02-16]. ISSN 0734-743X. Available from: <https://doi.org/10.1016/j.ijimpeng.2012.10.010>
- [33] SEIDT, J. D., GILAT, A., KLEIN, J. A., LEACH, J. R. High strain rate, high temperature constitutive and failure models for EOD impact scenarios. In: *SEM Annual Conference and Exposition on Experimental and Applied Mechanics: proceedings*. 2007. ISBN 9781604232226.
- [34] HAN, G., LEE, K. M., KIM, S. K. A study on improving dynamic characteristics of a front lower suspension arm and aerodynamic effects of a hand-made hybrid vehicle. *International Journal of Precision Engineering and Manufacturing* [online]. 2014, **15**(9), p. 1897-1908. Available from: <https://doi.org/10.1007/s12541-014-0544-1>
- [35] CHEN, W., HUO, D., TENG, X., SUN, Y. Surface generation modelling for micro end milling considering the minimum chip thickness and tool runout. *Procedia CIRP* [online]. 2017, **58**, p. 364-369. ISSN 2212-8271. Available from: <https://doi.org/10.1016/j.procir.2017.03.237>
- [36] DONG, Y., REN, Y., FAN, S., WANG, Y., ZHAO, S. Investigation of notch-induced precise splitting of different bar materials under high-speed load. *Materials* [online]. 2020, **13**(11), 2461. eISSN 1996-1944. Available from: <https://doi.org/10.3390/ma13112461>
- [37] TAK, S. K., IQBAL, M. A. Axial compression behaviour of thin-walled metallic tubes under quasi-static and dynamic loading. *Thin-Walled Structures* [online]. 2021, **159**, 107261. ISSN 0263-8231. Available from: <https://doi.org/10.1016/j.tws.2020.107261>
- [38] HARIS, S., AMDAHL, J. Analysis of ship-ship collision damage accounting for bow and side deformation interaction. *Marine Structures* [online]. 2013, **32**, p. 18-48. ISSN 0951-8339. Available from: <https://doi.org/10.1016/j.marstruc.2013.02.002>
- [39] SURYANTO, S., PRABOWO, A. R., MUTTAQIE, T., ISTANTO, I., ADIPUTRA, R., MUHAYAT, N., FAJRI, A., BRAUN, M., EHLERS, S. Evaluation of high-tensile steel using nonlinear analysis: experiment-FE materials benchmarking of LNG carrier structures under low-temperature conditions. *Energy Reports* [online]. 2023, **9**(9), p. 149-161. ISSN 2352-4847. Available from: <https://doi.org/10.1016/j.egy.2023.05.252>



This is an open access article distributed under the terms of the Creative Commons Attribution 4.0 International License (CC BY 4.0), which permits use, distribution, and reproduction in any medium, provided the original publication is properly cited. No use, distribution or reproduction is permitted which does not comply with these terms.

# STUDY OF THE STRENGTH OF THE OPEN WAGON HATCH DOOR WITH RECTANGULAR CORRUGATIONS UNDER STATIC LOADS

Juraj Gerlici, Alyona Lovska\*

University of Zilina, Zilina, Slovak Republic

\*E-mail of corresponding author: alyona.lovska@fstroj.uniza.sk

Juraj Gerlici 0000-0003-3928-0567,

Alyona Lovska 0000-0002-8604-1764

## Resume

Rail transport has been the leading sector of the whole transport network. In order to improve the efficiency of its functioning, it is important to develop measures that may help reduce the maintenance cost. To improve the open wagon hatch door strength, it is proposed to make it with rectangular corrugations. The results of calculations show that, taking into account the proposed solution, the weight of the improved hatch door is almost 10% lower than the weight of a typical one.

The strength of the hatch door under static loads was calculated. The results of calculations show that the strength of the hatch door under the diagrams considered is ensured.

The study will contribute to the development of best practices for modern structures of railway vehicles and increase their cost-effective operation.

## Article info

Received 12 April 2024

Accepted 11 June 2024

Online 27 June 2024

## Keywords:

open wagon

hatch door

strength of the hatch door

improved hatch door

Available online: <https://doi.org/10.26552/com.C.2024.039>

ISSN 1335-4205 (print version)

ISSN 2585-7878 (online version)

## 1 Introduction

The competitive struggle in the transport market makes it necessary to increase the efficiency of railway transport operation in order to maintain its leading positions [1-3]. It is known that one of the most common types of freight transported by rail is bulk cargo. It is transported in open wagons and unloaded through the discharge hatches (Figure 1), which form its floor, or by using mechanised unloading equipment.

A typical hatch door of an open wagon consists of a metal sheet to which strapping, locking brackets, and hinges are attached (Figure 2).

The sheet of a typical hatch door is a 5-mm thick metal plate with six longitudinal corrugations for higher rigidity (Figure 3).

It is important to note that under operating conditions, such a sheet does not have sufficient strength, and may be damaged (Figure 4).

The most common damages to the sheet are rupture and deformation, which cause the freight to spill out of an open wagon on the move, thus causing losses to the railway. In addition, these damages require additional capital investments due to unscheduled repairs of the wagon. In this regard, there is a need to develop

measures aimed at improving the strength of the hatch door sheet under operating load conditions.

Analysing modern publications on improved hatch doors of open wagons, we have come to the conclusion that at present this problem is quite relevant. A new design of the hatch door for an open wagon with convex configuration is proposed in [4]. This design increases the payload of the open wagon by one tonne compared to the payload of standard hatch doors. This solution is scientifically justified. However, the authors considered only one design mode for the hatch door of an open wagon. Moreover, it is rather costly in manufacture and maintenance.

The hatch door proposed in [5] has similar disadvantages. It consists of two corrugated sheets with energy-absorbing material in-between. The strapping of the hatch door has a W-shaped profile. Although this hatch door design has certain advantages over standard ones, its widespread implementation is constrained by a number of factors.

To improve the strength of the hatch door, the authors of [6] propose to reinforce it with additional belts with the rectangular profile which facilitates the production and installation. The authors substantiate this hatch door design by means of strength calculations.

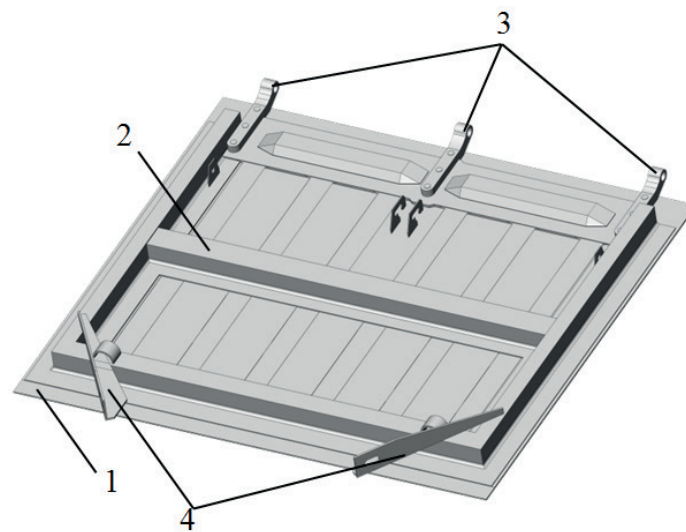




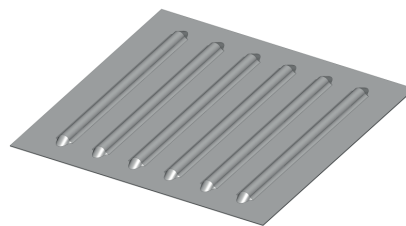
a) general view



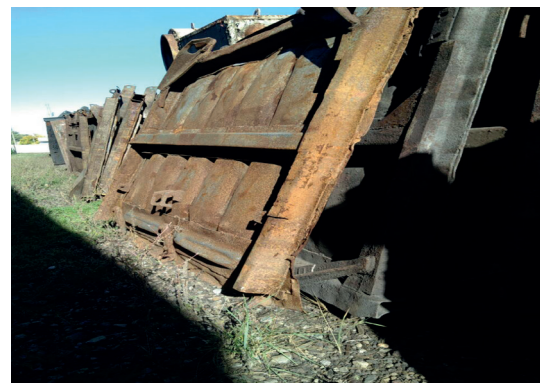
b) unloading process

**Figure 1** Open wagon with discharge hatches

1 - sheet; 2 - strapping; 3 - locking brackets; 4 - hinges

**Figure 2** Hatch door of an open wagon**Figure 3** Typical hatch door sheet

a) rupture



b) deformation

**Figure 4** Damage to the hatch door sheet

However, this improvement increases the hatch door weight and, consequently, the wagon tare.

An improved hatch door reinforced with additional belts is also proposed in [7]. Here, the hatch door sheet is made of smooth sheet metal, and the reinforcing belts have the form of struts. The hatch door has moulded hinges. The study presents the calculations of the static strength for the hatch door, that confirm the feasibility of the proposed solution. However, widespread implementation of such hatch doors requires substantial capital investments.

To ensure the durability of the hatch door, materials with improved physical and mechanical properties, rather than steel, can be used for the door's components. For example, in [8], the authors propose to improve the wagon strength by using composite materials for the floor. The research proved the rationality of this solution. However, the authors did not consider the use of these materials in the hatch door for an open wagon.

Work [9] investigates the feasibility of using composite materials for the hatch door sheet for open wagons. The results of strength calculation of the hatch door proved the possibility of this implementation. However, these materials will increase the production costs, moreover, this will require an appropriate maintenance and repair system.

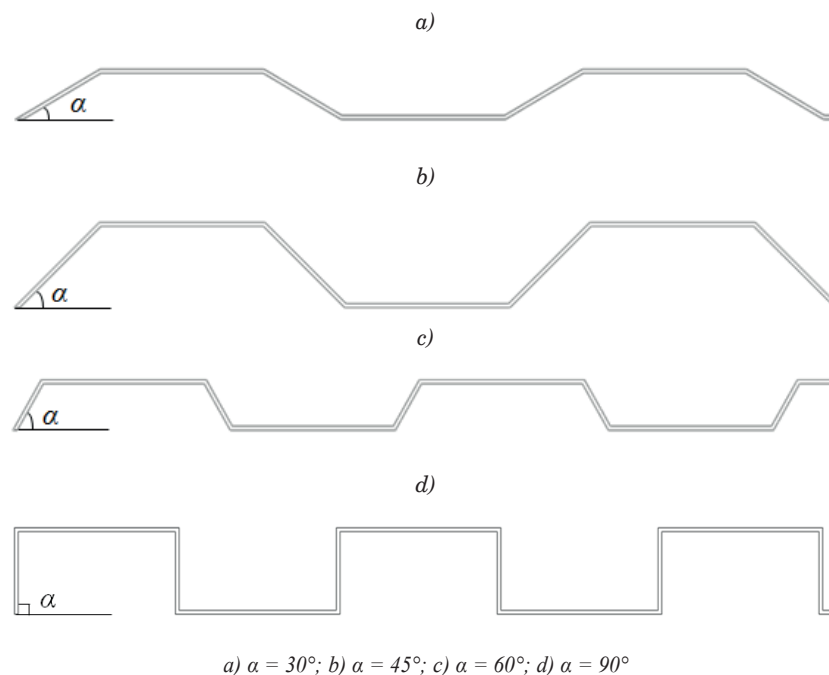
An improved hatch door for an open wagon is also proposed in [10]. Its structural feature is sandwich-type components. The hatch door consists of two smooth sheets with an energy-absorbing material in-between. The strapping has the  $\Omega$ -shaped profile. The strength is calculated under static and dynamic loads on the hatch door. However, among the disadvantages of this hatch door are high cost, complexity of maintenance, etc.

The analysis of publications has shown that the issue of how to improve the hatch door of an open wagon is relevant and requires extensive research. The purpose of this study is to scientifically substantiate the design of the hatch door for an open wagon and determine the main strength indicators under static loads.

## 2 Materials and methods

Higher strength of the hatch door of an open wagon can be achieved by increasing the rigidity of the door. For this purpose, several possible variants of corrugations were studied and different corrugation angles were taking into account (Figure 5).

The moment of resistance depends on the corrugation profile (Table 1) and for rectangular corrugations it is the highest.



**Figure 5** Different corrugations of the sheet

**Table 1** Inertia moments and resistance moments of cross-sections of the sheet

Corrugation angle ( $\alpha$ )	Moment of inertia ( $I$ ), $\text{mm}^4$	Moment of resistance ( $W$ ), $\text{mm}^3$
$30^\circ$	$3.79 \cdot 10^4$	$3.64 \cdot 10^3$
$45^\circ$	$12.52 \cdot 10^4$	$6.95 \cdot 10^3$
$60^\circ$	$4.66 \cdot 10^4$	$4.48 \cdot 10^3$
$90^\circ$	$19.53 \cdot 10^4$	$10.85 \cdot 10^3$



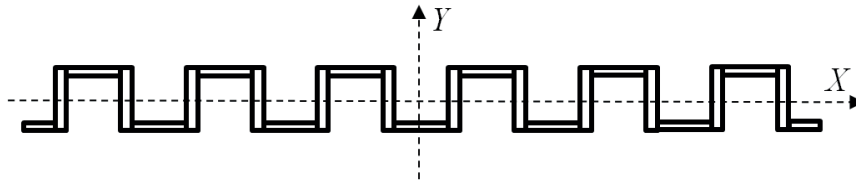


Figure 6 Cross-section of the hatch door sheet

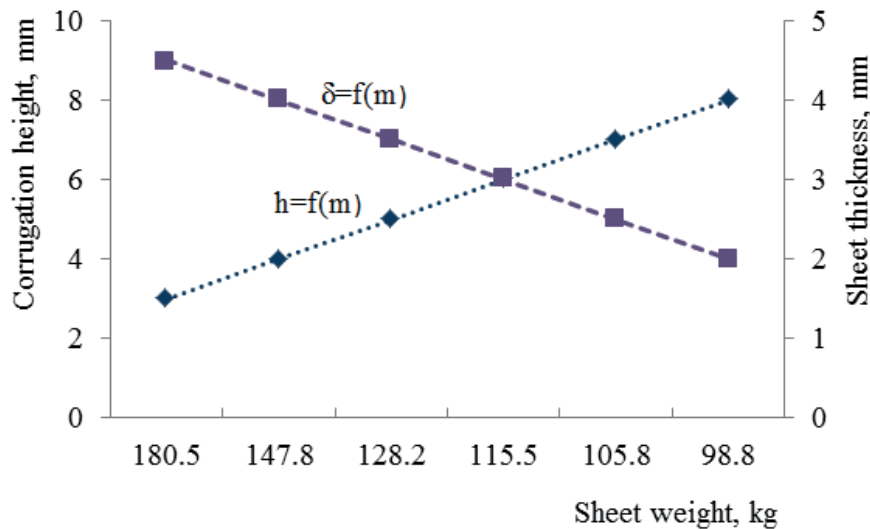


Figure 7 Dependence of the sheet weight on its parameters

Therefore, this study deals with the feasibility of rectangular corrugations for the hatch door used in open wagons.

The geometrical parameters of sheet corrugations are determined provided that its moment of inertia is higher than that of a typical hatch door sheet ( $W = 200.8 \cdot 10^3 \text{ mm}^3$ ).

The moment of resistance of the sheet is determined by dividing its cross-section into elementary rods (Figure 6).

Here, the moment of resistance is calculated based on the known moment of inertia. Thus, for a vertical rod [11-12] it is:

$$W = \frac{2 \cdot I}{h}, \quad (1)$$

where  $h$  is the rod height.

Herewith,

$$I = \frac{\delta \cdot h^3}{12}, \quad (2)$$

where  $\delta$  is the rod width.

The rational parameters of corrugations are determined with variational calculations. The target function of these calculations is the minimum weight of the sheet with such variational parameters as the corrugation height  $h$  and the corrugation thickness  $\delta$ .

The calculation has the following constraint: the moment of inertia of the sheet must be higher than that of a typical sheet.

The moment of resistance is determined by Equation (1). The sheet weight is calculated using the sheet volume. The calculation results are shown in Figure 7.

An analysis of Figure 7 shows that a rational solution is corrugations with a height of  $h = 60 \text{ mm}$  and a thickness of  $\delta = 3 \text{ mm}$ . The total sheet weight is about 110 kg. Importantly, the calculated sheet weight is almost 10% lower than the weight of a typical sheet.

### 3 Results

The strength of the hatch door sheet with rectangular corrugations is studied by means of the spatial model built in SolidWorks [13-14] (Figure 8).

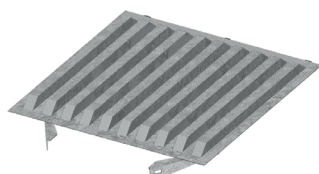
The strength of the hatch door is determined using the FEM in SolidWorks Simulation [15-17]. The model is built with tetrahedra (Figure 9), the number of which is determined graphically and analytically [18-20]. Thus, the finite element model has 180,572 elements and 566,450 nodes.

The strength is calculated based two design diagrams [21]:

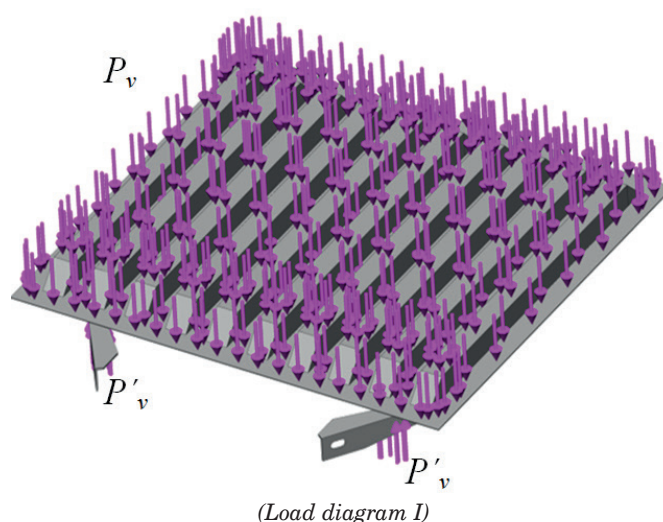
- the effect of a uniformly distributed load of 69.9 kN on the hatch door area; this force includes the gross weight force of the hatch door and the dynamic load (diagram I); and
- the effect of a load of 50 kN distributed in the hatch door centre across an area of 250x250 mm (diagram II).



**Figure 8** Spatial model of the hatch door



**Figure 9** Finite element model of the hatch door



**Figure 10** Design diagram of the hatch door

The design diagram of the hatch door under the action of the evenly distributed load  $P_v$  is shown in Figure 10.

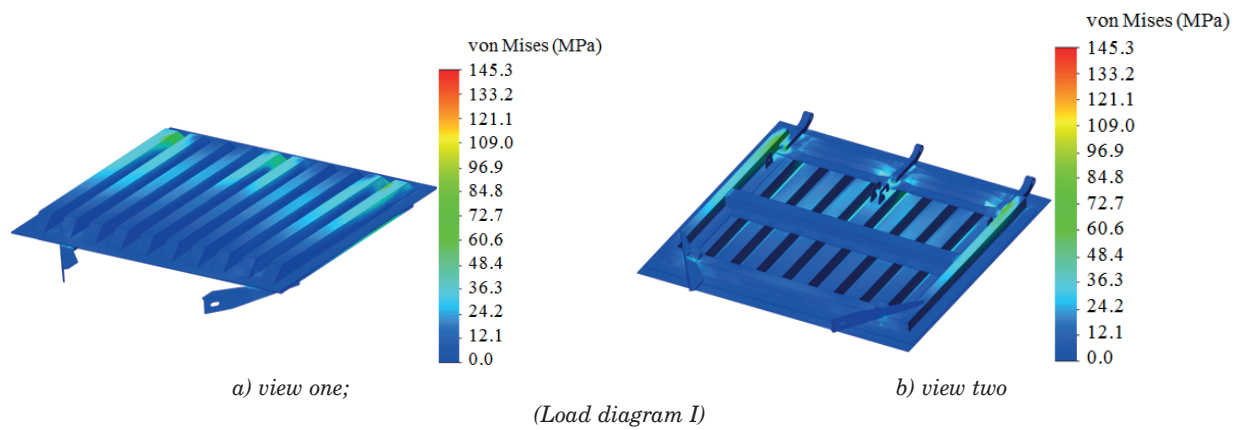
The hatch door is secured with the hinges, and the locking brackets are subject to the reactions  $P'_v$  to the vertical load  $P_v$ . The hatch door is made of Steel 09G2S.

The calculation results are shown in Figures 11-13. The maximum stresses in the hatch door are 145.3 MPa (Figure 11). However, they are lower than permissible by 30% [21]. This means that the safety factor of the hatch door is about 1.4 under specified load conditions. It should be noted that the resulting stresses in the hatch door are 23% lower than those in a typical structure. From Figure 12 it can be seen that the maximum stresses occur in the areas of interaction between the hinges and the strapping, because the model is secured by the hinges, and the load is applied to the sheet and the locking brackets.

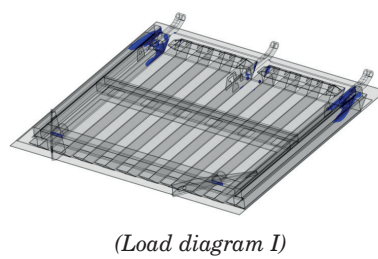
The maximum displacements in the hatch door occur in the locking brackets and amount to 2.27 mm (Figure 13). This distribution of displacement fields can be explained by the fact that the vertical reactions to the load  $P_v$  on the sheet are applied to the middle part of the bracket, while the end part of the bracket is free.

The following stage of the study included the determination of the hatch door strength under the vertical load  $P_v$  distributed in the centre across an area of 250x250 mm, which is equal to 50 kN. The design diagram of the hatch door is shown in Figure 14. The reactions  $P'_v$  to the vertical load  $P_v$  are applied to the locking brackets.

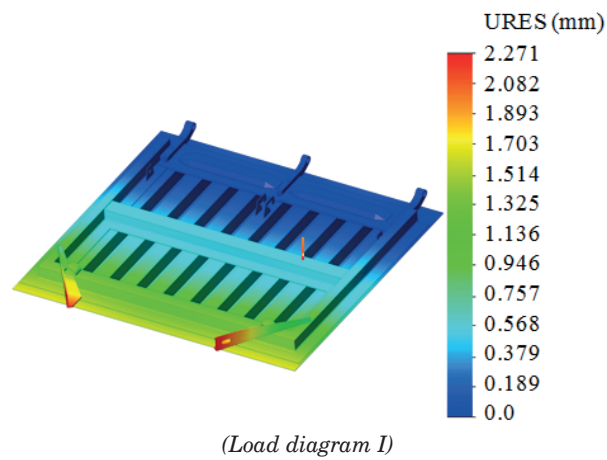
The results of calculations for the hatch door are shown in Figures 15-17. The maximum stresses are 161.5 MPa (Figure 15); they are 23% lower than permissible [21]. The safety factor of the hatch door under specified load conditions is 1.3. The resulting



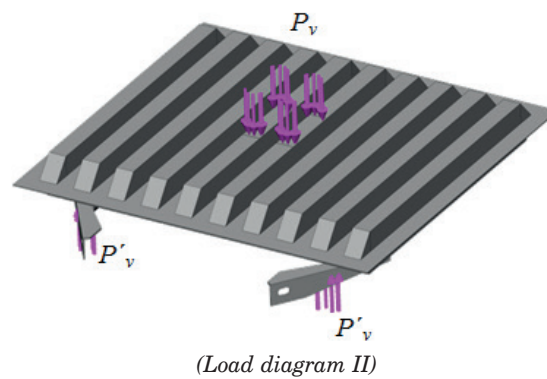
**Figure 11** Stress state of the hatch door



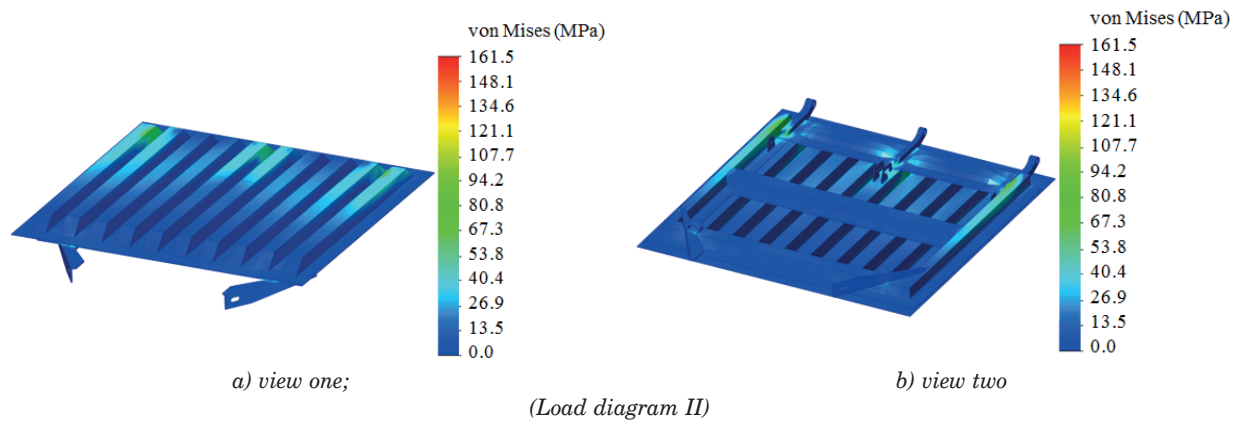
**Figure 12** Most loaded areas of the hatch door



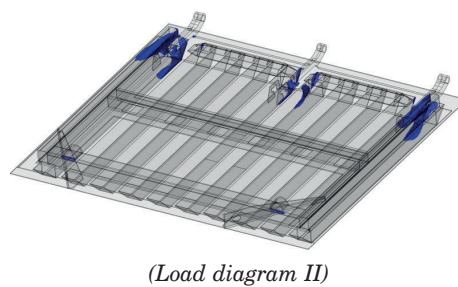
**Figure 13** Displacements in the hatch door



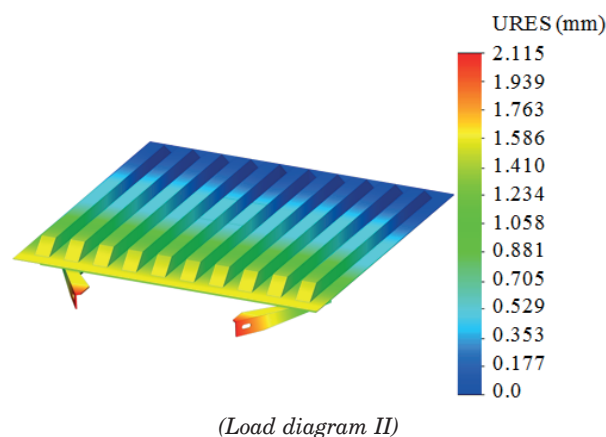
**Figure 14** Design diagram of the hatch door



**Figure 15** Stress state of the hatch door



**Figure 16** Most loaded areas of the hatch door



**Figure 17** Displacements in the hatch door

stresses in the hatch door are 23.5% lower than those in a typical structure. The maximum stresses are also concentrated in the areas of interaction between the edge hinges and the strapping. This is explained in the same way as for design diagram I.

The maximum displacements in the hatch door occur in the locking brackets (Figure 17); they amount to 2.1 mm. This distribution of displacement fields can be explained in the same way as for the previous design diagram.

The research shows that, taking into account the proposed improvement, the hatch door strength under the static loads is ensured.

#### 4 Discussion

In order to increase the strength of the hatch door for an open wagon, it is proposed to use rectangular corrugations to improve the hatch door sheet. In addition, possible corrugation profiles for the hatch door sheet are analysed (Figure 5). It is found that the cross-section of the sheet with rectangular corrugations has the maximum moment of resistance (Table 1). The geometrical parameters of corrugations are determined by means of the moment of resistance of the cross-section of the sheet. The results of calculations demonstrate that corrugations with a height of  $h=60$  mm and a thickness

of  $\delta = 3$  mm are a rational solution. The sheet weight is about 110 kg, which is almost 10% lower than the weight of a typical sheet (Figure 7).

The following stage of the calculation included the determination of the main strength indicators of the hatch door under static loads, namely, the action of a load of 69.9 kN uniformly distributed on the hatch door and the action of a load of 50 kN distributed in the centre of the hatch door on an area of 250x250 mm.

The calculation results show that the hatch door strength is ensured under the load diagrams in question. The maximum stresses in the hatch door are 145.3 MPa for load diagram I (Figure 11). These stresses are lower than permissible by 30%. The maximum displacements in the hatch door occur in the locking brackets and are 2.27 mm (Figure 13).

The maximum stresses in the hatch door at load diagram II are 161.5 MPa and they are lower than permissible by 23% (Figure 15). The maximum displacements in the hatch door occur in the locking brackets and they amount to 2.1mm (Figure 17). Therefore, the hatch door strength under static loads is ensured.

The restriction of this study is that the strength calculation of the hatch door included a rigid interaction between the hinges and the centre sill of an open wagon.

Moreover, it did not include the welds between the individual components of the hatch door. Thus, the hatch door was considered monolithic.

The advantage of this study in comparison with [4] is that the technical maintenance of the improved hatch door can be carried out at existing repair enterprises. Unlike the hatch door designs presented in [5, 7-10], the design proposed is less expensive in production thanks to lower costs of the structural materials used. In addition, unlike the solution described in [6], the proposed hatch door design does not increase the open wagon tare.

It is important to note that the proposed improved hatch door can be not only manufactured but also modernized at wagon building and repair enterprises.

The further research of the authors may include the determination of the hatch door strength under dynamic loads and experimental research into the hatch door strength.

## 5 Conclusions

1. The geometrical parameters of the corrugations of the hatch door of an open wagon are determined

using the moment of resistance of the cross-section, the sheet being considered as a set of rods. The calculation results show that the corrugations with a height of  $h = 60$  mm and a thickness of  $\delta = 3$  mm is a rational solution. The sheet weight is about 110 kg, which is almost 10% lower than the weight of a typical sheet.

2. The strength of the hatch door for an open wagon under static loads is calculated. The calculation results show that the maximum stresses in the hatch door are 145.3 MPa when it is subject to a load evenly distributed across its area; they are 30% lower than permissible. It is important to note that the calculated stresses are 23% lower than those in a typical structure. The safety factor of the hatch door is about 1.4. The maximum displacements occur in the locking brackets and are 2.27mm.

The calculation results show that the maximum stresses in the hatch door are 161.5 MPa under a vertical load distributed in its centre across an area of 250x250 mm; they are 23% lower than permissible. The stresses obtained are 23.5% lower than those in a typical structure; the safety factor is 1.3. The maximum displacements in the hatch door are 2.1 mm and occur in the locking brackets. Using the results obtained it can be concluded that the strength of the hatch door subjected to static loads is ensured.

The research will contribute to the development of best practices for modern designs of railway vehicles and increase their operational efficiency.

## Acknowledgment

This contribution was elaborated within execution of the project "New generation of freight railway wagons" (Project code in ITMS2014+: 313010P922), on the basis of support of the operational program Research and innovation financed from the European Regional Development Fund.

Funded by the EU NextGenerationEU through the Recovery and Resilience Plan for Slovakia under the project No. 09I03-03-V01-00131.

## Conflicts of interest

The authors declare that they have no known competing financial interests or personal relationships that could have appeared to influence the work reported in this paper.

## References

- [1] CABAN, J., BRUMERCIK, F., VRABEL, J., IGNACIUK, P., MISZTAL, W., MARCZUK, A. Safety of maritime transport in the Baltic Sea. *MATEC Web of Conferences* [online]. 2017, **134**, 00003. eISSN 2261-236X. Available from: <https://doi.org/10.1051/mateconf/201713400003>



- [2] DIZO, J., BLATNICKY, M., STEISUNAS, S., SKOCILASOVA, B. Assessment of a rail vehicle running with the damaged wheel on a ride comfort for passengers. *MATEC Web of Conferences* [online]. 2018, **157**, 03004. eISSN 2261-236X. Available from: <https://doi.org/10.1051/mateconf/201815703004>
- [3] DIZO, J. Analysis of a goods wagon running on a railway test track. *Manufacturing Technology* [online]. 2016, **16**, p. 667-672. ISSN 1213-2489, eISSN 2787-9402. Available from: <https://doi.org/10.21062/ujep/x.2016/a/1213-2489/MT/16/4/667>
- [4] BARANOVSKIY, D., BULAKH, M., MYAMLIN, S., KEBAL, I. New design of the hatch cover to increase the carrying capacity of the gondola car. *Advances in Science and Technology - Research Journal* [online]. 2022, **16**(6), p. 186-191. ISSN 2299-8624. Available from: <https://doi.org/10.12913/22998624/156205>
- [5] FOMIN, O., GERLICI, J., LOVSKA, A., GORBUNOV, M., KRAVCHENKO, K., PROKOPENKO, P., HAUSER, V. The improved hatch cover construction for universal open box-type wagon from the strength and durability point of view. *Manufacturing Technology*, 2019, **19**(2), p. 216-221. ISSN 1213-2489, eISSN 2787-9402. Available from: <https://doi.org/10.21062/ujep/272.2019/a/1213-2489/MT/19/2/216>
- [6] NIKITCHENKO, A., ARTIUKH, V., SHEVCHENKO, D., MISAILOV, A., MAKHOV, D. The use of nonlinear dynamic analysis in the calculation of cargo fall onto the hatch of the gondola car. *E3S Web of Conferences* [online]. 2019, **110**, 01050. eISSN 2267-1242. Available from: <https://doi.org/10.1051/e3sconf/201911001050>
- [7] VIZNYAK, R. I., CHEPURCHENKO, I. V., YATSENKO, A. O. Peculiarities of determining operational loads of a semi-car body and ways of improving its design in order to ensure durability and preservation (in Ukrainian). *Collection of Scientific Works of the Ukrainian State University of Railway Transport*. 2016, **159**, p. 91-97. ISSN 2413-3795.
- [8] ZAYNITDINOV, O. I., RUZMETOV, Y. O., RAHIMOV, R., LAFTA, W. M. Development of new polymer composite materials for the flooring of rail carriage. *International Journal of Engineering and Technology* [online]. 2020, **9**(2), p. 378-381. ISSN 1793-8236. Available from: <https://doi.org/10.14419/ijet.v9i2.30519>
- [9] KARAKAEV, A. K., ZARIPOV, R. Y. Composite materials in freight car building. *Science and Technology of Kazakhstan*. 2016, **1-2**, p. 39-47. ISSN 2788-8770.
- [10] LOVSKA, A., NERUBATSKYI, V., PLAKHTII, O., MYAMLIN, S. Determining the influence of sandwich-type components on the load of a hatch cover in a universal open wagon. *Eastern-European Journal of Enterprise Technologies* [online]. 2024, **1/7**(127), p. 6-13. ISSN 1729-3774, eISSN 1729-4061. Available from: <https://doi.org/10.15587/1729-4061.2024.296620>
- [11] PISARENKO, G. S., KVITKA, O. L., UMANSKYI, E. S. Resistance of materials: textbook (in Ukrainian). Kyiv: Higher school, 2004. ISBN 966-642-056-2.
- [12] SHVABYUK, V. I. *Resistance of materials: textbook* (in Ukrainian). Kyiv: Knowledge, 2016. ISBN 978-617-07-0360-4.
- [13] KOZYAR, M. M., FESHCHUK, Y. V., PARFENYUK, O. V. *Computer graphics: SolidWorks: tutorial* (in Ukrainian). Kherson: Oldi-plus, 2018. ISBN 978-966-289-191-1.
- [14] PUSTYLGA, S. I., SAMOSTYAN, V. R., KLAKE, Y. V. *Engineering graphics in SolidWorks: training manual*. (in Ukrainian). Lutsk: Tower, 2018.
- [15] CABAN, J., NIEOCZYM, A., GARDYNSKI, L. Strength analysis of a container semi-truck frame. *Engineering Failure Analysis* [online]. 2021, **127**, 105487. ISSN 1350-6307, eISSN 1873-1961. Available from: <https://doi.org/10.1016/j.engfailanal.2021.105487>
- [16] SOUKUP, J., SKOCILAS, J., SKOCILASOVA, B., DIZO, J. Vertical vibration of two axle railway vehicle. *Procedia Engineering* [online]. 2017, **177**, p. 25-32. ISSN 1877-7058. Available from: <https://doi.org/10.1016/j.proeng.2017.02.178>
- [17] PANCHENKO, S., GERLICI, J., VATULIA, G., LOVSKA, A., PAVLIUCHENKOV, M., KRAVCHENKO, K. The analysis of the loading and the strength of the FLAT RACK removable module with viscoelastic bonds in the fittings. *Applied Sciences* [online]. 2023, **13**(1), 79. eISSN 2076-3417. Available from: <https://doi.org/10.3390/app13010079>
- [18] PANCHENKO, S., GERLICI, J., LOVSKA, A., VATULIA, G., RYBIN, A., KRAVCHENKO, O. Strength assessment of an improved design of a tank container under operating conditions. *Communications - Scientific Letters of the University of Zilina* [online]. 2023, **25**(3), p. B186-B193. ISSN 1335-4205, eISSN 2585-7878. Available from: <https://doi.org/10.26552/com.C.2023.047>
- [19] SUPRIANTO, T., SYAIFUDIN, A., PAMUNGKAS, L. W., ARIATEDJA, J. B., FARID, A. R. Effect of fluctuating load on fatigue of PPCW flat wagon. *The International Journal of Mechanical Engineering and Sciences* [online]. 2023, **7**(1), p. 26-35. eISSN 2580-7471. Available from: <http://dx.doi.org/10.12962/j25807471.v7i1.14354>
- [20] KONDRATIEV, A., POTAPOV, O., TSARITSYNSKYI, A., NABOKINA, T. Optimal design of composite shelled sandwich structures with a honeycomb filler [online]. In: *Advances in design, simulation and manufacturing IV. DSMIE 2021. Lecture notes in mechanical engineering*. IVANOV, V., TROJANOWSKA, J., PAVLENKO, I.,

ZAJAC, J., PERAKOVIĆ, D. (eds.). Cham: Springer, 2021. ISBN 978-3-030-77718-0. eISBN 978-3-030-77719-7.  
Available from: [https://doi.org/10.1007/978-3-030-77719-7\\_54](https://doi.org/10.1007/978-3-030-77719-7_54)

- [21] DSTU 7598:2014. Freight wagons. General requirements for calculations and design of new and modernized wagons of 1520 mm track (non-self-propelled). (in Ukrainian). Kyiv: UkrNDNTS, 2015.



UNIVERSITY  
OF ŽILINA

In its over 70 years of successful existence, the University of Žilina (UNIZA) has become one of the top universities in Slovakia.



## World University Rankings by subject

Arts & humanities

Business & economics

Education

Law

Social sciences

Computer science

Engineering

Clinical & health

Life sciences

Physical sciences

Psychology

The University of Žilina is a public university located in Žilina, Slovakia and is the only university located in the north western region of Slovakia.

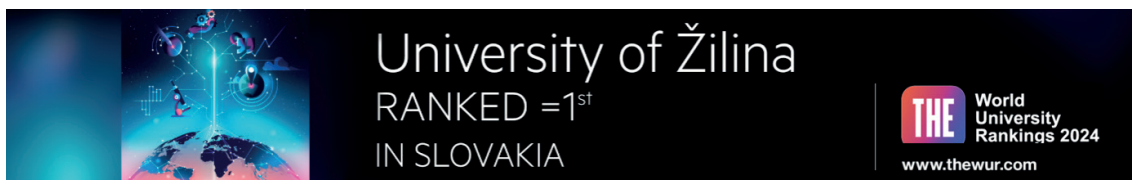
It first began as the College of Railways in 1953 and was subsequently renamed the University of Transport in 1959. It has been operating under its current name since 1996.

The university offers undergraduate, graduate and doctoral courses in wide range of subjects ranging from transport to marketing and humanities.

The university is well known for its engineering programs and has research partnerships with universities across the world.

The university is involved in a wide array of scientific projects such as the TEMPUS, COST, National Scholarship Programme, and the DAAD. The university also actively organises several scientific and professional events and is working to deepen its engagement through its University Science Park and Research Centre.

The university has a large and modern campus located near the serene forest park in Žilina. It offers students a wide range of amenities such as relaxation zones, libraries, dormitories and cafeterias. There are active student clubs which organise a wide range of events and activities every year.



Slovakia

**University of Žilina**

**1001–1200<sup>th</sup>**  
World University Rankings  
2024

**1501+**  
Impact Rankings 2024

📍 Univerzitná 8215/1, 010 26 Žilina, Slovakia

**UNIVERSITY OF ŽILINA**  
**Science & Research Department**

Univerzitná 8215/1,  
010 26 Žilina,  
Slovakia

Ing. Janka Macurová  
tel.: +421 41 513 5143  
e-mail: [janka.macurova@uniza.sk](mailto:janka.macurova@uniza.sk)



This is an open access article distributed under the terms of the Creative Commons Attribution 4.0 International License (CC BY 4.0), which permits use, distribution, and reproduction in any medium, provided the original publication is properly cited. No use, distribution or reproduction is permitted which does not comply with these terms.

# A PARTICLE SWARM OPTIMIZATION BASED FUZZY FLCPI-PSO CONTROLLER FOR QUADCOPTER SYSTEM

Mohammed Baba<sup>1,\*</sup>, Fateh Bounaama<sup>2</sup>, Sid Bennaceur<sup>3</sup>, Aissa Benhammou<sup>1</sup>, Mohammed Amine Soumeur<sup>1</sup>

<sup>1</sup>Laboratory of Smart Grids and Renewable Energies (SRGE), University Tahri Mohammed Bechar, Bechar, Algeria

<sup>2</sup>Laboratory of Energy in Arid Zones (ENERGARID), University Tahri Mohammed Bechar, Bechar, Algeria

<sup>3</sup>Laboratory of Renewable Energies and their Applications in Saharan areas (LDREAS), University Tahri Mohammed Bechar, Bechar, Algeria

\*E-mail of corresponding author: baba.mouhamed@univ-bechar.dz

Mohammed Baba 0000-0002-8644-3253,

Said Benaceur 0000-0003-4911-8694,

Mohammed Amine Soumeur 0000-0001-9303-4880

Fateh Bounaama 0000-0001-7230-5792,

Aissa Benhammou 0000-0003-3313-2571,

## Resume

The quadcopter persist as important roles across diverse applications, and the enhancement of their control efficacy has been the subject of extensive research.

In this work, the authors proposed optimal Proportional Integral (PI) controller based Fuzzy Logic Control (FLC) for the roll, pitch, altitude, and yaw motions of the quadcopter system.

The proposed technique uses the Particle Swarm Optimization (PSO) algorithm to tune the parameters of the FLC and enhance the quadcopter performance. The simulation results show that the proposed technique achieves smoothness of control and significant improvement over classical techniques, as the rise time and the settling time are reduced by 61 % and 66 %, respectively. These times are important for stabilizing the system's response speed and avoiding overshooting or oscillating. This indicates that the FLCPI-PSO can achieve the desired roll and altitude angles more rapidly and effectively.

## Article info

Received 21 September 2023

Accepted 18 March 2024

Online 4 April 2024

## Keywords:

quadcopter model  
fuzzy logic controller  
optimization  
FLCPI-PSO

Available online: <https://doi.org/10.26552/com.C.2024.027>

ISSN 1335-4205 (print version)

ISSN 2585-7878 (online version)

## 1 Introduction

Quadcopter drones, as autonomous aerial vehicles, have garnered significant attention from both researchers and manufacturers due to their versatility in exploration and study. Their compact size and unique capabilities for spatial monitoring and infrastructure inspection have spurred the evolution of such systems. Among the various drone configurations, Vertical Take-Off and Landing (VTOL) models are particularly noteworthy for their lightweight motors and efficient propeller arrangements that eliminate the need for a tail rotor, thus simplifying the control mechanism [1].

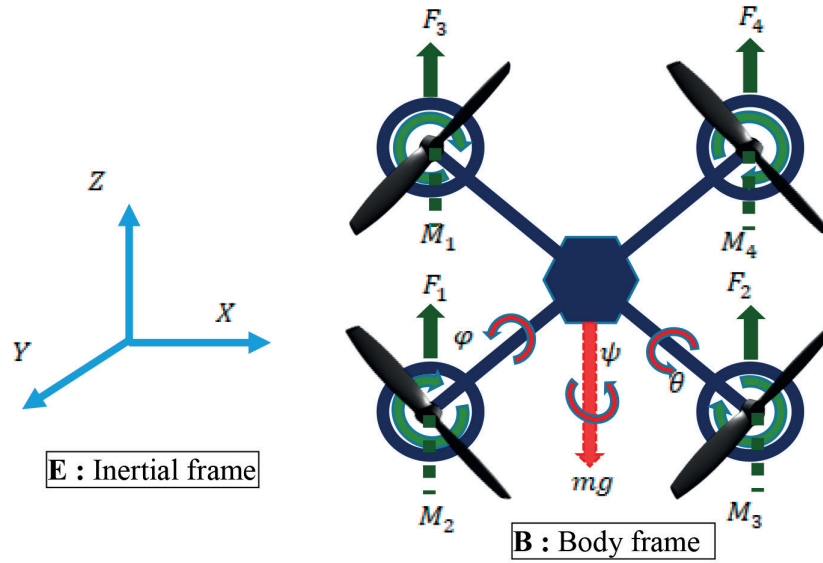
The topology of quadcopters typically involves front and rear motors of the same diameter rotating in opposite directions to their diametric counterparts, which negates gyroscopic effects and facilitates stable flight [2-4]. The study of the input forces influence on

output coordinates reveals a strongly coupled dynamic system [5].

Advancements in control methods have been applied across diverse fields, including electric cars [6-7], power electronics [8], and hybrid electric systems [9-10]. To meet the increasing performance demands of quadcopters, enhancements in controller design have been implemented, such as Feedback Linearity (FBL) [11-12], Sliding Mode Control (SMC) [13-14], and backstepping methods [15-16]. Comparative analyses of various controllers, including Proportional Integral Derivative (PID), linear quadratic regulator (LQR), and modified PID with LQR control, are well-documented [17-18].

Fuzzy logic models, specifically the Takagi-Sugeno (TS) and Mamdani types, are the two fundamental and distinct approaches in intelligent control systems that have been integrated into electrical systems alongside Neural Networks (NN) [4, 19-21], Neuro-





**Figure 1** The structure of quadcopter

Fuzzy methodology [22-23], and Iterative Learning Control (ILC) [24-25]. These intelligent control methods are adept at managing unpredictable, non-linear, time-varying, and non-deterministic systems [26]. Fuzzy logic, in particular, is capable of handling the disturbances and noises (rotor vibrations) that quadrotors frequently encounter [27].

It has been noted that fuzzy control necessitates precise technology for selecting input constants [28]. The modular architecture of the fuzzy controller facilitates its integration with various optimizers to circumvent limitations.

In this paper, the mathematical model was developed using the Newton-Euler method to control altitude  $Z$ , roll ( $\varphi$ ), pitch ( $\theta$ ), and yaw ( $\psi$ ) angles.

To accurately and steadily navigate the quadcopter, a FLC and an optimized fuzzy PID controller (FLCPI-PSO) are utilized for the control component, representing the core contribution of this work. The novelty of this paper lies in evaluating the quadcopter's behavior and performance through the optimization of a basic FLC with a swarm technique. This proposed control technique endows the quadcopter with acceptable response times, thereby enhancing its behavior—a facet not previously explored in other studies.

The remainder of this research paper is organized as follows: Section 1 presents the mathematical model, Section 2 discusses the control strategy, Section 3 contains the simulation results and discussion, and the paper concludes with the conclusions and future perspectives of this study.

## 2 Mathematical model

A quadcopter is an aerial vehicle equipped with four rotors that enable 360-degree maneuverability. To accurately describe the system dynamics, it is essential

to understand the concept of six degrees of freedom, which represents the location and orientation of the quadcopter in three-dimensional (3-D) space. The six degrees of freedom are defined using two reference frames as illustrated in the quadcopter structure shown in Figure 1:

1. The inertial or earth frame, a fixed coordinate system represented by the  $x$ ,  $y$ , and  $z$  coordinates, corresponding to the cardinal directions of north, east, and down. This frame serves as the initial reference point.
2. The body frame, a movable coordinate system centered around the quadcopter's center of gravity, described by the angles ( $\varphi$ ), ( $\theta$ ), and ( $\psi$ ) in relation to the inertial frame.

Given that the quadcopter has four inputs and six outputs, it is classified as an underactuated nonlinear system. To facilitate the controller design, sensible assumptions are made to model the system dynamics of the quadcopter effectively [29].

### 2.1 Kinematic model

To derive a model for the quadcopter motions it is necessary to examine different moments and forces acting on the quadcopter.

We assume  $\xi = [XYZ]$  to be the position and the linear velocity  $V = [uvw]$ , and let  $\eta = [\phi\theta\psi]$  to be rotational angles and angular velocity is  $\omega = [pqr]$ .

Using the Newton-Euler equations and the information proaccessed in Equation (1), one can determine the forces and moments acting on the quadcopter [30]:

$$\begin{bmatrix} F \\ \tau \end{bmatrix} = \begin{bmatrix} mI_{3 \times 3} & 0 \\ 0 & 1 \end{bmatrix} + \begin{bmatrix} \omega \times m\xi \\ \omega \times I\eta \end{bmatrix}, \quad (1)$$



where;  $F$  and  $\tau$  represent the force and torque vector, respectively, generated by the four motors' rotation acting on the quadcopter,  $m$  is the mass of the quadcopter,  $\dot{V}$  and  $\dot{\omega}$  represent linear and angular acceleration vector, respectively, all with respect to the body frame, and  $I_{3 \times 3}$  represents the moments of inertia matrix and is given as:

$$I = \begin{bmatrix} I_{xx} & 0 & 0 \\ 0 & I_{yy} & 0 \\ 0 & 0 & I_{zz} \end{bmatrix}. \quad (2)$$

Typically, the angular positions and velocities above are in a different frame, so we need some kind of transformation matrix to go from one reference frame to the other. The rotation  $R$  and transfer  $T$  matrices, respectively, are used to derive the translational and rotational kinematic equations [31]. Equations (3) and (4), respectively, processed the expressions for the rotation  $R$  and transfer  $T$  matrices.

$$R = \begin{bmatrix} c\phi c\theta & c\phi s\theta s\phi - s\phi c\phi & c\phi s\theta c\phi + s\phi c\phi \\ s\phi c\theta & s\phi s\theta s\phi - c\phi c\phi & s\phi s\theta c\phi - c\phi s\phi \\ -s\theta & c\theta s\phi & c\theta c\phi \end{bmatrix}, \quad (3)$$

$$T = \begin{bmatrix} 1 & t\theta s\phi & t\theta c\phi \\ 0 & c\phi & -s\phi \\ 0 & s\phi/c\theta & c\phi/c\theta \end{bmatrix}, \quad (4)$$

where,  $c\theta = \cos \theta$ ,  $s\theta = \sin \theta$ , and  $t\theta = \tan \theta$ .

- The translational kinematics:

$$\dot{\xi} = RV, \quad (5)$$

where  $\dot{\xi}$  are linear velocity vector with respect to the earth frame E and  $V$  is the linear velocity vector with respect to body frame B.

- The rotational kinematics:

$$\dot{\omega} = T \dot{\eta}, \quad (6)$$

where  $\dot{\omega}$  is the angular velocity vector with respect to the earth frame E and  $\dot{\eta}$  the angular velocity vector with respect to body frame B.

## 2.2 Dynamic model

The translational dynamic equations of the quadcopter are given as follows in accordance with the Euler's first rule of motion for rigid body dynamics:

$$m \begin{bmatrix} \ddot{X} \\ \ddot{Y} \\ \ddot{Z} \end{bmatrix} = \begin{bmatrix} 0 \\ 0 \\ -mg \end{bmatrix} + RU_1, \quad (7)$$

where  $g$  is the gravity acceleration and  $U_1$  is the total thrust generated by the four rotors:

$$U_1 = \sum_{i=1}^4 F_i = b \sum_{i=1}^4 \Omega_i^2, \quad (8)$$

where  $b[N s^2]$  is the thrust coefficient and  $\Omega[\frac{rad}{sec}]$  is the angular velocity of the rotor  $i$ .

From Equation (1) and the Newton-Euler formalism, we obtain the rotational motion equations:

$$I\ddot{\eta} = \tau - \dot{\eta} \times I\dot{\eta} - \dot{\eta} \times [0 \ 0 \ I_r \Omega_r], \quad (9)$$

where  $I$  is an inertia matrix of the quadcopter,  $I_r$  is the inertia of the rotors,  $\Omega_r$  is the relative speed and  $\tau$  is the moment acting on the quadcopter in the body frame.

$$\Omega_r = (-\Omega_1 - \Omega_3 + \Omega_2 + \Omega_4), \quad (10)$$

$$\tau = \begin{bmatrix} U_2 \\ U_3 \\ U_4 \end{bmatrix} = \begin{bmatrix} bl(\Omega_4^2 - \Omega_2^2) \\ bl(\Omega_3^2 - \Omega_1^2) \\ dbbl(\Omega_4^2 - \Omega_2^2 - \Omega_3^2 + \Omega_1^2) \end{bmatrix}, \quad (11)$$

where  $d[N m s^2]$  is the drag coefficient and  $l[m]$  is the distance between the center of the quadcopter and the center of a propeller.

From Equation (7) and Equation (9), the equations motion of the quadcopter are given as follows:

$$\dot{X} = (\sin \phi \sin \varphi + \cos \phi \sin \theta \cos \varphi) \frac{U_1}{m}, \quad (12)$$

$$\dot{Y} = (-\cos \phi \sin \varphi + \sin \phi \sin \theta \cos \varphi) \frac{1}{m} U_1, \quad (13)$$

$$\dot{Z} = -g + \frac{1}{m}(\cos \theta \cos \varphi) U_1, \quad (14)$$

$$\ddot{\phi} = \frac{\dot{\theta}\phi(I_{yy} - I_{zz})}{I_{xx}} - \frac{J_r}{I_{xx}} \Omega_r \dot{\theta} + \frac{U_2}{I_{xx}}, \quad (15)$$

$$\ddot{\theta} = \frac{\dot{\phi}\phi(I_{zz} - I_{xx})}{I_{yy}} + \frac{J_r}{I_{yy}} \Omega_r \phi + \frac{U_3}{I_{yy}}, \quad (16)$$

$$\ddot{\phi} = \frac{\dot{\theta}\phi(I_{xx} - I_{yy})}{I_{zz}} + \frac{U_4}{I_{zz}}. \quad (17)$$

## 3 Control strategy

### 3.1 Fuzzy logic controller (FLC)

The FLC is the consequence of Zadeh's fuzzy set notion in 1965. Fuzzy set theory was graded from non membership to membership. Thus, the boundaries of fuzzy sets might be unclear and ambiguous, making them suitable for approximation systems. If correct mathematical formulations are problematic, the FLC is the best accessible solution. Other FLC benefits include:

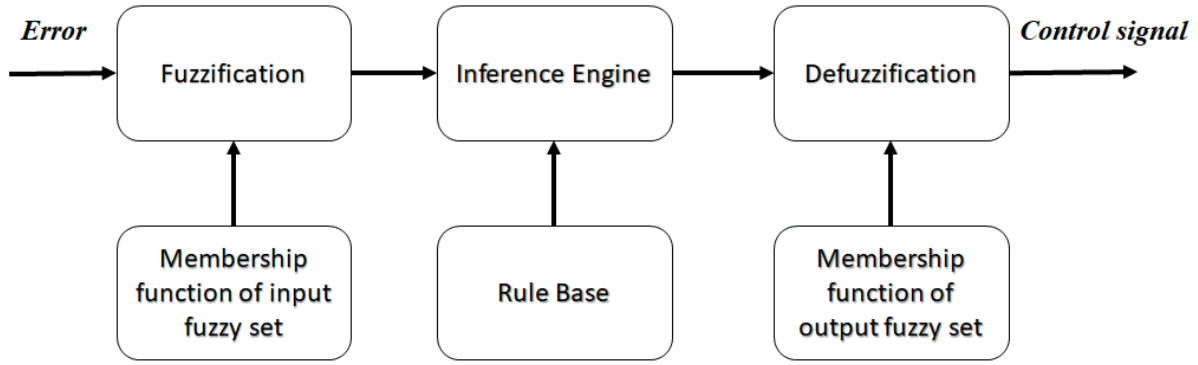


Figure 2 The structure of the Fuzzy Logic Control

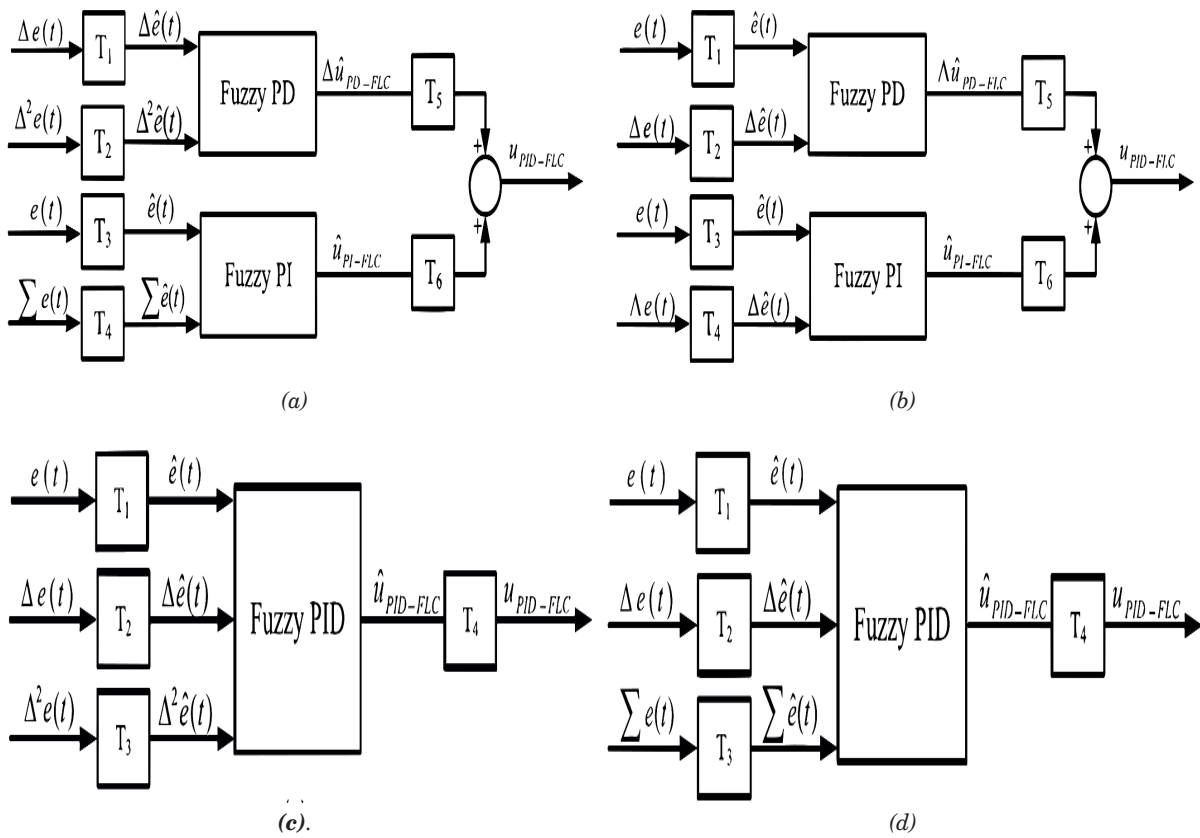


Figure 3 Common PID-type fuzzy logic controllers [28]

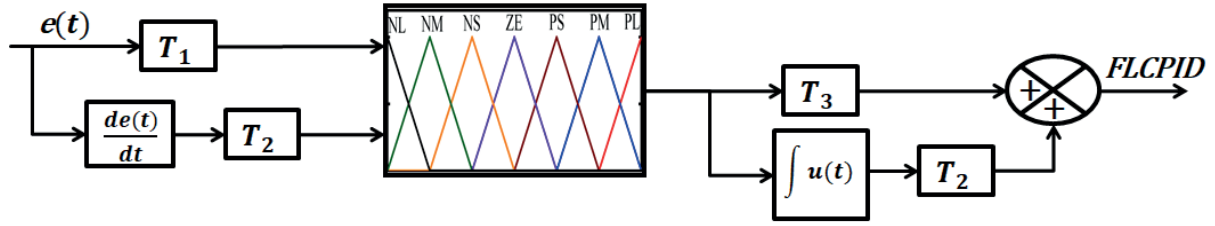
1. It may seek to proprocessed less precise outcomes.
2. There is no requirement for rapid processors.
3. It does not take as much data storage in the formula of rule and membership function MF as compared to typical controllers.

The structure of the FLC is given in Figure 2.

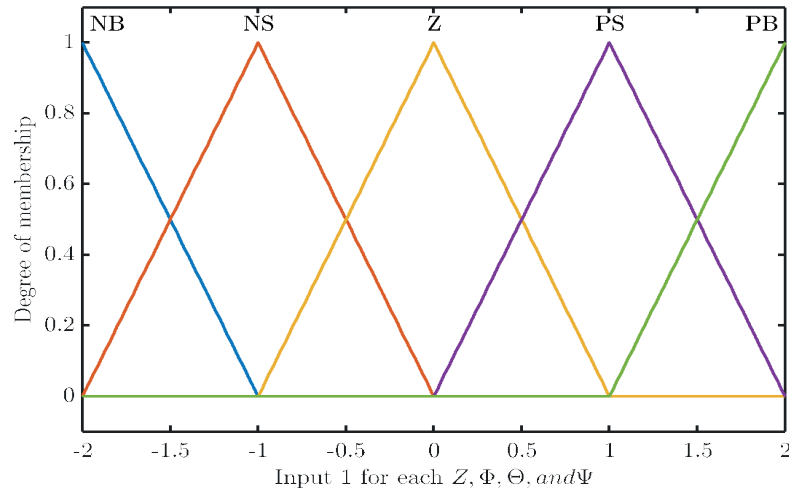
The direct action fuzzy controller structure is simply referred to as PID-type fuzzy controller or PID-FLC. However, the term fuzzy PID controller (or FLCPI) refers to the so-called gain scheduling-type PID controllers, which are not covered in this work. In these controllers, fuzzy logic is employed to generate the necessary KP, KI, and KD gains for the linear PID controller. The amount of inputs to the fuzzy PID controllers determines how

they are often categorized. The most prevalent fuzzy control architectures, in which a nonlinear PID-like performance is anticipated from the controller, are often two- and three-input fuzzy controllers. Figure 3 shows a few of the most widely utilized structures. It should be noted that the fuzzy controllers' input/output variables are normalized to fall between [1-1]. As a result, the first two structures (see Figure 3.a and 3.b) need the appropriate selection of six scaling factors, while the last two structures (see Figure 3.c and 3.d) require the proper selection of four scaling factors [28].

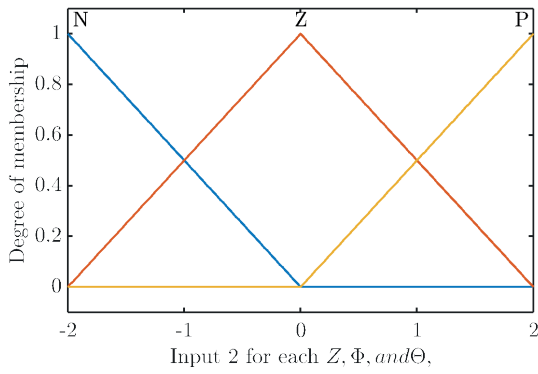
Throughout this study, a different structure is used; it is shown in Figure 4. The proprocessed structure has one single two-input fuzzy controller, which makes



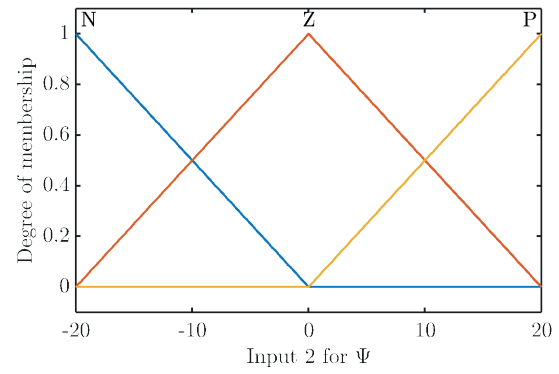
**Figure 4** Alternative fuzzy PID controller



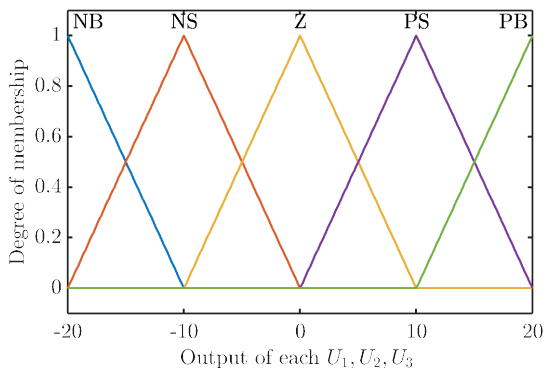
**Figure 5** The MF for the input variable error of altitude and three angle roll, pitch, yaw



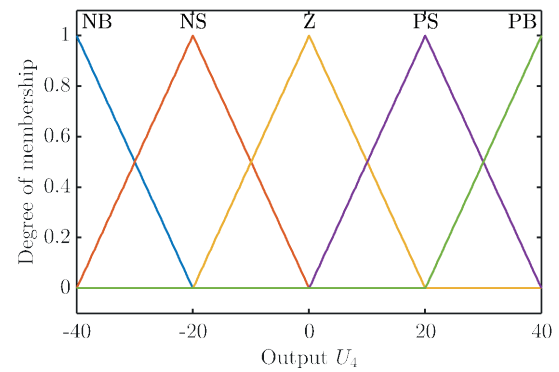
**Figure 6** The MF for the input variable (de) derivative error for roll and pitch angle and altitude



**Figure 7** The MF for the input variable (de) derivative error for the yaw angle



**Figure 8** The MF for the output variable ( $U_1, U_2, U_3$ )



**Figure 9** The MF for the output variable ( $U_4$ )

**Table 1** The rules base for the four fuzzy logic controllers (altitude, roll, pitch, and yaw Controllers)

e de	NB	NM	Z	PM	PB
N	NB	NM	NM	Z	PM
Z	NB	NM	Z	PM	PB
P	NM	Z	PM	PM	PB

it computationally more efficient for the real-time implementation when compared to that in Figure 3. In comparison to three-input architectures, the fuzzy controller only needs two inputs, hence fewer rule bases need to be constructed.

This study is thus limited to fuzzy controllers of the Mamdani-Type.

### 3.1.1 Fuzzification

The total control system for the quadcopter with the Fuzzy PID controllers for the four fundamental quadcopter movements thrust, roll, pitch, and yaw is depicted in Figure 4. The triangle membership function has been utilised for each of the inputs and the outputs and for all of the controllers. The inputs, errors are defined by five membership functions MF: NB (negative big), NS (negative small), Z (zero), PS (positive small), and PB (positive big), and the error derivative is defined by three membership functions: P(positive), Z(zero), N(negative). On the other hand, each of the outputs is specified by five membership functions: NB (negative big), NS (negative small), Z (zero), PS (positive small), and PB (positive big). The range of the fuzzy set for the error input for all controllers (altitude, roll, pitch, and yaw) has been chosen as  $[-2, 2]$ , and for the error derivative for (altitude, roll, and pitch controllers) as  $[-4, 4]$ , and  $[-20, 20]$  for the error derivative of yaw controller. Figures 5 to 7 show the membership functions for the inputs.

The range for the outputs fuzzy set has been chosen as follows:

- $[-20, 20]$  for  $U_1, U_2, U_3$ , and as indicated in Figure 8,
- $[-40, 40]$  for  $U_4$  and as indicated in Figure 9.

### 3.1.2 Rules base

After specifying the inputs and outputs for each fuzzy controller, we established the rules base.

The fuzzy rules suggest that “if error is  $E_i$  and error change is  $DE_i$ , then production is  $U_i$ ”. The fuzzy inference procedure of the controller parameters leverages the Mamdani approach. Five variables refer to errors, and three error changes are added to the 15 rules.

If the change in error is NB and the error is NB, then the outcome will be NB, as well. The response signal is fed back and subtracted from the set value to generate the error signal, and then the change in error

is determined after the subtraction. Those two signals are sent as inputs to the controller. Table 1 shows the rules base for each controller.

### 3.1.3 Defuzzification

Fuzzification’s counterpart is known as defuzzification. The fuzzy set generated by the FLC inference engine must be transformed to actual value (crisp output) in line with the real-world requirements. Defuzzification implies the weighted average approach. The weighted average strategy becomes the illustrating point, which is the centre of the region generated by the curve and abscissa of the fuzzy membership function. Theoretically, the centre of gravity of a set of sites within the output scope must be computed [32].

## 3.2 Particle swarm optimization algorithm

Finding the best solutions involves using a variety of optimisation techniques. Evolutionary and meta-heuristic approaches work best when employed for route planning.

Numerous evolutionary techniques have been demonstrated to be useless when route planning procedures have an excessively wide search area. The exciting findings from this vast area of study may help the meta-heuristic systems to overcome these limitations.

The population-based stochastic optimisation method, known as the particle swarm optimisation (PSO), is very similar to evolutionary computing methods like genetic algorithms (GA). The PSO has been effectively used in several research and application domains over the last few years because it produces better results more quickly with fewer parameters to alter.

The PSO uses particles to represent possible solutions, which follow the current optimal particles as they move around the problem space. According to their prior behaviours, particles move around the search space at velocities that are dynamically changed.

The system starts out with a population of random solutions and updates generations in an effort to find the best option. The location of a point  $X_i = (x_{i,1}, x_{i,2}, \dots, x_{i,d}) \in S$  in an S-dimensional space serves as the representation of the i-th particle. Each particle keeps track of three values during the process: its best position in previous cycles; its present position,

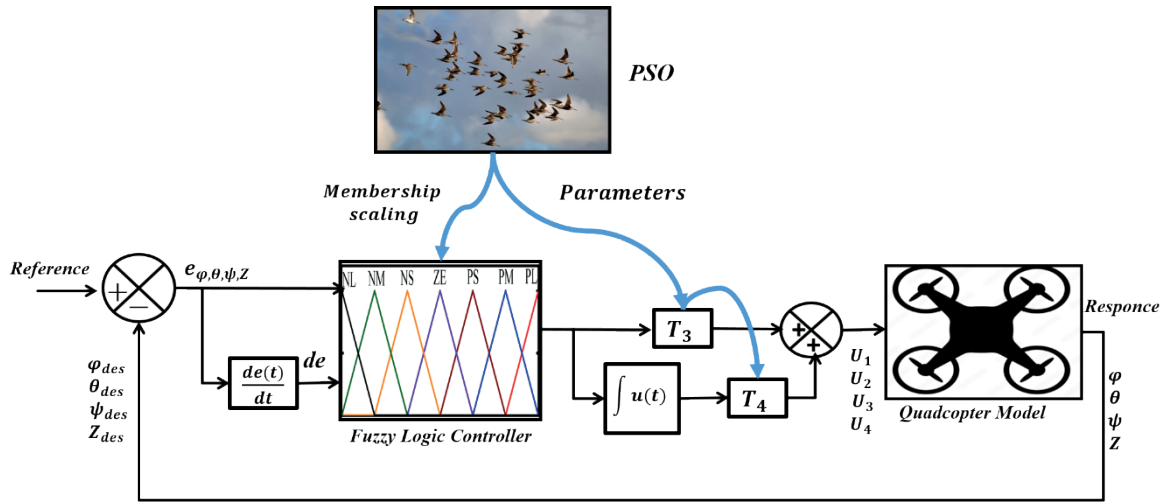


Figure 10 Structure of FLCPI-PSO controller

$X_i$ .  $pbest_i = (pbest_{i,1}, pbest_{i,2}, pbest_{i,3}, \dots, pbest_{i,d}) \in S$ ; and the speed of its flight  $V_i = (v_{i,1}, v_{i,2}, v_{i,3}, \dots, v_{i,d})$ . To catch up to the leading particle, each particle modifies its location and velocity, such as:

$$X_i(t+1) = X_i(t) + V_i(t+1), \quad (18)$$

$$V_i(t+1) = V_i(t) + c_1 r_{i,1}(t)(pbest_i(t) - X_i(t)) + c_2 r_{i,2}(t)(gbest(t) - X_i(t)). \quad (19)$$

The best track value for each particle in iteration  $t$  is denoted by  $pbest_i$ , and the best position of the entire swarm is denoted by  $gbest$ . The cognitive and social parameters are denoted, respectively, by  $c_1$  and  $c_2$ , two positive constants (acceleration coefficients), and  $r_{i,1}$  and  $r_{i,2}$ , two random functions in the  $[0, 1]$  range.

The following is a summary of an approach to determine the optimal placement vector for the PSO with  $n$  Agents:

1. Using the random numbers, the initial positioning vector  $X[n]$  and velocity vector  $V[n]$  are created.
2. Using Equation (1), agent  $i$ 's velocity vector  $V_i(t+1)$  is determined.
3. Equation (2) is used to determine agent  $i$ 's new positioning vector,  $X_i(t)$ .
4. The positioning vector  $X_i$  is set to  $pbest_i$  if  $F(X(t))$  is superior than  $F(pbest_i)$ . The positioning vector  $gbest$  is set to  $pbest_i$  if  $F(gbest)$  is superior than  $F(pbest_i)$ .
5. When the required number of iterations has been reached, stop. If not, go to step 2.

The first design is a Mamdani-type two-input PID-type fuzzy controller, as shown in Figures 2 and 3. The membership functions in the first level of tuning are uniformly distributed, and the meta-heuristic techniques must be used to tune the scaling factors and parameters  $T_1$ ,  $T_2$ ,  $T_3$ , and  $T_4$ . PSO is employed at this point to identify the ideal scaling factors and parameters

$T_1$ ,  $T_2$ ,  $T_3$ , and  $T_4$ . The optimisation approach is used to reduce many common time domain objective functions, including the integral time absolute of error (ITAE).

The structure of the FLCPI-PSO controller is depicted in Figure 10.

#### 4 Simulation results and discussion

In the design process and simulation studies, a 1-step unit is applied to each height and roll, pitch, and yaw angle concurrently at  $t = 0$  s. The simulation is carried out with Matlab 2017 programme and Simulink Toolbox. The simulation was done on an SGRE laboratory computer with a Intel(R) Core(TM) i7-5820K, 3.30 GHz, 64 GB of RAM, and Windows 10.

The MATLAB Simulink is used to mimic two type of controllers, FLCPI and FLCPI-PSO. These controllers were employed to control the quadcopter systems. The FLCPI with a one-of-a-kind configuration that is adjusted manually and FLCPI-PSO that is tuned via the PSO method Integral Time Absolute Error (ITAE) is used as a criterion for the control performance assessment as in Equation (20).

$$ITAE = \int t|e(t)|dt. \quad (20)$$

Figure 11 displays the objective function of PSO algorithm.

As a result, the tuned scaling factors and parameters of four controllers are presented in Table 2.

The quadcopter system response, after an occurrence of step-unit changes is depicted in Figures 12 to 15. The responses quadcopter system characteristics are summarized in Table 3.

The control signals ( $U_1$  through  $U_4$ ), which represent the desired thrust force and torques, are shown in Figures 16 to 19.

The results presented in Figures 12-15 and Table 3 illustrate the comparative performance of the FLC



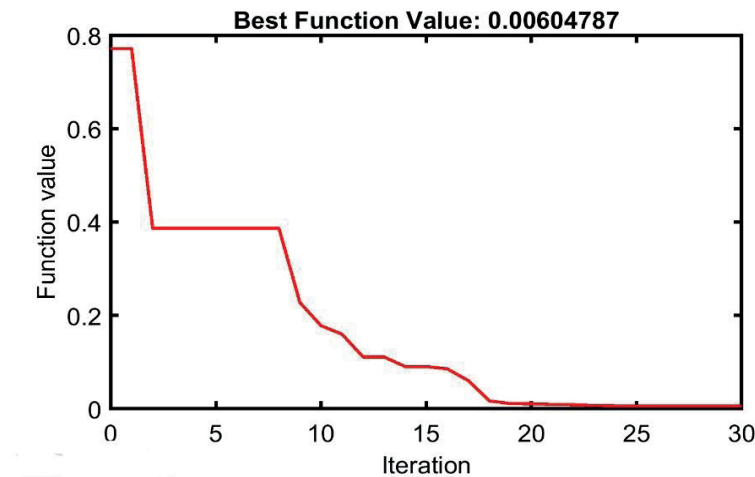


Figure 11 Objective function of PSO algorithm

Table 2 Scaling factors and parameters optimized by the PSO

	Scaling factors		Parameters	
	T1	T2	T3	T4
Altitude	6.1868	55.9443	88.8980	40.2961
Roll	100.0000	99.0577	23.0000	0.2000
Pitch	1.0000	99.1495	77.0602	1.0000
Yaw	9.2101	45.8878	9.0000	0.2300

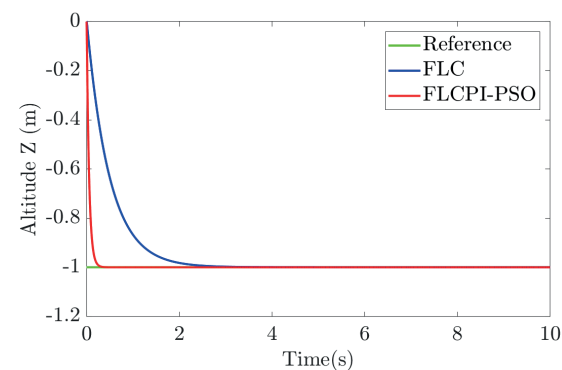


Figure 12 The altitude signal response for the FLC and the FLCPI-PSO controllers

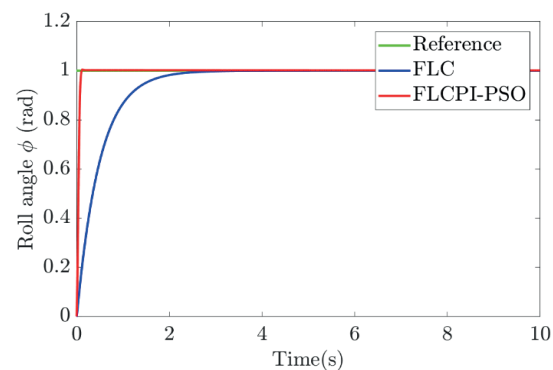


Figure 13 The roll signal response for the FLC and the FLCPI-PSO controllers

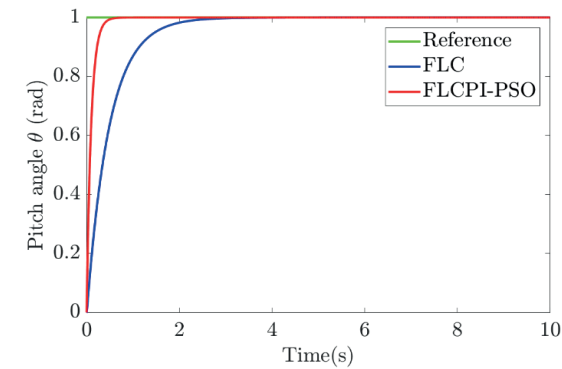


Figure 14 The pitch signal response for the FLC and the FLCPI-PSO controllers

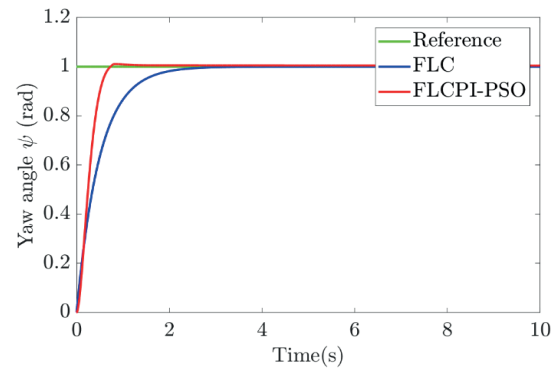
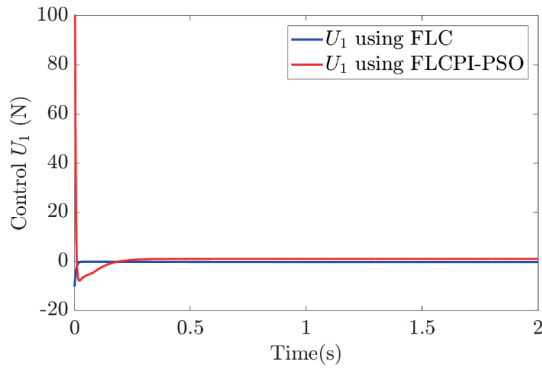
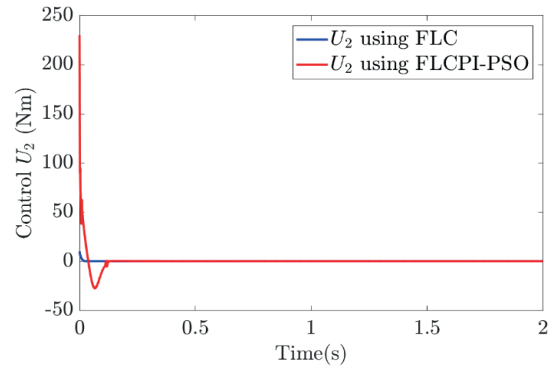


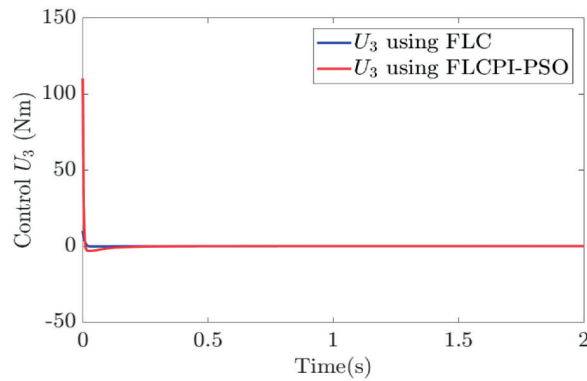
Figure 15 The yaw signal response for the FLC and the FLCPI-PSO controllers



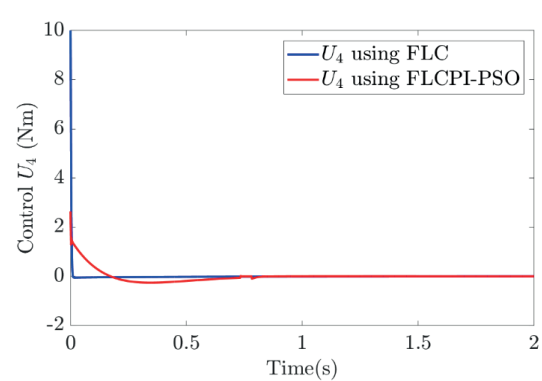
**Figure 16** Control signal  $U_1$  for the FLC and the FLCPI-PSO controllers



**Figure 17** Control signal  $U_2$  for the FLC and the FLCPI-PSO controllers



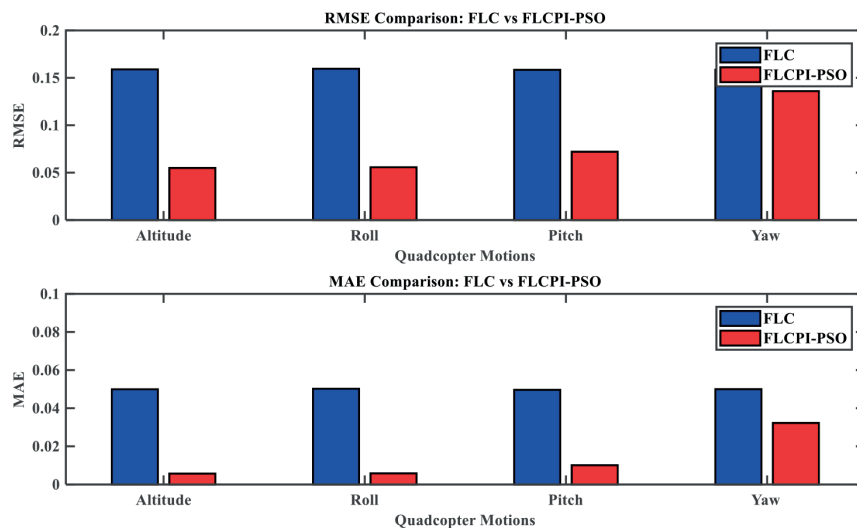
**Figure 18** Control signal  $U_3$  for the FLC and the FLCPI-PSO controllers



**Figure 19** Control signal  $U_4$  for the FLC and the FLCPI-PSO controllers

**Table 3** Responses to a step function with different control

Performances	Controllers							
	Altitude		Roll		Pitch		Yaw	
	FLC	FLCPI-PSO	FLC	FLCPI-PSO	FLC	FLCPI-PSO	FLC	FLCPI-PSO
RiseTime (s)	1.0839	0.1157	1.0869	0.0605	1.0801	0.2143	1.0924	0.4257
SettlingTime (s)	1.9395	0.2094	1.9429	0.0954	1.9334	0.3851	1.9492	0.6632
Overshoot (%)	0	1.9000	0	31.6100	0	0	0	64.1100



**Figure 20** Quadcopter control performance evaluation between the FLC and FLCPI-PSO

and FLCPI-PSO controllers in managing the altitude, roll, pitch, and yaw of a quadcopter. It is evident that the FLCPI-PSO controller consistently outperforms the FLC controller across all parameters. The rise time for altitude, roll, pitch, and yaw is significantly reduced with FLCPI-PSO, indicating a quicker response to changes. Similarly, the settling time is also lower for all the inputs under the FLCPI-PSO control, denoting faster stabilization.

In terms of overshoot percentage, the FLC controller exhibits a 1.9000% overshoot in altitude and a substantial 31.6100% in roll but none in pitch and yaw. In contrast, the FLCPI-PSO controller effectively eliminates overshoot in all parameters except for yaw where it records a 64.1100% overshoot.

These findings underscore the enhanced efficiency and reliability of the FLCPI-PSO controller over its FLC counterpart in ensuring the rapid response times and minimal overshoots during quadcopter operation. The data suggests that the integrating PSO with fuzzy logic control (FLCPI) yields superior control precision and responsiveness.

Comparison of the quadcopter performance evaluation using the KPIs indexes between the FLC and FLCPI-PSO, is shown in Figure 20.

## 5 Conclusion

Based on the comparative analysis of the FLC and FLCPI-PSO for altitude, roll, pitch, and yaw in the quadcopter system, the FLCPI-PSO demonstrates superior performance in terms of faster rise time and

settling time for altitude and roll control compared to the FLC. This indicates that the FLCPI-PSO can achieve the desired altitude and roll angles more efficiently and with quicker response times. The FLCPI-PSO offers advantages in terms of faster response times and shorter settling times for altitude and roll control in the quadcopter system. The trade-off is a potential increase in overshoot, particularly in the roll and yaw control. These findings highlight the importance of considering the specific requirements and trade-offs when selecting the appropriate controller for the quadcopter systems. Future research could focus on further optimizing the FLCPI-PSO to reduce the overshoot, while maintaining its performance advantages and its real-time implementation.

## Acknowledgements

The authors thank the Algerian research direction DGRSDT, and the Smart Grids and Renewable Energies (SGRE) Laboratory, laboratory of Energy in Arid Zones (ENERGARID), and Laboratory of Renewable Energies and their Applications in Saharan areas (LDREAS), for supporting this research.

## Conflicts of interest

The authors declare that they have no known competing financial interests or personal relationships that could have appeared to influence the work reported in this paper.

## References

- [1] PINES, D. J., BOHORQUEZ, F. Challenges facing future micro-air-vehicle development. *Journal of Aircraft* [online]. 2006, **43**(2), p. 290-305. ISSN 1533-3868. Available from: <https://doi.org/10.2514/1.4922>
- [2] HONG, M., BOUSBAINE, A., WU, M. H., POYI, G. T. Modelling and simulation of a quad-rotor helicopter. In: 6th IET International Conference on Power Electronics, Machines and Drives PEMD 2012: proceedings [online]. IEEE. 2012. eISBN 978-1-84919-616-1. Available from: <https://doi.org/10.1049/cp.2012.0318>
- [3] LUPASHIN, S., SCHOLLIG, A., SHERBACK, M., D'ANDREA, R. A simple learning strategy for high-speed quadcopter multi-flips. In: IEEE International Conference on Robotics and Automation: proceedings [online] [accessed 2023-09-21]. 2010, ISSN 1050-4729, p. 1642-1648. ISSN 1050-4729. Available from: <https://doi.org/10.1109/ROBOT.2010.5509452>
- [4] MOHAMMED, B., SAID, B., FATEH, B. Feedforward neural network emulation of a PID continuous-time controller for quadcopter attitude digital control. *International Journal of Power Electronics and Drive Systems* [online]. 2023, **14**(2), p. 799-808 [accessed 2023-09-19]. ISSN 2088-8694. Available from: <https://doi.org/10.11591/ijpeds.v14.i2.pp799-808>
- [5] ELAJRAMI, M., SATLA, Z., BENDINE, K. Drone control using the coupling of the PID controller and genetic algorithm. *Communications - Scientific Letters of the University of Zilina* [online]. 2021, **23**(3), p. C75-C82 [accessed 2024-01-18]. ISSN 1335-4205, eISSN 2585-7878. Available from: <https://doi.org/10.26552/COM.C.2021.3.C75-C82>
- [6] BENHAMMOU, A., HARTANI, A.M., TEDJINI, H., REZK, H., AL-DHAIFALLAH, M. Improvement of autonomy, efficiency, and stress of fuel cell hybrid electric vehicle system using robust controller. *Sustainability* [online]. 2023, **15**(7), 5657 [accessed 2024-01-18]. eISSN 2071-1050. Available from: <https://doi.org/10.3390/SU15075657>
- [7] BENHAMMOU, A., TEDJINI, H., GUETTAF, Y., SOUMEUR, M. A., HARTANI, M. A., HAFSI, O., BENABDELKADER, A. Exploitation of vehicle's kinetic energy in power management of tow-wheel drive electric

- vehicles based on ANFIS DTC-SVM comparative study. *International Journal of Hydrogen Energy* [online]. 2021, **46**(54), p. 27758-27769. ISSN 0360-3199. Available from: <https://doi.org/10.1016/J.IJHYDENE.2021.06.023>
- [8] TOUFIK, T., TAHRI, U., BECHAR, M., ABDELKHALEK, O., AHMED, A., ABDELKADER, B., OTHMANE, A., AISSA, B., OUSSAMA, H. Dynamic voltage restorer using sliding mode controller: experimental studies Benhammou Aissa Dynamic voltage restorer using sliding mode controller: experimental studies. *International Journal of Applied Power Engineering* [online]. 2021, **10**(4), p. 337-346. ISSN 2252-8792. Available from: <https://doi.org/10.11591/ijape.v10.i4.pp337-346>
- [9] BOUNAAMA, F., LAMMARI, K., DRAOUI, B., BOUNAAMA, F., LAMMARI, K., DRAOUI, B. Greenhouse air temperature control using fuzzy PD+I and neuro-fuzzy hybrid system controller. *International Journal on Numerical and Analytical Methods in Engineering (IRENA)* [online]. 2016, **4**(6), p. 172-178 [accessed 2024-01-18]. ISSN 2533-1736. Available from: <https://doi.org/10.15866/IRENA.V4I6.12055>
- [10] AISSA, B., HAMZA, T., YACINE, G., AMINE, H. M. Impact of artificial intelligence in renewable energy management of hybrid systems. *Physical Sciences Forum* [online]. 2023, **6**(1), 5 [accessed 2024-01-18]. ISSN 2673-9984. Available from: <https://doi.org/10.3390/PSF2023006005>
- [11] ALQAISI, W., BRAHMI, B., GHOMMAM, J., SAAD, M., NERGUIZIAN, V. Vision-based leader-follower approach for uncertain quadrotor dynamics using feedback linearisation sliding mode control. *International Journal of Modelling, Identification and Control* [online]. 2019, **33**(1), p. 9-19 [accessed 2023-09-21]. ISSN 1746-6180. Available from: <https://doi.org/10.1504/IJMIC.2019.103980>
- [12] KUANTAMA, E., TARCA, I., TARCA, R. Feedback linearization LQR control for quadcopter position tracking. In: 2018 5th International Conference on Control, Decision and Information Technologies CoDIT 2018: proceedings [online] [accessed 2023-09-21]. IEEE: 2018. eISSN 2576-3555, 204-209. Available from: <https://doi.org/10.1109/CODIT.2018.8394911>
- [13] CHIEW, T. H., LEE, H. E., LEE, Y. K., CHANG, K. M., ONG, J. J., EU, K. S. Second order sliding mode controller for altitude and yaw control of quadcopter. In: 2021 11th IEEE International Conference on Control System, Computing and Engineering ICCSCE 2021: proceedings [online]. IEEE. 2021. eISBN 978-1-6654-1281-0, p. 97-102. Available from: <https://doi.org/10.1109/ICCSCE52189.2021.9530850>
- [14] SURAJ, S. K., GEORGE, V. I., THIRUNAVUKKARASU, I., VALSA PAUL, T. Design and simulation of a sliding mode-based control design for a quadrotor UAV. *Lecture Notes in Electrical Engineering* [online]. 2021, **750**, p. 495-507 [accessed 2023-09-19]. ISSN 1876-1119. Available from: [https://doi.org/10.1007/978-981-16-0336-5\\_41/COVER](https://doi.org/10.1007/978-981-16-0336-5_41/COVER)
- [15] BOUCHAIB, A., TALEB, R., MASSOUM, A., MEKHILEF, S. Geometric control of quadrotor UAVs using integral backstepping. *Indonesian Journal of Electrical Engineering and Computer Science* [online]. 2021, **22**(1), p. 53-61 [accessed 2023-09-21]. ISSN 2502-4760. Available from: <https://doi.org/10.11591/IJEECS.V22.I1.PP53-61>
- [16] MOEINI, A., LYNCH, A. F., ZHAO, Q. A backstepping disturbance observer control for multirotor UAVs: theory and experiment. *International Journal of Control* [online]. 2022, **95**(9), p. 2364-2378 [accessed 2023-09-19]. ISSN 1366-5820. Available from: <https://doi.org/10.1080/00207179.2021.1912393>
- [17] ARGENTIM, L. M., REZENDE, W. C., SANTOS, P. E., AGUIAR, R. A. PID, LQR and LQR-PID on a quadcopter platform. In: 2013 International Conference on Informatics, Electronics and Vision ICIEV 2013: proceedings [online]. IEEE. 2013. ISBN 978-1-4799-0397-9, eISBN 978-1-4799-0400-6. Available from: <https://doi.org/10.1109/ICIEV.2013.6572698>
- [18] AHMAD, F., KUMAR, P., BHANDARI, A., PATIL, P. P. Simulation of the quadcopter dynamics with LQR based control. *Materials Today: Proceedings* [online]. 2020, **24**(2), p. 326-332. ISSN 2214-7853. Available from: <https://doi.org/10.1016/j.matpr.2020.04.282>
- [19] ELTAYEB, A., RAHMAT, M. F., ELTOUM, M. A. M., IBRAHIM, M. H. S., BASRI, M. A. M. Trajectory tracking for the quadcopter UAV utilizing fuzzy PID control approach. In: 2020 International Conference on Computer, Control, Electrical, and Electronics Engineering, ICCCEEE 2020: proceedings [online]. IEEE. 2021. eISBN 978-1-7281-9111-9. Available from: <https://doi.org/10.1109/ICCCEEE49695.2021.9429636>
- [20] TALHA, M., ASGHAR, F., ROHAN, A., RABAH, M., KIM, S. H. Fuzzy logic-based robust and autonomous safe landing for UAV quadcopter. *Arabian Journal for Science and Engineering* [online]. 2019, **44**(3), p. 2627-2639 [accessed 2023-09-19]. ISSN 2191-4281. Available from: <https://doi.org/10.1007/S13369-018-3330-Z/METRICS>
- [21] BREESE, B., SCOTT, D., BARAWKAR, S., KUMAR, M. Fuzzy logic controller for force feedback control of quadcopter via tether. In: ASME 2020 Dynamic Systems and Control Conference DSCC 2020: proceedings [online] [accessed 2023-09-19]. 2021. Available from: <https://doi.org/10.1115/DSCC2020-3275>
- [22] DARWITO, P. A., INDAYU, N. Adaptive neuro-fuzzy inference system based on sliding mode control for quadcopter trajectory tracking with the presence of external disturbance. *Journal of Intelligent Systems and Control* [online]. 2023, **2**(1), p. 33-46 [accessed 2023-09-19]. ISSN 2957-9805. Available from: <https://doi.org/10.56578/JISC020104>

- [23] KORKMAZ, D., ACIKGOZ, H., USTUNDAG, M. Altitude and attitude control of a quadcopter based on neuro-fuzzy controller. *Lecture Notes in Electrical Engineering* [online]. 2022, **829**, p. 1009-1015 [accessed 2023-09-19]. ISSN 1876-1119. Available from: [https://doi.org/10.1007/978-981-16-8129-5\\_154/COVER](https://doi.org/10.1007/978-981-16-8129-5_154/COVER)
- [24] ABDOLAH, Y., REZAEIZADEH, A. Black-box identification and iterative learning control for quadcopter. In: 2018 6th International Conference on Control Engineering and Information Technology CEIT 2018: proceedings [online]. IEEE. 2018. eISBN 978-1-5386-7641-7. Available from: <https://doi.org/10.1109/CEIT.2018.8751795>
- [25] PIPATPAIBUL, P., OUYANG, P. R. Application of online iterative learning tracking control for quadrotor UAVs. *International Scholarly Research Notices* [online]. 2013, **2013**, 476153. ISSN 2356-7872. Available from: <https://doi.org/10.5402/2013/476153>
- [26] BEHERA, L., KAR, I. *Intelligent systems and control: principles and applications*. New Delhi, India: Oxford University Press, 2010. ISBN 9780198063155.
- [27] PEDRO, J. O., KALA, P. J. Nonlinear control of quadrotor UAV using Takagi-Sugeno fuzzy logic technique. In: 2015 10th Asian Control Conference ASCC: proceedings [online]. IEEE. 2015. eISBN 978-1-4799-7862-5. Available from: <https://doi.org/10.1109/ASCC.2015.7244739>
- [28] NOSHADI, A., SHI, J., LEE, W. S., SHI, P., KALAM, A. Optimal PID-type fuzzy logic controller for a multi-input multi-output active magnetic bearing system. *Neural Computing and Applications* [online]. 2016, **27**(7), p. 2031-2046 [accessed 2024-01-17]. ISSN 0941-0643. Available from: <https://doi.org/10.1007/S00521-015-1996-7/METRICS>
- [29] BOUABDALLAH, S. Design and control of quadrotors with applications to autonomous flying [online]. Lausanne, EPFL, 2007. Available from: <https://doi.org/10.5075/epfl-thesis-3727>
- [30] SAUD, L. J., MOHAMMED, S. R. Performance evaluation of a PID and a fuzzy PID controllers designed for controlling a simulated quadcopter rotational dynamics model. *Journal of Engineering* [online]. 2017, **23**(7), p. 74-93 [accessed 2024-01-13]. ISSN 2520-3339. Available from: <https://doi.org/10.31026/J.ENG.2017.07.05>
- [31] BRESCIANI, T. Modelling, identification and control of a quadrotor helicopter. MSc theses [online]. 2008 [accessed 2024-01-13]. ISSN 0280-5316. Available from: <http://lup.lub.lu.se/student-papers/record/8847641>
- [32] MATTAVELLI, P., ROSSETTO, L., SPIAZZI, G., TENTI, P. General-purpose fuzzy controller for DC-DC converters. *IEEE Transactions on Power Electronics* [online]. 1997, **12**(1), p. 79-86 [accessed 2023-09-21]. ISSN 0885-8993. Available from: <https://doi.org/10.1109/63.554172>





This is an open access article distributed under the terms of the Creative Commons Attribution 4.0 International License (CC BY 4.0), which permits use, distribution, and reproduction in any medium, provided the original publication is properly cited. No use, distribution or reproduction is permitted which does not comply with these terms.

# THE POWER ANALYSIS OF SEMICONDUCTOR DEVICES IN MULTI-PHASE TRACTION INVERTER TOPOLOGIES APPLICABLE IN THE AUTOMOTIVE INDUSTRY

Jakub Šimčák\*, Michal Frivaldský, Patrik Resutík

Department of Mechatronics and Electronics, Faculty of Electrical Engineering and Information Technologies, University of Zilina, Zilina, Slovakia

\*E-mail of corresponding author: jakub.simcak@uniza.sk

Jakub Simcak 0009-0000-9628-7752,  
Patrik Resutik 0000-0001-6643-4045

Michal Frivaldsky 0000-0001-6138-3103,

## Resume

The article deals with the power analysis of semiconductor devices nowadays commonly used in perspective traction inverter topologies suitable for automotive industry applications. The power analysis is devoted to topologies, which are the Voltage Source Inverter (VSI) topology and perspective three-level alternatives, which are the Neutral Point Clamped (NPC) and T-type Neutral Point Clamped (T-NPC) traction inverter topologies. The main part of the power analysis of the proposed topologies is done on multi-phase versions (specifically six-phase). Mentioned topologies are modelled through the use of the simulation environment PLECS, while the focus is given on the accurate determination of semiconductor devices' power losses. Collected data of each analyzed topology are then processed using the MATLAB environment. The analysis of power parameters aims to find out which of the mentioned topologies achieves the highest efficiency as an VSI system at various power levels using the same input parameters.

## Article info

Received 18 March 2024

Accepted 9 May 2024

Online 14 June 2024

## Keywords:

multi-phase traction inverter

multi-level traction inverter

VSI

NPC

T-NPC

power loss analysis

Available online: <https://doi.org/10.26552/com.C.2024.034>

ISSN 1335-4205 (print version)

ISSN 2585-7878 (online version)

## 1 Introduction

At this moment, the sales of electrified vehicles are rising due to political support, battery technology improvements, growing charging infrastructure, and more and more new models from vehicle manufacturers. Electrification of the automotive industry is also spreading to new divisions of the road transport, which sets the new possible changes across the automotive industry. In the year 2022, electrified vehicles had a 14 % share of sales in the passenger cars category. This percentage number has risen every year since 2015, and it is predicted that this trend will continue. The global sales of electrified passenger cars in 2022 have grown by around 40 % compared to 2021. The largest share of the increase in global sales of electrified vehicles was recorded in China. Their global sales share doubled as compared to 2021 [1-4].

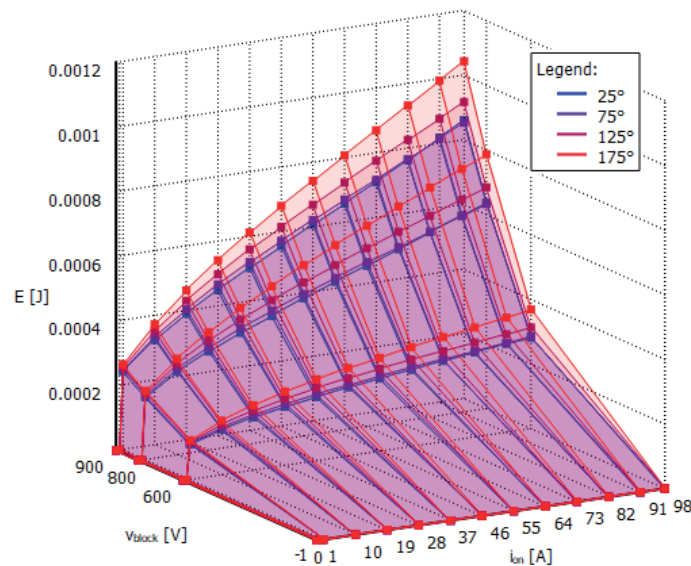
Due to targets for reaching the carbon neutrality in road transport by 2050, research on the new possible

improvements is needed across the entire traction drive of electrified vehicles [5].

There are several traction inverters possibility to enhance the power parameters. A traction inverter is a part of the traction drive of electrified vehicles and there are several possible ways to improve its power parameters. Since the commonly used traction drive now uses, mostly IGBT (Insulated gate bipolar transistor) - based, two-level Voltage Source Inverter topology (one leg contains the half-bridge connection of the semiconductor switching devices) [2], which can be seen in Figure 1, the first possible change that occurs, which can improve the power parameters of the inverter, is to replace the IGBT with wide-bandgap (WBG) devices as SiC MOSFETs. These WBG devices have several advantages compared to Si IGBT. Operation at higher temperatures, higher breakdown voltages, lower switching losses at higher frequencies, and lower chip size are the reasons why Silicon Carbide (SiC) and Gallium Nitride (GaN) MOSFETs are suitable for IGBT

**Table 1** Common input parameters for all the analyzed traction inverter topologies

Electrical variable/unit	value
DC-Link input voltage [V]	800
DC-Link capacitor [ $\mu$ F]	300
Switching frequency [kHz]	20
Continuous output power [kW]	10 - 100
Power factor [-]	0.75
Estimated efficiency [%]	98

**Figure 1** Thermal model of the NTBG020N120SC1 - Turn on switching losses

replacement [6-10].

Apart from that, there are other options for achieving the higher efficiency of the traction inverter. For example, a change in the number of phases of the traction inverter from three-phase drives to multi-phase ones. In the case of automotive traction drives, the closest development step would be six-phase drives. Multi-phase drives split the power into a higher number of phases, which means that the power ratings per phase are lower [4]. Improved current handling, enhanced fault tolerance, reduced DC-Link capacitor requirements, as well as modularity are the main strengths of the multiphase inverters [11-14].

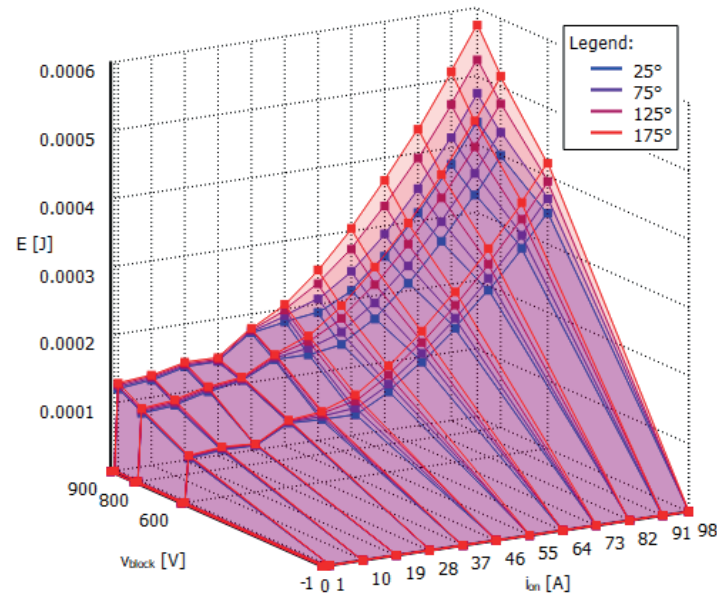
Another possible traction drive enhancement is to change the two-level VSI topology with an alternative topology. Three-level inverters were, based on advanced studies, presented as the most viable alternative for the nowadays used VSI architecture. There were studies, that suggested that the two most competitive three-level topologies that have been developed are T-type Neutral Point Clamped (T-NPC) and Neutral Point Clamped (NPC). The efficiency of the VSI topology is higher than the mentioned two topologies only at lower switching frequencies than 10 kHz. At a higher switching frequency than 10, but lower than 30 kHz, T-NPC topology is expected to be more efficient, while at the higher switching frequencies than 30 kHz the NPC

topology provides higher efficiency than both mentioned topologies. Apart from that the three-level topologies offer lower harmonic distortion of the output voltage and offer reduced requirements for the EMI filter. However, the volume of DC-Link capacitors is twice that big compared to the VSI topology. In addition, the costs of producing three-level inverters are higher and the control is more complex [15-18].

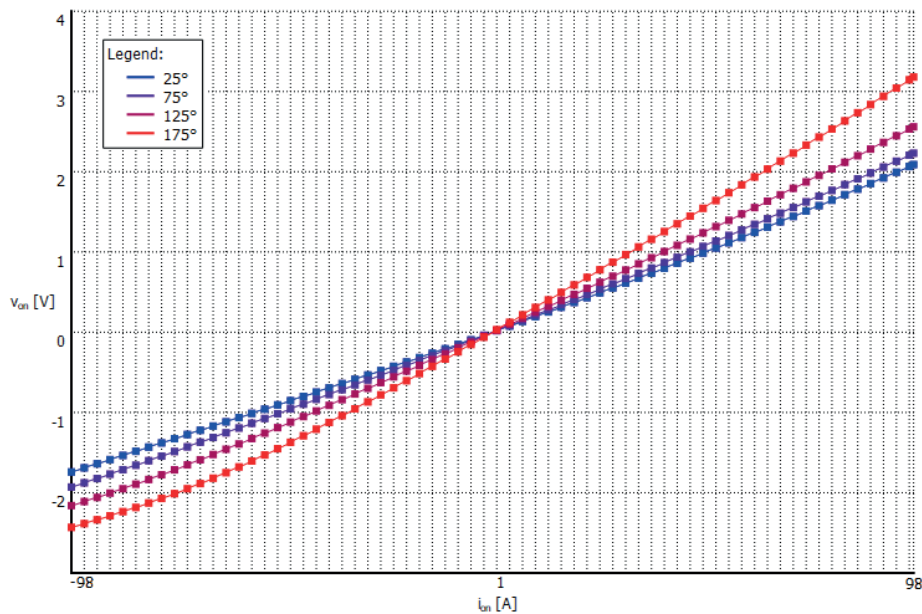
This study is devoted to analyzing the power losses of the semiconductor devices of the three-phase VSI, its six-phase version, and six-phase three-level topologies NPC and T-NPC, at the same power levels. The power analysis performed in the PLECS software deals with the power losses of the semiconductor switching devices, from which the all analyzed traction inverter topologies are composed. Output power parameters obtained from the analysis are compared to each other to investigate the highest efficiency of the traction inverter system topology.

## 2 Operational parameters of the simulation models of investigated VSI alternatives

All the analyzed topologies are built based on the same input parameters, semiconductor switching devices (ones that are directly connected to a DC-Link),



**Figure 2** Thermal model of the NTB020N120SC1 - Turn-off switching losses



**Figure 3** Thermal model of the NTB020N120SC1 - Conduction losses

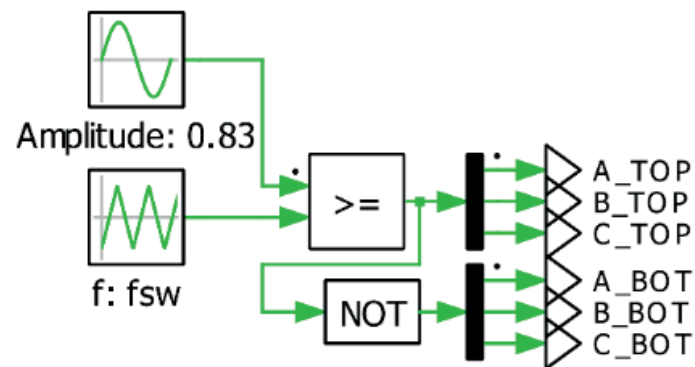
simulation model of the cooling system, control technique, and parameters of the AC load. The input parameters are shown in Table 1.

These input parameters were selected based on the literature that deals with future trends in automotive traction drive systems described in [3-5]. The value of the DC-Link capacitor was determined based on the calculations using the method mentioned in [7]. In all the proposed analyses of the topologies, discrete silicon carbide semiconductor devices from *onsemi* were used. To be able to reach the high-power levels, such as 100 kW, with the use of discrete packages of semiconductor devices, their parallel connection is necessary to be applied.

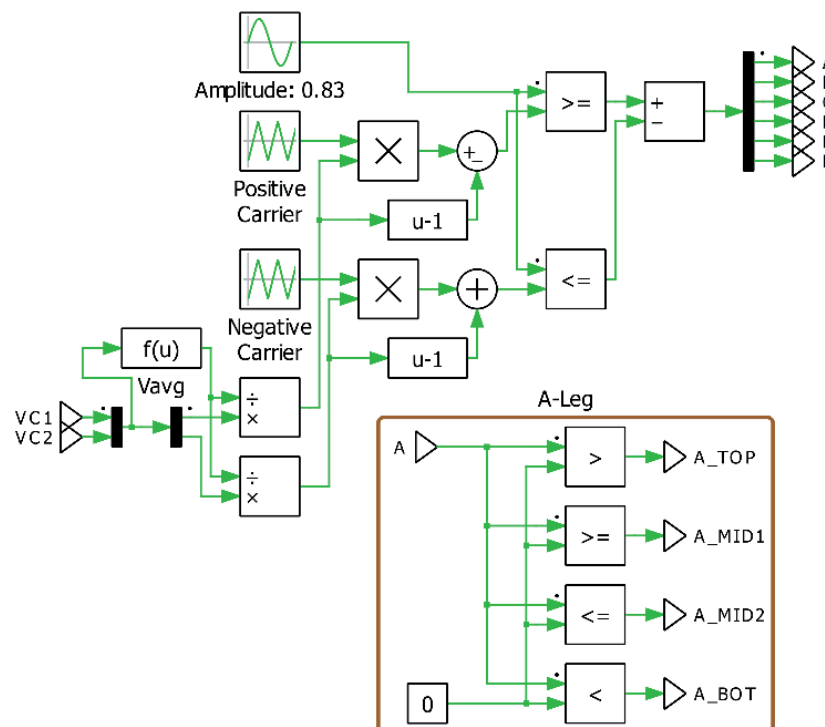
Based on the previous work with the PLECS simulation software, the power loss calculations

using this software are considered accurate, which enables fast-analyzing power losses of any circuit, that contains semiconductor devices. Since the PLECS works with thermal modelling of the semiconductor devices, it is possible to analyze the power losses of each semiconductor device of each proposed traction inverter topology suitable for automotive applications. The example of the thermal model of the switching device used in majority of the analyzed topologies NTB020N120SC1 SiC MOSFET by *onsemi* can be seen in Figure 1 to Figure 3.

Any other semiconductor device, used in power parameters analysis in PLECS, must have its thermal model. This is what the thermal models of all used semiconductor devices in the power parameters analysis look like. These thermal models can be created based on



**Figure 4** Block scheme of the two-level three-phase SinePWM control technique



**Figure 5** Block scheme of the three-level six-phase SinePWM control technique with the example of comparison for each switching device

the datasheet information, or some of the manufacturers nowadays offer these thermal models already created on their website or the PLECS website. Apart from the loss's waveforms, the PLECS thermal models contain information about the change of switching losses based on the change of the gate resistance or the thermal chain table.

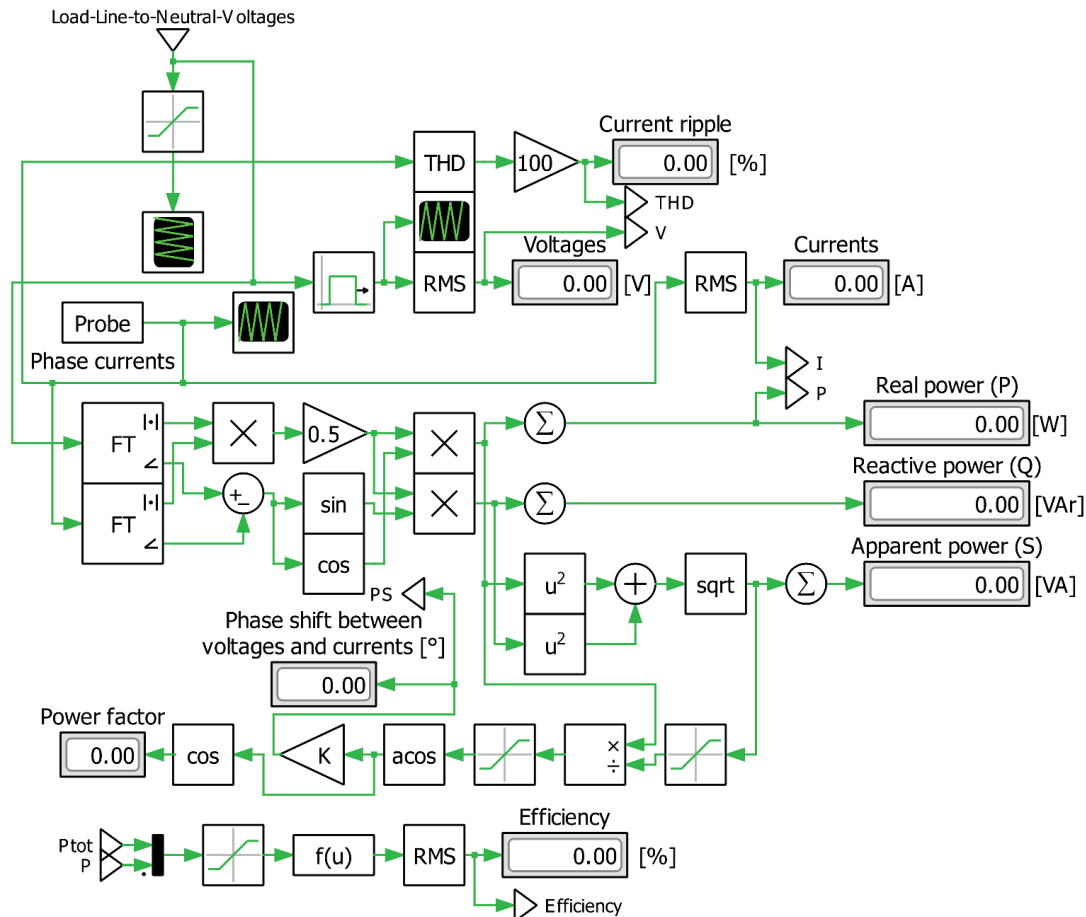
Apart from the common input parameters, the used control technique, for all the analyzed topologies, is a sinusoidal pulse width modulation (SinePWM). It is because of its simplicity. The SinePWM control method is the most often used across the industry [19-21].

The block scheme of the two-level SinePWM, which is used as a control technique for the three-phase VSI topology analysis in PLECS can be seen in the block scheme in Figure 4. The same control technique, but modified to a three-level one, was used for the NPC

and T-NPC topologies of the traction inverter. The block scheme of the modified SinePWM for three-level topologies can be seen in Figure 5, where the division algorithm for the A-Legs switching devices of the three-level inverter topology is also shown.

### 3 Power loss analysis of the traction inverter topologies simulation models

The analyzed topologies of the traction inverter suitable for automotive applications are the three-phase Voltage Source Inverter (nowadays commonly used across the automotive industry), its six-phase version, and the three-level six-phase topologies, which are NPC and T-NPC. These topologies were analyzed in PLECS, where based on the input parameters the power loss calculation was performed.



**Figure 6** Calculation scheme for the efficiency evaluation of the investigated VSI alternatives

As it was mentioned in the previous section, SiC MOSFET NTB020N120SC1 is used in the majority of analyzed topologies. This MOSFET blocking voltage is 1200 V. Since the selected input voltage is 800 V, the closest suitable power SiC MOSFET value of the blocking voltage category is 1200 V. MOSFETs with a blocking voltage of 900 V are also commercially available, but in order not to damage the given switching device with overvoltage, it is necessary to take into consideration a 20% margin of the blocking voltage, which at the value of the input voltage of 800 V is 160 V above its limit value. It means that these 900 V blocking voltage MOSFETs are not suitable for this application. The 1200 V blocking voltage switching device is used in both versions of the VSI topology and T-NPC as a switching device connected to the DC-Link (TOP and BOT ones).

The required blocking voltage level of the semiconductor devices used in the NPC topology is the half value of the DC-Link input voltage plus a 20% reserve. For this reason, 650 V blocking voltage MOSFETs NTB015N065SC1 were selected. Their value of continuous drain current varies based on the temperature but even at 100 °C does not drop below 103 A. These MOSFETs are also used as a bipolar switch in the T-NPC topology.

The NPC topology also contains clamping Schottky diodes, which should be zero recovery ones. The voltage

level of these diodes is the same as the MOSFETs. So, based on these key parameters of the clamping diodes, the FFSH5065B-F085 from *onsemi* was selected.

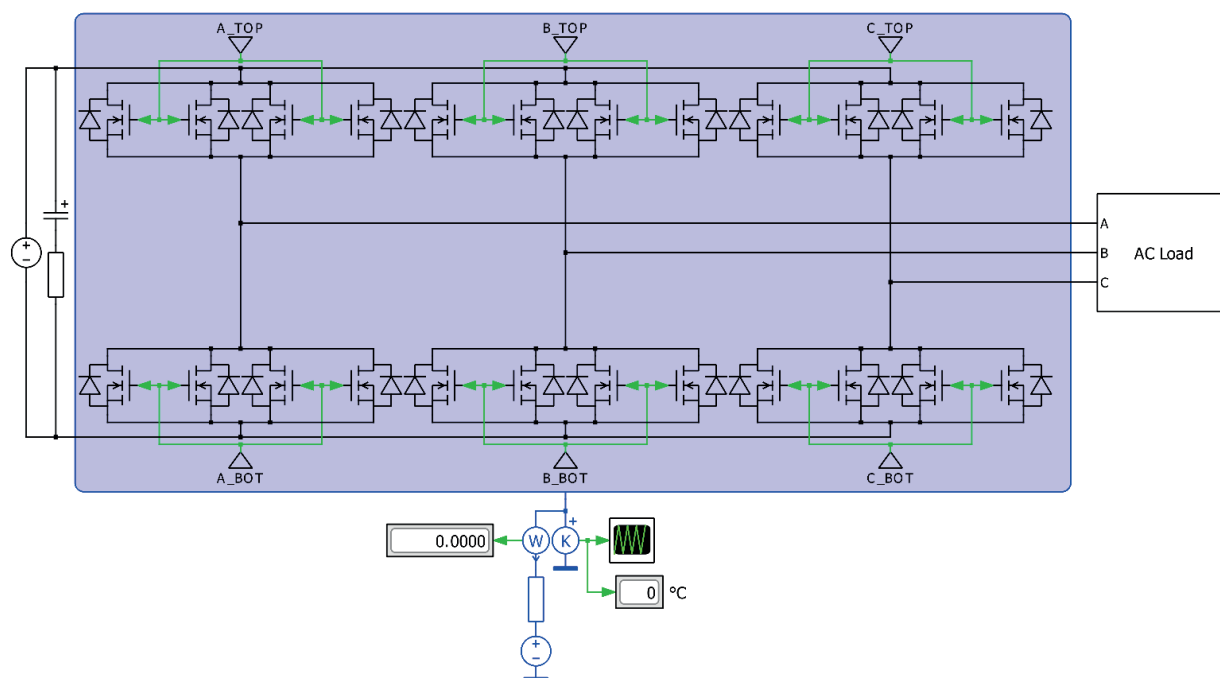
For the estimation of efficiency of individual VSI alternatives, the calculation scheme was used (Figure 6). As is seen from the figure, the circuit connection contains Fourier transformation blocks, in order to evaluate individual power components, i.e. the active power, reactive power and apparent power. Instead of evaluation of the total system efficiency, power factor is evaluated, as well. The power losses of the inverters are estimated for active and passive (filter components) devices of the main circuit, while built-in block of the simulation environment have been used (Switch Loss Calculator for power semiconductors and periodic averaging scheme for passive components).

### 3.1 The three-phase voltage source inverter topology

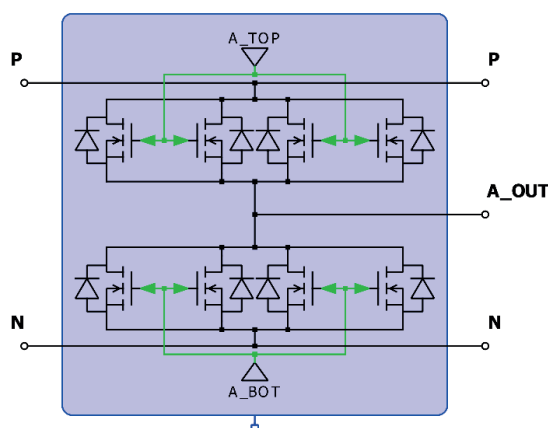
Voltage Source Inverter topology is commonly used topology in automotive traction inverters due to its reliability, robustness, and relatively high efficiency at lower costs [3].

A simulation model of the three-phase Voltage Source Inverter topology, assembled by the discrete





**Figure 7** Three-phase Voltage Source Inverter topology



**Figure 8** A-Leg of the analyzed circuit of the three-phase VSI topology

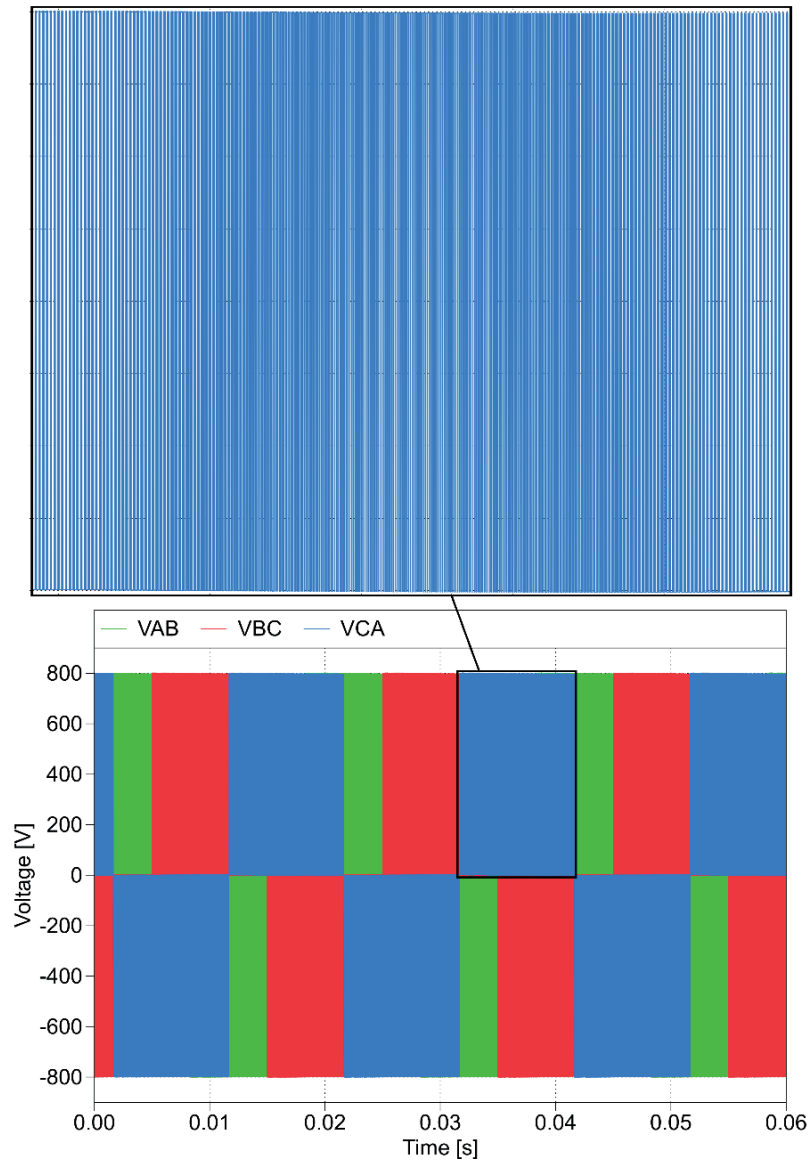
switching devices, is shown in Figure 7. The VSI topology consists of a half-bridge connection of two switching devices for each phase.

Figure 8 shows a closer look at the one phase of the three-phase VSI topology. As can be seen, one switch consists of four parallel connected NTB020N120SC1 SiC MOSFETs to be able to reach the current requirements for the maximum of 100 kW output power, at an acceptable junction temperature of SiC MOSFETs (lower than 175 °C). At 20 kHz switching frequency, the RMS value of junction temperature of each parallel connected SiC MOSFET was at 74.4 °C. A parallel connection of the switching devices is needed because the maximum value of NTB020N120SC1 continuous drain current is only 98 A, where the value is lowered by circa 20 A when the 20% reserve rule is applied.

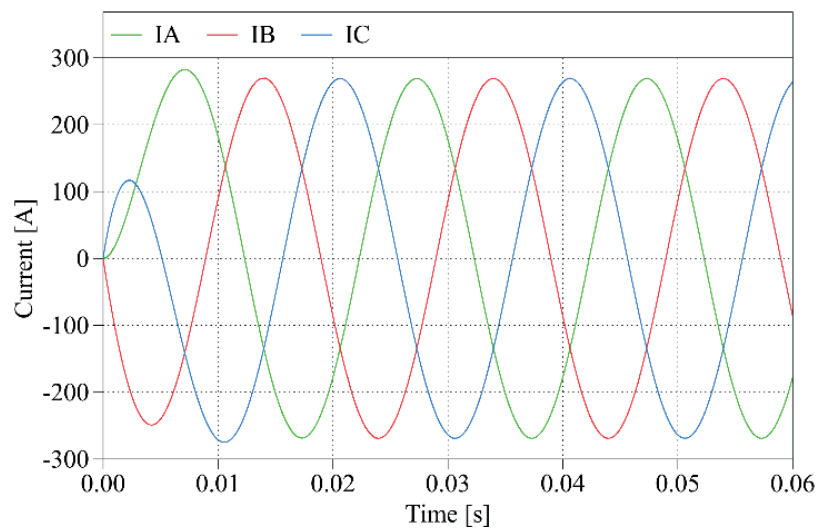
Before the power parameters analysis (determination of power loss values), it is important to verify the system's functionality. In Figure 9 and Figure 10, the

output waveforms of line voltages and phase currents of the AC Load can be seen, which demonstrate the correct functionality of the three-phase VSI topology system. The RMS value of the AC load line-to-neutral voltage, at all power levels, was on average 234.39 V. The two-level character of the line-to-line voltages is easily observable in Figure 8. The AC load current RMS value at the highest power level (100 kW) was 190.18 A. As can be seen in Figure 9, the total harmonic distortion (THD) of the phase current is low. The value of the phase current THD, at all power levels, for the three-phase VSI topology is 0.19%.

Power losses of the three-phase VSI topology at the different power levels are shown in Figure 11. In this figure, it can be noticed that at output power values lower than 30 kW, the switching losses form most of the total power losses. From the 30 kW conduction losses form most of the power losses. When using these semiconductor devices, the power losses reach



**Figure 9** Line-to-line voltage waveforms of the three-phase VSI at 100 kW output power



**Figure 10** Phase current waveforms of the three-phase VSI at 100 kW output power

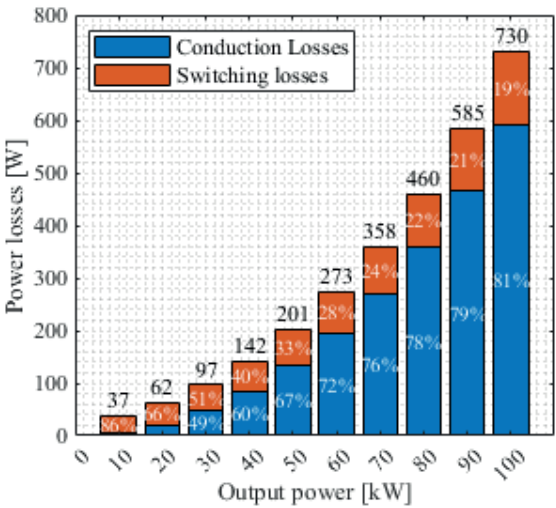


Figure 11 Power losses of the three-phase VSI topology

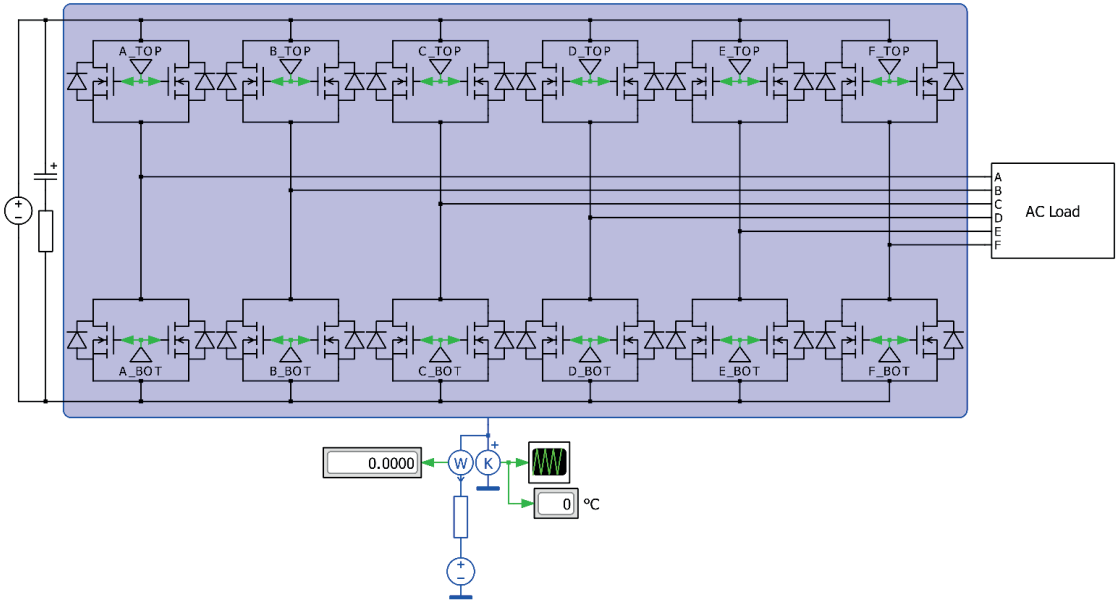


Figure 12 The six-phase Voltage Source Inverter topology

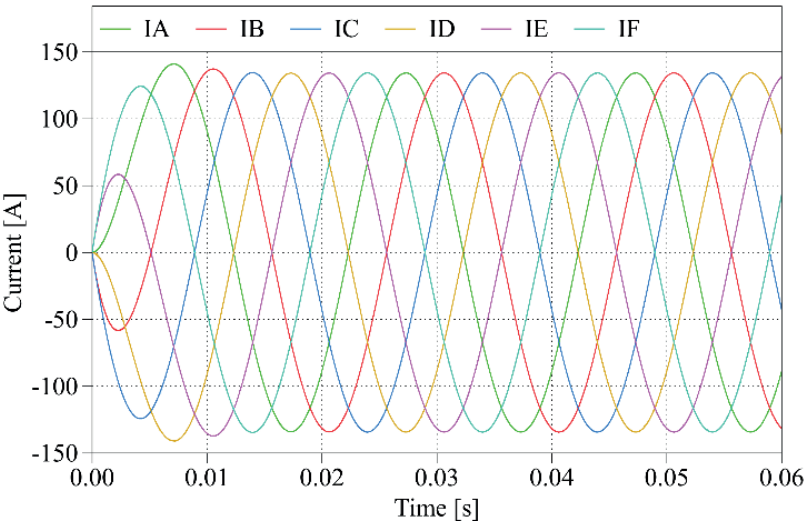


Figure 15 Phase current waveforms of the six-phase VSI at 100 kW output power

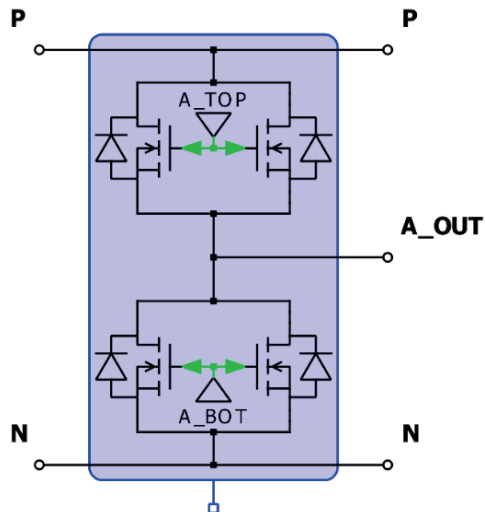


Figure 13 A-Leg of the analyzed circuit of the six-phase VSI topology

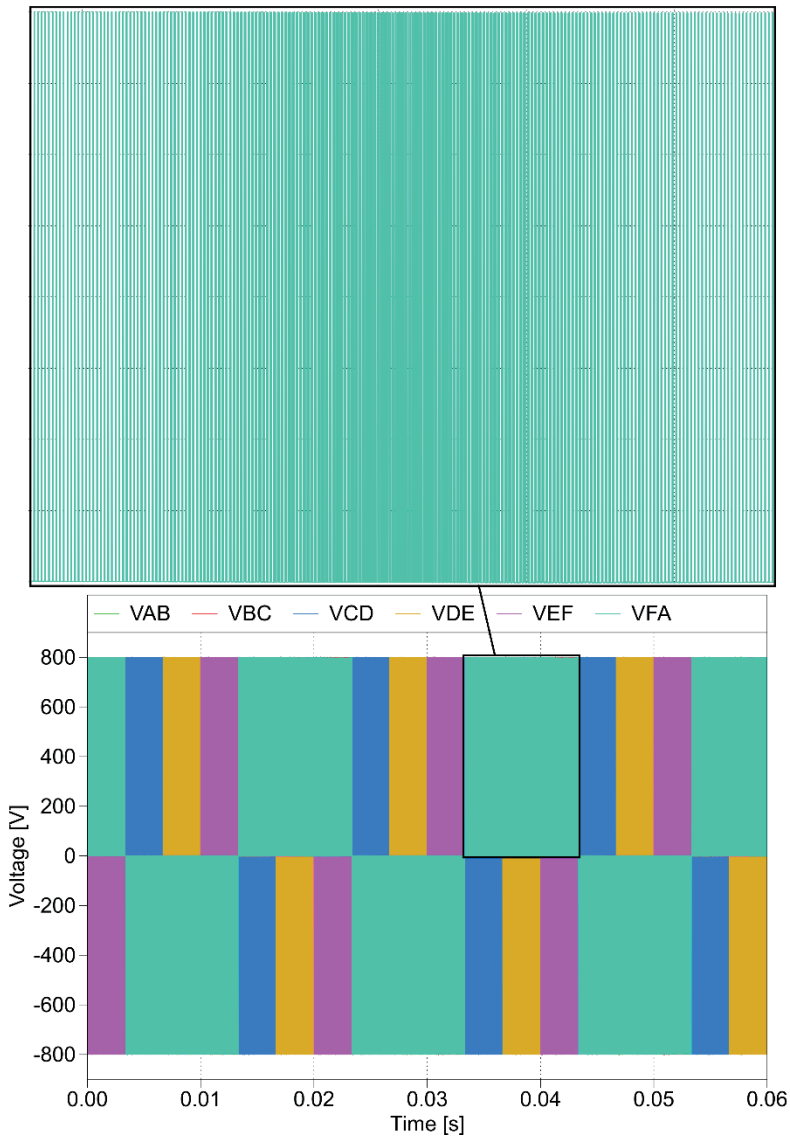
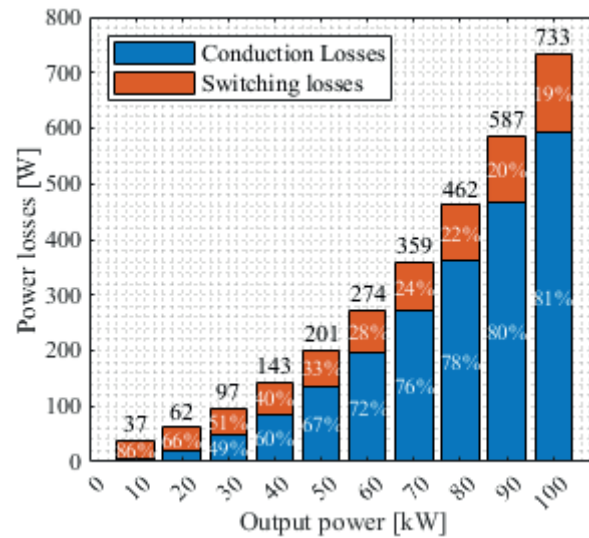


Figure 14 Line-to-line voltage waveforms of the six-phase VSI at 100 kW output power



**Figure 16** Power losses of the six-phase VSI topology

a maximum value of 730 W at a maximum output power of 100 kW.

These values of power losses are obtained when the temperature of the thermal domain is stable. The maximum temperature of the modelled heatsink reached a value of 61.5 °C at 100 kW.

### 3.2 The six-phase voltage source inverter topology

This topology (shown in Figure 12) is the same as the previous one, from the point of view of the configuration of the switching devices, but it is enhanced by the number of phases, which is doubled. This change was also made based on the future trends, which were mentioned in the section dedicated to input parameters of simulation models.

The multi-phase topologies have several advantages over the three-phase ones. One of them is, for example, half the phase current (which can be observed by comparing Figure 10 and Figure 15) or lower DC-Link current ripples, which lower the requirements for selection of a DC-Link capacitor [4].

Since the current requirements of the switching devices are lowered, the number of parallel connected SiC MOSFETs is also reduced. As shown in Figure 13, the one switching device contains two parallel connected SiC MOSFETs. The selection of switching semiconductor devices for this six-phase application was based on the same criteria as for the three-phase version, which means that the same MOSFETs with a blocking voltage of 1200 V are used. The junction temperature of each MOSFET is also almost the same as in the three-phase version, which is around 74.3 °C. All the analyzed topologies have almost the same values of the RMS line-to-neutral voltage (Figure 14) as was mentioned in the three-phase VSI topology subsection (on average 234.4

V). Since these first two topologies are the same apart from the number of phases, the character of the line-to-line voltage is the same, but the output phase current is significantly lower, as it was predicted to be.

In numbers, compared to the three-phase VSI topology the RMS value of the six-phase VSI topology's phase current at the highest power level (100 kW) is 94.94 A, which proves that the statement about half the phase current in a doubled number of phases is correct. The total harmonic distortion of the phase current of the six-phase VSI topology is also the same as for the three-phase version, around 0.19%.

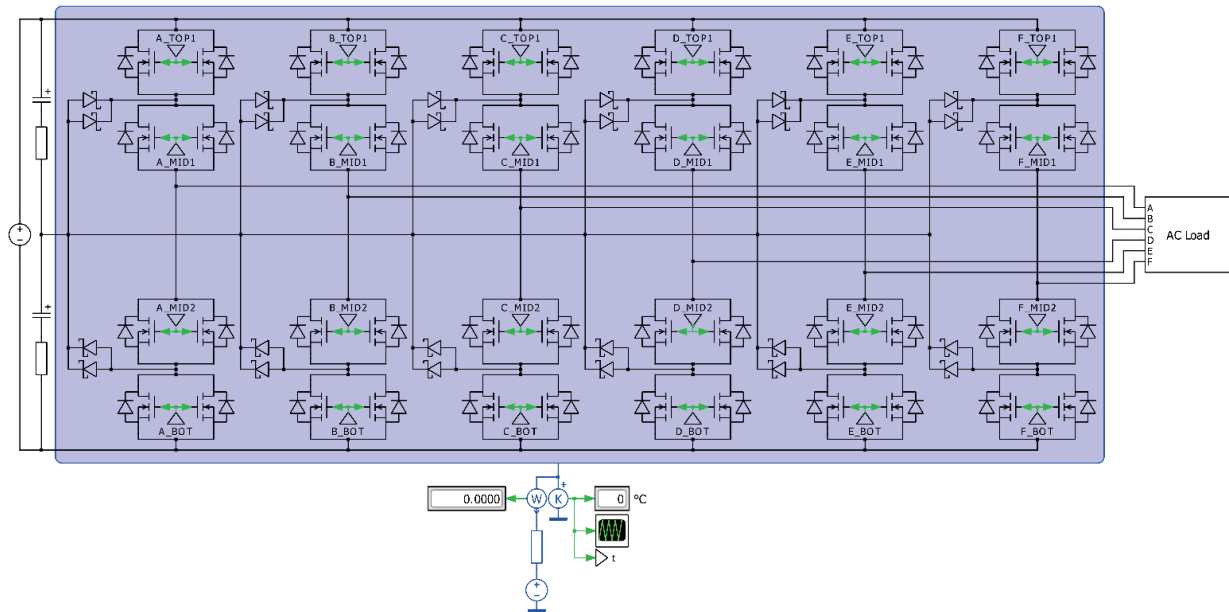
The power loss values at different power levels and stabilized heatsink temperatures, which are shown in Figure 16, are the almost same as the power losses of the three-phase one. That is because the number of semiconductor devices, their method of connection, and their use in these two analyzed circuits are the same. This fact means that the costs of both versions would be the same.

There is no difference between the two VSI topologies in the case of the stabilized temperature of the modeled heatsink. Both three-phase and six-phase topologies reached the maximal temperature of 61.5 °C.

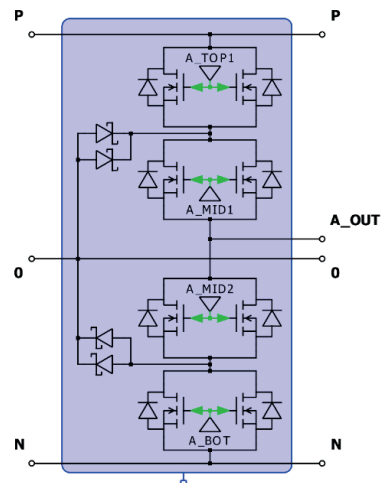
### 3.3 The six-phase neutral point clamped topology

The first analyzed three-level topology is Neutral Point Clamped (shown in Figure 17). This topology uses the clamping diodes to connect the half-bridge outputs and neutral point, which generates an additional voltage level [8]. The three-level topologies were introduced as a possible successor of the VSI topology in the automotive industry, because of lower harmonic distortion, reduced demands of EMI filters, and improved motor efficiency. These are the superior features compared to the VSI topology. The disadvantages are that the volume of





**Figure 17** The six-phase Neutral Point Clamped topology



**Figure 18** A-Leg of the analyzed circuit of the six-phase NPC topology

the DC-Link capacitor is doubled, and the number of semiconductor components is higher [3].

One phase of the NPC topology contains four switching devices and two clamping diodes. The voltage level compared to VSI topology is halved, which means that the demands on the blocking voltage of the switching devices, used in the NPC topology are reduced. A detailed look at one phase of this topology is displayed in Figure 18.

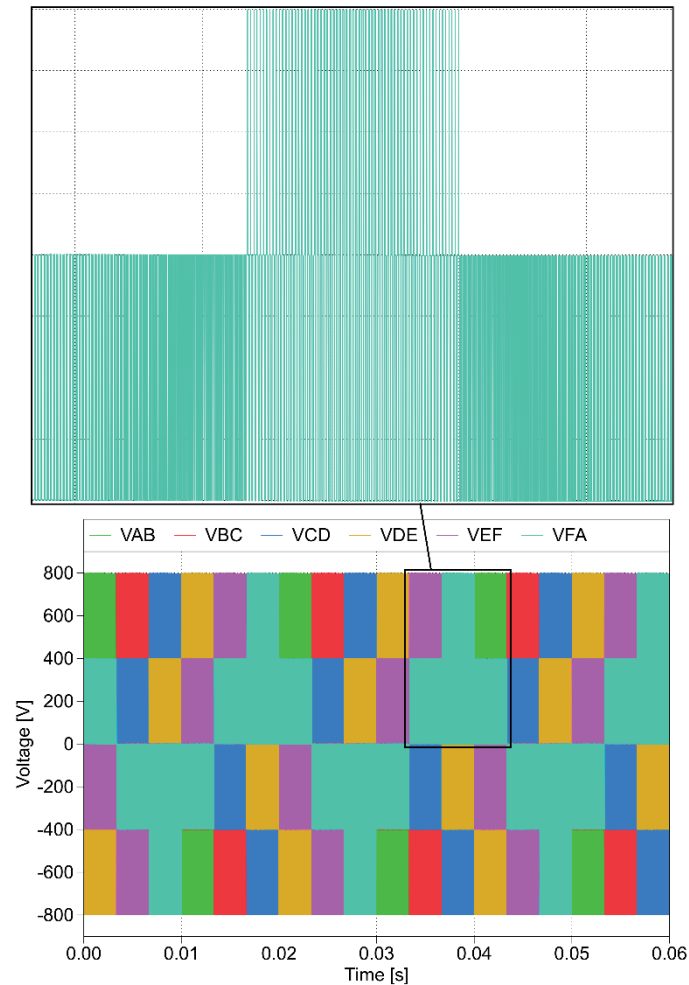
Two NTBG015N065SC1 MOSFETs, with a blocking voltage level of 650 V, are connected in parallel as one switching device, and two Schottky diodes FFSH5065B-F085 are connected in parallel as one clamping device. The junction temperature of each TOP and BOT MOSFET was 71.5 °C, each MID1 and MID2 one had a higher temperature of 2 °C, and the junction temperature of each Schottky diode was 77.4 °C.

As shown in Figure 19, compared to the two-level VSI topology the characteristics of the line-to-line

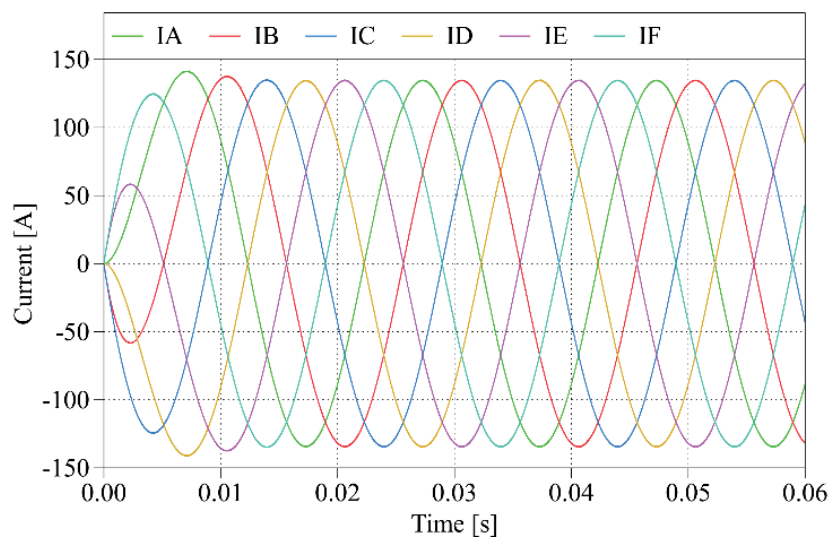
voltage waveforms differ. As the category name of this topology implies, the character of the line-to-line voltage waveforms is enhanced to three levels.

The output line-to-line voltage and phase current waveforms of NPC topology at 100 kW are shown in Figure 19 and Figure 20. Despite the change in the characteristics of the line-to-line voltage waveforms, the output phase current remains unchanged and could be considered identical compared to the previously analyzed circuit (six-phase VSI). However, its total harmonic distortion is slightly higher compared to the mentioned VSI topology, at the level of 0.24 %.

Power losses of the NPC topology contain apart from MOSFETs conduction and switching losses, the conduction losses of the diodes (Figure 21). These three categories make the total power losses of the NPC topology. Conduction losses of the clamping diodes make up a large part of the total power losses of the NPC topology, where at the maximum analyzed power



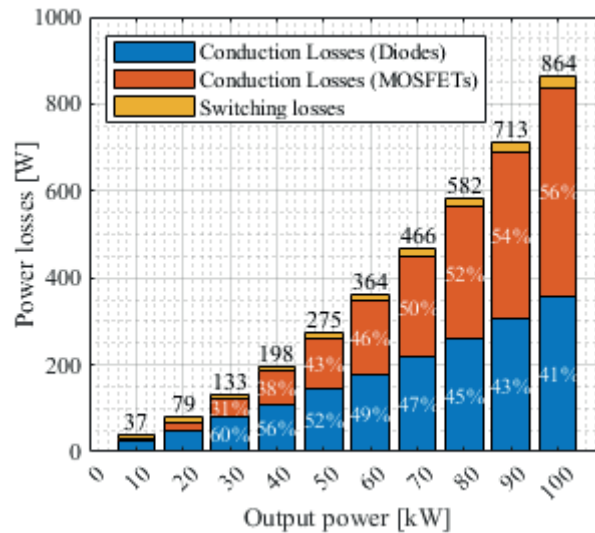
**Figure 19** Line-to-line voltage waveforms with closer look of VFA waveform of the six-phase NPC at 100 kW output power



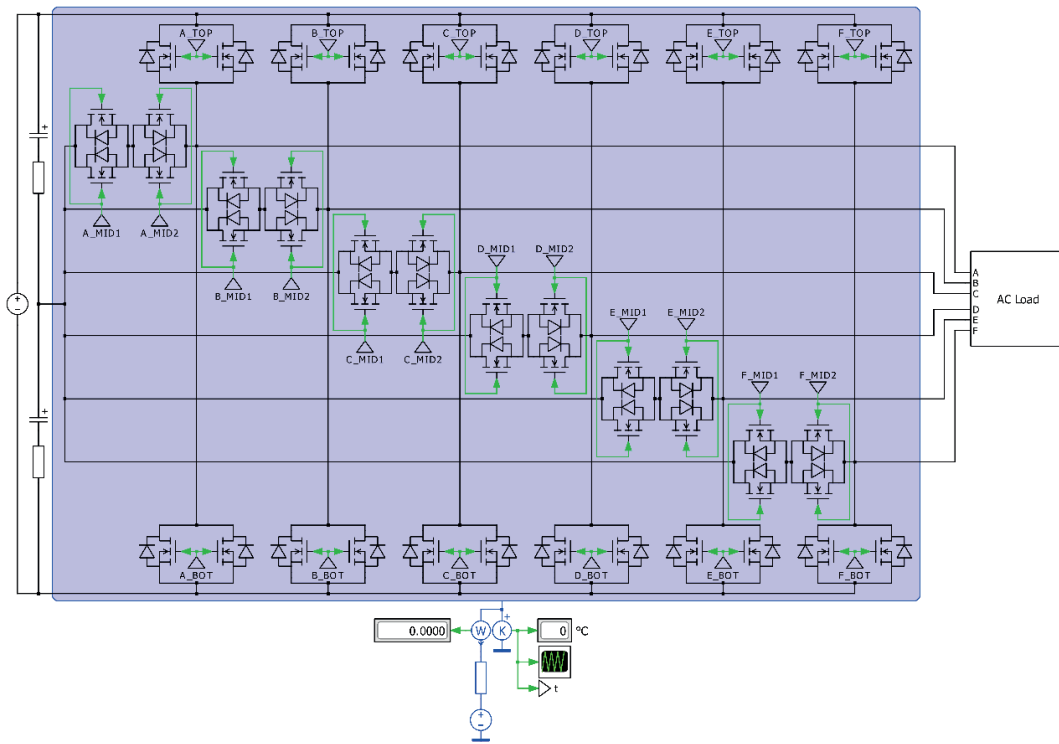
**Figure 20** Phase current waveforms of the six-phase NPC at 100 kW output power

level of 100 kW their share is up to 41%. Compared to the previously analyzed topologies, the total power loss values of the NPC topology, due to the conduction losses of the diodes, are higher. As it can be seen in Figure 21

the switching losses of the MOSFETs are much lower than the switching losses of the VSI topology MOSFETs. It creates just 3% at the maximum of the total power losses of this topology.



**Figure 21** Power losses of the six-phase NPC topology



**Figure 22** The six-phase T-type Neutral Point Clamped topology

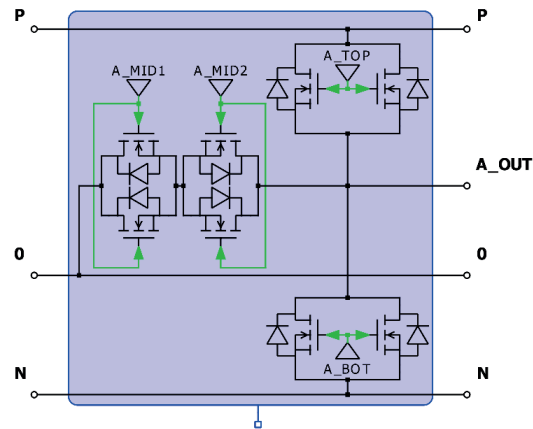
The power losses were calculated at the stabilized modeled heatsink, with its maximum temperature at an output power of 100 kW of 68.2 °C, which is an increase of almost 7 °C compared to the VSI topology.

### 3.4 The six-phase T-type neutral point clamped topology

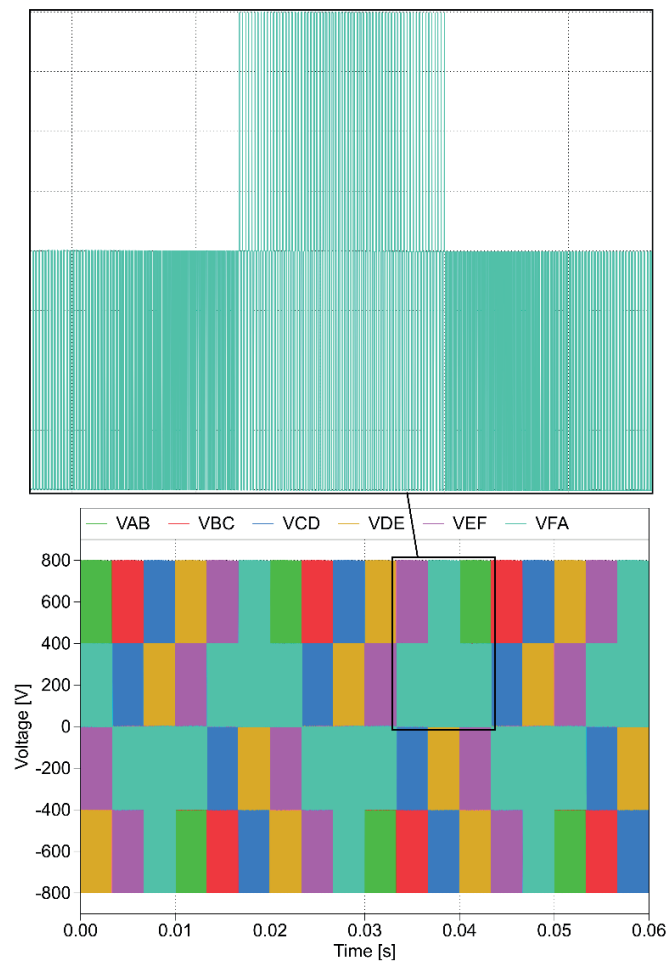
The last analyzed perspective automotive traction inverter topology is a three-level T-type Neutral Point Clamped topology. This topology's circuit can be seen in Figure 22.

The T-NPC topology is considered to be the most competitive solution for an automotive traction inverter. Compared to its three-level previously analyzed alternative, the number of semiconductor devices is lower, because of the clamping diodes absence. This results in the prediction that the power losses are expected to be lower than for the NPC topology. This three-level topology uses a bipolar switch as a connection between the output and neutral point. A close-up view of one phase of the T-NPC traction inverter topology is displayed in Figure 23.

The TOP and BOT in this topology are the switching devices with a 1200 V blocking voltage level. The



**Figure 23** A-Leg of the analyzed circuit of the six-phase T-NPC topology



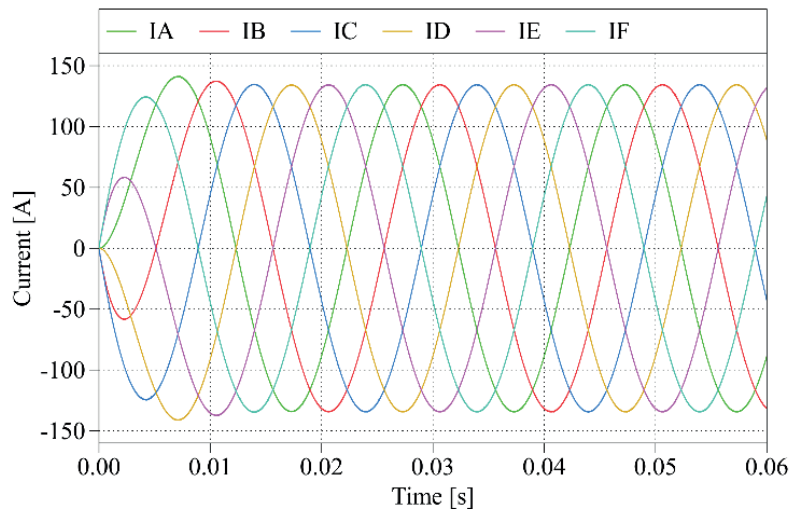
**Figure 24** Line-to-line voltage waveforms with closer look of VFA waveform of the six-phase T-NPC at 100 kW output power

NTBG020N120SC1 as TOP and BOT MOSFETs are used. The bipolar switch (MID1 and MID2 MOSFETs) are built with the NTBG015N065SC1 which has a 650 V blocking voltage. For the same reason, as in the previously analyzed topologies, the switching device consists of two parallel connected MOSFETs. The junction temperature of each TOP and BOT MOSFET was 63.1 °C and for the bipolar switch MOSFETs (MID1 and MID2) it was 61.2 °C. These values are the lowest

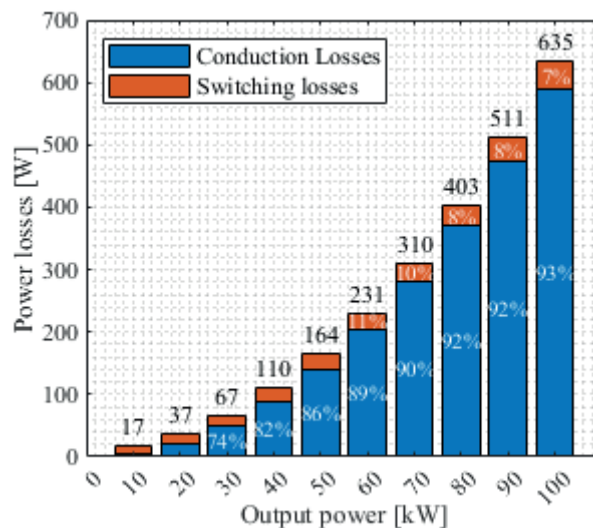
compared to all the other analyzed topologies at the maximum power level (100 kW). The output line-to-line voltage and phase current waveforms of NPC topology at 100 kW are shown in Figure 24 and Figure 25.

The output waveforms, with their parameters such as RMS values of line-to-neutral voltage or phase current of the T-NPC topology, are identical compared to the previously analyzed three-level topology.

The total power losses of the T-NPC topology are



**Figure 25** Phase current waveforms of the six-phase T-NPC at 100 kW output power



**Figure 26** Power losses of the six-phase T-NPC topology

shown in Figure 26. These power losses are the lowest compared to all the other analyzed topologies. The three-level topologies are well known for their reduced switching losses. At the maximum power level of the analysis of T-NPC topology, the switching losses form only 7% of the total 635 W power losses.

What makes this topology even superior to the other analyzed topologies, apart from the lowest power losses, is that the maximum value of the modeled heatsink temperature at the maximum power level reached 56.7 °C.

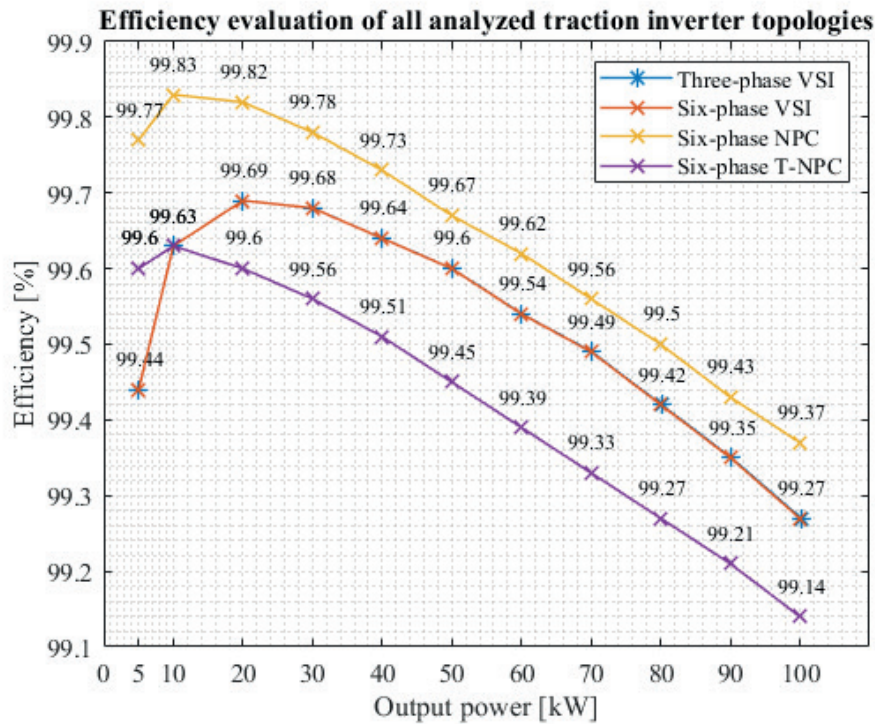
#### 4 Efficiency evaluation of proposed traction inverter topologies

To be able to determine the best traction inverter topology suitable for automotive applications based on the power parameter analysis, it is necessary to express the efficiency of each topology at each power level. Based

on the results of the total power losses of each analyzed traction inverter topology, the efficiency evaluation was performed.

The evaluation of the efficiency of each analyzed traction inverter topology is shown in Figure 27. The efficiency values at each power level of both analyzed versions of the VSI topology are the same. After analyzing these two versions of the VSI topology, it can be concluded that increasing the number of phases does not increase the efficiency of the traction inverter. However, the current requirements per phase, which are important when choosing the switching devices, and their involvement, were reduced. More specifically, the number of parallel connected switching devices were reduced, but the number of switching devices of the inverter stayed the same. The lowest reached efficiency was achieved by the NPC topology due to high power losses due to the high number of semiconductor devices (double the number of MOSFETs and additional clamping diodes compared to VSI topology), even





**Figure 27** Efficiency evaluation of all analyzed traction inverter topologies

**Table 2** The costs of the analyzed traction inverter topologies

Topology/Device	650 V MOSFET	1200V MOSFET	650V Diode	Cost of topology
3-ph VSI	0	24	0	\$481.92
6-ph VSI	0	24	0	\$481.92
6-ph NPC	48	0	24	\$821.04
6-ph T-NPC	24	24	0	\$843.84

though the switching losses were significantly reduced compared to both versions VSI topology. The most perspective topology for automotive applications based on the power parameters analysis is a three-level T-NPC topology. The number of switching devices of the six-phase T-NPC topology is doubled compared to the six-phase VSI topology, but the power losses are lower. This is mostly because of reduced switching losses.

These data on efficiencies of individual topologies at different power levels were built on the fact that the individual topologies were assembled using discrete WBG (SiC) devices. To achieve the maximum power of 100 kW, it was necessary to connect these devices in parallel, which increased the number of these devices in the circuit. Although the two-level topologies contained the same switching devices and in the same number, which was twice as low compared to the three-level ones, their achieved efficiency was not the highest at any power level. The three-level topologies contained twice the number of switching devices compared to the two-level VSI topology. However, only with the T-NPC topologies was the efficiency higher compared to the other analyzed topologies.

The device's pricing information is obtained from the official manufacturer's website. The costs of the whole topologies, which are determined in Table 2, were calculated based on the manufacturer's pricing stated on their official website, and the calculations were made only for the used semiconductor devices. The price per unit of the 650 V MOSFETs NTBG015N065SC1 was \$15.08, the 1200 V MOSFETs NTBG020N120SC1 was \$20.08, and 650 V Schottky diodes was \$4.05. The price of these semiconductor devices is higher at retail stores.

The topology used nowadays in the automotive traction drives Voltage Source Inverter's cost is the lowest compared to the perspective alternative three-level topologies. The cost of the most efficient T-NPC topology is almost double the cost of VSI. These cost data are key to the practical implementation of traction drive's mass production of electrified vehicles. The higher the traction drive's efficiency, the longer the driving distance range of the electrified vehicle, and to achieve this, it would be necessary to enhance the traction inverter, for example by the change of switching devices from IGBTs to SiC MOSFETs, or the very topology of the connection of these devices. However, this comes at the expense of a higher price.

## 5 Conclusions

A description of the input parameters that were defined based on the automotive future trends for the power loss analysis of the semiconductor devices of traction inverter topologies suitable for automotive applications was determined. All the necessary parts of the thermal model of the semiconductor device, which is necessary for the power loss calculations, were created in PLECS, where the power loss analysis was performed. A closer look at sinusoidal PWM control algorithms was used for the two-level (VSI) and three-level (NPC and T-NPC) inverter topologies expressed by block diagrams. Before the actual analysis of the power losses, the selection procedure of discrete semiconductor devices that were used in the given topology was defined. For each of the analyzed topologies (VSI, NPC, and T-NPC) a simulation model was created in PLECS, the key properties of which were described. A close-up look at one phase of the inverter was displayed for each topology. The power loss analysis of all proposed topologies was performed at multiple power levels, but its line-to-line voltage and phase current waveforms were shown only at maximal power level. The results of the analysis of power losses were graphically displayed for each topology separately. The comparison of the analyzed topologies was based on the highest reached efficiency and on the costs of purchasing semiconductor devices.

It is seen from the results, that NPC converter exhibits the highest efficiency within the whole power range that was evaluated. Approximately 0.1% up to 0.3% efficiency value is higher compared to the

other evaluated topologies, even the higher amount of switching devices is presented within the main circuit of the NPC converter compared to standard VSI converter. Another advantage of multilevel inverter is better quality of electrical variables, thus lowering the negative impact on the electrical machine operation. The design technique that is being described makes it possible to evaluate the outcomes of different operational trials and offers a quick and dependable way to investigate multi-phase, multi-level power converter topologies. The 6-phase T-NPC inverter (100 kW) laboratory prototype is presently being developed. More thorough and in-depth analysis of the efficiency estimation using various methods (mathematical calculations, simulations, and laboratory experiments) is intended to be provided in future studies.

## Acknowledgment

The authors would like to thank to the National grant agency APVV for project funding APVV-20-0500 and to national grant agency Vega for project funding 1/0274/24.

## Conflicts of interest

The authors declare that they have no known competing financial interests or personal relationships that could have appeared to influence the work reported in this paper.

## References

- [1] MCKERRACHER, C., O'DONOVAN, A., SOULOPOULOS, N., GRANT, A., LYU, J., MI, S., DOHERTY, D., FISHER, R., CANTOR, C., YANG, M., AMPOFO, K., SEKINE, Y., LEACH, A., STOIKOU, E., SHI, J., XU, P., MALO YAGUE, L., HARING, A., GEURTS, P., ADRIAENSSENS, CH., ABRAHAM, A. T., KAREER, K. Electric vehicle outlook 2023 [online]. Available from: <https://about.bnef.com/electric-vehicle-outlook/>
- [2] GOLI, C. S., ESSAKIAPPAN, S., SAHU, P., MANJREKAR, M., SHAH, N. Review of recent trends in design of traction inverters for electric vehicle applications. In: 2021 IEEE 12th International Symposium on Power Electronics for Distributed Generation Systems PEDG: proceedings [online]. IEEE. 2021. eISBN 978-1-6654-0465-5, eISSN 2329-5767, p. 1-6. Available from: <https://doi.org/10.1109/PEDG51384.2021.9494164>
- [3] WU, Y., MUSTAFEEZ-UL-HASSAN, LUO, F. Design and optimization of a modular multiphase drive for multiphase machines. In: 2023 IEEE Applied Power Electronics Conference and Exposition APEC: proceedings [online]. IEEE. 2023. eISBN 978-1-6654-7539-6, eISSN 2470-6647, p. 1423-1428. Available from: <https://doi.org/10.1109/APEC43580.2023.10131621>
- [4] KESBIA, N., SCHANEN, J. -L., ALAWIEH, H., GARBUIO, L., AVENAS, Y. Design by optimization of multiphase inverter for electric vehicle drive. In: 2020 22nd European Conference on Power Electronics and Applications EPE'20 ECCE Europe: proceedings [online]. IEEE. 2020. eISBN 978-9-0758-1536-8. p. 1-8. Available from: <https://doi.org/10.23919/EPE20ECCEEurope43536.2020.9215677>
- [5] BRAZHNIKOV, A. V., BELOZEROV, I. R. Non-traditional control and advantages of multiphase AC inverter drives. In: 2011 International Conference on Energy, Automation and Signal: proceedings [online]. IEEE. 2011. eISBN 978-1-4673-0136-7, p. 1-6. Available from: <https://doi.org/10.1109/ICEAS.2011.6147207>
- [6] ARENA, G., AIELLO, G., SCALBA, G., CACCIATO, M., GENNARO, F. A cost-effective hardware in the loop implementation of dual active bridge for fast prototyping of electric vehicles charging controls. In:

- 2021 23rd European Conference on Power Electronics and Applications EPE'21 ECCE Europe: proceedings [online]. IEEE. 2021. eISBN 978-9-0758-1537-5, p. P.1-P.10. Available from: <https://doi.org/10.23919/EPE21ECCEurope50061.2021.9570652>
- [7] CHOLEWA, D., DROZDOWSKI, P. Simulink modeling of multiphase induction motors. In: 2018 14th Selected Issues of Electrical Engineering and Electronics WZEE: proceedings [online]. IEEE. 2018. eISBN 978-1-5386-8299-9, p. 1-6. Available from: <https://doi.org/10.1109/WZEE.2018.8749007>
- [8] GLEISSNER, M., HARING, J., BAKRAN, M. -M., WONDRAK, W., HEPP, M., AG, M.-B. Advantageous fault-tolerant multilevel and multiphase inverter systems for automotive electric powertrains. In: 2020 Fifteenth International Conference on Ecological Vehicles and Renewable Energies EVER: proceedings [online]. IEEE. 2020. eISBN 978-1-7281-5641-5, p. 1-8. Available from: <https://doi.org/10.1109/EVER48776.2020.9243131>
- [9] WANI, R., PATIL, S. L., SHINDE, P. Modeling and simulation of average current-mode controlled bidirectional multiphase dc-dc converters used in hybrid vehicles. In: 2021 6th International Conference for Convergence in Technology I2CT: proceedings [online]. IEEE. 2021. eISBN 978-1-7281-8876-8, p. 1-7. Available from: <https://doi.org/10.1109/I2CT51068.2021.9418219>
- [10] REIMERS, J., DORN-GOMBA, L., MAK, C., EMADI, A. Automotive traction inverters: current status and future trends. *IEEE Transactions on Vehicular Technology* [online]. 2019, **68**(4), p. 3337-3350. ISSN 0018-9545, eISSN 1939-9359. Available from: <https://doi.org/10.1109/TVT.2019.2897899>
- [11] SCHUCK, M., PILAWA-PODGURSKI, R. C. N. Ripple minimization through harmonic elimination in asymmetric interleaved multiphase DC-DC converters. *IEEE Transactions on Power Electronics* [online]. 2015, **30**(2), p. 7202-7214. ISSN 0018-9545, eISSN 1939-9359. Available from: <https://doi.org/10.1109/TPEL.2015.2393812>
- [12] SALEM, A., NARIMANI, M. A review on multiphase drives for automotive traction applications. *IEEE Transactions on Transportation Electrification* [online]. 2019, **5**(4), p. 1329-1348. ISSN 0018-9545, eISSN 1939-9359. Available from: <https://doi.org/10.1109/TTE.2019.2956355>
- [13] TAHA, W., AZER, P., CALLEGARO, A. D., EMADI, A. Multiphase traction inverters: state-of-the-art review and future trends. *IEEE Access* [online]. 2022, **10**, p. 4580-4599. eISSN 2169-3536. Available from: <https://doi.org/10.1109/ACCESS.2022.3141542>
- [14] AULAGNIER, G., ABOUDA, K., ROLLAND, E., COUSINEAU, M., MEYNARD, T. Benefits of multiphase buck converters in reducing EME (electromagnetic emissions) analysis and application to on-chip converters for automotive applications. In: 2015 IEEE International Symposium on Electromagnetic Compatibility EMC: proceedings [online]. IEEE. 2015. eISBN 978-1-4799-6616-5, ISSN 2158-110X, eISSN 2158-1118, p. 102-107. Available from: <https://doi.org/10.1109/ISEMC.2015.7256140>
- [15] CHEN, L., GE, B. High power traction inverter design and comparison for electric vehicles. In: 2018 IEEE Transportation Electrification Conference and Expo ITEC: proceedings [online]. IEEE. 2018. eISBN 978-1-5386-3048-8, p. 583-588. Available from: <https://doi.org/10.1109/ITEC.2018.8450259>
- [16] ZAIDI, E., MAROUANI, K., BOUADI, H., NOUNOU, K., AISSANI, M., BENTOUHAMI, L. Control of a multiphase machine fed by multilevel inverter based on sliding mode controller. In: 2019 IEEE International Conference on Environment and Electrical Engineering and 2019 IEEE Industrial and Commercial Power Systems Europe IEEEIC / I&CPS Europe: proceedings [online]. IEEE. 2019. eISBN 978-1-7281-0653-3, p. 1-6. Available from: <https://doi.org/10.1109/IEEEIC.2019.8783559>
- [17] BUTT, O. M., BUTT, T. M., ASHFAQ, M. H., TALHA, M., RAIHAN, S. R. S., HUSSAIN, M. Simulative study to reduce DC-link capacitor of drive train for electric vehicles. *Energies* [online]. 2022, **15**(12), 4499. eISSN 1996-1073. Available from: <https://doi.org/10.3390/en15124499>
- [18] RODRIGUEZ, J., BERNET, S., STEIMER, P. K., LIZAMA, I. E. A survey on neutral-point-clamped inverters. *IEEE Transactions on Industrial Electronics* [online]. 2010, **57**(7), p. 2219-2230. ISSN 0278-0046, eISSN 1557-9948. Available from: <https://doi.org/10.1109/TIE.2009.2032430>
- [19] PADMANABAN, S., WHEELER, P., BLAABJERG, F., ERTAS, A. H., OJO, J. O., SZCZESNIAK, P. Proposed novel multiphase-multilevel inverter configuration for open-end winding loads. In: 2016 18th European Conference on Power Electronics and Applications EPE'16 ECCE Europe: proceedings [online]. IEEE. 2016. eISBN 978-9-0758-1524-5, p. 1-9. Available from: <https://doi.org/10.1109/EPE.2016.7695537>
- [20] BOTTARO, E., CACCIATO, M., RAFFA, A., RIZZO, S. A., SALERNO, N., VENEZIANO, P. P. Development of a SPICE modelling strategy for power devices in GaN technology. In: 47th Annual Conference of the IEEE Industrial Electronics Society IECON 2021: proceedings [online]. IEEE. 2021. eISBN 978-1-6654-3554-3, eISSN 2577-1647, p. 1-6. Available from: <https://doi.org/10.1109/IECON48115.2021.9589710>
- [21] KYSLAN, K., LACKO, M., FERKOVA, Z., ZASKALICKY, P. V/f control of five phase induction machine implemented on DSP using Simulink coder. In: 2020 ELEKTRO: proceedings [online]. IEEE. 2020. eISBN 978-1-7281-7542-3, p. 1-6. Available from: <https://doi.org/10.1109/ELEKTRO49696.2020.9130358>









This is an open access article distributed under the terms of the Creative Commons Attribution 4.0 International License (CC BY 4.0), which permits use, distribution, and reproduction in any medium, provided the original publication is properly cited. No use, distribution or reproduction is permitted which does not comply with these terms.

# GENERALIZED ORDERED LOGIT MODEL WITH TESTING ASSUMPTIONS: A CASE STUDY OF USING URBAN LIGHT RAIL IN BURSA

Nurten Akgun<sup>1</sup>, Tiziana Campisi<sup>2,\*</sup>, Muhammed Talha Sunar<sup>1</sup>

<sup>1</sup>Faculty of Engineering and Natural Sciences, Bursa Technical University, Bursa, Turkey

<sup>2</sup>Faculty of Engineering and Architecture, University of Enna Kore, Enna, Italy

\*E-mail of corresponding author: tiziana.campisi@unikore.it

Nurten Akgun 0000-0003-3888-3913,  
Muhammed Talha Sunar 0000-0003-4747-2868

Tiziana Campisi 0000-0003-4251-4838,

## Resume

Logistic regression has been a widely used prediction technique to analyze categorical variables. However, if the assumptions are violated the results may be biased. The study in this paper applied an analytical technique namely generalized ordered logit model. A case study of using urban light rail under pandemic conditions was applied for the analysis. The results suggested that logistic regression should not be applied before exploring the multicollinearity and applying the test of parallel lines. If the assumptions are violated, generalized ordered logit model should be considered. Regarding the predictive variables, sociodemographic, socioeconomic and travel pattern, related variables were found to have a statistically significant impact on the perception of safety and infrastructure of urban light rail. The outcomes of the study would provide a deeper understanding of developing regression models for categorical variables for future studies.

## Article info

Received 20 December 2023

Accepted 16 March 2024

Online 29 April 2024

## Keywords:

public transport  
comparison tests  
Covid-19  
assumption

Available online: <https://doi.org/10.26552/com.C.2024.028>

ISSN 1335-4205 (print version)  
ISSN 2585-7878 (online version)

## 1 Introduction

The Covid-19 pandemic has changed urban travel behaviors in many countries [1-2]. The travel distance was reduced by approximately 60% [3]. Not only the need for travel, but the mode choice behavior has changed significantly, as well

. A shift from public transport use to private motor vehicle use, cycling, and walking was observed [4]. Transport authorities claimed that a 95% reduction in public transport use was observed during the peak period of the pandemic [5]. Although there has been a significant decrease in travel distance during the first months of the pandemic, it increased gradually during the post-pandemic period [6]. The study [4] suggested that private motor vehicle use and walking came back to normal levels during the post-pandemic period. However, public transport use could not reach the pre-pandemic level [3]. Due to the remote working option and the discomfort in crowded spaces, a straightforward return to the pre-pandemic status of the public transport use

is not achievable [7]. In addition, the lack of emergency readiness in the public transport sector for a pandemic situation is an important reason for decreased ridership [8]. These cause unsustainable transportation modes to be used more than the public transport [9]. Using the public transport should be encouraged to reduce the level of private motor vehicle use [6]. It was suggested [4] that a deeper investigation should be carried out to understand the reason behind the low level of public transport use due to the pandemic effects. Several socioeconomic groups of people have experienced travel mode shifts to varying degrees [10-11]. Therefore, this reason should be examined by considering survey-based socioeconomic parameters such as gender, age, education, travel pattern, household size, and personal values, such as perceptions of the mobility system [3, 12]. In addition, study [13] explored the long-term impact of a pandemic on travel behavior and it was suggested that safety concerns should be investigated to reduce the significant and permanent influence on public transport users.



The study in this paper aimed to fill this gap by investigating the influence of the social, travel pattern, and perception-related parameters on urban light rail use under pandemic concerns. The objectives of the study are given as follows: i) examining the level of change in travel patterns before and after the pandemic, ii) selecting the most appropriate prediction model by testing the statistical assumptions, iii) developing the model to explore the impacts on participants' perceptions on urban light rail after the pandemic period.

## 2 Literature review

Depending on the measures taken by the governments to prevent the spread of the pandemic, there has been a change in the public transportation habits of people trying to deal with this situation [14]. During the peak period of the pandemic-related disturbances, the number of passengers using public transportation decreased by 50 % to 90 % worldwide [15]. Particularly, there were substantial reductions in metro service durations, with up to a 40 % decrease in travel times [16]. The decrease in the use of public transport was in correlation with the rising number of Covid-19 cases [17-19]. It is stated that the most important challenge after the Covid-19 pandemic is to re-establish trust in public transportation [20-22]. Travel behavior, sociodemographic and latent characteristics of the road users were found to be significant for the reason of switch from public transport to other modes during the pandemic [23]. In a study [24], focused on the effectiveness of incentives aimed at promoting public transport usage in China after the pandemic, it was found that while there was a minor increase in public transport use, the impact of the incentives remained limited in achieving significant behavioral change. The safety of individual or social transportation needs can be achieved with sustainable transportation systems [25]. To achieve this goal, the factors affecting the perceptions of users regarding transportation safety should be carefully evaluated at the planning stage [26].

As stated in the United Nations Agenda 30, prepared for sustainable development, it is a human right to feel safe in public [20]. The Great Walk of Athens (GWA) has been determined that the use of public transportation has decreased due to the decrease in the desire to share indoor space after the pandemic and the public did not show the expected interest in the GWA project, and the most important reason for this was that the public was not sufficiently included in the planning stage [27]. This outcome supports the emergency of understanding the reason behind the preference change and planning the transportation system including users' perceptions.

Before exploring the applied studies in this research area, it should be noted that the influence of emergencies on public transportation use may not be at the same level in different regions or among different modes

or societies [28]. Particularly, metro and bus modes were affected more than other public transportation options. Environmental and economic concerns are also determinants of people's preference for public transportation [14]. For instance, the UK based study found that users in poor neighborhoods return to public transport faster than people living in more affluent areas [29]. In addition, the regional differences can be influential such as the study [30] suggested that a decrease in the use of public transportation was observed in American and European cities at a similar level, while this rate was found to be less in Asian countries.

Concerning this given information in the literature, there have been several studies, which were conducted in different regions to investigate the reasons behind the decrease in using public transport and not returning to its former levels. One of the major reasons for reduced public transport usage was the sociodemographic background of road users. Women and elder road users exhibited higher susceptibility to using public transport during the pandemic situation [31-32]. The effects of the pre- and post-pandemic on public transport users have been investigated in three different Scandinavian cities; Stockholm, Bergen and Oslo [20]. The results suggested that women experienced more stress and had less confidence while using public transportation during the pandemic period. In addition, elderly individuals significantly reduced their use of public transport. This situation was reduced but not fully recovered post pandemic period. This cannot be explained by the negative service level but by the decrease in the number of individuals who prefer public transportation [20]. The study [33] carried out in Lahore, Pakistan indicated that elderly individuals were less likely to use public transport in the absence of necessary precautions, while individuals with lower levels of education exhibited higher usage, highlighting the potential for attitude change through the implementation of sanitation measures and informative activities [34]. The decrease in public transport use occurred among mid-high age users, however, people under the age of 30 had to keep using public transportation because the majority of the young road users did not have access to private vehicles in India [35]. Mostly elder groups tended to switch their travel mode from public transport to private motor vehicles, and this preference has not been recovered yet. The study carried out in Germany suggested that women and those living in the suburbs tended to use private vehicles more during the pandemic period [36]. Total of 19 % of the participants, who did not own a car, were tempted to buy a car even though they could live without a car. These results clearly showed that the public transport behavior has been changing among different sociodemographic and socioeconomic groups [37]. Consequently, a permanent modal shift behavior was observed.

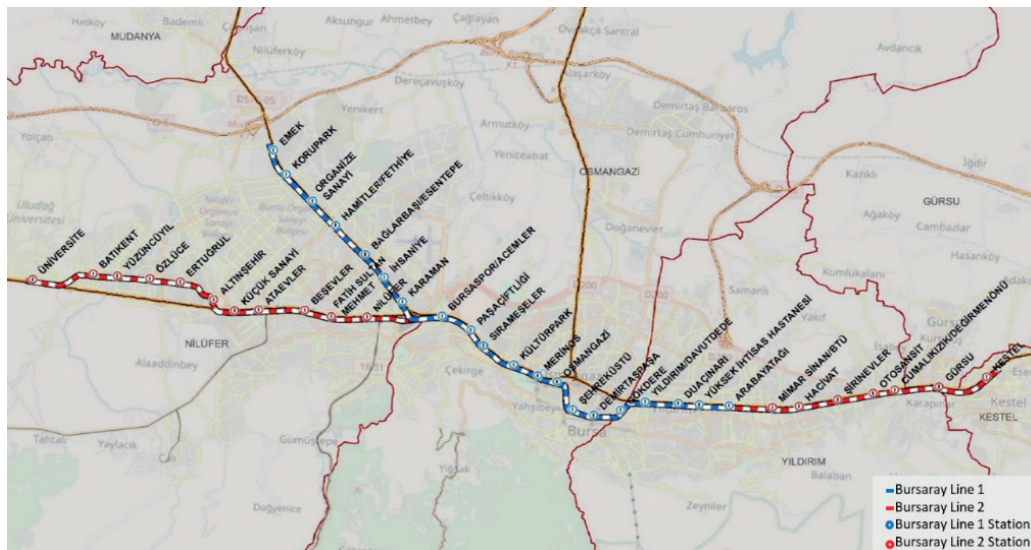
In a comprehensive study [38], conducted in

Warsaw, it was found that there was a substantial transition away from traditional public transportation towards individual modes of transportation. Individuals in the high-income group, and those who primarily use motorcycles as their mode of transportation, exhibited a strong preference against using public transportation due to their significant dependency on private means of transportation, regardless of adherence to pandemic safety protocols [39]. The outcomes of the study [40], conducted in Scotland, suggested that the post-pandemic preference for private vehicle usage over public transportation was likely to result in adverse environmental consequences, while the adoption of remote working arrangements and increased bicycle usage was expected to have positive environmental effects. In a survey based comprehensive study [41] conducted in Greece, it was uncovered that the transportation behaviors adopted during the pandemic, specifically walking and cycling, were anticipated to persist among individuals even after its resolution, particularly in the short term. The data obtained from the public transport service providers in Spain was analyzed and it was found that in the post-pandemic “new normal,” there has been a notable increase in the use of bicycles as shared transportation and a higher overall traffic density compared to the utilization of public transport [42]. The study [23], conducted in Athens, suggested that self-employed individuals and owners of private cars were less inclined to revert to using public transport after the pandemic. During the two waves of the pandemic in Australia, surveys indicated that the use of public transport was influenced by the adoption of remote work practices, and it was further concluded that government incentives would be a determining factor in shaping public transport behavior [43].

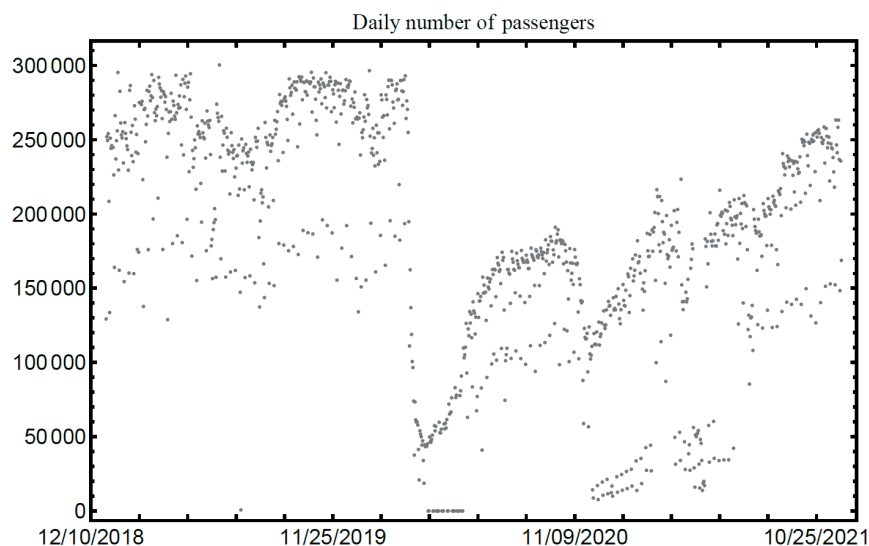
Further studies focused on the road users’ perception of public transport use under comprehensive health issues. A survey was conducted online with the participation of 700 people across Sicily island of Italy. It was concluded that policymakers should investigate the psychological and emotional aspects of using the public transport against private motor vehicle mode shift [44]. A survey-based study [45], covering 8 cities in China, suggested that taking temperature measurements in public vehicles can be useful in reducing health concerns caused by Covid-19. Through an examination conducted during the Covid-19 pandemic in Santiago, a comprehensive analysis was performed using 455 valid survey responses obtained from both an online survey conducted on the Qualtrics platform and a face-to-face survey [46]. The data were investigated to assess users’ perceptions of mask-wearing and their attitudes toward crowded vehicles. The results indicated a heightened reluctance towards crowded vehicles, even when all occupants were wearing masks, in comparison to the pre-pandemic period [46]. Based on the data obtained from the smart card system used in public

transportation, it was revealed that users modified their public transportation routes and opted for destinations where the pandemic-induced isolation policies were not implemented [47]. Through a study [48] tracking 48 users with GPS before and during the pandemic, it was discovered that the key considerations in the selection of transportation mode and route were the avoidance of crowds and travel time. The study [49] emphasized the importance of commissioning bus lines with small crossing distances to alleviate overcrowding concerns during the pandemic and prevent potential inconvenience to passengers who may be skipped at stops. According to a study [50] analyzing data from the local public transportation service provider in Tampere, Finland, it was found that the public transportation usage declined across the country during the pandemic, and specifically in the eastern part of the city, the crowdedness ratio was higher compared to other areas. The survey conducted with the participation of 420 public transport users in Addis Ababa, Ethiopia revealed that approximately one-third of the participants were found to have symptoms indicative of general anxiety disorder related to the pandemic [31]. Another study [51] conducted in India, which examined the factors affecting the choice of public transport mode, revealed that the key consideration for individuals is the capacity of the mode of transport to provide social distancing. In a study [52] addressing policies for managing public transportation systems during the epidemic periods, several measures, including vehicle disinfection and mask usage, were recommended as a part of a transportation emergency response plan to prevent the spread of the epidemic while ensuring continued service to meet the demand. The study [53] conducted in Gdansk, Poland revealed that the Covid-19 pandemic could lead to subjective safety concerns regarding public transport, resulting in a significant proportion (25%) of participants losing confidence in its safety. The survey conducted in Germany with the participation of 918 individuals revealed that users are expected to experience lingering fear of infection related to public transport even after the pandemic [54].

Regarding the information given in the literature, investigating the factors affecting the perception of public transport use emerges to be carried out. The previous studies mainly carried out a survey and aimed to explore the importance of the parameters by applying several analysis methods, such as structural equation modelling [20, 39], exploratory factor analysis [33], binary logistic regression [36], multivariate regression analysis [37], two-parameter probit model [40], Mann Whitney U test [44], multi-group analysis method [45] and multinomial logit model [23]. The analysis in this paper aimed to focus not only on examining the factors, but also on applying a deeper methodology for investigating categorical variables. The following section explains the case study area, data collection and analytical approach of the analysis.



**Figure 1** Bursa urban light rail system



**Figure 2** The daily number of passenger data for Bursaray

### 3 Methodology

The case study area in this paper is Bursa city, which has approximately 2 million populations. The south part of the city is narrowed by Uludag mountains and the north part is covered with agricultural lands. Therefore, the city form has a linear structure and the majority of the daily travel movement occurs on the east-west line. Accordingly, the most used public transport mode in the city is the Bursa urban light rail system (i.e., Bursaray) (see Figure 1). Bursaray consists of 2 lines with a total length of 39km. It has 38 stations and the platforms for each station are 120m in length. The lines are merged at 13 stations. The system has a 70 km/h operating speed with a fixed blocked signalling system. Average travel times are 34 min and 55 min, for line 1 and line 2, respectively. Station waiting time is between 20 s and 40 s for all platforms. Each train has

4 railcars with 8 doors total. The railcar length, width and height are 28.20 m, 2.65 m, and 3.88 m, respectively. The number of passenger seats located in one railcar is 50.

The transportation network in Bursa primarily relies on the Bursaray rail system, serving as the backbone of public transit in the city. Bursaray is the preferred mode of transportation for many residents, offering linear accessibility to various parts of the city. Notably, the Acemler station serves as a major interchange point, where the rail lines diverge and connect with minibuses heading to outlying districts such as Harmancık, Buyukorhan, and Keles.

Additionally, it is important to note that the University, Emek, and Kestel stations serve as key launch points for the Bursaray system, facilitating connections to different transportation modes. While buses and minibuses complement the Bursaray lines,

they are often hampered by traffic congestion, leading to inconsistent travel times. This has been a common concern among the public transport users, highlighting the need for improved efficiency and reliability across all modes of transportation in Bursa.

The daily number of passenger data for Bursaray was obtained from the Bursa Municipality Department of Transportation for the period between January 2019

and November 2021 (see Figure 2). Before the Covid-19 pandemic, the daily number of passengers was up to 300.000; however, the demand dropped significantly during the first phase of the pandemic. The demand increased in the third quarter of year 2020; but it dropped slightly during the second phase of the pandemic. During 2021, the demand has increased slowly; however, it could not have reached the pre-pandemic conditions.

**Table 1** Descriptive statistics for sociodemographic and working status

Parameters	Units (frequency)
Gender	Female (489); Male (498)
Age group	18-25 (538); 26-40 (374); 41-55 (62); 56-70 (13)
Education	Primary (11); High school (461); Undergraduate (416); Post-graduate (99)
Employment	Unemployed (54); Part-time employed (43); Full-time employed (385); Self-employed (33); Student (472)
Working status	Unemployed (54); Office (452); Flexible (481)

**Table 2** Descriptive statistics for travel pattern

Parameters	Units (frequency)
Daily average commuting distance	Less than 2km (288); 2-5km (192); 5-10km (166); Over 10km (341)
Travel mode before	Micromobility (17); Private motor vehicle (348); Taxi (5); Public Transport (573); Walking (44)
Travel mode after	Micromobility (26); Private motor vehicle (564); Taxi (15); Public Transport (272); Walking (110)
Frequency of using public transport before	Less than 5 days (461); 5 days (236); 6 days (142); 7 days (148)
Frequency of using public transport after	Less than 5 days (827); 5 days (100); 6 days (41); 7 days (19)
Frequency of using private motor vehicle before	Less than 5 days (690); 5 days (93); 6 days (32); 7 days (172)
Frequency of using private motor vehicle after	Less than 5 days (563); 5 days (102); 6 days (63); 7 days (259)
Frequency of walking before	Less than 5 days (449); 5 days (191); 6 days (90); 7 days (257)
Frequency of walking after	Less than 5 days (647); 5 days (128); 6 days (55); 7 days (157)
Motivation of choosing the travel mode before	Environmental concerns (51); Costs (393); Travel time (444); Social distance (99)
Motivation for choosing the travel mode after	Environmental concerns (31); Costs (133); Travel time (132); Social distance (691)

**Table 3** Descriptive statistics for perceptions on urban light rail

Parameters	Survey questions	Units (frequency)
Infrastructure	What is your perception on URL infrastructure? Likert Scale 1-6, where 6 corresponds to the best possible score and 1 to the worst.	1 (127); 2 (155); 3 (245); 4 (286); 5 (145); 6 (29)
Safety	What is your health-related safety perception on using URLs after the pandemic?	Definitely unsafe (469); Unsafe (384); Moderate (107); Safe (23); Definitely safe (4)
Stress/anxiety	Do you feel stressed/anxious while using URLs after the pandemic? Likert scale 1-5, where 1 corresponds to completely yes and 5 to completely no	1 (18); 2 (31); 3 (67); 4 (383); 5 (488)
Improvement on infrastructure	Do you prefer using URLs after the pandemic condition if the infrastructure improves? Likert scale 1-5, where 1 corresponds to completely no and 5 to completely yes	1 (99); 2 (158); 3 (260); 4 (380); 5 (90)



As mentioned in the literature review, passengers had significant hesitations or concerns about using the public transport during the pandemic crises. Therefore, the study in this paper has surveyed to understand passengers' perceptions.

The survey was conducted with randomly selected 987 local participants in December 2020. The participants had been using the light rail at least once a week before the pandemic. The questions were distributed via the Google survey platform. The minimum sample size for the study area was calculated using the Krejcie and Morgan formula [55] (Equation (1)). In this study, the population size was 2,056,140 [56] and the p-value was 0.5 (maximum variability). The confidence level was decided at 95% ( $\chi^2 = 3.841$ ) and the margin of error was  $\pm 5\%$ . The minimum required sample size was calculated as 384, which was less than the sample size of 987 in this study. The survey questions were divided into three categories: sociodemographic variables, travel patterns and perceptions of public transport. The frequency analysis for each variable is given in Tables 1, 2 and 3.

$$n = \frac{\chi^2 N p(1-p)}{e^2(N-1) + \chi^2 p(1-p)}, \quad (1)$$

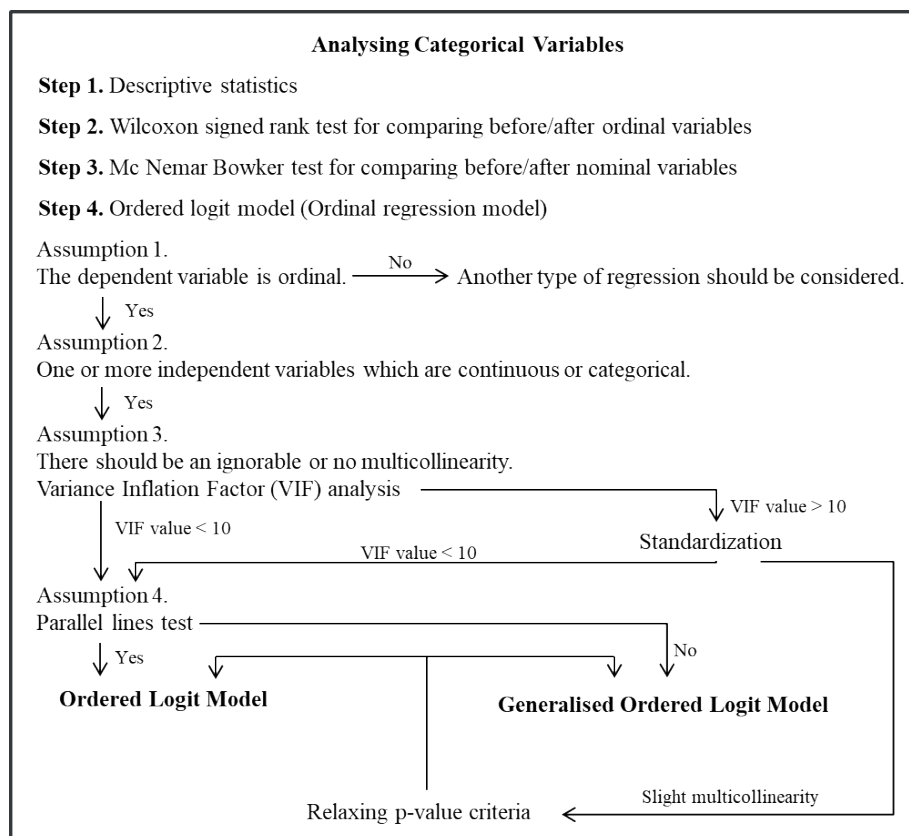
where:  $N$  is the population size,  
 $n$  is the sample size,

$e$  is the margin of error,

$\chi$  is the value of the chi-square distribution having a degree of freedom of one at a certain confidence level,  
 $p$  is population proportion.

The method for analyzing the categorical variables was carried out in four steps (see Figure 3). After gaining a fundamental understanding of the dataset by descriptive statistics in step 1, before-after comparison analysis was conducted in step 2 and step 3. Wilcoxon signed rank test is a non-parametric analysis for comparing pairs of data for the ordinal variables [57]. In this study, the variables, namely frequency of using public transport, frequency of using private motor vehicle and frequency of walking were analyzed with Wilcoxon signed rank test. When the variables are in a nominal structure, McNemar-Bowker test should be conducted [58]. Therefore, before-after comparison analysis for the variables, namely the travel mode and motivation of choosing the travel mode, were analyzed with McNemar-Bowker test.

In step 4, a prediction model was developed. The investigated dependent variables were on a categorical Likert Scale from 1 to 5. Therefore, the ordered logit model was selected to be applied to develop a prediction regression [51]. The assumptions of the ordered logit model should be met: i) the dependent variable is ordinal categorical, ii) independent variables are either categorical or continuous, iii) ignorable or no multicollinearity and iv) parallel lines [59]. Meeting



**Figure 3** Methodological framework



these assumptions is compulsory for applying the ordered logit regression; however, they are frequently violated in studies [60]. If the assumptions are violated, generalized ordered logit model should be applied to relax the assumptions [61]. The study in this paper examined each assumption of the ordered logit model in step four and developed the prediction model based on the results. The equation generalized ordered logit model is given as follows [59]:

$$P(Y_i > j) = g(X_i\beta_j) = \frac{\exp(\alpha_j + X_i\beta_j)}{1 + \{\exp(\alpha_j + X_i\beta_j)\}}, \quad (2)$$

$$j = 1, 2, \dots, M - 1,$$

where M is a number of categories of the ordinal ranked responses of the dependent variable, and j is a number of compared categories. If M = 3, the number of compared categories is two: for j = 1 category 1 is contrasted with categories 2 and 3, and for j = 2 categories 1 and 2 are contrasted with category 3. The probability Y can be estimated as given below:

$$P(Y_i = 1) = 1 - g(X_i\beta_i), \quad (3)$$

$$P(Y_i = j) = g(X_i\beta_{j-1}) - g(X_i\beta_j), \quad (4)$$

$$j = 2, \dots, M - 1,$$

$$P(Y_i = M) = g(X_i\beta_{M-1}). \quad (5)$$

#### 4 Results

Wilcoxon signed rank test showed that there has been a statistically significant decrease in public transport use and walking frequency after the pandemic, compared to before. However, a reverse outcome was observed

for private motor vehicle frequency after compared to before. The participants had a model shift from public transport and walking to private car use (see Table 4). This outcome has been supported by the results of McNemar-Bowker test that there has been a statistically significant travel mode change comparing before and after the pandemic. In addition, the motivation for choosing the travel mode has been different before and after the pandemic (see Table 5). Before the pandemic, the participants tended to choose their daily travel mode regarding mostly costs and travel time. However, after the pandemic period, the participants started to prioritize social distancing.

The results from the comparative analysis suggested that the pandemic has changed the participants' daily travel behavior. The further step of the analysis was exploring the perceptions of the participants on public transport, to identify the impacts on their modal shift. A prediction analysis was carried out by applying an ordered logit model with examining the four assumptions. The analysis started with checking the first assumption which was "the dependent variable should be ordinal". The study in this paper had four prediction models for each dependent variable, namely perception on infrastructure (Model 1), safety (Model 2), stress/anxiety (Model 3), and improvement on infrastructure (Model 4). These dependent variables were collected on the Likert Scale (from 1 to 5); therefore, the dependent variables in the models were in ordinal structure and the first assumption was approved. The second assumption was "there should be one or more predictor variables and these should be continuous, ordinal or categorical". The predictor variables in this study were gender, age group, education, employment, working status and daily average commuting distance. Therefore, the second assumption was approved. The third assumption was "there should be ignorable or no multicollinearity

**Table 4** Wilcoxon signed-rank test

Variables	Z	Negative mean ranks <sup>c</sup>	Positive mean ranks <sup>d</sup>	Asymptotic Significance (2-tailed)
Public transport use frequency before vs. after the pandemic	-17.273 <sup>a</sup>	215.63	125.26	0.00*
Private motor vehicle use frequency before vs. after the pandemic	-8.778 <sup>b</sup>	122.97	150.66	0.00*
Walking frequency before vs. after the pandemic	-10.054 <sup>a</sup>	211.13	172.80	0.00*

<sup>a</sup>based on positive ranks; <sup>b</sup>based on negative ranks; <sup>c</sup>frequency after < frequency before; <sup>d</sup>frequency after > frequency before; \*statically significant at 95% confidence level

**Table 5** McNemar-Bowker test

Variables	Value	Degrees of freedom	Asymptotic Significance (2-sided)
Travel mode before vs. after the pandemic	251.394	8	0.00*
Motivation of choosing the travel mode before vs. after the pandemic	590.378	6	0.00*

\*statically significant at 95% confidence level

**Table 6** Testing multicollinearity for predictor variables with Variance Inflation Factors (VIF)

Predictor variables	VIF Values			
	Model 1	Model 2	Model 3	Model 4
Gender	1.05	1.05	1.04	1.04
Age group	1.36	1.37	1.37	1.35
Education	1.39	1.38	1.38	1.37
Daily average commuting distance	1.25	1.25	1.25	1.17
PT frequency	1.06	1.06	1.06	-
PT infrastructure	-	1.06	1.13	-
PT safety	1.27	-	1.10	-
PT stress/anxiety	1.29	1.05	-	-

PT = public transport

**Table 7** Test of parallel lines

Model <sup>a</sup>	Dependent variable	Chi-Square	Degrees of freedom	Significance
Model 1	PT infrastructure	104.64	84	0.06
Model 2	PT safety	1321.09	66	0.00*
Model 3	PT stress/anxiety	126.61	66	0.00*
Model 4	Improvement on PT infrastructure	63.24	30	0.00*

<sup>a</sup>the null hypothesis stated that the location parameters (slope coefficients) were the same across response categories

\*statistically significant at 95% confidence level

**Table 8** Model 1 - Ordered Logit Model

Variables	Coefficient	P- Value	Odds ratio	95 % confidence interval for odds ratio	
				Lower	Upper
Infrastructure <sup>a</sup> dependent variable					
Gender	-0.07	0.56	0.93	0.74	1.17
Age group	-0.31	0.00*	0.77	0.61	0.89
Education	-0.06	0.52	0.94	0.78	1.14
Daily average commuting distance	-0.13	0.01*	0.88	0.80	0.97
ULR using frequency	0.07	0.48	1.07	0.88	1.30
Safety	0.66	0.00*	1.93	1.64	2.27
Stress/anxiety	-0.10	0.20	0.91	0.79	1.05

\*statistically significant at 95% confidence level

<sup>a</sup>outcome variable

between predictor variables". The VIF analysis was carried out to explore multicollinearity (see Table 6). The VIF values less than 10 for each predictor suggested that there has been no multicollinearity and the third assumption was approved.

The fourth assumption was test of parallel lines, which was given in Table 7. The results suggested that the assumption was violated for Models 2, 3 and 4. Therefore, ordered logit model was applied only for the Model 1. Generalized ordered logit model was used for the Models 2, 3 and 4 in order to relax the fourth assumption of ordinal regression. The Model 1 suggested that an increase in daily average commuting distance reduces the level of perception on infrastructure (see Table 8). The road users who travel longer distance

found the ULR system infrastructure of lower quality. In addition, the level of perception on infrastructure reduced for the higher age groups. On the other hand, one unit increase in safety perception increased the perception on infrastructure by 93%.

Generalized ordered logit was applied in the Model 2, Model 3 and Model 4. In these three models, the dependent variables were road users' perceptions in Likert Scale from 1 to 5. Therefore, the number of comparison groups was four ( $j = 1, 2, 3$  and 4). As shown in Model 2, higher quality of infrastructure had a consistent positive impact on feeling safer while using the ULR ( $p=0.00$ ) (see Table 9).

The other consistent impact for all the comparison groups was observed for education. The participants,

**Table 9** Model 2 - Generalized Ordered Logit Model

Variables	j = 1		j = 2		j = 3		j = 4	
	Coefficient	P- Value	Coefficient	P- Value	Coefficient	P- Value	Coefficient	P- Value
Safety perception <sup>a</sup>								
Gender	0.39	0.01**	-0.20	0.34	-0.95	0.04**	-0.47	0.70
Age group	0.05	0.68	0.05	0.68	0.05	0.68	0.05	0.68
Education	0.21	0.06*	0.21	0.06*	0.21	0.06*	0.21	0.06*
Daily average commuting distance	0.02	0.77	0.02	0.77	0.02	0.77	0.02	0.77
PT frequency	-0.08	0.47	-0.08	0.47	-0.08	0.74	-0.08	0.47
PT infrastructure	0.41	0.00**	0.41	0.00**	0.41	0.00**	0.41	0.00**
PT stress/anxiety	-1.07	0.00**	-0.97	0.00**	-1.53	0.00**	-1.86	0.00**

\*statistically significant at 90 % confidence level

\*\*statistically significant at 95 % confidence level

<sup>a</sup>outcome variable**Table 10** Model 3 - Generalized Ordered Logit Model

Variables	j =1		j =2		j =3		j =4	
	Coefficient	P- Value	Coefficient	P- Value	Coefficient	P- Value	Coefficient	P- Value
PT Stress/Anxiety <sup>a</sup>								
Gender	4.06	0.00**	0.13	0.69	0.19	0.39	0.59	0.00**
Age group	-2.95	0.00**	0.13	0.61	0.02	0.91	-0.24	0.05**
Education	0.16	0.15	0.16	0.15	0.16	0.15	0.16	0.15
Daily average commuting distance	1.29	0.00**	-0.01	0.96	0.09	0.33	0.10	0.11
PT frequency	-0.13	0.24	-0.13	0.24	-0.13	0.24	-0.13	0.24
PT infrastructure	-0.07	0.21	-0.07	0.21	-0.07	0.22	-0.07	0.21
PT safety	0.22	0.57	-1.36	0.00**	-1.27	0.00**	-1.44	0.00**

\*statistically significant at 90 % confidence level

\*\*statistically significant at 95 % confidence level

<sup>a</sup>outcome variable**Table 11** Model 4 - Generalized Ordered Logit Model

Variables	j =1		j =2		j =3		j =4	
	Coefficient	P- Value	Coefficient	P- Value	Coefficient	P- Value	Coefficient	P- Value
Improvement on PT infrastructure <sup>a</sup>								
Gender	0.73	0.00**	0.37	0.01**	0.02	0.89	-0.76	0.00**
Age group	-0.26	0.09*	-0.27	0.02**	-0.10	0.37	-0.57	0.01**
Education	0.05	0.65	0.05	0.65	0.05	0.65	0.05	0.65
Daily average commuting distance	0.02	0.64	0.02	0.64	0.02	0.64	0.02	0.64

\*statistically significant at 90 % confidence level

\*\*statistically significant at 95 % confidence level

<sup>a</sup>outcome variable

who had lower education level, perceived less safe while using ULR ( $p = 0.06$ ). In addition, the participants tended to feel less stressed when they feel safer ( $p = 0.00$ ). In addition, the same result was observed in the Model 3 (see Table 10). The participants in higher age groups tended to not prefer using URL after the pandemic condition even if the quality of infrastructure would be improved (see Table 11). The influence of each variable, namely gender in Models 2, 3 and 4, age groups and daily average commuting distance in Model 3, on the dependent variables were not found consistent between comparison groups. Therefore, a further investigation should be carried out by considering the limitations of the study in this paper.

## 5 Discussion

Logistic regression has been a widely used prediction technique to analyse the categorical variables. However, if the assumptions are violated, the results may be biased. Therefore, the assumptions should be checked carefully. The study in this paper applied a deeper analytical technique namely a generalized ordered logit model to analyse the categorical dependent variable. The results suggested that logistic regression should not be applied before exploring the multicollinearity and applying the test of parallel lines.

Regarding the outcomes of the statistical tests and prediction models, the literature review revealed a global decrease in public transportation use during the peak of the Covid-19 pandemic [6], which aligns with our findings indicating a statistically significant decrease in public transport use and walking frequency after the pandemic compared to before. These changes were further supported by the results demonstrating a shift in travel behavior among participants. However, the observed reverse outcome for private motor vehicle frequency after the pandemic highlights a noteworthy mode shift that warrants a detailed examination. This shift was more pronounced than suggested in some studies [10, 16], emphasizing the need to explore the nuances of travel behavior changes in different contexts. It was highlighted that the regional, sociodemographic and socioeconomic variations occurred in public transportation use during the pandemic [15]. Our results support these findings, indicating that participants exhibited a model shift away from the public transport and walking, particularly notable among certain sociodemographic groups. This aligns with the studies [24, 34], which indicated that elderly individuals were less likely to use public transport, emphasizing

the role of sociodemographic factors in shaping travel behavior.

The importance of rebuilding trust in public transportation was a recurrent theme in the literature [13, 23-25, 54], and our study underscores this challenge. The observed mode shift has significant implications for urban planning and transportation policies. Policymakers need to address the newfound emphasis on social distancing in travel mode choices and consider measures that enhance the perceived safety of public transportation to encourage to use. The literature emphasized the impact of governmental measures on public transportation habits and creating different strategies [44], and our study corroborates these trends.

A shift in motivation for choosing the travel modes before and after the pandemic emerged from our results, echoing the findings from the literature [1-4]. The change from cost and travel time considerations to prioritizing social distance suggests a fundamental shift in public perceptions and priorities. This aligns with the study [27] conducted in Athens, which found that the use of public transportation decreased due to a decrease in the desire to share indoor space after the pandemic. As clearly seen in the discussion, unexpected and traumatic health conditions can deeply affect the travel behavior, preferences and perceptions. A further study focused on sustainable transportation design after Covid-19 for Melbourne and it was stated that the infrastructure of electric vehicles was insufficient and reducing carbon emission was not achievable due to the shift from public transport to private motor vehicles [62]. Associating this result with the outcomes in this paper suggests that future studies should focus on improving the sustainable transport infrastructure to reduce the safety concerns under the health issues. It is also noted here that governmental authorities should consider income support program in ensuring the continuity of public transportation services [63].

## Acknowledgements

The authors received no financial support for the research, authorship and/or publication of this article.

## Conflicts of interest

The authors declare that they have no known competing financial interests or personal relationships that could have appeared to influence the work reported in this paper.

## References

- [1] CAMPISI, T., BASBAS, S., SKOUFAS, A., AKGUN, N., TICALI, D., TESORIERE, G. The impact of COVID-19 pandemic on the resilience of sustainable mobility in Sicily. *Sustainability* [online]. 2020, **12**(21), 8829. eISSN 2071-1050. Available from: <https://doi.org/10.3390/su12218829>
- [2] DE WEERT, Y., GKIOTSALITIS, K. A COVID-19 Public transport frequency setting model that includes short-turning options. *Future Transportation* [online]. 2021, **1**(1), p. 3-20. eISSN 2673-7590. Available from: <https://doi.org/10.3390/futuretransp1010002>
- [3] HINTERMAN, B., SCHOEMAN, B., MOLLOY, J., SCHATZMANN, T., TCHERVENKOV, CH., AXHAUSEN, K. W. The impact of COVID-19 on mobility choices in Switzerland. *Transportation Research Part A: Policy and Practice* [online]. 2023, **169**, 103582. ISSN 0965-8564, eISSN 1879-2375. Available from: <https://doi.org/10.1016/j.tra.2023.103582>
- [4] MONTERDE-I-BORT, H., SUCHA, M., RISSER, R., KOCHETOVA, T. Mobility patterns and mode choice preferences during the COVID-19 situation. *Sustainability* [online]. 2022, **14**(2), 768. eISSN 2071-1050. Available from: <https://doi.org/10.3390/su14020768>
- [5] NAVEEN, B. R., GURTOO, A. Public transport strategy and epidemic prevention framework in the context of Covid-19. *Transport Policy* [online]. 2022, **116**, p. 165-174. ISSN 0967-070X, eISSN 1879-310X. Available from: <https://doi.org/10.1016/j.tranpol.2021.12.005>
- [6] VAN DER DRIFT, S., WISMANS, L., KALTER, M.-J. O. Changing mobility patterns in the Netherlands during COVID-19 outbreak. *Journal of Location Based Services* [online]. 2021, **16**(1), p. 1-24. ISSN 1748-9725, eISSN 1748-9733. Available from: <https://doi.org/10.1080/17489725.2021.1876259>
- [7] VICKERMAN, R. Will Covid-19 put the public back in public transport? A UK perspective. *Transport Policy* [online]. 2021, **103**, p. 95-102. ISSN 0967-070X, eISSN 1879-310X. Available from: <https://doi.org/10.1016/j.tranpol.2021.01.005>
- [8] TORI, S., DE SEJOURNET, A., MACHARIS, C. Reactions of the public transport sector to the COVID-19 pandemic. Insights from Belgium. *Travel Behaviour and Society* [online]. 2023, **31**, p. 244-253. ISSN 2214-367X, eISSN 2214-3688. Available from: <https://doi.org/10.1016/j.tbs.2023.01.001>
- [9] OESTREICH, L., RHODEN, P. S., DA SILVA VIEIRA, J., RUIZ-PADILLO, A. Impacts of the COVID-19 pandemic on the profile and preferences of urban mobility in Brazil: challenges and opportunities. *Travel Behaviour and Society* [online]. 2023, **31**, p. 312-322. ISSN 2214-367X, eISSN 2214-3688. Available from: <https://doi.org/10.1016/j.tbs.2023.01.002>
- [10] HOSSAIN, S., ISLAM, M. A., AKTHER, M. S. COVID-19 impact on travel and work habits of office workers in Bangladesh. *Transportation Engineering* [online]. 2023, **11**, 100162. eISSN 2666-691X. Available from: <https://doi.org/10.1016/j.treng.2023.100162>
- [11] WANG, J., HUANG, J., YANG, H., LEVINSON, D. Resilience and recovery of public transport use during. *npj Urban Sustainability* [online]. 2022, **2**, 18. eISSN 2661-8001. Available from: <https://doi.org/10.1038/s42949-022-00061-1>
- [12] ALMLOF, E., RUBENSSON, I., CEBECAUER, M., JENELIUS, E. Who continued travelling by public transport during COVID-19? Socioeconomic factors explaining travel behavior in Stockholm 2020 based on smart card data. *European Transport Research Review* [online]. 2021, **13**, 31. Available from: <https://doi.org/10.1186/s12544-021-00488-0>
- [13] AADITYA, B., RAHUL, T. M. Long-term impacts of COVID-19 pandemic on travel behavior. *Travel Behaviour and Society* [online]. 2023, **30**, p. 262-270. ISSN 2214-367X, eISSN 2214-3688. Available from: <https://doi.org/10.1016/j.tbs.2022.10.005>
- [14] ANWAR, M. A., DHIR, A., JABEEN, F., ZHANG, Q., SIDDIQUEI, A. N. Unconventional green transport innovations in the post-COVID-19 era. A trade-off between green actions and personal health protection. *Journal of Business Research* [online]. 2023, **155**(A), 113442. ISSN 0148-2963, eISSN 1873-7978. Available from: <https://doi.org/10.1016/j.jbusres.2022.113442>
- [15] GKIOTSALITIS, K., CATS, O. Public transport planning adaption under the COVID-19 pandemic crisis: literature review of research needs and directions. *Transport Reviews* [online]. 2021, **41**(3), p. 374-392. ISSN 0144-1647, eISSN 1464-5327. Available from: <https://doi.org/10.1080/01441647.2020.1857886>
- [16] ZHANG, Z., CHAI, H., GUO, Z. Quantitative resilience assessment of the network-level metro rail service's responses to the COVID-19 pandemic. *Sustainable Cities and Society* [online]. 2023, **89**, 104315. ISSN 2210-6707, eISSN 2210-6715. Available from: <https://doi.org/10.1016/j.scs.2022.104315>
- [17] RASCA, S., MARKVICA, K., IVANSCHITZ, B. P. Impacts of COVID-19 and pandemic control measures on public transport ridership in European urban areas - the cases of Vienna, Innsbruck, Oslo, and Agder. *Transportation Research Interdisciplinary Perspectives* [online]. 2021, **10**, 100376. eISSN 2590-1982. Available from: <https://doi.org/10.1016/j.trip.2021.100376>



- [18] ZAVAREH, M. F., MEHDIZADEH, M., NORDFJAERN, T. Demand for mitigating the risk of COVID-19 infection in public transport: the role of social trust and fatalistic beliefs. *Transportation Research Part F: Traffic Psychology and Behaviour* [online]. 2022, **84**, p. 348-362. ISSN 1369-8478, eISSN 1873-5517. Available from: <https://doi.org/10.1016/j.trf.2021.12.010>
- [19] BECK, M. J., HENSHER, D. A., NELSON, J. D. Public transport trends in Australia during the COVID-19 pandemic: an investigation of the influence of bio-security concerns on trip behavior. *Journal of Transport Geography* [online]. 2021, **96**, 103167. ISSN 0966-6923, eISSN 1873-1236. Available from: <https://doi.org/10.1016/j.jtrangeo.2021.103167>
- [20] BOCKER, L., OLSSON, L. E., UTENG, T. P., FRIMAN, M. Pandemic impacts on public transport safety and stress perceptions in Nordic cities. *Transportation Research Part D: Transport and Environment* [online]. 2023, **114**, 103562. ISSN 1361-9209, eISSN 1879-2340. Available from: <https://doi.org/10.1016/j.trd.2022.103562>
- [21] BAUER, M., BAUER, K. Analysis of the impact of the COVID-19 pandemic on the future of public transport: example of Warsaw. *Sustainability* [online]. 2022, **14**(2), 7268. eISSN 2071-1050. Available from: <https://doi.org/10.3390/su14127268>
- [22] KOPSIDAS, A., MILIOTI, CH., KEPAPTSOGLU, K., VLACHOGIANNI, E. I. How did the COVID-19 pandemic impact traveler behavior toward public transport? The case of Athens, Greece. *Transportation Letters* [online]. 2021, **13**(5-6), p. 344-352. ISSN 1942-7867, eISSN 1942-7875. Available from: <https://doi.org/10.1080/19427867.2021.1901029>
- [23] VALLEJO-BORDA, J. A., RICARDO GIESEN, R., BASNAK, P., REYES, J. P., MELLA LIRA, B., BECK, M. J., HENSHER, D. A., DE DIOS ORTUZAR, J. Characterising public transport shifting to active and private modes in South American capitals during the COVID-19 pandemic. *Transportation Research Part A: Policy and Practice* [online]. 2022, **164**, p. 186-205. ISSN 0965-8564, eISSN 1879-2375. Available from: <https://doi.org/10.1016/j.tra.2022.08.010>
- [24] DAI, J., LIU, Z., LI, R. Improving the subway attraction for the post-COVID-19 era: the role of fare-free public transport policy. *Transport Policy* [online]. 2021, **103**, p. 21-30. ISSN 0967-070X, eISSN 1879-310X. Available from: <https://doi.org/10.1016/j.tranpol.2021.01.007>
- [25] LITMAN, T. Developing indicators for comprehensive and sustainable transport planning. *Transportation Research Record: Journal of the Transportation Research Board* [online]. 2017, **2017**(1), p. 10-15. ISSN 0361-1981, eISSN 2169-4052. Available from: <https://doi.org/10.3141/2017-02>
- [26] FRIMAN, M., LATTMAN, K., OLSSON, L. E. Public transport quality, safety, and perceived accessibility. *Sustainability* [online]. 2020, **12**(9), 3563. eISSN 2071-1050. Available from: <https://doi.org/10.3390/su12093563>
- [27] KYRIAKIDIS, C., CHATZHOANNOU, I., ILIADIS, F., NIKITAS, A., BAKOGIANNIS, E. Evaluating the public acceptance of sustainable mobility interventions responding to Covid-19: the case of the Great Walk of Athens and the importance of citizen engagement. *Cities* [online]. 2023, **132**, 103966. ISSN 0264-2751, eISSN 1873-6084. Available from: <https://doi.org/10.1016/j.cities.2022.103966>
- [28] SIEWWUTTANAGU, S., JITTTRAIROM, P. The impact of COVID-19 and related containment measures on Bangkok's public transport ridership. *Transportation Research Interdisciplinary Perspectives* [online]. 2023, **17**, 100737. eISSN 2590-1982. Available from: <https://doi.org/10.1016/j.trip.2022.100737>
- [29] LONG, A., CARNEY, F., KANDT, J. Who is returning to public transport for non-work trips after COVID-19? Evidence from older citizens' smart cards in the UK's second largest city region. *Journal of Transport Geography* [online]. 2023, **107**, 103529. ISSN 0966-6923, eISSN 1873-1236. Available from: <https://doi.org/10.1016/j.jtrangeo.2023.103529>
- [30] NIKOLAIDOU, A., KOPSACHEILIS, A., GEORGIADIS, G., NOUTSIAS, T., POLITIS, I., FYROGENIS, I. Factors affecting public transport performance due to the COVID-19 outbreak: a worldwide analysis. *Cities* [online]. 2023, **134**, 104206. ISSN 0264-2751, eISSN 1873-6084. Available from: <https://doi.org/10.1016/j.cities.2023.104206>
- [31] KASSAW, CH., PANDEY, D. COVID-19 Pandemic related to anxiety disorder among communities using public transport at Addis Ababa, Ethiopia, March 2020: cross-sectional Study Design. *Human Arenas* [online]. 2021, **5**, p. 312-321. ISSN 2522-5790, eISSN 2522-5804. Available from: <https://doi.org/10.1007/s42087-020-00166-y>
- [32] SHELAT, S., CATS, O., VAN CRANENBURGH, S. Traveller behavior in public transport in the early stages of the COVID-19 pandemic in the Netherlands. *Transportation Research Part A: Policy and Practice* [online]. 2022, **159**, p. 357-371. ISSN 0965-8564, eISSN 1879-2375. Available from: <https://doi.org/10.1016/j.tra.2022.03.027>
- [33] ABDULLAH, M., ALI, N., JAVID, M. A., DIAS, CH., CAMPISI, T. Public transport versus solo travel mode choices during the COVID-19 pandemic: self-reported evidence from a developing country. *Transportation Engineering* [online]. 2021, **5**, 100078. eISSN 2666-691X. Available from: <https://doi.org/10.1016/j.treng.2021.100078>
- [34] ABDULLAH, M., ALI, N., DIAS, CH., CAMPISI, T., JAVID, M. A. Exploring the traveler's intentions to use public transport during the COVID-19 pandemic while complying with precautionary measures. *Applied Sciences* [online]. 2021, **11**(8), 3630. eISSN 2076-3417. Available from: <https://doi.org/10.3390/app11083630>

- [35] DAS, S., BORUAH, A., BANERJEE, A., RAONIAR, R., NAMA, S., MAURYA, A. K. Impact of COVID-19: a radical modal shift from public to private transport mode. *Transport Policy* [online]. 2021, **109**, p. 1-11. ISSN 0967-070X, eISSN 1879-310X. Available from: <https://doi.org/10.1016/j.tranpol.2021.05.005>
- [36] EISENMANN, C., NOBIS, C., KOLAROVA, V., LENZ, B., WINKLER, CH. Transport mode use during the COVID-19 lockdown period in Germany: the car became more important, public transport lost ground. *Transport Policy* [online]. 2021, **103**, p. 60-67. ISSN 0967-070X, eISSN 1879-310X. Available from: <https://doi.org/10.1016/j.tranpol.2021.01.012>
- [37] SCHAEFER, K. J., TUITJER, L., LEVIN-KEITEL, M. Transport disrupted - substituting public transport by bike or car under Covid 19. *Transportation Research Part A: Policy and Practice* [online]. 2021, **153**, p. 202-217. ISSN 0965-8564, eISSN 1879-2375. Available from: <https://doi.org/10.1016/j.tra.2021.09.002>
- [38] KLOS-ADAMKIEWICZ, Z., GUTOWSKI, P. The outbreak of COVID-19 pandemic in relation to sense of safety and mobility changes in public transport using the example of Warsaw. *Sustainability* [online]. 2022, **14**(3), 1780. eISSN 2071-1050. Available from: <https://doi.org/10.3390/su14031780>
- [39] JAVID, M. A., ABDULLAH, M., ALI, N., DIAS, CH. Structural equation modeling of public transport use with COVID-19 precautions: an extension of the norm activation model. *Transportation Research Interdisciplinary Perspectives* [online]. 2021, **12**, 100474. eISSN 2590-1982. Available from: <https://doi.org/10.1016/j.trip.2021.100474>
- [40] DOWNEY, L., FONZONE, A., FOUNTAS, G., SEMPLE, T. The impact of COVID-19 on future public transport use in Scotland. *Transportation Research Part A: Policy and Practice* [online]. 2022, **163**, p. 338-352. ISSN 0965-8564, eISSN 1879-2375. Available from: <https://doi.org/10.1016/j.tra.2022.06.005>
- [41] NIKIFOIADIS, A., MITROPOULOS, L., KOPELIAS, P., BASBAS, S., STAMATIADIS, N., KROUSTALI, S. Exploring mobility pattern changes between before, during and after COVID-19 lockdown periods for young adults. *Cities* [online]. 2022, **125**, 103662. ISSN 0264-2751, eISSN 1873-6084. Available from: <https://doi.org/10.1016/j.cities.2022.103662>
- [42] ORRO, A., NOVALES, M., MONTEAGUDO, A., PEREZ-LOPEZ, J.-B., BURGARIN, M. R. Impact on city bus transit services of the COVID-19 lockdown and return to the new normal: the case of a Coruna (Spain). *Sustainability* [online]. 2020, **12**(17), 7206. eISSN 2071-1050. Available from: <https://doi.org/10.3390/su12177206>
- [43] BECK, M. J., HENSHER, D. A., WEI, E. Slowly coming out of COVID-19 restrictions in Australia: implications for working from home and commuting trips by car and public transport. *Journal of Transport Geography* [online]. 2020, **88**, 102846. ISSN 0966-6923, eISSN 1873-1236. Available from: <https://doi.org/10.1016/j.jtrangeo.2020.102846>
- [44] CAMPISI, T., BASBAS, S., AL-RASHID, M. A., TESORIERE, G., GEORGIADIS, G. A region-wide survey on emotional and psychological impacts of COVID-19 on public transport choices in Sicily, Italy. *Transactions on Transport Sciences* [online]. 2021, **12**(3), p. 34-43. ISSN 1802-9876. Available from: <https://doi.org/10.5507/tots.2021.010>
- [45] DONG, H., MA, S., JIA, N., TIAN, J. Understanding public transport satisfaction in post COVID-19 pandemic. *Transport Policy* [online]. 2021, **101**, p. 81-88. ISSN 0967-070X, eISSN 1879-310X. Available from: <https://doi.org/10.1016/j.tranpol.2020.12.004>
- [46] BASNAK, P., GIESEN, R., MUNOZ, J. C. Estimation of crowding factors for public transport during the COVID-19 pandemic in Santiago, Chile. *Transportation Research Part A: Policy and Practice* [online]. 2022, **159**, p. 140-156. ISSN 0965-8564, eISSN 1879-2375. Available from: <https://doi.org/10.1016/j.tra.2022.03.011>
- [47] GRAMSCH, B., GUEVARA, C. A., MUNIZAGA, M., SCHWARTZ, D., TIRACHINI, A. The effect of dynamic lockdowns on public transport demand in times of COVID-19: evidence from smartcard data. *Transport Policy* [online]. 2022, **126**, p. 136-152. ISSN 0967-070X, eISSN 1879-310X. Available from: <https://doi.org/10.1016/j.tranpol.2022.06.012>
- [48] MARRA, A. D., SUN, L., CORMAN, F. The impact of COVID-19 pandemic on public transport usage and route choice: evidences from a long-term tracking study in urban area. *Transport Policy* [online]. 2022, **116**, p. 258-268. ISSN 0967-070X, eISSN 1879-310X. Available from: <https://doi.org/10.1016/j.tranpol.2021.12.009>
- [49] GKIOTSALITIS, K. A model for modifying the public transport service patterns to account for the imposed COVID-19 capacity. *Transportation Research Interdisciplinary Perspectives* [online]. 2021, **9**, 100336. eISSN 2590-1982. Available from: <https://doi.org/10.1016/j.trip.2021.100336>
- [50] TIIKKAJA, H., VIRI, R. The effects of COVID-19 epidemic on public transport ridership and frequencies. a case study from Tampere, Finland. *Transportation Research Interdisciplinary Perspectives* [online]. 2021, **10**, 100348. eISSN 2590-1982. Available from: <https://doi.org/10.1016/j.trip.2021.100348>
- [51] BANDYOPADHYAYA, V., BANDYOPADHYAYA, R. Understanding public transport use intention post Covid-19 outbreak using modified theory of planned behavior: case study from developing country perspective. *Case Studies on Transport Policy* [online]. 2022, **10**(4), p. 2044-2052. ISSN 0967-070X, eISSN 1879-310X. Available from: <https://doi.org/10.1016/j.cstp.2022.09.002>

- [52] ZHOU, J.-B., MA, CH.-X., DONG, S., ZHANG, M.-J. Unconventional epidemic prevention strategy for urban public transport systems during the COVID-19 Outbreak: the example of Ningbo. *China Journal of Highway and Transport* [online]. 2020, **33**(11), p. 1-10. ISSN 1001-7372. Available from: <https://doi.org/10.19721/j.cnki.1001-7372.2020.11.001>
- [53] PRZYBYŁOWSKI, A., STELMAK, S., SUCHANEK, M. Mobility behavior in view of the impact of the COVID-19 pandemic - public transport users in Gdansk case study. *Sustainability* [online]. 2021, **13**(1), 364. eISSN 2071-1050. Available from: <https://doi.org/10.3390/su13010364>
- [54] HELFERS, A., REISERER, M., SCHNEIDER, N., EBERSBACH, M., SOMMER, C. Should I stay or should I go? Risk perception and use of local public transport during the COVID-19 pandemic. *Frontiers in Psychology* [online]. 2022, **13**, 926539. eISSN 1664-1078. Available from: <https://doi.org/10.3389/fpsyg.2022.926539>
- [55] KREJCIE, R. V., MORGAN, D. W. Determining sample size for research activities. *Educational and Psychological Measurement* [online]. 1970, **30**(3), p. 607-610. ISSN 0013-1644, eISSN 1552-3888. Available from: <https://doi.org/10.1177/001316447003000308>
- [56] BURSA governorship (in Turkish) [online]. Available from: <http://bursa.gov.tr/ilcelerimiz>
- [57] WOOLSON, R. F. Wilcoxon signed-rank test [online]. In: *Wiley encyclopedia of clinical trials*. D'AGOSTINO, R., MASSARO, J., SULLIVAN, L. (Eds.). Hoboken, New Jersey: John Wiley and Sons, Inc., 2008. ISBN 9780471352037, eISBN 9780471462422, p. 1-3. Available from: <https://doi.org/10.1002/9780471462422.eoct979>
- [58] ABDULLAH, M., DIAS, CH., MULEY, D., SHAHIN, M. Exploring the impacts of COVID-19 on travel behavior and mode preferences. *Transportation Research Interdisciplinary Perspectives* [online]. 2020, **8**, 100255. eISSN 2590-1982. Available from: <https://doi.org/10.1016/j.trip.2020.100255>
- [59] WILLIAMS, R. Generalized ordered logit/partial proportional odds models for ordinal dependent variables. *The Stata Journal: Promoting Communications on Statistics and Stata* [online]. 2006, **6**(1), p. 58-82. ISSN 1536-867X, eISSN 1536-8734. Available from: <https://doi.org/10.1177/1536867X06006001>
- [60] LONG, J. S., FREESE, J. Regression models for categorical dependent variables using Stata. Texas: Stata press, 2006. ISBN 1-59718-011-4.
- [61] WILLIAMS, R. Understanding and interpreting generalized ordered logit models. *The Journal of Mathematical Sociology* [online]. 2016, **40**(1), p. 7-20. ISSN 0022-250X, eISSN 1545-5874. Available from: <https://doi.org/10.1080/0022250X.2015.1112384>
- [62] PAWLUK DE-TOLEDO, K., O'HERN, S., KOPPEL, S. A city-level transport vision for 2050: reimagined since COVID-19. *Transport Policy* [online]. 2023, **132**, p. 144-153. ISSN 0967-070X, eISSN 1879-310X. Available from: <https://doi.org/10.1016/j.tranpol.2022.12.022>
- [63] SUNIO, V., LI, W. J., PONTAWE, J., DIZON, A., VALDERRAMA, J. B., ROBANG, A. Service contracting as a policy response for public transport recovery during the Covid-19 pandemic: a preliminary evaluation. *Transportation Research Interdisciplinary Perspectives* [online]. 2022, **13**, 100559. eISSN 2590-1982. Available from: <https://doi.org/10.1016/j.trip.2022.100559>



This is an open access article distributed under the terms of the Creative Commons Attribution 4.0 International License (CC BY 4.0), which permits use, distribution, and reproduction in any medium, provided the original publication is properly cited. No use, distribution or reproduction is permitted which does not comply with these terms.

# EXAMINING THE EFFECT OF GEOMETRIC DESIGN FEATURES ON THE SPEED IN HORIZONTAL CURVE ON MOUNTAIN ROAD

Ehsan Ramezani-Khansari<sup>1\*</sup>, Fereidoon Moghadas Nejad<sup>2</sup>, Sina Moogehi<sup>2</sup>

<sup>1</sup>Civil Engineering Department, Imam Khomeini International University, Qazvin, Iran

<sup>2</sup>Civil Engineering Department, Amirkabir University of Technology (Tehran Polytechnic), Tehran, Iran

\*E-mail of corresponding author: E.R.Khansari@eng.ikiu.ac.ir

Ehsan Ramezani-Khansari 0000-0001-9642-6134,

Fereidoon Moghadas Nejad 0000-0003-3830-4555

## Resume

In this study, the effect of five geometric design features, including radius, superelevation, longitudinal grade, lane and shoulder width, on the average speed in the horizontal curve on a two-lane undivided rural road was investigated. The standardized regression coefficients showed that the most important factor affecting the speed was the radius (10.47) followed by the longitudinal grade (4.46). Superelevation and lane width had little effect. Shoulder width had no significant effect. This would be due to the wide width of the lanes. It was found that the relationships between speed and radius, longitudinal grade, superelevation and lane width were radical, quadratic, linear and linear, respectively. Increasing the longitudinal grade has increased the speed of the drivers. Increasing the superelevation was effective when its value changed from negative to positive.

## Article info

Received 12 March 2024

Accepted 5 June 2024

Online 27 June 2024

## Keywords:

horizontal curve  
driving behavior  
driving simulator  
geometric design

Available online: <https://doi.org/10.26552/com.C.2024.037>

ISSN 1335-4205 (print version)

ISSN 2585-7878 (online version)

## 1 Introduction

Improper driving strategy is one of the main causes of accidents (roughly 65 %). In general, speed, changes in acceleration and vehicle trajectory are a reflection of the driving strategy. Researches have shown that horizontal curves are a critical location on rural two-lane roads due to the possibility of skidding or overturning [1]. Improper perception and expectation of horizontal curve sharpness also affects the driver's strategy and can lead to dangerous speeds and accidents. Investigating the effect of horizontal curve properties on driver performance has remained a major road safety issue [2].

Accidents are more likely to occur in horizontal curves than on straight segments, as the need for the driver attention is increased and the drivers may take the wrong speed and path. The average number of accidents reported in the United States indicates that the number of accidents in horizontal curves is higher than straight segments. In 2008, the rate of accidents on horizontal curves has been 3 times higher than accidents on other segments of highways.

About 75 % of road fatal crashes have been caused

by a car going off the road and hitting fixed objects such as trees [3]. Studies in other countries have also confirmed it [4]:

- The rate of crashes in curves was 1.5 to 4 times than that of straight segments.
- 25 to 30 % of injury accidents occur in horizontal curves.
- Approximately 60 to 70 % of fatal crashes in curves are single-vehicle crashes.

Among all the features of horizontal curves, factors such as small radius, narrow lane width and cross section (including lanes and shoulders) can be mentioned [5]. Andjus and Maletin studied speed in horizontal curves. Nine horizontal curves on rural two-lane roads with radii in the range of 50 to 750 m were examined. The curves were more than 2 km away from any intersection and free flow speed were extracted from data with a time headway of more than 7 sec. The results showed that with the increase in the radius, not only does the average speed increase, but the range between the 85th and 15th percentile speeds increases as well [6]. Dell'Acqua provided equation (1) for environmental speed ( $V_{ENV}$ ) that depended on two variables: curvature



**Table 1** Relationship between operating speed in horizontal curves and geometric design features

Researcher(s)	Estimated relationship
Castro at al. [10]	$V_{85} = 102.048 - \frac{3990.26}{R}, R \leq 400 \text{ m}$
Camacho et al. [11]	$V_{85}^2 = 127 * R \left( f + \frac{e}{R} \right), R \leq 70 \text{ m}$
Kanellaidis at al. [12]	$V_{85} = 129.88 - \frac{623.1}{\sqrt{R}}$
Abbas at al. [13]	$V_{85MC} = 129.88 - \frac{623.1}{\sqrt{R}} + 0.307 V_{85AT}$
Misaghi and Hassan [14]	$V_{85MC} = 94.3 + 8.67 * 10^{-6} * R^2$
Jacob and Anjaneyulu [15]	$V_{85} = 56.75 - \frac{739.21}{R} - 0.034 * CL$
Dilling [16]	$V_{85} = 5.32 - 1.12 * V_{AVG}$ $V_{AVG} = 25.1 + 5.57b + 0.05R - 0.05CCR$

$V_{85MC}$ : 85<sup>th</sup> speed in the middle of the curve,  $V_{85AT}$ : 85<sup>th</sup> speed in straight segment,  $CCR$ : curvature change rate,  $b$ : lane width,  $V_{AVG}$ : Average of speed in the curve,  $R$ : Radius,  $e$ : superelevation,  $f$ : skid resistance,  $CL$ : length of curve

change rate (CCR) in terms of gradient per kilometer and road width (L) in terms of meter:

$$V_{ENV} = 82.84 - 0.1033 * CCR + 3.44 * L. \quad (1)$$

It should be noted that the environmental speed defined as a maximum velocity of 85 % in straight segments or curves with a high radius [7]. Dhahir and Hassan used naturalistic driving study (NDS) data prepared by the second strategic highway research program (SHRP2) to examine driver behavior on curves. They selected 24 curves in flat areas and 25 curves in mountainous areas for study. They presented Equation (2) for the speed in the middle of the horizontal curve. The dependent variable of this model was the operating speed in the middle of the curve ( $V_{85MC}$ ) and the independent variables included the radius (R), the speed limit (VL) and a dummy variable T (0 for flat, 1 for mountainous areas) [8]:

$$V_{85MC} = 80.352 + \frac{3289.296}{R} + 0.261 * V_L + 5.969 * T \quad (R_{adj}^2 = 0.829). \quad (2)$$

Malaghan et al. equipped a vehicle with GPS device to study driving behavior in curves. The participants in this study were 49 people in the age range of 21 to 59 years. Six undivided two-lane roads in India were examined. The absolute grade of all curves was less than 4 %. They modeled operating speed ( $V_{85}$ ) by applying radius (R) and degree of curvature (DC). Equations (3), (4) and (5) show the regression models [9]:

$$V_{85} = 11.68 + 10.37 * \ln(R) \quad (R^2 = 0.87), \quad (3)$$

$$V_{85} = 84.72 + 10.37 * \ln(D_C) \quad (R^2 = 0.87), \quad (4)$$

$$V_{85} = 71.7 + 0.01 * R + 1.12 + D_C \quad (R^2 = 0.87), \quad (5)$$

There are other papers estimated the operating speed in horizontal curves that the Table 1 has

summarized.

These studies have used the field data to study the horizontal curves. Driving simulator is another source of data that has been used in many researches, some of which are mentioned below. Calvi investigated the features of horizontal curves such as radius, transition, sight distance and cross-section. He examined 34 drivers in 72 different curves under 3 different scenarios in both directions using a driving simulator. The results showed that by improving the geometric conditions, the speed has been also increased [5].

Wang et al. built a highway in China in a driving simulator. They recruited 22 drivers who drove 4 different types of curves (horizontal curve with positive and negative longitudinal grade, horizontal curve with crest and sag vertical curve). For each type of the curves, a model for estimating the maximum lateral acceleration was proposed, in which the radius, the longitudinal grade and the length of the segment were examined. According to the models, the radius was the only affecting factor in all the cases. The length of the road was effective in horizontal curves with crest vertical curve [17]. Shuo et al. examined the effects of lane width, lane position, and shoulder width on driving behavior on a three-lane urban highway tunnel. By using a driving simulator, 24 volunteers were examined. The results showed that lane and shoulder width had significant effect on driving speed [18].

Mecheri et al. investigated the effect of shoulder and lane width and their combinations on drivers. 34 drivers of an average age of 30 years (range of 25-52) participated in the experiment. Their research showed that the best combination of shoulder and lane width was 0.5 and 3 m, respectively, which allowed the driver to find and adjust her/his position in the road properly. The lane width could also be reduced to 2.75 m, where the passage of heavy vehicles such as trucks and buses was very low [19].

Melo et al. investigated the effect of lane and shoulder width on free flow speed using a driving simulator by 15 participants. The results demonstrated the minimum



lane-shoulder width combination, after which no further increase in free-flow speed was observed, was 3.6 and 0.8 m for lane and shoulder, respectively [20]. Rosey et al. examined the difference between the effect of lane width reduction on speed and lateral position in real-world and simulation conditions. One of their purposes was to driving simulator validation in this area. The results showed that reducing the lane width has no effect on speed. Furthermore, by comparing the simulator results and reality, the results were relatively valid [21].

Ben-Bassat et al. studied the effects of a combination of three road design features, including shoulder width, barrier (guard rail) and horizontal curve, on driving behavior (speed and position in the lane) and mental measures (understanding safe driving speed and estimating road safety) by recruiting 22 drivers. The results showed that there was a significant effect of road geometry on driver behavior. Shoulder width had significant effect on speed and position on the lane, but this effect was only apparent when there was a barrier or guardrail. These findings demonstrated the role of a barrier in determining the perceived safety margin across different shoulder widths. When there was no guardrail, shoulder width lost many of its benefits and effects on driving behavior [22].

Using the high-fidelity driving simulators, Wang et al. examined the effect of lane width in mountain highways on driving behaviors (lateral positions and speed). First, the validity of the driving simulator was studied. 46 drivers (20 women and 26 men, age range of 23-56 years) were participated in the experiment. Due to the fact that there are many curved segments, including horizontal and vertical curves in mountain roads, they studied the lateral positions and speed in curves. The results showed that the effect of radius on speed was statistically significant and showed that the simulator can be used for mountain road studies. In addition, vehicle trajectory and speed analysis showed that lane width and horizontal curve radius had significant effects on driving behavior. The wider the lane, the greater the speed deviations [23]. Wang et al. used a driving simulator to investigate the amplitude of the effect of the horizontal curves on driver behavior on mountain roads. They found that curves could affect driver behavior, including speed and lateral position, at a distance of 300 m [24]. Zolali et al. studied the effect of experience, sight distance and geometric design on the average speed on a suburban road. It was observed that sight was the most important factor influencing the choice of average speed.

Furthermore, the presence of curves on the simulated road, as a parameter in geometric design, encourages drivers to slow down [25].

One of the applications of studying the effect of geometric characteristics on driving behavior is the investigation of fuel consumption and environmental effects, which is important in sustainability studies. A study using real-world driving data in Madrid, Spain, showed that traffic conditions, driving behavior and the road topology were effective on fuel consumption [26]. Another study in Spain showed that vehicle CO<sub>2</sub> emissions decreased as the consistency level of a homogeneous road segment increased. In other words, when the parameters of the geometric design were considered consistent in different road segments, the fuel consumption was reduced [27].

As aforementioned, various studies have been conducted to determine the effect of geometric design features on driver behavior and speed. However, they have considered two or three features of the geometric design. In this research, the simultaneous effect of 5 geometric design features on mountain roads has been investigated. The effect of superelevation has also been studied, which has been rarely addressed in previous research.

In the next section, the methodology and design of experiments has been explained. The third section describes the data collection, apparatus and materials. The properties of the applied driving simulator have been introduced in this section. The fourth section has been devoted to analyze of the results and discussion. The research has been concluded in the fifth section.

## 2 Methodology

In this research, a driving simulator is used to study the driver behavior in different geometric designs. Features of the geometric design that are studied are: longitudinal grade, superelevation, radius, lane width and shoulder width. Each geometric design is made of a combination of different levels of features or factors. The levels of a feature divide it into different intervals, so its effect can be examined. Table 2 shows the features and levels are used in this research.

After determining the number of features and levels to be tested, the required number of tests must be determined. If a study with all the levels of factors is required, all permutations must be considered in which

**Table 2** Levels of geometric design features of the driving simulator tests

Feature Level	Radius (m)	Lane width (m)	Longitudinal grade (%)	Superelevation (%)	Shoulder width (m)
1	20	2	0	-2	0.5
2	40	2.5	-10	0	0.8
3	60	3	-15	2	*
4	80	*	-20	4	*

**Table 3** The geometric designs selected for testing

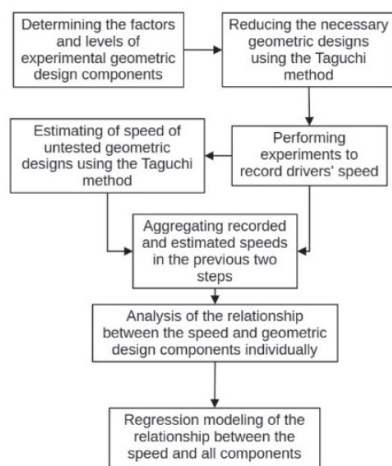
Road-Geometric design	Radius (m)	Lane width (m)	Longitudinal grade (%)	Superelevation (%)	Shoulder width (m)
1-1	80	3	-20	-2	0.5
1-2	60	2.5	0	2	0.5
1-3	40	2	-15	4	0.5
1-4	20	2.5	-20	4	0.8
1-5	20	2.5	-10	0	0.5
2-1	80	2.5	0	4	0.8
2-2	80	2.5	-15	0	0.5
2-3	60	2	-20	0	0.8
2-4	40	3	0	0	0.8
2-5	20	2	0	-2	0.5
3-1	80	2	-10	2	0.8
3-2	60	3	-10	4	0.5
3-3	60	2.5	-15	-2	0.8
3-4	40	2.5	-10	-2	0.8
3-5	40	2.5	-20	2	0.5
3-6	20	3	-15	2	0.8

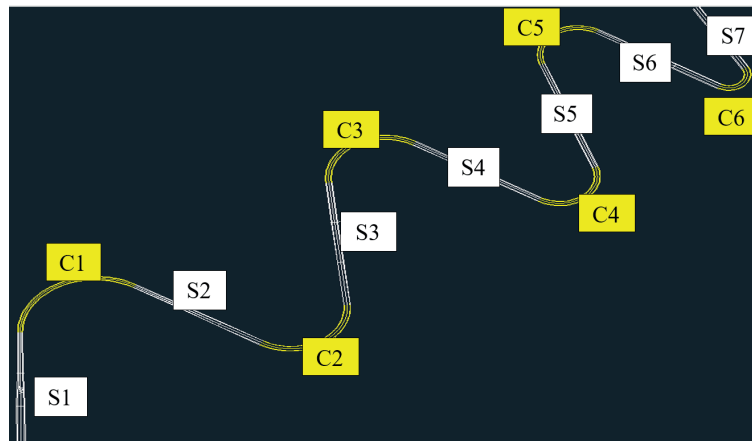
384 ( $4 * 4 * 4 * 2 * 3$ ) tests are needed. Performing this number of experiments by using driving simulator is impractical. Therefore, the number of experiments is reduced to 16 using the Taguchi method. The efficiency of the Taguchi method has been tested in comparison to the full factorial in transportation studies [28]. Using the Taguchi method, only 16 geometric designs are needed to be tested in the driving simulator, and the speed of other geometric designs can be estimated by Taguchi method.

It is not appropriate to put all the geometric designs in one route, because it may make the drivers tired and it is possible to affect the results. Therefore, the geometric designs are divided into three groups and three routes are built accordingly. The geometric designs are randomly distributed between the routes. By doing so, the numbers of geometric designs in routes are 5, 5 and 6.

Table 3 shows the combination of levels of factors for each geometric designs in 3 routes. In the first column of Table 3, the first and second numbers represent the route number and the geometric design number in that route.

Finally, statistical analyses are performed on the speed data that were obtained directly from the driving simulator experiments and the speed data that estimated by the Taguchi method. The relationship between the speed and each of the geometric design features (factors) is first examined separately, then relationship between the speed and all the features is investigated by regression models. Figure 1 depicts the flowchart of methodology. All the speed data recorded in a curve of participants are averaged and it is used in further analyses (each participant drove the experiment path twice).

**Figure 1** Flowchart of methodology**Figure 2** The simulated two-lane undivided rural road



**Figure 3** The scheme of a simulated experiment roads

### 3 Apparatus and materials

Thirty men between 21 and 33 years old were recruited to drive a personal car in driving simulator. Driving simulator are accepted tool for the driving behavior studies that has been used in many articles and its validity has been demonstrated [29-30]. Male drivers recruited in driving test to omit the effect of gender, which is out of scope of this paper. The scope of this study was two-lane undivided rural roads in mountainous area (Figure 2).

The weather was sunny with no precipitation and there was no other vehicle on the road. Amirkabir University driving simulator was used for the experiments, which has been used in previous researches [31-33].

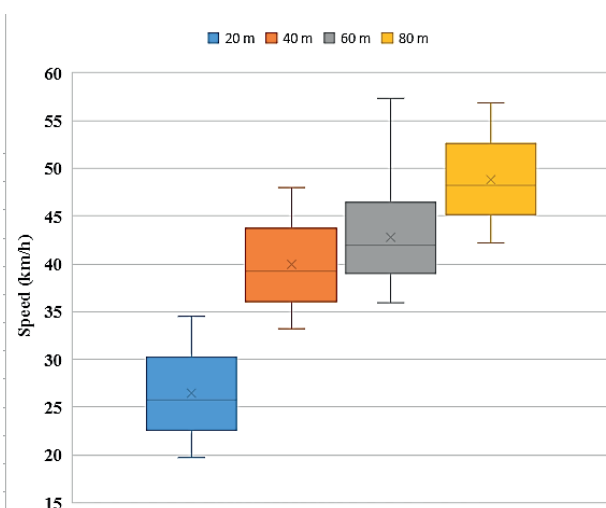
Figure 3 depicts one of the experiment roads, in which there are straight segments (S1, S2...) between curves (C1, C2...). The straight segments were added to the experiment to avoid the effect of curves on each other. The effect of curves was found 300 m in Wang et al.'s research [24], to ensure that the straight segments were considered 500 m. There was no vertical curve in the road.

### 4 Results and discussion

The effect of each geometric design feature on the speed in the horizontal curve was investigated by using box plot and one-way ANOVA (Analysis of variance).

**Table 4** Speed of different radius levels

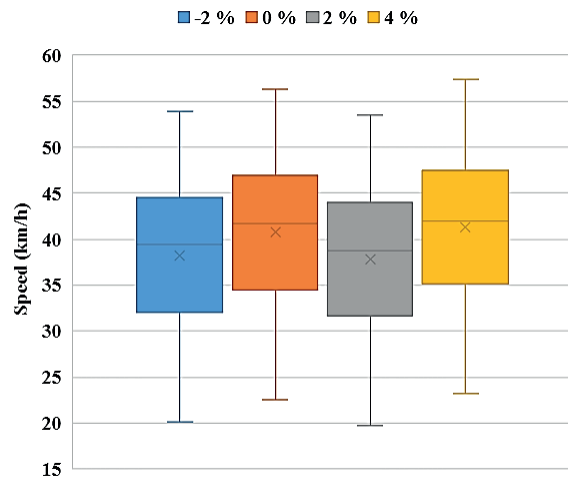
Radius (m)	Speed mean (km/h)	Standard Deviation	Confidence interval (95%)
20	26.93	4.146	(25.687, 28.172)
40	39.926	4.808	(38.684, 41.169)
60	42.942	4.256	(41.700, 44.184)
80	49.112	4.212	(47.870, 50.355)



**Figure 4** Boxplot of speed based on the radius

**Table 5** Speed of different superelevation levels

Superelevation (%)	Speed mean (km/h)	Standard Deviation	Confidence interval (95 %)
-2	38.25	9.09	(36.417,40.091)
0	40.70	9.14	(38.865,42.540)
2	37.83	9.14	(35.995,39.669)
4	41.35	9.24	(39.508,43.182)

**Figure 5** Boxplot of speed based on the superelevation

#### 4.1 Radius

Radius can be considered as the most important factor affecting the speed in the horizontal curve. Table 4 and Figure 4 show the speed data for each radius level. As can be seen, the speed has increased by increasing the radius, which is logical. Furthermore, it can be seen that the radius of less than 20 m has been critical for the drivers, and has had a significant effect on the speed. It is obvious from Figure 4. Also, it can be seen that by reducing the radius from 80 to 40 m, the speed mean has reduced by 9.84 km/h while the speed mean has reduced by 13 km/h by reducing the radius from 40 to 20 m.

#### 4.2 Superelevation

Table 5 and Figure 5 show the speed data for each superelevation level. Intuitively, there was no direct relationship between them and indicates an irregular pattern. It is discussed by using a regression model in next sections.

#### 4.3 Longitudinal grade

Increasing the longitudinal grade can affect the speed in two ways, on the one hand, it would increase the risk of the car fall that may lead to speed reduction. On the other hand, it would encourage the driver to

higher speed because of the car dynamics. In other words, increasing the longitudinal grade simultaneously can have positive and negative effects on the driver's safety and speed in the curve. Table 6 and Figure 6 demonstrate that the longitudinal grade has had a direct relationship with the speed. Due to the high similarity of speed data of the two levels of longitudinal grade of 0 % and -10 %, it can be concluded that the drivers have not been significantly sensitive to longitudinal grade less than -10 %.

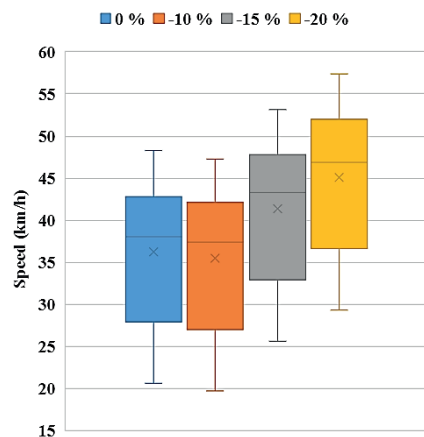
#### 4.4 Lane width

The lane width can influence the safety perceived by the driver, and the speed data for each lane width level have been depicted in Table 7 and Figure 7. It can be seen that the driving speeds recorded at different lane width levels were similar. It can be due to the features of routes and traffic. The drivers could use two lanes as the road was undivided with no traffic. AASHTO (American Association of State Highway and Transportation Officials) [34] mentions that standard lane width for highways is 3.65 m, while here the total width of the road was at least 4 m (excluding shoulders), so it can be said that the road width has been always too large to affect and limit the driver's speed. Therefore, its increase has not had a significant effect on the driver's speed.

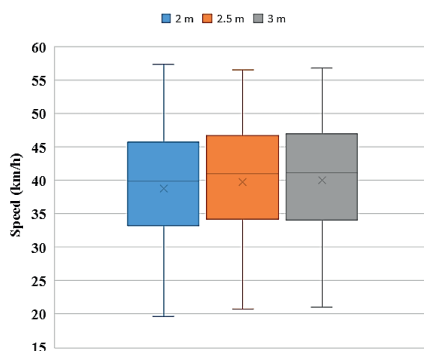
It is worth noting that if the road is undivided and

**Table 6** Speed of different longitudinal grade levels

longitudinal grade (%)	Speed mean (km/h)	Standard Deviation	Confidence interval (95%)
0	36.26	8.36	(34.58, 37.95)
-10	35.42	8.39	(33.74, 37.11)
-15	41.35	8.38	(39.66, 43.03)
-20	45.11	8.45	(43.42, 46.79)

**Figure 6** Boxplot of speed based on the longitudinal grade**Table 7** Speed of different lane width levels

Lane width (m)	Speed mean (km/h)	Standard Deviation	Confidence interval (95%)
2	38.85	9.31	(37.244, 40.461)
2.5	39.74	9.20	(38.128, 41.345)
3	40.01	9.25	(38.403, 41.619)

**Figure 7** Boxplot of speed based on the lane width

there is no traffic, then all lanes (even the opposite direction) can be used by the driver. In other words, the effect of the road width was examined by changing the lane width as the road width is equal to the sum of the lanes and shoulders. The road width is directly related to the lane width, and the road width was checked by the lane width.

#### 4.5 Shoulder width

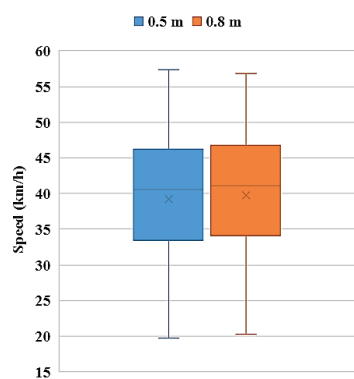
As the shoulder width increases, the car is less likely to deviate from the road and the driver has

more space to control the car, so the driver can achieve higher speeds in horizontal curves. Although a direct relationship is expected between the speed and the shoulder width, Table 8 and Figure 8 demonstrate that the speed difference between the shoulder widths was negligible in this study. As seen earlier, lane width had no significant effect on drivers' speed, so the shoulder width is not expected to be effective, since both of them determine the width of the road. So, when the lane width was sufficient (or even large), the driver would not use the shoulder width. It can be due to the specific experimental conditions of current study including absence of oncoming traffic, lack of guardrails along



**Table 8** Speed of different shoulder width levels

Lane width (m)	Speed mean (km/h)	Standard Deviation	Confidence interval (95%)
0.5	39.276	9.29	(37.963, 40.589)
0.8	39.791	9.214	(38.478, 41.103)

**Figure 8** Boxplot of speed based on the shoulder width**Table 9** ANOVA of geometric design features

Feature	P-value
Radius	0.000
Longitudinal grade	0.016
Superelevation	0.000
Lane width	0.579
Shoulder width	0.586

**Table 10** Comparison between different speed models

Model Num.	R-sqr (%)	RMSE	MAE
1	61.2	6.9	5.7
2	63.4	6.3	5.2
3	63.8	6.3	5.2
4	65.9	5.4	4.5

the edges, and the absence of lateral distractions in the peripheral vision.

#### 4.6 Statistical analysis of geometric design features

To examine the differences in experiment levels more accurately, ANOVA was used for each of the geometric factors (Table 9).

#### 4.7 Regression models

Four regression models were applied to simultaneously examine the effect of geometric design features, is given by:

$$\text{Model \#1: } V = \alpha * R + \beta * G + \gamma * e + \delta * LW + \theta * SHL + \text{Constant}$$

$$\text{Model \#2: } V = \alpha * \hat{R}^2 + \beta * G + \gamma * e + \delta * LW + \theta * SHL + \text{Constant}$$

$$\text{Model \#3: } V = \alpha * R + \beta * G^2 + \gamma * e + \delta * LW + \theta * SHL + \text{Constant}$$

$$\text{Model \#3: } V = \alpha * \hat{R}^2 + \beta * G^2 + \gamma * e + \delta * LW + \theta * SHL + \text{Constant}$$

$V$ : Speed (km/h),  $R$ : Radius (m),  $G$ : Longitudinal grade (%),  $e$ : Superelevation (%),  $LW$ : Lane width (m),  $SHL$ : Shoulder width (m),  $\alpha, \beta, \gamma, \delta, \theta$ : Coefficients.

In the first step of modelling, the shoulder width was found insignificant ( $p\text{-value} > 0.005$ ), so it was removed from the model. Three goodness of fit criteria MEA (mean absolute error), RMSE (root mean square error) and coefficient of determination (R-sqr), were used to compare regression models (Table 10).

It can be seen that model 4 has the best fit, so the coefficients of this model are analyzed (Equation 6).

$$V = 4.78 * \sqrt{R} - 0.02 * G^2 + 0.32 * e + 0.88 * LW + 15.01. \quad (6)$$

To show the order of importance of the variables, model with standardized coefficients was applied.

The greater the absolute value of the standardized coefficient of each variable, the greater the importance of that variable. The absolute standardized coefficient for radius, longitudinal grade, superelevation and lane width were 10.47, 4.46, 0.96 and 0.44, respectively. It shows that the radius was the most effective factor, followed by longitudinal grade. The other two factors have had very small effect on the speed.

The estimated model showed that shoulder width was not effective in determining the driver's speed. However, there are some researches by driving simulator that demonstrated the effect of shoulder width on the drivers' behavior [18-19]. Melo et al. examined shoulder width by driving simulator and real data, simultaneously. They found the shoulder width as one of the effective factors [20].

Ben-Bassat and Shinar found that the shoulder width had a significant effect on speed and lane position, but this effect was only evident when there was a guardrail [22]. Dixon et al. showed that the shoulder width was significant when the adjacent lane was 3.35 m wide, and had no effect on the 3.65 m lane width, indicating that the shoulder width was less important as lane width increased [30]. Their research can confirm the results of this paper. Here, although the width of one lane was less than 3.65 m, considering that the driver could use both lanes, the shoulder effect became meaningless.

Other factors, such as sight distance, can also affect the driver's speed in horizontal curves.

It is obvious that the sight distance is one of the important factors in determining the driver's speed. In this research, the presence of a mountain (continuously) has reduced the sight distance, so the effect of sight distance cannot be examined directly, and instead, other factors, such as the radius and the width of the lane and shoulder, have been studied. These factors can affect the sight distance.

In this research, very high or low values of geometric design criteria have been investigated because there are roads that must have an extreme and unusual geometric design due to environmental conditions. For example, we can refer to military roads and access roads to mines or residences in the mountains. These types of roads have very little traffic, but in critical conditions and also at sometimes, they have a lot of function, so it is necessary to study the speed of the cars in them. In other words, these types of roads are not normal because there are many limitations for their geometric design.

It should be mentioned that if female drivers were also checked, then the number and time of experiments would have to be doubled, which was not practical. It can be said about different age groups. So, this study has focused only on young male drivers, while women and other age groups should be examined as well.

## 5. Conclusions

Horizontal curves are one of the most important segments of the roads because crash rate is high and can also affect driving behavior. Therefore, it is important to study the effect of curve geometric design features on driving behavior such as speed selection. In this research, a driving simulator has been used to investigate the effect of five features of the geometric design of horizontal curves of an undivided two-lane mountain road, including: radius, longitudinal grade, superelevation, lane width and shoulder width. The experiments were determined using the Taguchi method. The results indicated that the radius was the most important factor affecting the speed, followed by the longitudinal grade. The two other features, lane width and superelevation, had very small effect. Shoulder width did not have a significant effect, which would be due to the large lane width, so drivers did not use the shoulder width to cross or maintain safety.

Regression demonstrated that the relationships between the speed and radius, longitudinal grade, superelevation and lane width were radical, quadratic, linear and linear, respectively. Although increasing the longitudinal grade can be dangerous, it has increased the speed of the drivers. Increasing the superelevation was effective when its value changed from negative to positive.

In this article, it has been tried to study the average speed in the curves. However, it is interesting to investigate other driving behaviors, such as lateral position or speed profile. Furthermore, it is better to investigate validity of the Taguchi method for human behavior such as speed. It suggests studying the effect of gender and age groups. This research helps managers and decision makers to estimate the ratio of improvement of geometric criteria to increase the speed of drivers and to choose the optimal point in terms of road construction cost. Also, the results of this research can be used in traffic safety by determining speed reduction in sharp curves.

## Acknowledgements

The authors received no financial support for the research, authorship and/or publication of this article.

## Conflicts of interest

The authors declare that they have no known competing financial interests or personal relationships that could have appeared to influence the work reported in this paper.

## References

- [1] CHOUDHARI, T., MAJI, A. Socio-demographic and experience factors affecting drivers' runoff risk along horizontal curves of two-lane rural highway. *Journal of Safety Research* [online]. 2019, **71**, p. 1-11. ISSN 0022-4375, eISSN 1879-1247. Available from: <https://doi.org/10.1016/j.jsr.2019.09.013>
- [2] CHARLTON, S. G. The role of attention in horizontal curves: a comparison of advance warning, delineation, and road marking treatments. *Accident Analysis and Prevention* [online]. 2007, **39**(5), p. 873-885. ISSN 0001-4575, eISSN 1879-2057. Available from: <https://doi.org/10.1016/j.aap.2006.12.007>
- [3] ZHU, L., LU, L., ZHANG, W., ZHAO, Y., SONG, M. Analysis of accident severity for curved roadways based on Bayesian networks. *Sustainability* [online]. 2019, **11**(8), 2223. eISSN 2071-1050. Available from: <https://doi.org/10.3390/su11082223>
- [4] SRINIVASAN, R., BAEK, J., CARTER, D. L., PERSAUD, B., LYON, C., ECCLES, K. A., GROSS, F. B., LEFLER, N. Safety evaluation of improved curve delineation. United States: Federal Highway Administration, 2009.
- [5] CALVI, A. A study on driving performance along horizontal curves of rural roads. *Journal of Transportation Safety and Security* [online]. 2015, **7**(3), p. 243-267. ISSN 1943-9962, eISSN 1943-9970. Available from: <https://doi.org/10.1080/19439962.2014.952468>
- [6] ANDJUS, V., MALETIN, M. Speeds of cars on horizontal curves. *Transportation Research Record* [online]. 1998, **1612**(1), p. 42-47. ISSN 0361-1981, eISSN 2169-4052. Available from: <https://doi.org/10.3141/1612-06>
- [7] DELL'ACQUA, G. Modeling driver behavior by using the speed environment for two-lane rural roads. *Transportation Research Record* [online]. 2015, **2472**(1), p. 83-90. ISSN 0361-1981, eISSN 2169-4052. Available from: <https://doi.org/10.3141/2472-10>
- [8] DHAHIR, B., HASSAN, Y. Modeling speed and comfort threshold on horizontal curves of rural two-lane highways using naturalistic driving data. *Journal of Transportation Engineering, Part A: Systems* [online]. 2019, **145**(6), 4019025. ISSN 2473-2907, eISSN 2473-2893. Available from: <https://doi.org/10.1061/JTEPBS.0000246>
- [9] MALAGHAN, V., PAWAR, D. S., DIA, H. Modeling operating speed using continuous speed profiles on two-lane rural highways in India. *Journal of Transportation Engineering, Part A: Systems* [online]. 2020, **146**(11), 4020124. ISSN 2473-2907, eISSN 2473-2893. Available from: <https://doi.org/10.1061/JTEPBS.0000447>
- [10] CASTRO, M., PARDILLO-MAYORA, J. M., JURADO, R. Development of a local operating speed model for consistency analysis integrating laser, GPS and GIS for measuring vehicles speed. *The Baltic Journal of Road and Bridge Engineering* [online]. 2013, **8**(4), p. 281-288. ISSN 1822-427X, eISSN 1822-4288. Available from: <https://doi.org/10.3846/bjrbe.2013.36>
- [11] PEREZ ZURIAGA, A. M., GARCIA GARCIA, A., CAMACHO-TORREGROSA, F. J., D'ATTOMA, P. Modeling operating speed and deceleration on two-lane rural roads with global positioning system data. *Transportation Research Record* [online]. 2010, **2171**, p. 11-20. ISSN 0361-1981, eISSN 2169-4052. Available from: <https://doi.org/10.3141/2171-0>
- [12] KANELLAIDIS, G., GOLIAS, J., EFSTATHIADIS, S. Drivers' speed behaviour on rural road curves. *Traffic Engineering and Control* [online]. 1990, **31**(7-8), pp. 414-415. ISSN 0041-0683. Available from:
- [13] ABBAS, S. K. S., ADNAN, M. A., ENDUT, I. R. Exploration of 85th percentile operating speed model on horizontal curve: a case study for two-lane rural highways. *Procedia - Social and Behavioral Sciences* [online]. 2011, **16**, p. 352-363. ISSN 1877-0428. Available from: <https://doi.org/10.1016/j.sbspro.2011.04.456>
- [14] MISAGHI, P., HASSAN, Y. Modeling operating speed and speed differential on two-lane rural roads. *Journal of Transportation Engineering* [online]. 2005, **131**(6), p. 408-418. ISSN 2473-2907, eISSN 2473-2893. Available from: [https://doi.org/10.1061/\(ASCE\)0733-947X\(2005\)131:6\(408\)](https://doi.org/10.1061/(ASCE)0733-947X(2005)131:6(408))
- [15] JACOB, A., ANJANEYULU, M. Operating speed of different classes of vehicles at horizontal curves on two-lane rural highways. *Journal of Transportation Engineering* [online]. 2013, **139**(3), p. 287-294. ISSN 2473-2907, eISSN 2473-2893. Available from: [https://doi.org/10.1061/\(ASCE\)TE.1943-5436.0000503](https://doi.org/10.1061/(ASCE)TE.1943-5436.0000503)
- [16] SEPORAITS, M., VOROBOVAS, V., VAITKUS, A. Evaluation of horizontal curve radius effect on driving speed in two lane rural road. Pilot study. *Baltic Journal of Road and Bridge Engineering* [online]. 2020, **15**(4), p. 252-270. ISSN 1822-427X, eISSN 1822-4288. Available from: <https://doi.org/10.7250/bjrbe.2020>
- [17] WANG, X., WANG, T., TARKO, A., TREMONT, P. J. The influence of combined alignments on lateral acceleration on mountainous freeways: a driving simulator study. *Accident Analysis and Prevention* [online]. 2015, **76**, p. 110-117. ISSN 0001-4575, eISSN 1879-2057. Available from: <https://doi.org/10.1016/j.aap.2015.01.003>
- [18] LIU, S., WANG, J., FU, T. Effects of lane width, lane position and edge shoulder width on driving behavior in underground urban expressways: a driving simulator study. *International Journal of Environmental Research and Public Health* [online]. 2016, **13**(10), 1010. eISSN 1660-4601. Available from: <https://doi.org/10.3390/ijerph13101010>

- [19] MECHERI, S., ROSEY, F., LOBJOIS, R. The effects of lane width, shoulder width, and road cross-sectional reallocation on drivers' behavioral adaptations. *Accident Analysis and Prevention* [online]. 2017, **104**, p. 65-73. ISSN 0001-4575, eISSN 1879-2057. Available from: <https://doi.org/10.1016/j.aap.2017.04.019>
- [20] MELO, P., LOBO, A., COUTO, A., RODRIGUES, C. M. Road cross-section width and free-flow speed on two-lane rural highways. *Transportation Research Record* [online]. 2012, **2301**(1), p. 28-35. ISSN 0361-1981, eISSN 2169-4052. Available from: <https://doi.org/10.3141/2301-04>
- [21] ROSEY, F., AUBERLET, J.-M., MOISAN, O., DUPRE, G. Impact of narrower lane width: comparison between fixed-base simulator and real data. *Transportation Research Record* [online]. 2009, **2138**(1), p. 112-119. ISSN 0361-1981, eISSN 2169-4052. Available from: <https://doi.org/10.3141/2138-15>
- [22] BEN-BASSAT, T., SHINAR, D. Effect of shoulder width, guardrail and roadway geometry on driver perception and behavior. *Accident Analysis and Prevention* [online]. 2011, **43**(6), p. 2142-2152. ISSN 0001-4575, eISSN 1879-2057. Available from: <https://doi.org/10.1016/j.aap.2011.06.004>
- [23] WANG, P., FANG, S., WANG, J. Impact of lane width of mountain highway on vehicle lateral position and speed. *Advances in Transportation Studies*. 2014, **32**, p. 51-64. ISSN 1824-5463.
- [24] WANG, X., GUO, Q., TARKO, A. P. Modeling speed profiles on mountainous freeways using high resolution data. *Transportation Research Part C: Emerging Technologies* [online]. 2020, **117**, 102679. ISSN 0968-090X, eISSN 1879-2359. Available from: <https://doi.org/10.1016/j.trc.2020.102679>
- [25] ZOLALI, M., MIRBAHA, B., LAYEGH, M., BEHNOOD, H. R. A behavioral model of drivers' mean speed influenced by weather conditions, road geometry, and driver characteristics using a driving simulator study. *Advances in Civil Engineering* [online]. 2021, **2021**, p. 1-18. ISSN 1687-8086, eISSN 1687-8094. Available from: <https://doi.org/10.1155/2021/5542905>
- [26] BOGGIO-MARZET, A., MONZON, A., RODRIGUEZ-ALLOZA, A. M., WANG, Y. Combined influence of traffic conditions, driving behavior, and type of road on fuel consumption. Real driving data from Madrid Area. *International Journal of Sustainable Transportation* [online]. 2022, **16**(4), p. 301-313. ISSN 1556-8318. Available from: <https://doi.org/10.1080/15568318.2020.1871128>
- [27] LLOPIS-CASTELLO, D., CAMACHO-TORREGROSA, F. J., GARCIA, A. Analysis of the influence of geometric design consistency on vehicle CO2 emissions. *Transportation Research Part D: Transport and Environment* [online]. 2019, **69**, p. 40-50. ISSN 1361-9209, eISSN 1879-2340. Available from: <https://doi.org/10.1016/j.trd.2019.01.029>
- [28] GUNAY, B., HINISLIOGLU, S. Traffic microsimulation scenario tests by the Taguchi method. *Proceedings of the Institution of Civil Engineers - Transport* [online]. 2011, **164**(1), p. 33-42. ISSN 0965-092X, eISSN 1751-7710. Available from: <https://doi.org/10.1680/tran.9.00029>
- [29] ARNOLD, M. L., VANHOUTEN, R. Increasing following headway in a driving simulator and transfer to real world driving. *Journal of Organizational Behavior Management* [online]. 2020, **40**(1-2), p. 63-81. Available from: <https://doi.org/10.1080/01608061.2020.1746475>
- [30] MAXWELL, H., WEAVER, B., GAGNON, S., MARSHALL, S., BEDARD, M. The validity of three new driving simulator scenarios: detecting differences in driving performance by difficulty and driver gender and age. *Human Factors* [online]. 2021, **63**(8), p. 1449-1464. ISSN 0018-7208, eISSN 1547-8181. Available from: <https://doi.org/10.1177/0018720820937520>
- [31] RAMEZANI KHANSARI, E., MOGHADAS NEJAD, F., MOOGHEHI, S. Comparing time to collision and time headway as safety criteria. *Pamukkale University Journal of Engineering Sciences*. 2021, **27**(6), p. 669-675. ISSN 1300-7009, eISSN 2147-5881.
- [32] RAMEZANI-KHANSARI, E., TABIBI, M., MOGHADAS NEJAD, F., MESBAH, M. Comparing the effect of age, gender, and desired speed on car-following behavior by using driving simulator. *Journal of Advanced Transportation* [online]. 2021, **2021**, 9922321. eISSN 2042-3195. Available from: <https://doi.org/10.1155/2021/9922321>
- [33] RAMEZANI-KHANSARI, E., TABIBI, M., MOGHADAS NEJAD, F. Validating driving simulator for car-following distance. *Iranian Journal of Science and Technology, Transactions of Civil Engineering* [online]. 2021, **45**(1), p. 281-290. ISSN 2228-6160, eISSN 2364-1843. Available from: <https://doi.org/10.1007/s40996-020-00576-6>
- [34] American Association of State Highway and Transportation Officials. A policy on geometric design of highways and streets. 6. ed. Washington, DC: American Association of State Highway and Transportation Officials, 2011. ISBN 978-1-56051-508-1.



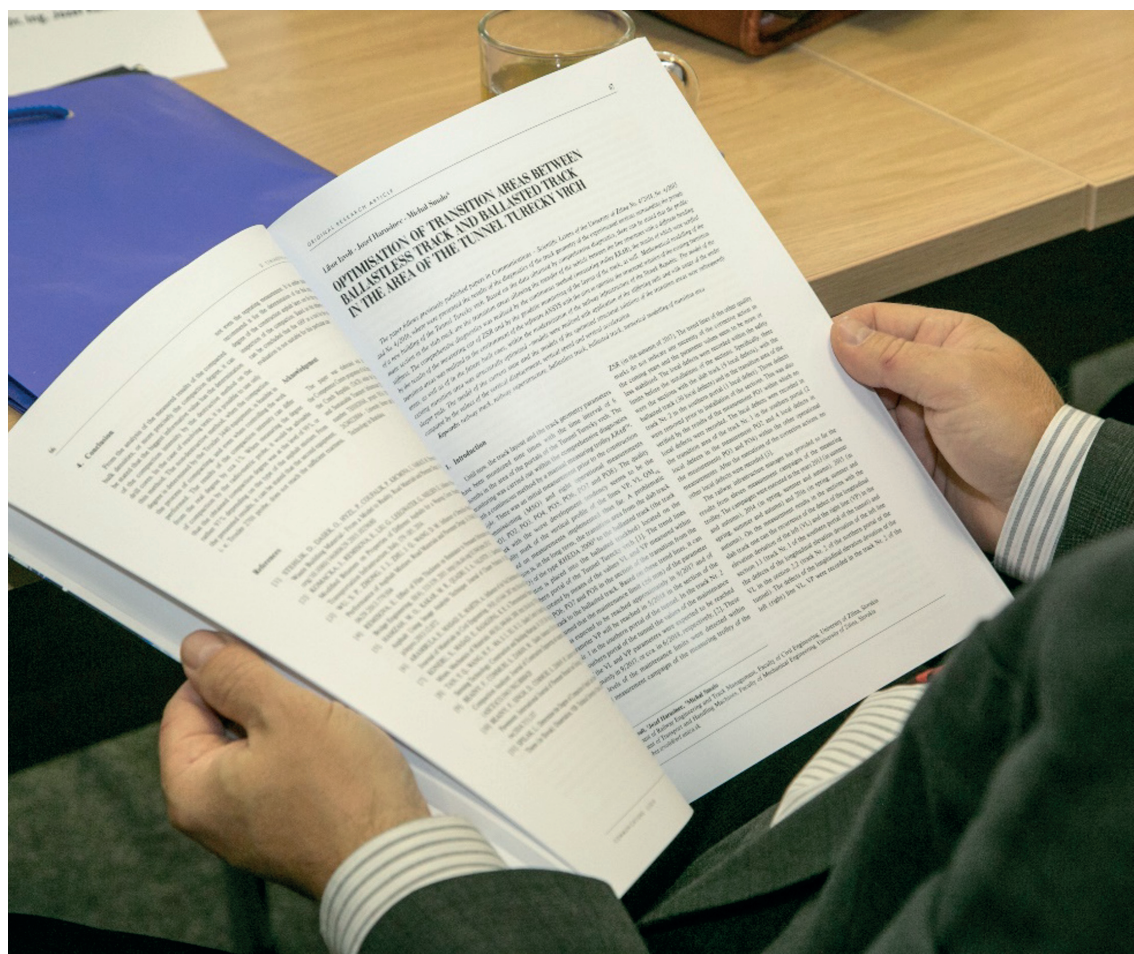


UNIVERSITY  
OF ŽILINA

In its over 70 years of successful existence, the University of Žilina (UNIZA) has become one of the top universities in Slovakia.

The journal *Komunikácie-vedecké listy Žilinskej univerzity v Žiline / Communications-Scientific Letters of the University of Žilina, Slovakia*, began publication in 1999 with the expectation that it would provide sufficient space for presentation of the latest scientific knowledge and trends in the field of transport, telecommunications, and information technology. The scientific scope of the journal was mainly focused on the issues of transport, telecommunications, structures, materials, technologies and new areas of the university development. As of September 2018, the journal has been profiled as a scientific journal focusing on the topic of transportation.

The journal *Communications-Scientific Letters of the University of Žilina* is now an established open access scientific journal focusing primarily on topics related to the field of transport. The main areas, related to transport, include Civil Engineering, Electrical Engineering, Management and Informatics, Mechanical Engineering, Operations and Economics, Safety and Security, Travel and Tourism Studies. Research in the field of education also falls under these categories.



UNIVERSITY OF ŽILINA  
Science & Research Department

Univerzitná 8215/1,  
010 26 Žilina,  
Slovakia

Ing. Janka Macurová  
tel.: +421 41 513 5143  
e-mail: janka.macurova@uniza.sk





This is an open access article distributed under the terms of the Creative Commons Attribution 4.0 International License (CC BY 4.0), which permits use, distribution, and reproduction in any medium, provided the original publication is properly cited. No use, distribution or reproduction is permitted which does not comply with these terms.

# IMPACT OF AI TECHNOLOGIES ON OPERATIONS OF SMALL AND MEDIUM TRANSPORT BUSINESSES

Vojislava Nićin<sup>1,\*</sup>, Slobodan Nićin<sup>2</sup>, Milovan Mirkov<sup>3,4</sup>

<sup>1</sup>The College of Vocational Studies for Management and Business Communication, Belgrade, Serbia

<sup>2</sup>The College of Academic Studies "DOSITEJ", Belgrade, Serbia

<sup>3</sup>ONB Veljko Petrovic, Zabalj, Serbia

<sup>4</sup>University Business Academy in Novi Sad, Novi Sad, Serbia

\*E-mail of corresponding author: nicin.vojislava@gmail.com

Vojislava Nićin 0000-0002-9984-2632,  
Milovan Mirkov 0009-0008-0568-5121

Slobodan Nićin 0009-0001-6579-5321,

## Resume

In this article, the authors present a study on artificial intelligence (AI) integration in transportation and storage SMEs, focusing on research questions, literature reviews, hypotheses, sample selection, and data analysis. They explored current AI support and perceptions and plans of SMEs in this sector. The authors addressed the lack of literature on AI use in transport SMEs and investigated factors, such as AI adoption, benefits perception, company size correlation, and investment willingness. Data was collected from 163 SMEs in Serbia and Slovakia, revealing challenges in participant identification due to low AI use. Declining AI adoption rates authors attributed to financial, technological, regulatory, and awareness issues. The research aims to enhance the AI adoption in transportation and storage SMEs and give some directions for future work.

## Article info

Received 16 April 2024

Accepted 6 June 2024

Online 27 June 2024

## Keywords:

artificial intelligence  
small and medium enterprises  
transportation  
storage  
logistics  
perception  
technology adoption

Available online: <https://doi.org/10.26552/com.C.2024.038>

ISSN 1335-4205 (print version)  
ISSN 2585-7878 (online version)

## 1 Introduction

The transport and logistics sectors face challenges like congestion, delays, and traffic accidents leading to time, cost, and environmental impacts, which affect economic sectors and overall growth. The AI innovations effectively address these challenges by leveraging generative artificial intelligence (AI) technology. Recent advancements include OpenAI's ChatGPT and GPT-4, Anthropic's generative AI, Claude, and Google's new AI-driven features, [1]. The AI plays a crucial role in combinatorial optimization for transport and logistics problems, solving various issues such as vehicle routing and warehousing location. The AI applications, as seen in Drydak's research [2], are predominantly used in recruitment (~ 14 %), customer communication (28 %), and online targeting (30.54%). The number of applications used per company is 1.6, while 52.72 % of SMEs do not use a single AI application. Despite

the small businesses (SMEs)<sup>1</sup> lagging in AI adoption [3], the accessibility of AI suggests a potential narrowing of this gap in the future, offering automation, improved customer experiences, and support for business growth.

The AI in small businesses automates tasks, enhances customer experience, and supports growth. For instance, platforms like ChatGPT aid in customer service, marketing, and sales [4]:

- *Customer Experience:* Chatbots improve service by mimicking human conversations, reducing wait times, and offering personalized support, fostering loyalty.
- *Marketing:* AI enables personalized campaigns, recommendations, and targeted offers across various platforms. As AI advances, investing in AI-powered marketing solutions offers a competitive edge.
- *Content Creation:* As in large businesses, in SMEs, AI assists in generating content, analyzing

<sup>1</sup> There is no single definition for SMEs [22], and we used the European SME definition in our work [32].

preferences, and maintaining quality and brand alignment.

The AI is a crucial technological component that enhances existing productivity methods in Industry 4.0, without replacing them [5]. It empowers companies, enabling smart task performance, strategic decision-making support for managers, and real-time remote operations management. Notably, sectors such as transportation, logistics, automotive, and technology are early adopters of AI, as evidenced in the literature [6].

While many associate AI with autonomous vehicles, its application extends deeper into the transportation processes and logistics chains. The integration of AI has revolutionized decision-making in transport and logistics, leading to improved efficiency, safety, and sustainability. Key impacts include predictive analytics for demand forecasting, optimized route planning, enhanced freight security, real-time tracking, and intelligent inventory management [7]. The MHI/Deloitte research indicates that only 12 % of businesses currently utilize AI in warehouses, highlighting opportunities for further adoption and growth.

Transportation SMEs can leverage AI differently, including services and low-tech solutions, to enhance their operations and participation in supply chains [8]. The AI-powered tools optimize efficiency in autonomous vehicles and ride-sharing services, improving traffic forecasting and route optimization through sensor networks. Transport and logistics SMEs specifically benefit from transforming practices, reducing accidents, and savings in maintenance, insurance, and fuel consumption [9].

However, the SMEs exhibit slower adoption rates of data analytics compared to larger enterprises, as evidenced by OECD data, indicating that big data analysis was conducted by 34.1 % of large firms, 18.8 % of medium-sized enterprises, and only 10.6 % of small enterprises in OECD countries in 2018. A significant gap in data analytics adoption between the large and small businesses is especially evident in countries like Belgium, Denmark, the Netherlands, and Slovenia, where large corporations position themselves as late majority adopters [8].

The business environment impact of AI on SMEs is profound due to their reliance on business ecosystems and resource allocation strategies. The SMEs dedicate more resources to administrative tasks and trade smaller volumes to manage fixed costs, making them susceptible to framework constraints, market deficiencies, and economic instabilities. Limited infrastructure hampers their market access and availability of critical resources, hindering their ability to secure funding, skilled workforce, and innovation support. Public policies and governance play a pivotal role in influencing the SME performance outcomes [8].

The AI, such as Generative Pre-trained Transformers (GPT), can have a profound impact on several facets of the SME business landscape. These include:

- *Public administration*: The integration of AI and automation boosts efficiency, streamlines tasks for civil servants, and enhances the comprehension of user requirements. Policymakers can leverage machine learning techniques for improved decision-making [10].
- *Tax compliance*: The adoption of AI empowers tax authorities to combat tax evasion and implement a proactive “tax compliance by design” strategy tailored for SMEs [11].
- *Courts*: AI-driven efficiencies in case analysis, law enforcement processes, and dispute resolution mechanisms can reduce the resources SMEs allocate to resolving commercial conflicts [12].
- *Market competition*: Given the significance of market competitiveness for SMEs, algorithms wield influence over market dynamics, potentially fostering tacit collusion practices and sustaining profits beyond equitable competitive levels [13].
- *Infrastructure*: While the AI fortifies digital security measures for information and communication technology (ICT), transportation, and energy infrastructure, it introduces vulnerabilities to cyber-attacks, as well.
- *Access to finance*: AI tools enhance credit assessment procedures, mitigate default risks, and streamline SMEs’ access to credit facilities, even catering to those lacking established credit histories [14].
- *Labor markets*: The advent of AI and “people analytics” will reshape recruitment, termination practices, occupational health guidelines, data privacy protocols, performance evaluations, and skills alignment processes within SMEs [15].
- *Knowledge and innovation access*: The AI automation accelerates scientific breakthroughs, curtails experimentation costs, and bolsters data-sharing practices and reproducibility standards within the realm of SME operations [8].

## 2 Background to the study

Artificial intelligence is currently a highly relevant topic, with experts examining it from diverse angles, ranging from technology to practical application, encompassing security and societal implications.

Sustainable practices play a pivotal role in defining the growth within the AI transportation market. Emphasizing environmental stewardship, societal impact, and ethical governance has emerged as critical benchmarks for success in this dynamic market space, fostering innovation, collaboration, global engagement, and sustainability to propel progressive advancement [16].

The TNO/TKI [17] position paper (from 2020) underscores the three key dimensions of implementing artificial intelligence within the transportation and logistics sectors:

**Table 1** SMEs and transportation and storage businesses having performed big data analysis and using AI in 2023 [21]

Activity →	Big data analysis			Application of artificial intelligence		
Indicator →	Small and Medium Businesses having performed big data analysis (%)		Transportation and storage companies performing big data analysis (%)	Small and medium businesses using artificial intelligence (%)		Transportation and storage companies using artificial intelligence (%)
Breakdowns→	Small - 10 to 49 employees	Medium - 50 to 249 employees		Small - 10 to 49 employees	Medium - 50 to 249 employees	
↓Country						
Denmark	44.09	69.28	43.80	12.37	22.56	15.16
Hungary	51.11	62.58	52.14	2.98	5.54	2.23
Slovak Republic	25.16	44.27	25.18	5.95	8.57	3.32
Croatia	47.67	69.84	59.20	6.98	11.17	7.58
Romania	19.10	30.99	26.45	1.07	2.38	0.36
Average	28.55	48.34	28.17	6.42	12.96	6.03
Median	29.83	50.38	25.81	5.77	11.17	5.61

Data extracted on 17 Feb 2024 from OECD.Stat [21]

1. *Sense*: Building a data fusion-based worldview to interpret the environment poses challenges in system communication and interaction with external entities during the development of AI systems.
2. *Think*: Analyzing the world model with AI systems to forecast the future scenarios and outcomes entails complexities, particularly in intricate mobility and logistics scenarios. For instance, in predicting the traffic congestion, leveraging real-time roadwork status, traffic flow data, radar imagery, and historical information could prove beneficial.
3. *Act*: Recognizing potential actions, envisioning outcomes, and delivering decision-making guidance autonomously or under human oversight. The current constraints of fully autonomous decision-making AI systems encounter uncertainties.

The SMEs are progressively integrating AI into their operations, utilizing it for enhancements across multiple functions, such as automating customer service, extracting data insights, and facilitating decision-making. Despite facing challenges like cost implications and skill gaps, the availability of user-friendly AI tools is fueling increased adoption rates. Successful SMEs are positioning themselves for expansion and competitiveness in today’s technology-driven realm. In the domain of logistics and supply chain management, AI systems streamline route optimization, monitor shipments, oversee inventory, and predict demand, leading to cost efficiencies and heightened delivery effectiveness [18].

According to Eurostat [19], SMEs account for 99.8 % of European non-financial companies, illustrating their significant presence in the economy. Therefore, the economic growth of any country hinges on development of SMEs and their adoption of technology. While the AI presents a competitive advantage for SMEs, there exists a lack of acceptance and understanding. Simplifying the utilization of AI, quantifying its benefits, and

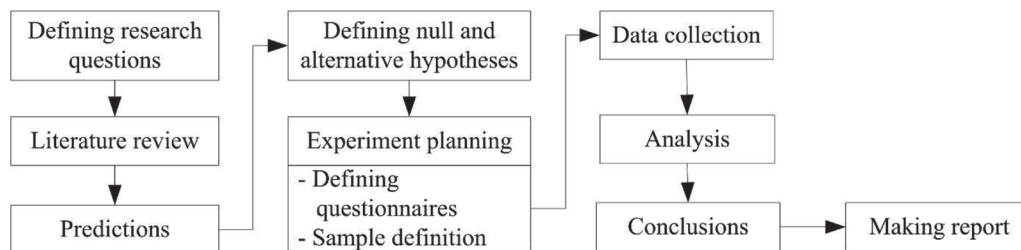
elucidating the potential time and cost savings can aid SMEs in effectively embracing AI to enhance operational efficiency and effectiveness [20].

A considerable portion of SMEs operate in the transport and logistics sector, with a particular focus on last-mile delivery. Despite its criticality, the SMEs in this sector are often overlooked. Hence, exploring the applications of AI in transport SMEs becomes an imperative.

The analysis of big data forms a pivotal aspect of artificial intelligence, enabling machines to derive insights from vast volumes of data and identify patterns and trends. Table 1 displays the percentages of SME companies, as well as companies involved in transportation and storage, in 2023 that engaged in big data analysis. The data indicates that, across fifteen countries, the reported values for transport and storage companies are slightly higher than those for small companies, but notably lower than those for medium-sized enterprises. The average value for transport companies in the analyzed countries closely aligns with that of small companies, with a similar pattern observed for the median values. Medium-sized companies exhibit a more advanced standing in both categories.

The implementation of artificial intelligence in transport and storage companies lags behind big data analysis. The adoption of AI within the industry across just ten countries exceeds that of small businesses. Furthermore, the average and median rates of AI adoption are significantly lower (4.7 and 4.6 times less, respectively). This disparity stems from the timing of widespread artificial intelligence deployment. Additionally, various factors influence AI adoption among SMEs, including cost and resource limitations, skill gaps, data quality and availability issues, change management challenges, integration hurdles with existing systems, ethical and privacy concerns, scalability issues, and a lack of awareness.

To tackle these obstacles, SMEs are embracing



**Figure 1** Methodological approach to the creation of the paper

proactive and strategic approaches, such as meticulous budgeting, exploring cost-effective solutions, engaging in pilot projects, seeking expert guidance, collaborating with industry associations, and drawing insights from successful AI implementations in other SMEs. Those who can navigate these challenges ahead of the curve will stand at a significant competitive advantage.

### 3 Research methodology and sample

This research was motivated by a keen interest in exploring the impact of artificial intelligence on the operational dynamics of small and medium-sized enterprises (SMEs) operating within the realm of transportation and supply chain management. The methodological framework employed in this study is outlined in Figure 1.

One of the inherent challenges in investigating social phenomena lies in the absence of controlled laboratory settings. Consequently, researchers often resort to statistical analysis to mitigate this limitation, striving to minimize extraneous variables that could potentially confound their results. Despite the thorough preparations, unforeseen factors may still influence the outcomes, accentuating the importance of cautious interpretation and generalization of findings to ensure reliability. Therefore, a prudent approach involves beginning with the study of simpler phenomena before delving into more complex subjects, recognizing distinct patterns within each research phase and methodological strategy [22].

This study delves into how the integration of artificial intelligence impacts the performance and sustainability of SMEs at the microeconomic level. An empirical approach was adopted in this research, as a synthesis of theoretical and empirical insights is imperative for generating meaningful and relevant data. Categorized under the integral research group, this investigation encompasses logical, epistemological, technical, and scientific-strategic components reflective of the scientific method. Primarily exploratory, this research also comprises elements of explanatory and descriptive analyses, shedding light on the “what,” “why,” “how much,” and “how” aspects underpinning the integration of AI in SME operations.

#### 3.1 Defining research questions, reviewing literature, and setting scientific hypotheses

##### *Research Question*

The study delves into the multidisciplinary nature of transport SMEs and their varied activities. Current AI implementations in this sector reflect a diverse range of applications, with no singular dominant technology in use among SMEs. In 2021, only a small percentage, around 1 to 2%, of transportation and storage companies have integrated artificial intelligence, with a focus on areas such as ICT security (28%), logistics (24%), and operational efficiency [3].

The convergence of artificial intelligence and management in small and medium-sized enterprises operating within logistics chains was investigated in this study. Specifically, investigated were the managerial functions and evaluated how the AI can potentially enhance the SME operations and outcomes.

Objective of this study was to address the following questions:

RQ<sub>1</sub>. To what extent does AI currently support transport and storage SMEs?

RQ<sub>2</sub>. What are the perceptions of transport and storage SMEs regarding AI applications, and what are their plans for the future AI implementation?

##### *Literature review*

In 2021, 293.48 thousand papers about AI were published in journals, and 85.09 thousand at conferences. The number of AI repository publications was 65,210 [23, p. 32, 36, 40]. To address the research question, we selected key terms (such as Artificial Intelligence, SMEs, Transport\*, and Management) and conducted a thorough review of the available literature from the WoS database, Scopus Source List (1-4 quartile), the EBSCO database, and the OECD iLibrary. Additionally, we utilized official reports and statistics from reputable organizations and leading institutions available online when appropriate. Most of our sources were of open-access type.

For the keywords “Artificial Intelligence + SME\*,” the Clarivate Master Journal List (MJL) offered 286 academic journals (103 with open access). For “Artificial Intelligence + Transport\*,” MJL provided access to 426 academic journals (163 with open access), and for “SME\* + Transport,” 150 academic journals are available on



MJL (65 with open access), [24].

Of the academic journals from the Scopus list that dealt with artificial intelligence, less than 4% simultaneously dealt with management, and less than 1 % dealt with logistics and transportation [25].

For the keywords AI + SMEs, the EBSCO database offered 115 peer-reviewed journals with 117 papers. Only one paper included the “logistics and supply chain management” criterion, and another corresponded to the third keyword, “Transport\*.” From such a modest result, we concluded that the application of AI in SMEs dealing with transport services, for now, is insufficiently researched.

Based on the analysis, we also concluded that very few academic journals deal with the problems of applying artificial intelligence to the needs of transport and SMEs. As a result, the number of published works in this area is small, and this work should contribute to improving the understanding of the potential impact of artificial intelligence on SMEs.

### Hypotheses

In setting hypotheses, how a hypothesis is formulated is crucial. When drawing statistical conclusions, it is expedient to start with the null hypothesis ( $H_0$ ), which essentially serves as a general statement or default position positing no association between two measured phenomena or no differences between the observed groups [26].

Based on the research question, study area, studied literature, defined variables, limit values, and our expectations, we have set the null hypotheses. To answer the first research question, we set null hypotheses  $H_{0,1}$  and  $H_{0,2}$ .

$H_{0,1}$ : Transportation and storage SMEs have not widely adopted the implementation of artificial intelligence in their operations.

$H_{0,2}$ : There is no strong correlation between the size of transportation and storage SMEs and the adoption level of artificial intelligence implementation in business operations.

To answer the second research question, we set the null hypotheses  $H_{0,3}$  to  $H_{0,5}$ .

$H_{0,3}$ : Transportation and storage SMEs are hesitant to adopt artificial intelligence in their operations, as they doubt its potential benefits.

$H_{0,4}$ : There is no strong correlation between a company having a defined strategy for integrating artificial intelligence into business processes and utilizing some form of artificial intelligence in its operations.

$H_{0,5}$ : Transportation and storage SMEs are reluctant to invest in the application of artificial intelligence.

We also set the alternative hypotheses:

$H_{A,1}$ : Transportation and storage SMEs have widely adopted the implementation of artificial intelligence in their operations.

$H_{A,2}$ : There is a strong correlation between the size of transportation and storage SMEs and the adoption

level of artificial intelligence implementation in business operations.

$H_{A,3}$ : Transportation and storage SMEs are willing to adopt artificial intelligence in their operations, as they believe it will bring benefits.

$H_{A,4}$ : There is a strong correlation between a company having a defined strategy for integrating artificial intelligence into business processes and utilizing some form of artificial intelligence in its operations.

$H_{A,5}$ : Transportation and storage SMEs enthusiastically invest in artificial intelligence.

### 3.2 Defining the sample and the questionnaire and data processing

#### Sample

We interviewed a balanced number of respondents from all the SME categories in the transportation and storage sector without differentiation based on their primary focus, as their shared sectoral similarities and activities justified this approach. We conducted the study in Serbia and Slovakia, with 210 SMEs surveyed. Of these, 163 SMEs responded to the survey, including 47 medium-sized enterprises, 54 small enterprises, and 62 micro-enterprises. Challenges we faced in identifying suitable survey participants due to low levels of artificial intelligence utilization. For instance, in Serbia in 2021, only 1.1 % of companies used AI, with the transportation and storage sector representing 6 % of this figure [3]. In 2023, Slovakia reported a 3.3 % utilization rate of AI technologies [27]. Unexpectedly, there was a decline in AI adoption rates in 2023 compared to 2021, with Denmark experiencing a decrease from 21.3 % to 15.2 % and Slovenia from 12.5 % to 7.5 %. Factors contributing to this decline include financial constraints, technological challenges, regulatory issues, and the impact of the pandemic. One significant factor was the lack of awareness regarding the benefits of artificial intelligence. However, the introduction of ChatGPT and other technologies has sparked increased interest in AI. By 2024, there was a noticeable improvement in AI adoption, although official data for 2024 is pending. In Slovakia, the utilization rate of AI among transportation and storage companies stood at 3.32 %.

#### Questionnaire

For the experiment, we developed a structured questionnaire with 26 questions and 16 sub-questions. It included predefined answer options and open-ended questions to ensure unbiased feedback from diverse SMEs and avoid unintentional bias. The questionnaire was designed to collect company information, digitization level, AI relationship, past experiences, elements used, plans, and investment size. The target group included owners (6.75 %), directors (3.07 %), PR (11.04 %), and other high-ranking employees (49.08 %), with one respondent per company. A total of 49 (30.06 %) respondents were included.



of the surveyed did not give data about who filled the questionnaire out. Potential risks include respondent comprehension and availability of information, as well as variations based on the specific nature of each SME. Despite the individual variances, the sample size aimed to provide a general overview.

### **Data processing**

The survey data have been organized in an Excel spreadsheet and can be requested via e-mail from interested parties. Statistical analysis of the experimental data was conducted using the Excel ANOVA tool.

### **3.3 Analysis of results with discussion**

We grouped the analysis results into two categories: literature review findings and experimental research results. Within the experimental research category, we further divided the data into two subgroups based on research questions RQ<sub>1</sub> and RQ<sub>2</sub>. Statistical methods were then applied to test and determine the rejection of null hypotheses using predefined limits.

### **3.4 Defining conclusions**

The study's conclusions were derived from the analysis and interpretation of collected data and research findings, following these key steps:

1. Review relevant results to identify trends, patterns, and deviations.
2. Interpret results within the research question framework, linking them to existing theories.
3. Discuss implications, emphasizing research significance, practical applications, theoretical contributions, and future research directions.
4. Confirm or reject hypotheses based on results, guiding subsequent research efforts.
5. Formulate conclusions summarizing main findings, addressing research questions, and providing guidance for future studies.

## **4 Results and discussion**

### **4.1 Benchmarking criteria for successful implementation of AI in SMEs**

The application of artificial intelligence in logistics, transportation, and other industries is still in its early stages. To assess the success of AI implementation in SMEs engaged in transportation and storage, the following criteria can be used:

- Companies using at least one AI application rank among the top 8 % of companies in the EU in terms of AI implementation success.

- Companies in the transportation and storage sector using AI applications place among the top 0.48 % in successful AI implementation.
- Companies employing AI for autonomous decision-making in machine movement rank among the top 1 % of most automated companies in the EU.
- Companies utilizing AI software/systems in logistics are among the top 10 % of advanced companies.

### **4.2 Literature review findings**

The AI technology and machine learning can support small and medium-sized enterprises by enhancing their data comprehension and automating intricate and routine tasks [28].

A recent McKinsey Global Survey indicates a growing adoption and significant benefits from AI. As businesses increasingly utilize AI, tools and best practices are more refined. Companies experiencing the highest AI-driven earnings boost employ a core and advanced practices combination, including machine-learning operations, allocate the AI spending more effectively, leverage cloud technologies, and actively address the AI-related risks (a shortfall in many AI strategies). Most companies prioritize data science and make significant investments in it. This study shows an increase in the adoption of artificial intelligence across various functions, rising from 50 % in 2020 to 56 % in 2021. Additionally, 27 % of respondents reported that at least 5 % of earnings were driven by AI applications, up from 22 % in the previous year [29].

McKinsey's latest survey from 2023 affirms the rapid growth of generative artificial intelligence (gen AI) tools. In less than a year since their introduction, a third of respondents report regular gen AI use in business functions. The AI has transitioned from a tech-focused topic to a leadership priority, with C-suite executives and boards increasingly leveraging gen AI. As advances in gen AI drive investment, 40 % of organizations plan to boost their overall AI funding. However, managing gen AI risks is still in its early stages. Less than half of respondents indicated sufficient mitigation efforts within their organizations. Even the risk they consider the most relevant: inaccuracy [30]. The survey results demonstrate widespread business adoption and personal use of gen AI across regions, industries, and job levels. A total of 79 % of respondents have interacted with genetic artificial intelligence, with 22 % regularly incorporating it into their professional tasks. One-third of respondents, representing 60 % of organizations with AI adoption, regularly employ generative AI in a business function. Additionally, 40 % of AI adopters expect increased overall investments into generative AI, and 28 % have board discussions on its implementation. Common functions for these tools align with broader AI usage, including marketing, sales, product development, and service operations. This focus on high-value areas

reflects the potential for significant annual value from generative AI. The share of reported gen AI uses in companies participating in supply chain management was only 3 %. The situation is better with service operations (10 %), product and service development (13 %), and marketing and sales (14 %) [30].

There is a high optimism about the impact of gen AI. Three-quarters of respondents anticipated significant competitive changes in the next three years, particularly in the tech and financial sectors. The level of impact is projected to vary across industries, with knowledge-intensive sectors likely to experience greater disruption and value creation. Tech firms are poised to benefit the most, potentially increasing global revenue by up to 9%, followed by knowledge-driven industries (up to 5 %) and education (up to 4 %). Conversely, manufacturing sectors, like aerospace, automotive, and advanced electronics may see more modest effects, compared to past technological shifts focused on production improvement [1, p. 3].

The generative AI is revolutionizing work structures by automating tasks that currently absorb 60 to 70 % of employees' time. With the advancements in natural language understanding, the generative AI can now streamline activities that involve speech comprehension, accounting for 25 % of work time. Industries requiring higher education levels will experience a more significant impact as automation potential increases. The workforce transition will intensify over time, with predictions suggesting that up to half of all work activities could be automated between 2030 and 2060 [1, p. 3].

However, the SMEs have encountered challenges in the AI project preparation and implementation. Oldemeyer, Jede, and Tauteberg [31] identified lack of knowledge, costs, and inadequate infrastructure as the most common barriers to implementation, emphasizing social, economic, and technological aspects.

#### 4.3 Research according to the null hypothesis $H_{0,1}$

As a criterion for the reference level of implementation of artificial intelligence, a limit of 8 % was adopted, which corresponds to the EU average for

SMEs [3]. Out of 163 surveyed SMEs, 17 of them (10.4 %) use some artificial intelligence applications. The reason for this result may lie in the current mass availability of ChatGPT to which business individuals turn for help and advice on matters related to the company's current operations. The situation would be different when looking at strictly dedicated AI applications. However, the use of AI is even more intense considering that many business software applications are powered by artificial intelligence (e.g. MS Office, Grammarly, Google Translate, etc.). In that case, 130 respondents (79.8%) declared that they use artificial intelligence. The obtained results provide sufficient evidence to reject the null hypothesis  $H_{0,1}$  that "transportation and storage SMEs have not widely adopted the implementation of artificial intelligence in their operations."

#### 4.4 Research according to the null hypothesis $H_{0,2}$

There is no clear definition of the readiness of an enterprise to accept or not to accept the implementation of AI. To be able to gain insight into the company's readiness to accept AI, we created a coefficient ( $K_{AI}$ ) that included three significant elements:

- Use of decision support tools ( $\xi_D$ )
- Having a strategy for applying AI ( $\xi_S$ )
- Use of artificial intelligence (at least one AI application) ( $\xi_A$ ).
- Given that these criteria have different weights, we weighted them and created an expression:

$$K_{AI} = 0.4 \xi_D + 0.2 \xi_S + 0.4 \xi_A. \quad (1)$$

Table 2 shows the results obtained by analyzing the entire sample to determine the correlation between the company size and AI adoption coefficient.

In the observed sample, 116 companies have  $K_{AI}$  equal to 0, which significantly affects the obtained results. One company did not provide enough data to create the  $K_{AI}$  coefficient. The analysis of the sample where the  $K_{AI}$  is greater than zero (46 cases) gave the results shown in Table 3.

In this case, the obtained P-value was close to zero,

**Table 2** Results of the regression analysis of the company size and  $K_{AI}$  coefficient correlation

ANOVA						
	df	SS	MS	F	Significance F	
Regression	1	0.402505	0.402505	13.43214	0.000335	
Residual	161	4.824489	0.029966			
Total	162	5.226994				

	Coefficients	Standard Error	t Stat	P-value	Lower 95%	Upper 95%
Intercept	0.056884	0.017206	3.306131	0.001166	0.022906	0.090863
X Variable 1	0.0007	0.000191	3.664989	0.000335	0.000323	0.001077

**Table 3** Results of the regression analysis of the company size and  $K_{AI}$  coefficient correlation for cases when  $K_{AI} > 0$ 

ANOVA						
	df	SS	MS	F	Significance F	
Regression	1	0.115485	0.115485	3.866825	0.055577	
Residual	44	1.314081	0.029865			
Total	45	1.429565				
	Coefficients	Standard Error	t Stat	P-value	Lower 95%	Upper 95%
Intercept	0.289347	0.035919	8.05546	3.36E-10	0.216956	0.361737
X Variable 1	0.000619	0.000315	1.966424	0.055577	-1.5E-05	0.001254

**Table 4** Results of the regression analysis of the correlation between SME size and lack of knowledge or resources for artificial intelligence applications.

ANOVA						
	df	SS	MS	F	Significance F	
Regression	1	0.138566	0.13856613	0.626164	0.42993	
Residual	161	35.62831	0.22129382			
Total	162	35.76687				
	Coefficients	Standard Error	t Stat	P-value	Lower 95%	Upper 95%
Intercept	0.6520689	0.046757	13.9459409	1.72E-29	0.559733	0.744405
X Variable 1	0.0004107	0.000519	0.79130499	0.42993	-0.00061	0.001436

as well, which means that for this sample there is no linear correlation between the size of the company and the coefficient of acceptance of AI and that there is no basis for rejecting the null hypothesis  $H_{0,2}$  that “*there is no strong correlation between the size of a transportation and storage SMEs and the adoption level of artificial intelligence implementation in business operations.*”

#### 4.5 Research according to the null hypothesis $H_{0,3}$

The value of 66.6 % supports the application of artificial intelligence we adopted as a reference criterion. We believe that a two-thirds majority would strongly separate belief and disbelief in AI applications. Out of 162 answers, 133 SMEs (82.1 %) believed that the use of AI would be beneficial for the company's work. This means that companies would like to use AI, and why they do not use it yet, the reasons we sought in the lack of IT experts (in 71 out of 162 surveyed companies, or 43.8 %), lack of AI experts (in 146 out of 162, or 90.1 %), and lack of funds (in 146 out of 162, or 90.1 %).

For a deeper analysis, we analyzed the impact of SME size on the use of AI in SMEs. We started with the hypothesis that the lack of knowledge or resources is not correlated with the size of the SME. Regression analysis of the survey data gave the results shown in Table 4.

The P-value of 0.4299 indicates a high probability that the relationship between the number of employees

in SMEs and the lack of knowledge or resources for artificial intelligence is random. Therefore, there are no grounds for rejecting the hypothesis that the lack of knowledge or resources is independent of the SME size.

In addition, 113 companies (69.8 %) expressed readiness for outsourcing in the implementation of AI. The survey showed that the vast majority consider the application of AI to be useful, which created the conditions to reject the null hypothesis  $H_{0,3}$  that “*transportation and storage SMEs are hesitant to adopt artificial intelligence in their operations, as they doubt its potential benefits*” at the expense of the alternative hypothesis  $H_{A,3}$ .

#### 4.6 Research according to the null hypothesis $H_{0,4}$

Within the sample of 162 SMEs, 27 of them had a strategy for application of AI, and 17 used at least one AI application in practice. Based on the results of the analysis, the findings presented in Table 5 were obtained.

A P-value of 0.957 indicates a very strong correlation between these two values. However, due to the existence of many businesses that neither have a strategy nor use AI, the P-value is exaggerated. If we exclude those companies from the analysis and look only at companies that have at least one element, 42 SMEs remain for

**Table 5** Results of the regression analysis of the correlation between a having strategy and using AI applications.

ANOVA						
	df	SS	MS	F	Significance F	
Regression	1	0.000274	0.000274	0.0029	0.957119	
Residual	161	15.22672	0.094576			
Total	162	15.22699				
	Coefficients	Standard Error	t Stat	P-value	Lower 95%	Upper 95%
Intercept	0.103704	0.026468	3.918058	0.000132	0.051434	0.155973
X Variable 1	0.003439	0.063861	0.053853	0.957119	-0.12267	0.129553

**Table 6** Results of the regression analysis of the correlation between a having strategy and using AI applications when an SME has at least one of the parameters not equal to zero.

ANOVA						
	df	SS	MS	F	Significance F	
Regression	1	7.440476	7.440476	111.1111	4.14E-13	
Residual	40	2.678571	0.066964			
Total	41	10.11905				
	Coefficients	Standard Error	t Stat	P-value	Lower 95%	Upper 95%
Intercept	1	0.06916	14.45914	1.77E-17	0.860222	1.139778
X Variable 1	-0.89286	0.084704	-10.5409	4.14E-13	-1.06405	-0.72166

analysis. In this case, the statistical analysis gave the results shown in Table 6.

The obtained results show that the P-value is very close to zero, indicating no linear correlation (higher-order correlation not excluded). The number of companies with an AI deployment strategy is significantly higher than those using AI. Furthermore, 14 companies using AI have no strategy. From this, we can infer that SMEs need to put considerable effort into translating their strategies into practice and that AI deployment is currently more responsive to immediate needs and opportunities rather than pre-planned strategies.

Based on the results, we can conclude that the analysis of this reduced sample does not provide sufficient evidence to reject the null hypothesis  $H_{0,4}$  that ‘there is no strong correlation between a company having a defined strategy for integrating artificial intelligence into business processes and utilizing some form of artificial intelligence in its operations.’

#### 4.7 Research according to the null hypothesis $H_{0,5}$

To assess the readiness of SMEs to invest in AI applications in their business, we considered two criteria. The first criterion was the company’s plan to invest in AI in the next year, and the second criterion was the company’s plan to invest in the next three years. We adopted 66.6 % as the threshold value by which

the SMEs would clearly express their willingness to finance in AI. Processing the sample according to the first criterion, we saw that 54 of the 157 companies that answered this survey question plan to invest in AI in the next year. Unlike them, 103 companies (65.6 %) do not plan investments in the next year. A total of 86 out of 152 companies, or 56.6 %, indicated their intention to invest in artificial intelligence over the next three years. Based on the analysis of the answers received it can be concluded that the SMEs are still hesitant to invest in the application of AI. The results are more favorable in terms of investing in AI in the next three years. They are still lower, but they are closer to the set criterion. However, they should be taken with a grain of salt, as they may be the result of optimistic expectations and planning.

Based on the obtained results, we can conclude that there is no evidence to reject the null hypothesis  $H_{0,5}$  that “SMEs doing business in transportation and storage are reluctant to invest in the application of artificial intelligence”, and that it can be considered that SMEs are still hesitant to invest in AI.

For a more in-depth analysis of AI investments, we analyzed the impact of the SME size on the decision to invest in AI. We started from the assumption that SME size does not affect the AI investment planning. Through the regression analysis of the data from the survey, we obtained the results shown in Table 7.

A P-value of 0.489 suggests a high probability that the relationship between the willingness to invest in

**Table 7** Results of the regression analysis of the correlation between MSP size and readiness to invest in AI applications.

ANOVA						
	df	SS	MS	F	Significance F	
Regression	1	0.107488	0.10748875	0.480674	0.489116	
Residual	161	36.00294	0.22362075			
Total	162	36.11043				

	Coefficients	Standard Error	t Stat	P-value	Lower 95%	Upper 95%
Intercept	0.31122685	0.047002	6.6215549	5.05E-10	0.21841	0.404047
X Variable 1	0.00036173	0.0005217	0.6933068	0.489116	-0.00067	0.001392

artificial intelligence and the number of employees in the company is not significant. Therefore, we cannot reject the hypothesis that the size of SMEs does not affect the company's willingness to invest in AI.

We can conduct a  $\chi^2$  test for SMEs' willingness to invest in AI by classes, separately for small and medium enterprises. Assuming that the company size does not affect the willingness to invest in AI, we get a value of  $\chi^2 = 0.05933$ . In our case, it corresponds to a P-value of about 0.80494. Therefore, there are no grounds for rejecting the hypothesis that company size and willingness to invest are mutually independent.

However, we must mention that statistical significance does not necessarily mean practical significance. It is possible that although there is a statistically insignificant relationship, it may be practically significant in a real business context. The most common reasons for this can be:

1. Sample size: It may happen that the statistical test does not show significance because there is not enough data to confirm the relationship even if it exists.
2. High variability: This may lead to a smearing of the effect and may result in statistically insignificant results.
3. Measurement error: Improperly filling out the survey form can cause statistically insignificant results.

In our case, the main risk is related to the fact that the implementation of AI in SMEs is still in its initial phase. The relations of SMEs to application of AI have not yet been established, so it is difficult to establish the interdependencies of individual parameters. The more massive application of AI would stabilize results, so possible inaccuracies in conclusions would be lower.

## 5 Conclusions

Artificial intelligence (AI) and machine learning analyze traffic data, predict behavior, optimize flow, and enhance transport efficiency, particularly in urban settings, crucial for SMEs. The AI technology benefits small businesses by optimizing operations, reducing costs, enhancing safety, and supporting decision-

making. It improves the customer service, marketing, content creation, and overall competitiveness, as well. This research addressed the readiness of SMEs to leverage these advantages.

### ***RQ<sub>1</sub>. To what extent does AI currently support transport and storage SMEs?***

Based on the survey results and discussion of application of artificial intelligence in SMEs in today's conditions, in sections 4.2, 4.3.1, and 4.3.2, one can conclude that it is still at an early stage when individual initiatives are more pronounced than the planned approach. Many SMEs (89.6 % of surveyed) do not use AI as a specific application, although 79.8% use AI indirectly as a part of their business software; 16.67 % of surveyed SMEs have created strategies for application of artificial intelligence.

### ***RQ<sub>2</sub>. What are the perceptions of transport and storage SMEs regarding AI applications, and what are their plans for future AI implementation?***

Most of the transport and warehousing SMEs are now recognizing the potential of AI applications, but are currently hesitant to fully leverage them. Various factors contribute to this hesitation, ranging from limited financial resources for AI utilization, shortage of AI experts, and inadequate IT support. Moreover, the reluctance to invest in necessary equipment and software to implement AI cannot be understated. These decisions are often influenced by fragile business conditions and insufficient management and owners' commitment toward AI adoption.

### ***Future of AI application in transport and storage SMEs***

The rapid advancement of artificial intelligence (AI) is paving the way for its extensive integration across various sectors, including transportation and storage. The potential implementation of AI in these industries presents significant opportunities for transformation. AI technologies can optimize route planning and logistical operations, leading to more streamlined transportation networks and decreased fuel consumption. The AI can enhance inventory management by accurately forecasting demand trends and maximizing storage



space efficiency within storage facilities.

Furthermore, the AI-powered predictive maintenance systems can preempt equipment malfunctions, limiting downtime, enhancing overall operational efficiency, and reducing operational costs. The AI-driven analytics hold the potential to deliver invaluable insights into supply chain operations, empowering companies to make the real-time data-informed decisions.

Transitioning from sporadic instances, the adoption of AI is on track to become pervasive, necessitating the integration of this technology within small and medium-sized enterprises for their survival. The willingness of managers and proprietors to outsource AI-related tasks may hasten the uptake of AI in SMEs within the transportation and warehousing sectors. Early implementation positions these businesses more competitively in the market. One can expect that SMEs will leverage AI for diverse purposes, even for operations not demanding advanced technological acumen.

Nevertheless, the successful integration of AI hinges on its harmonization with human cognition and collaboration, as AI serves as a complementary tool to personal reflection, societal norms, and cultural values. Apart from the willingness to adopt the AI, ensuring essential prerequisites for its application is imperative. Key among these is proficient employee training in AI system operations. Before widespread implementation, addressing ethical considerations is crucial to preclude potential conflicts. Consequently, taking a multidisciplinary and all-encompassing approach towards these matters in the forthcoming years is fundamental. States and large-scale enterprises will undoubtedly play pivotal roles in these endeavors, while the SMEs stand to reap the benefits from these ongoing discussions.

Finally, if we would like to provide some recommendations to SMEs involved in transport and storage regarding the future application of artificial intelligence, they could be summarized as follows:

- Utilize AI to automate as many routine tasks as possible,

- Implement artificial intelligence systems for predictive maintenance,
- Utilize data analytics and machine learning for data analysis,
- Use artificial intelligence to optimize business operations, track inventory, and find more efficient solutions,
- Invest in training employees on how to use the AI tools and technologies, and most importantly,
- Immediately initiate these activities.

These recommendations can help all the SMEs leverage artificial intelligence to enhance the efficiency and competitiveness of their transport and warehousing operations. As we are still in the early stages of AI adoption, these recommendations could be universally applicable and are relevant for companies in Slovakia and Serbia, as well.

**Authors contribution:** Conceptualization, VN, SN, and MM; methodology VN, SN, and MM; formal analysis VN and SN; data curation VN and SN; writing original draft preparation VN, SN, and MM; review and editing VN, SN, and MM; visualization MM; All authors have read and agreed to the version of the manuscript.

**Data availability:** On request, which should be delivered to the address of the author in charge of correspondence.

## Acknowledgements

The authors received no financial support for the research, authorship and/or publication of this article.

## Conflicts of interest

The authors declare that they have no known competing financial interests or personal relationships that could have appeared to influence the work reported in this paper.

## References

- [1] CHUI, M., HAZAN, E., ROBERTS, R., SINGLA, A., SMAJE, K., SUKHAREVSKY, A., YEE, L., ZEMMEL, R. The economic potential of generative AI: the next productivity frontier [online]. McKinsey and Company, 2023. Available from: <https://www.mckinsey.com/capabilities/mckinsey-digital/our-insights/the-economic-potential-of-generative-ai-the-next-productivity-frontier#business-and-society>
- [2] DRYDAKIS, N. Artificial intelligence and reduced SMEs' business risks. a dynamic capabilities analysis during the COVID-19 pandemic. *Information Systems Frontiers* [online]. 2022, **24**, p. 1223-1247 [accessed 2024-03-01]. ISSN 1387-3326, eISSN 1572-9419. Available from: <https://doi.org/10.1007/s10796-022-10249-6>
- [3] Eurostat. Use of artificial intelligence in enterprises [online] [accessed 2024-03-01]. Available from: [https://ec.europa.eu/eurostat/statistics-explained/index.php?title=Use\\_of\\_artificial\\_intelligence\\_in\\_enterprises#Enterprises\\_using\\_artificial\\_intelligence\\_technologies](https://ec.europa.eu/eurostat/statistics-explained/index.php?title=Use_of_artificial_intelligence_in_enterprises#Enterprises_using_artificial_intelligence_technologies)
- [4] Paysafe. 3 ways small businesses can use AI to drive growth [online] [accessed 2024-03-10]. Available from: <https://hbr.org/sponsored/2023/03/3-ways-small-businesses-can-use-ai-to-drive-growth>

- [5] RUESSMANN, M., LORENZ, M., GERBERT, P., WALDNER, M., ENGEL, P., HARNISCH, M., JUSTUS, J. Industry 4.0: the future of productivity and growth in manufacturing industries [online] [accessed 2024-03-01]. Available from: [https://www.bcg.com/publications/2015/engineered\\_products\\_project\\_business\\_industry\\_4\\_future\\_productivity\\_growth\\_manufacturing\\_industries](https://www.bcg.com/publications/2015/engineered_products_project_business_industry_4_future_productivity_growth_manufacturing_industries)
- [6] KUEPPER, D., LORENZ, M., KUHLMANN, K., BOUFFAULT, O., WYCK, J. V., KOECHER, S., SCHLAGETER, J. AI in the factory of the future: the ghost in the machine [online] [accessed 2024-03-01]. Available from: <https://www.bcg.com/publications/2018/artificial-intelligence-factory-future>
- [7] BROWN, T. V. The impact of artificial intelligence on freight transportation [online] [accessed 2024-03-02]. Available from: <https://medium.com/@teressavbrown/the-impact-of-artificial-intelligence-on-freight-transportation-ef8d865f29f0>
- [8] OECD. Artificial intelligence: changing landscape for SMEs [online] [accessed 2024-03-02]. Available from: <https://www.oecd-ilibrary.org/sites/01a4ae9d-en/index.html?itemId=/content/component/01a4ae9d-en>
- [9] OECD. OECD digital economy outlook 2020. Paris: OECD Publishing, 2020.
- [10] CORBETTA, M. An insight into the innovative start-up landscape of Friuli-Venezia Giulia: a tale of two sub-regions? *OECD Local Economic and Employment Development (LEED) Papers* [online]. 2020, **2020**(8), p. 1-68. eISSN 2079-4797. Available from: <https://doi.org/10.1787/20794797>
- [11] BERRYHILL, J., HEANG, K. K., CLOGHER, R., MCBRIDE, K. Hello, world: artificial intelligence and its use in the public sector. OECD Observatory of Public Sector Innovation (OPSI), 2019.
- [12] OECD. OECD SME and entrepreneurship outlook 2019. Paris: OECD Publishing, 2019.
- [13] OECD. Algorithms and collusion: competition policy in the digital age. Paris: OECD, 2017.
- [14] OECD. Financing SMEs and entrepreneurs 2020: an OECD scoreboard. Paris: OECD Publishing, 2020.
- [15] OECD. OECD employment outlook 2019: the future of work. Paris: OECD Publishing, 2019.
- [16] MIG. 2024-2030: artificial intelligence in transportation market share, by product, by application and forecast. Frankfurt, DE: Market Insight Group, 2024.
- [17] OMMEREN, C. V., WILLEMS, F., PAARDEKOOPEL, J.-P., BAKRI, T., BEEKELAAR, R. Artificial intelligence in mobility and transport / Artificiele intelligentie in mobiliteit en transport (in Dutch) [online] [accessed 2024-03-08]. Available from: <https://nlaic.com/wp-content/uploads/2020/07/Position-Paper-AI-in-Mobiliteit-en-Transport-1.pdf>
- [18] KARANPURIYA, H. The AI revolution: how SMEs are harnessing the power of artificial intelligence to supercharge their businesses [online] [accessed 2024-03-08]. Available from: <https://www.linkedin.com/pulse/ai-revolution-how-smes-harnessing-power-artificial-karanpuriya>
- [19] Eurostat. Small and medium-sized enterprises: an overview [online] [accessed 2024-03-06]. <https://ec.europa.eu/eurostat/web/products-eurostat-news/-/ddn-20200514-1>
- [20] RAFIQUE, S., MUJAWINKINDI, F. Changing the future. Umea: Umea School of Business, Economic and Statistics, 2023.
- [21] OECD. ICT access and usage by businesses [online] [accessed 2024-03-06]. Available from: [https://stats.oecd.org/Index.aspx?DataSetCode=ICT\\_BUS#](https://stats.oecd.org/Index.aspx?DataSetCode=ICT_BUS#)
- [22] BOGAVAC, M. Research of the influence of digitalization on small and medium enterprises. Doctoral dissertation. Belgrade: Faculty of Business and Law, 2019.
- [23] MASLEJ, N., FATTORINI, L., BRYNJOLFSSON, E., ETCHEMENDY, J., LIGETT, K., LYONS, T., MANYIKA, J., NGO, H., NIEBLES, J. C., PARLI, V., SHOHAM, Y., WALD, R., CLARK, J., PERRAULT, R. The AI index 2023 annual report. Stanford, CA: AI Index Steering Committee, Institute for Human-Centered AI, Stanford University, 2023.
- [24] Clarivate. Master journal list [online] [accessed 2024-03-06]. Available from: <https://mjl.clarivate.com/search-results>
- [25] Scopus. Sources [online] [accessed 2024-03-06]. Available from: <https://www.scopus.com/sources.uri>
- [26] EVERITT, B. The Cambridge dictionary of statistics. Cambridge, UK New York: Cambridge University Press, 1998.
- [27] EC. Artificial intelligence by NACE Rev.2 activity [online] [accessed 2024-03-29]. Available from: [https://ec.europa.eu/eurostat/databrowser/view/isoc\\_eb\\_ain2\\_custom\\_10370113/default/bar?lang=en](https://ec.europa.eu/eurostat/databrowser/view/isoc_eb_ain2_custom_10370113/default/bar?lang=en)
- [28] Oracle. What is AI? Learn about artificial intelligence [online] [accessed 2024-03-06]. Available from: <https://www.oracle.com/artificial-intelligence/what-is-ai/>
- [29] CHUI, M., HALL, B., SINGLA, A., SUKHAREVSKY, A. The state of AI in 2021 [online] [accessed 2024-03-20]. Available from: <https://www.mckinsey.com/capabilities/quantumblack/our-insights/global-survey-the-state-of-ai-in-2021>
- [30] CHUI, M. The state of AI in 2023: generative AI's breakout year [online] [accessed 2024-03-29]. Available from: <https://www.mckinsey.com/capabilities/quantumblack/our-insights/the-state-of-ai-in-2023-generative-ais-breakout-year#research>

- 
- [31] OLDEMEYER, L., JEDE, A., TEUTEBERG, F. Investigation of artificial intelligence in SMEs: a systematic review of the state of the art and the main implementation challenges. *Management Review Quarterly*. 2024, **2024**, p. 1-43. ISSN 2198-1620, eISSN 2198-1639. Available from: <https://doi.org/10.1007/s11301-024-00405-4>
- [32] 2003/361/EC. Commission recommendation concerning the definition of micro, small and medium-sized enterprises. Official Journal of the European Union. 2003, p. L 124/36 - L 124/41.